La borsa di dottorato è stata cofinanziata con risorse del
Programma Operativo Nazionale Ricerca e Innovazione 2014-2020 (CCI 2014IT16M2OP005),
Fondo Sociale Europeo, Azione I.1 "Dottorati Innovativi con caratterizzazione Industriale"

UNIONE EUROPEA
Fondo Sociale Europeo

Ministero dell'Università e della Ricerca

PON RICERCA E INNOVAZIONE

Università degli Studi di Salerno

DIPARTIMENTO DI CHIMICA E BIOLOGIA

"A. Zambelli"

Dottorato in Chimica - XXXIII ciclo

Ph. D. Tesi

New elastomeric materials obtained by biosourced monomers for high performance tyres

Tutor:

Prof. Carmine Capacchione

Co-Tutor:

Prof. Gaetano Guerra

PhD Coordinator

Prof. Claudio Pellecchia

Candidate:

David Hermann Lamparelli

8800100045

2018-2021

Contents

List of abbreviations and compounds

4MPD 4-methyl-1,3-pentadiene

6-PPD N-(1,3-Dimethylbutyl) N'-phenyl-p-phenylenediamine

BHT 2,6-bis(1,1-dimethylethyl)-4-methylphenol

BUNA CB 25 neodymium polybutadiene (high cis)

Buna VSL 2438-2 HM solution of styrene-butadiene rubber in **TDAE** oil

CBS N-cyclohexyl-2-benzothiazylsulphenamide

CCTP coordinative chain transfer polymerization

CRX 1391 CB commercial carbon black

CTA chain transfer agent

DSC differential scanning calorimetry

E ethylene

exKT extendet Kelen-Tudos method

F farnesene

F^{T} *trans*-1,4 farnesene

F^{V} 1,2 farnesene

HP755B (TDAE) mixture of 100 parts by weight of styrene-butadiene rubber with 37.5 parts by weight of **TDAE** oil

IB TUADS isobutyl thiuram disulfide

Kristalek F85 hydrocarbon resin

KT Kelen-Tudos method

Kristalek F85 commercial hydrocarbon resin

M myrcene

MAO methylaluminoxane

***m*-MAO** modified methylaluminoxane

MHD 3-methylenehepta-1,6-diene

M^{T} *trans*-1,4 myrcene

M^{V} 1,2 myrcene

NMR nuclear magnetic resonance

NR natural rubber

Novares TT30-TT90 commercial hydrocarbon resins

O ocimene

O^{T} *trans*-1,4 ocimene

O^{V} 1,2 ocimene

P propylene

PB polybutadiene

PF polyfarnesene

PI polyisoprene

PM polymyrcene

PO polyocimene

PSM styrene-myrcene copolymer

PSO styrene-ocimene copolymer

PVI N-cIclohexylthiophthalimide

RAP retarded anionic polymerization

Riowax BN01: commercial paraffin wax

S styrene

SI 69 bis(3-triethoxysilylpropyl) tetrasulfide

Silane JH75S blend of bis(triethoxysilylpropyl) tetrasulfide (TESPT 50%) supported on carbon black

SIR 20 P 91 commercial natural rubber

T_g glass transition temperature

TBSS N-tert-butyl-2-benzothiazyl-sulfenamide

TDAE treated distillate aromatic extract

TCDE 1,1,2,2 tetrachloroethane-d2

TGA thermogravimetric analysis

TMQ 2,2,4-Trimethyl-1,2-dihydroquinoline

TESPT Silane Bis[3-(triethoxysilyl) propyl] liquid tetrasulfide

T_m melting temperature

Vivatec® 500 commercial plasticizer

WCA water contact angle

ZEOSIL 1165 MP precipitated synthetic amorphous silica

Abstract

Elastomeric materials (commonly called rubbers) play a fundamental role in human life, having myriad applications ranging from wiper blades to spacecraft seals, albeit most of the world's rubber ends up in tyre production. An elastomer can be defined as a polymeric material with the following typical characteristics: (1) the glass transition temperature should be lower than room temperature; (2) amorphous in unstrained conditions and (3) characterized by low Young modulus and high failure strain.

Generally, elastomers are obtained either from natural sources (known as 'Natural Rubber') or by synthesis. Modern industry and technology could not exist as they are today without synthetic rubber since natural rubber fails to meet the growing demand for worldwide rubber. The research described in this thesis focuses on the development of new synthetic elastomeric materials, obtained from renewable natural resources, for tyre production. Currently, the synthetic elastomers used in the tyre compounds (mainly polybutadiene and styrene-butadiene copolymers) are synthesized from monomers coming from fossil sources such as butadiene, isoprene and styrene. The need to abate the current environmental issues, such as global warming, and the massive amount of fossil-based plastic pollution that wind up in the oceans every year, urges a reduction in the usage of fossil-based materials, and their replacement with more sustainable alternatives. These issues have inspired many scientists to design and implement more sustainable approaches for polymer synthesis. The identification and assessment of new and renewable biobased monomers have become a major topic of interest en route to a circular economy. In this context, a natural, potentially alternative source of hydrocarbons is represented by the large family of terpenes, molecules characterized by the presence of one or more double bonds with a cyclic or acyclic unsaturated structure. They are formally oligomers of isoprene units produced by many plants, animals, and some insects. Despite their structural similarity with 1,3-alkadienes, their use as monomers for polymer synthesis has been scarcely investigated and gained attention only in recent times. The aim of this project was, therefore, the synthesis of polymeric materials starting from terpene monomers, testing their mechanical properties, and preparing the first compounds for high-performance tires, in order to partially replace the rubbers obtained from fossil sources. These researches were conducted in collaboration with Pirelli S.p.a. (Milan, Italy), in whose laboratories the mechanical properties of compound formulations, obtained from terpene-based elastomers synthesized, have been studied.

Summary

This thesis is divided into six chapters:

Chapter 1 is devoted to important background information. This chapter introduces the category of treated materials, the elastomers, with a brief historical mention of the origin of natural rubber and the development of synthetic elastomers. The viscoelastic properties that make these materials unique as well as the main types of rubbers and industrial applications are highlighted.

Chapter 2 is dedicated to terpenes, in particular to acyclic ones that in last years have received a lot of attention from academia and industry for their possible uses as starting monomers for more sustainable elastomers. The biological origins of these molecules, current applications, and an overview of their stereoregular polymerization are proposed and discussed.

In **Chapter 3**, the stereoselective copolymerizations of renewable terpene monomers such as ocimene, myrcene, and farnesene with butadiene were investigated. For this purpose, [OSSO]-type bis(phenolate) titanium-based complexes, activated by modified methylalumoxane under mild reaction conditions, were used. The study was then extended to the synthesis and characterization of terpolymers, in particular employing ocimene, butadiene, and styrene.

In the synthesis of new elastomers, the influence of another transition metal centre, a cobalt complex with phosphane ligands, on the stereoselectivity and the catalytic activity were further investigated. The results are described in **Chapter 4.**

In **Chapter 5**, soluble alkillithium-free heterocomplexes consisting of sodium hydride in combination with trialkylaluminum derivatives were used as anionic initiating systems for the production of various elastomers. Homo-, co- and ter-polymerization of myrcene with styrene and isoprene were reached.

The scale-up of selected elastomeric samples is illustrated in **Chapter 6**. The study (in the laboratories of Pirelli) of the mechanical properties of the polymers obtained and their use for the formulation of innovative compounds for high-performance tires were carried out and here presented.

A detailed description of the main experimental procedures and characterization techniques is reported in **Appendix 7**.

«A man has cause for regret only when he sows and no one reaps»

Charles Goodyear (1800 – 1860)

Chapter 1

Elastomers: an introduction

1.1 From natural rubber to synthetic elastomers

The first documents on rubber date back to the mid-16th century. Originating from a flowering plant (*Hevea brasiliensis*) found in the jungles of the Amazon, rubber was used for centuries in its raw form by indigenous tribes who called it cauchu (means 'weeping wood'). Cristoforo Colombo was (probably) the first European to see natural rubber (**NR**) during his voyage to the *New World* (1493-96). The polymer arrived in Europe from South America after a few centuries, brought by Charles de la Condamine (1736-1743); in 1770, Joseph Priestley highlighted the usefulness of little pieces of **NR** to erase undesirable pencil marks on paper by *rubbing*, hence the English term rubber. However, **NR** remained unused until 1823, when Charles Macintosh patented the use of **NR** solutions in light oils to waterproof cloths.[1,2]

Figure 1 - Charles Goodyear photographed by Southworth and Hawes

The poor elastic properties and the lack of dimensional stability greatly limited its use until 1839 when, in the United States, Charles Goodyear discovered that superior qualities could be given to rubber by heating it with sulfur. Hancock exploited this process, introducing the term 'vulcanization' (from the Latin God Vulcanus), to prepare materials that are less sticky when hot and insoluble in common solvents.[2,3]

Rubber began to circulate more and its demand soon far exceeded supply: exports from Brazil grew rapidly, from a few hundred tons in 1846 to 10,000 tons in 1880. The increase in demand led the British to consider the possibility of cultivating *Hevea brasiliensis* in Asia as well. Thus, in 1876, in an act of blatant bio-piracy (or entrepreneurial far-sightedness, depending on point of view), Sir Henry Alexander Wickham shipped about 70,000 seedlings of *Hevea brasiliensis* from Brasil to Kew Gardens (London), falsely claiming as "academic specimens".[4] Some of the imported seeds were sent to Ceylon (now Sri Lanka); those surviving plants (only about 2,400 germinated) gave rise to the first plantations in Malaysia, Indonesia, Thailand, and Sri Lanka,

countries that currently produce 80% of the world's natural rubber. Since the early 1900s, rubber, initially considered a raw material of secondary interest, used as an ingredient in textile colors, paper, and sweetmeats, has become a fundamental element in civil life as well as in war.[2]

Rubber's breakthrough was mainly determined due to the rise of the motor vehicle because cars, trucks, motorcycles, and bicycles needed rubber for tires. During the 19th century, Brazil has met most of the demand for rubber from its wild-growing Amazonian *Hevea brasiliensis* trees, but in 1915 British Malaysia has become the most important rubber supplier with a global market share of 41 %.[5] Simultaneously with the development of technologies to improve and preserve the properties of **NR**, studies flourished with the aim of reproducing it synthetically in the laboratory, starting from conjugated dienes such as 1,3-pentadiene, 2,3-dimethyl-1,3-butadiene, and butadiene. However, the great availability of **NR** made the research on this subject unattractive at that time.

The situation suddenly changed with the First World War causing, especially in Germany and Russia, a serious shortage of rubber; Germans, under the stimulus of the blockade imposed by the Allies, began production of "methyl rubber". This was an inferior substitute and, after the war, german manufacturers returned to the cheaper and more satisfactory **NR**. It was always in Germany that the industrial production of polybutadiene (Buna rubber, 1926) and, subsequently, of the styrene-butadiene (Buna S, 1929) and styrene-acrylonitrile copolymers (the 1940s) began. The products were called **Buna**, from **bu**tadiene as raw material and **na**trium (sodium) as catalyst. No type of synthetic rubber was used commercially until almost 1940.[6] During the Second World War with Japan occupying prime rubber-producing areas in Southeast Asia, the U.S. feared it would run out of the vital material: every tire, hose, seal, valve, and inch of wiring required rubber. The war represented once again the push towards the research and development of new synthetic elastomeric materials capable of compensating for the limited supply of **NR** from Asia.[1,2]

In the 1950s the discovery of Ziegler-Natta organometallic catalysts has stimulated a strong research activity in the field of stereospecific catalysis of dienes, which was led to the preparation of synthetic rubbers with different microstructures, thus opening a new exciting chapter of this story.

1.2 Mechanical behavior of elastomers

A wide range of stress-strain behaviors exhibits polymeric materials that can be categorized into three main types as shown in figure 2: brittle plastic, tough plastic, and elastomer.[7]

Brittle plastics (green line), by virtue of stronger intermolecular bonding, have a linear stress-strain curve up to the fracture point with small deformation (normally from 2% to 5 % elongation) and high Young's modulus of a few GPa. At room temperature, these polymers are mostly in the glassy state, have higher strength and lower flexibility with a high glass transition temperature (T_g) such as polystyrene (T_g = ~100 °C).[8]

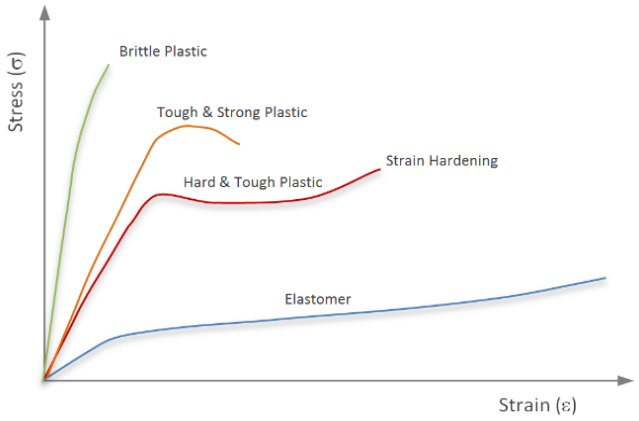

Figure 2 - Stress-strain curve

The orange and red curves represent the behavior of tough plastics: an initial linear elastic deformation is observed then followed by a region of plastic deformation.

The blue curve belongs to the plastic polymers, known as elastomers, the deformations of which are totally elastic.

Elastomers are amorphous polymers composed of long flexible chain-like molecules existing above their T_g that have the ability to elastically deform under stress and then almost to quickly recover their initial state (shape and size) as soon as the forces causing deformation are removed. They are also able to dissipate energy thanks to their viscoelastic nature. To achieve and improve these specific properties it is necessary for the polymer to come subjected to a crosslinking process (vulcanization or curing) (Figure 3).[9] This process changes rubber from plastic material to an elastic or hard material, greatly improves rubber strength and eliminates its deficiencies at temperature extremes. It is generally accomplished by the formation of a cross-linked molecular network with sulfur bridges, formed by a sulfur atom or

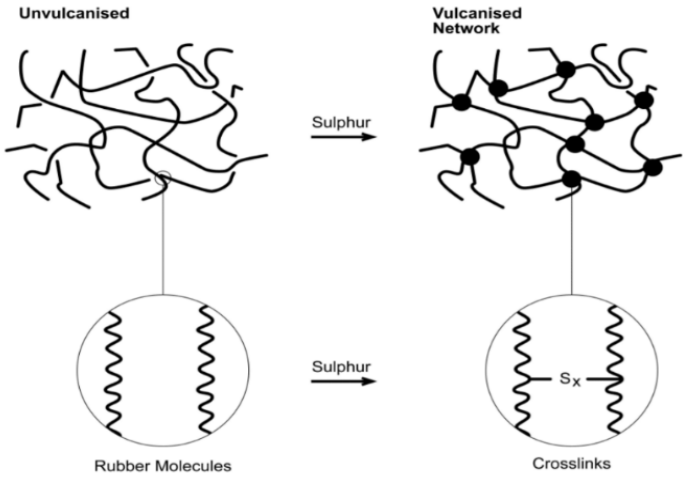

Figure 3 – Vulcanization process

a short chain of sulphur atoms. Rubbers are also capable of adhering to most other materials, enabling different hybrid constructions.

1.3 Classification of elastomers

Elastomers are obtained from two sources: naturally from **NR** or synthetically from man-made polymeric processes. They are classified according to **ASTM** D-1418 (American Society for Testing and Materials International) and are abbreviated as reported in **Table 1**.[7,10,11]

Table 1. Classifications of elastomers

Last letter in the abbreviation	Examples*
M: saturated chains of carbon atoms, no double bonds	**EPDM**, **FKM**, **FFKM**
R: double bonds in the carbon chain (unsaturated)	**NR**, **CR**, **BR**, **SBR**, **NBR**, **HNBR**, **IIR**
O: oxygen in the polymer chain	Epichlorohydrin rubber (**ECO**)
Q: silicon and oxygen in the polymer chain	**VMO**, **FVMQ**
T: sulfur in the polymer chain	Polysulphide elastomer
U: carbon, oxygen, and nitrogen in the polymer chain	Polyurethane rubber (**PU**)

* The abbreviations will be made explicit in the text.

NR is is the most ancient natural polymer known used in the production of elastomers. It is harvested from *Hevea Brasiliensis*, by making incisions in the bark and collecting the fluid as a colloidal white suspension in vessels (Figure 4), in a process called "tapping" usually done once every 2–3 days for 9 months each year.[12] The amount of milky latex obtained on each tapping is about 300 mL. **NR** combines high strength (tensile and tear) with outstanding resistance to fatigue; it shows low hysteresis (which leads to low heat generation), low rolling resistance, high resistance to cutting, chipping, and tearing but moderate resistance to environmental damage by heat, light, and ozone. These properties derive from its composition and unique molecular structure. Indeed, fresh **NR** latex comprises approximately 94% rubber hydrocarbon and 6% nonrubber constituents (proteins, phospholipids, glycolipids, fatty acids, etc).[13] The rubber hydrocarbon inside the rubber, as disclosed by nuclear magnetic resonance (**NMR)** studies, is essentially consisting of the initiating group (referred to as ω), two *trans*-1,4 isoprene units, a long sequence of *cis*-isoprene units, and terminal group (referred to as α), as shown in Figure 5.[13,14]

Figura 4 – Tapping of NR

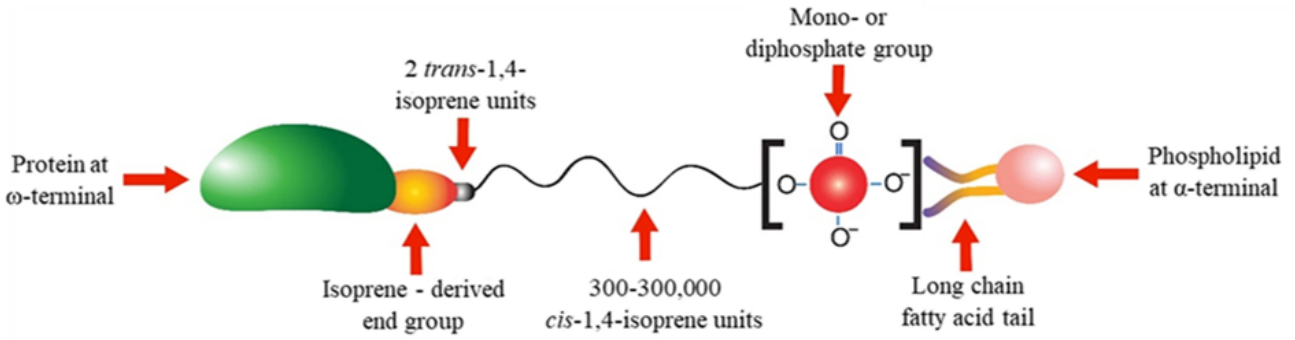

Figure 5 –Proposed structure of natural rubber molecule

In the last years, the production of synthetic rubber greatly exceeded the production of **NR** because on one hand the cultivation of *Hevea Brasiliensis* is circumscribed to few climatic areas of the planet, and on the other hand the final properties of synthetic rubber can be precisely tailored by a judicious choice of the reaction parameters (feed composition, catalyst, reaction conditions, etc.). Thailand, Malaysia, and Indonesia are among the world's largest producers of **NR** (Figure 6); China is currently the largest consumer utilizing (~33%).[15]

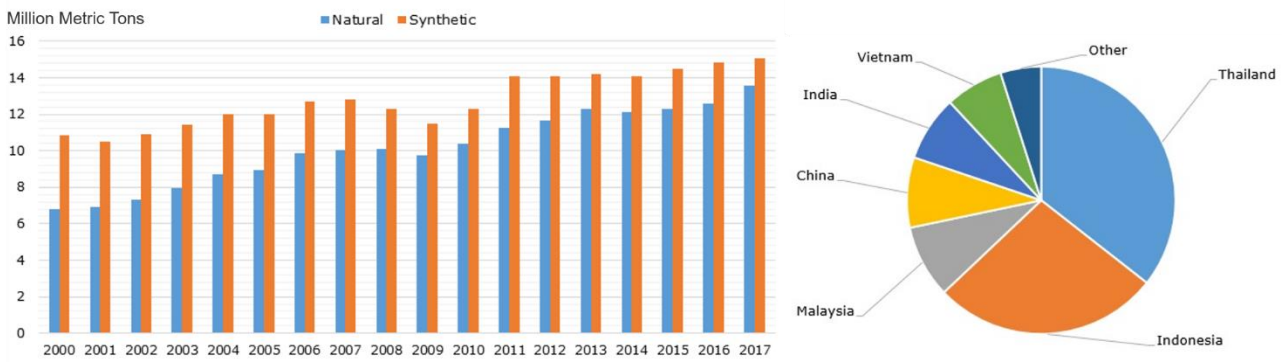

Figura 6 - On the left, the world production of NR and synthetic rubber (2000-2017); on the right, leading natural rubber producers. Source: International Rubber Study Group.

Synthetic rubbers include many types of elastomers:[9,11] styrene-butadiene rubber (**SBR**), polybutadiene rubber (**BR**), polyisoprene rubber (**IR**), ethylene propylene diene monomer rubber (**EPDM**), chloroprene rubber (**CR**), and so on. Specialty rubbers mainly include nitrile rubber (**NBR** or **HNBR**), epichlorohydrin rubber (**ECO**), butyl rubber (**IIR**), silicone rubber (**VMO**), fluorosilicone (**FVMQ**), fluororubber (**FKM**), perfluoroelastomers (**FKKM**), **PU** rubber, etc. **BR** and **SBR**s are by far the two largest volume synthetic rubber produced, being main players in the tyre industry. Both these elastomers are derived from butadiene that is obtained as by-product of ethylene production from steam crackers. **SBR** is a random copolymer of butadiene and 10–25% (mol) styrene produced on a large scale from emulsion (E-**SBR**) and solution (S-**SBR**) polymerization.[16] The addition of styrene lowers the price and improves the

abrasion and aging resistance, and blend properties of **BR**.[11] Indeed, **SBR** combines the properties of **BR**, which is a highly rubbery polymer (T_g = -100 °C) having low hysteresis and thus offering low rolling resistance in addition to wear resistance, with the properties of polystyrene (**PS**), which is a glassy polymer (T_g = 100 °C) characterized by high hysteresis and thus offering good wet grip properties.

1.4 Uses of elastomers and tires

For their unique properties, elastomers have been developed and applied for many industrial applications: seals, adhesives, belts, gloves, implants and prosthetics, footwear, molded flexible parts, and, above all, automotive products. Indeed, 70% of world rubber consumption goes into the tire industry. The growth in world tire production has been in response to the growth in the automotive sector, in particular in those countries, such as China, India, and Brazil, where there has been a demographic and industrial increase in the last 20 years. Therefore, the number of vehicles in the world's major markets is constantly and progressively increasing. This trend is especially evident for China, where it is expected to move from 147 million passenger cars in 2016 to 309 million in 2024.[17]

The word tire is a short form of *attire*, from the idea that a wheel with a tire is a dressed wheel. The main structural components of tires are the tread, body, sidewalls, and beads, composed of elastomeric compounds, steel, fabric and, in addition, a variety of other raw materials including tire cord, carbon black (or silica-based compounds), curatives, antidegradants, reinforcing fibers and processing oils. Figure 7 provides an internal view of the composition of a tire. Tire components are assembled like a puzzle and molded together in the curing process, which causes the tire components and rubber compounds to adhere to their surrounding components to create a singular product. The make-up of tires varies depending on the type – truck or passenger vehicle – manufacturer and place of manufacture (i.e. locally or internationally).

Figura 7 - Parts of a tyre

The most commonly used material in the composition of the car tire compound is the **SBR** polymer, while the truck tire compound is mainly composed of **NR**. The limitations of **SBR** are

inferior mechanical properties, low resilience, low tear strength, and poor resistance to oil and ozone. Thus, **SBR** dominates in the car and motorcycle tread for the possibility of adjusting T_g and the resistance to high temperatures. Hence, **NR** is used in a 100% in the heaviest and most severe uses, such as tires for buses and aircraft.

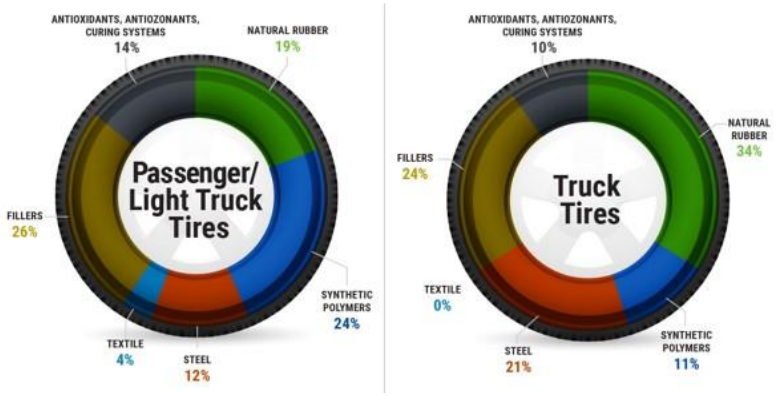

Figura 8- Typical tyre composition. Source: https://www.ustires.org/

BR is the second-largest volume of synthetic rubber produced, next to **SBR**. It in the cured state exhibits high elasticity and resilience (the ability to recover size and shape after stress) with resultant excellent low heat buildup, abrasion resistance, low-temperature flexibility, and resistance to flex cracking and cut growth (growth in the size of an initial cut in the cured rubber), but it is characterized by poor wet traction due to low transition glass temperature because of low vinyl content. For this reason, it is usually blended with other elastomers for tread compounds.

As seen above, rubber represents more than 40 % of a tire's composition. The tread is the part of the tire in direct contact with the soil; the composition of the tread is of fundamental importance since it must ensure high mechanical properties during the rolling of the wheel.

Taking into consideration the large volumes of global tire production, the replacement of synthetic rubber from fossil monomers with rubber derived from renewable resources could guarantee in the near future the desirable shift to more environmentally sustainable materials.[18] The term "sustainable development" was introduced by the Brundtland Commission (1987), with the definition as "development that meets the needs of the present without compromising the ability of future generations to meet their own needs".[19]

Among all the compounds derived from biomass, terpenes belong to a large family of hydrocarbons, present mainly in plants and insects, with a cyclic or linear unsaturated structure. Recently, they emerged as viable candidates to serve as building blocks for the synthesis of polymers and elastomers. In the next chapter, terpenes will be discussed.

«Study and in general the pursuit of truth and beauty is a sphere of activity in which we are permitted to remain children all our lives»

Albert Eistein (1879 – 1955)

Chapter 2

Terpenes as renewable raw materials for polymers

2.1 Introduction: the reasons for seeking alternative resources

The reduction in the consumption of fossil fuels is one of the most significant challenges of the modern era. The chemical industry still relies heavily on materials derived from petroleum, which is a complex mixture of hydrocarbons and other compounds (from 2009 to 2018, the worldwide daily demand for crude oil increased by 18% and is predicted to continue to increase).[20,21] Our life is deeply linked to this resource since petroleum products include transportation fuels, combustible oils for heating and electricity generation, asphalt, and raw materials for the production of various chemicals and materials such as plastics and synthetic rubber. In the last years, there is a growing body of evidence that the largest driver of the warming of Earth's surface and troposphere (the lowest layer of the atmosphere) is the emission of gases that create a greenhouse effect, of which more than 90% are carbon dioxide and methane.[22] Fossil fuel burning (coal, oil, and natural gas) for energy consumption is the main source of these emissions, with additional contributions from agriculture, deforestation, and manufacturing. Besides, another relevant concern of our time is widespread of large quantities of single-use plastic waste into the environment without controlled disposal.[23,24] Indeed, their accumulation in the oceans endangers marine organisms and, due to the formation of micro-plastics, potentially causes health risks of all links on the food chain.[24–26]

For these reasons, the search for more sustainable and renewable resources capable of replacing, or at least limiting, the consumption of fossil resources is constantly developing and is an active task of research in both industry and academia. Currently, more than 90% of existing polymers are obtained from non-renewable raw materials of fossil origin, while only a small percentage (<5%) is from renewable sources.[27,28]

Fortunately, nature offers many different not fully exploited compounds, which are excellent building blocks for constructing advanced materials: polysaccharides and their derivatives,

lignin, suberin, vegetable oils, tannins, monomers originating from sugars, furan derivatives, lactic acid, and fatty acid, which are just a few examples.[29–35] Among the wide range of molecules derived from biomass, a natural source of unsaturated hydrocarbons coming from cheap non-food crops is represented by the vast family of terpenes (>80.000 members).[36,37]

2.2 Terpenes: origin, classification, and applications

Terpenes and terpenoids (oxygenated derivatives) are ubiquitous unsaturated hydrocarbons molecules. Although they can be found in nature with various chemical structures (acyclic, monocyclic, bicyclic, and polycyclic structures), their classification is based on the number of isoprenes (**I**) structural units (C5), linked in a regular (head-tail) or irregular (head-head) arrangement, that a given molecule contains: monoterpenes (C10), sesquiterpenes (C15), diterpenes (C20), sesterpenes (C25), triterpenes (C30) and so on. This classification is known as the "biogenetic isoprene rule", formulated by Leopold Ruzicka (1887-1976).

These molecules have been known for hundreds of years, being the main components of essential oils extracted from the leaves, flowers, and fruits of various plants (mainly conifers). Also, a limited number of insects, marine microorganisms, and fungi are capable of producing them. Indeed, in the majority of organisms (bacteria, fungi, mammals, and plants), the biosynthesis of terpenes occurs via a common synthesis, the mevalonate pathway (MEP) (Scheme 1).[38,39] MEP starts from three acetyl-CoA units leading to the formation of mevalonic acid, the central precursor for isopentyl pyrophosphate (IPP) and its isomer dimethylallyl pyrophosphate (DMAPP). DMAPP and IPP condense to give geranyl pyrophosphate (GPP), which

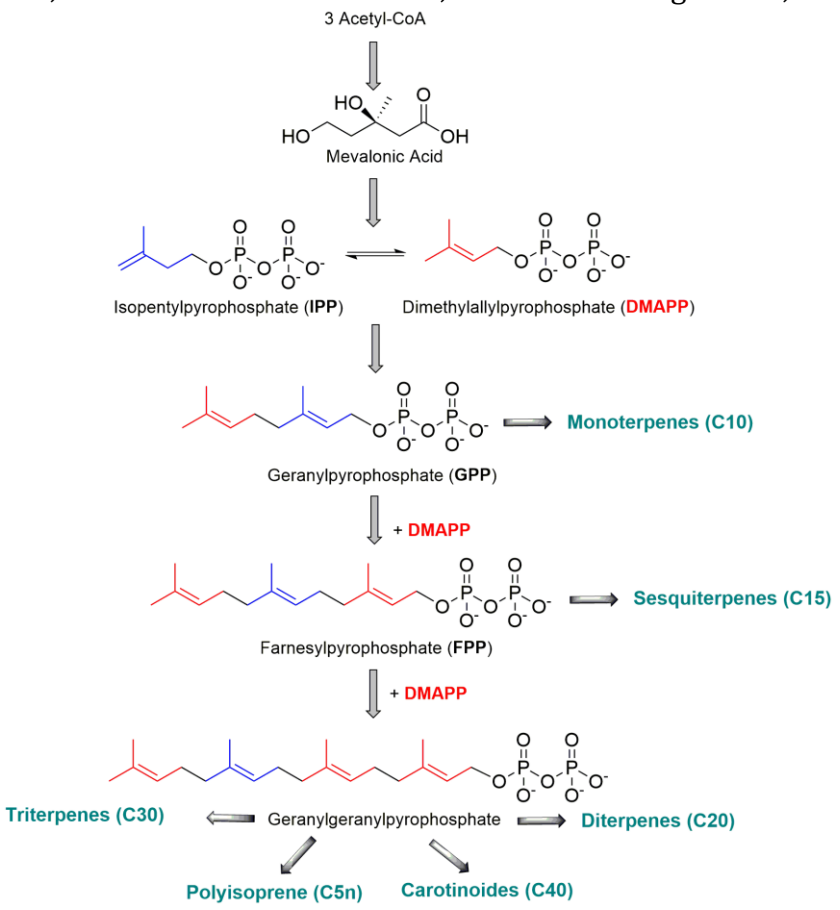

Scheme 1- MEP pathway

in turn reacts with another DMAPP to form farnesyl pyrophosphate (FPP). By this synthetic sequence, all terpene compounds can be stepwise generated, from monoterpenes to polyisoprene (natural rubber), through enzymatic catalysis (terpene synthases).

The largest natural source of terpenes is turpentine (world production is approximately 350000 tons per year),[40] the volatile fraction particularly isolated from resins of the genus Pinus belonging to the Pinaceae family. This plant resin has the important biological role of defending plants from attacks by insects and bacteria and of providing for rapid closure of wooden wounds. Turpentine has a distinctive odor and is a colorless liquid but turns yellow for the tendency of terpenes to easily oxidize. Its chemical composition can vary depending on the species, age of the tree, geographical location, extraction method, etc.[41] Pinenes, bicyclic monoterpenes that exist in the form of two structural isomers, namely *α*-pinene and *β*-pinene, are major turpentine constituents (up to 45-97 % and 0.5-28 % for *α*- and *β*-isomers, respectively) with smaller amounts of other monoterpenes such as 3-carene, limonene, camphene, *β*-phellandrene, and *β*-myrcene (**M**) (Figure 9). From the pyrolysis of pinenes, it's possible to isolate on an industrial scale acyclic monoterpenes such as *β*-ocimene (**O**) (from *α*-pinene) and its isomer **M** (from *β*-pinene).

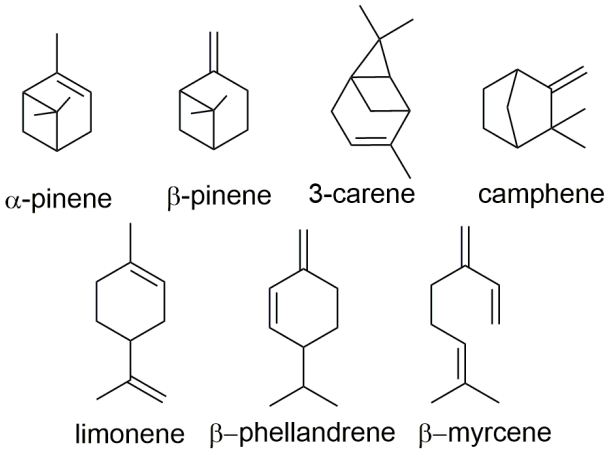

Figure 9 - Major turpentine components

Although the biological functions of terpenes are not yet fully understood, it is ascertained their function as secondary metabolites in many plants, playing important ecological roles as a plant defense against herbivory and insects (repellents), disease resistance, as well as potentially plant-plant communication, growth regulators, and activators of symbiotic mechanisms (attracting specific insects to stimulate cross-pollination processes).[42,43]

Nowadays, in terms of uses, terpenes are important sources of intermediates and ingredients for flavorings and fragrances, tackifiers, solvent, diluting agents for varnishes and dyes, fuels cosmetics, food additives, pharmaceuticals, insect repellents, biodegradable surfactants, chain transfer agents, and much more.[44–46]

2.3 Acyclic terpenes

Terpenes are divided into cyclic and acyclic (or linear) compounds. Among these compounds, some linear ones - due to the structural similarity to classical petrochemicals such **I** and butadiene (**B**) - have recently aroused growing attention as building blocks for the synthesis of a vast range of polymers, including elastomers.[30,34,35,47]

Acyclic monoterpenes as **O** and **M** (Figure 2) have certainly been the most studied for wide availability and low cost. **O**, **M** and their isomer allocimene (**A**) can be considered unsaturated derivatives of 2,6-dimethyloctane.[41]

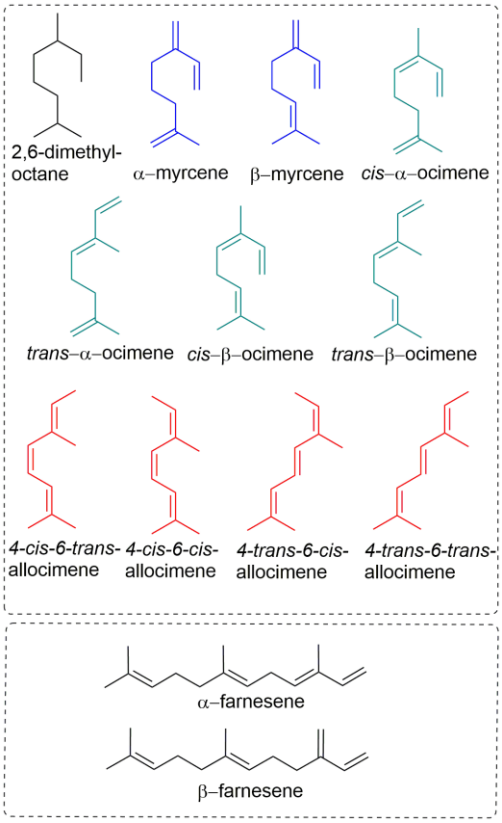

Figure 10 – Acyclic terpenes

M (7-methyl-3-methylene-octa-1,6-diene) is a colorless oil that exists as two isomers, *α*- and *β*-**M**. The *α*-isomer (2-methyl-6-methylene-1,7-octadiene) has not been found in nature and therefore the *β*-isomer is simply indicated as myrcene. **M** is industrially generated by pyrolysis of *β*-pinene and new developments on its production from microbial synthesis via metabolically engineered *Escherichia coli* were also investigated.[48] **M** found in smaller percentages, up to 2 %, in the hop, celery, ginger root, rosemary, nutmeg, and sage. By using different polymerization techniques (radicalic, anionic, cationic, and coordinative polymerization), **M** can be polymerized. Really, the first works on **M** date back to the 40s of the last century and concern an emulsion polymerization and a study to avoid the deterioration of the monomer during storage due to its reactivity.

O is produced from the thermal cracking of *α*-pinene, while **A** can be obtained by **O** isomerization at high temperature in a mixture of four isomers which undergo a cyclization on heating, giving mainly *β*-pyronene. **O** and its derivative ocimenol, which is produced by acid-catalyzed hydration, are mainly used as perfume components.

F is a linear polymerizable sesquiterpene that can be found in nature in the form of six isomers. *α*- and *β*- isomers of **F** differ only by the location of one double bond. Constituent of many higher plants and communication pheromone,[49] **F** can be obtained through fermentation of sugar

feedstocks[50] and is gaining increasing attention in the last years as a biofuel,[51] and precursor for a wide variety of commercial molecules.

For their characteristics, these molecules can be considered as alternative bio-sourced monomers since they can also be easy polymerized and functionalized giving access to a large variety of macromolecules,[52–54] such as polyketones, polyesters, polyamides, cycloolefinic polymers via controlled/living cationic polymerization or ring-opening polymerization (ROP).[55,56]

Furthermore, the presence of a double bond, replaced with electron donor groups, makes the cationic mechanism a concrete way for the polymerization of terpenes. Indeed, one of the first works (1937) concerned *α*-pinene, using $AlCl_3$ as the initiator of cationic polymerization.[57] Afterwards, in the literature examples of polymerization of cyclic and acyclic terpenes through anionic, cationic, or radical polymerization have been reported.[58] However, with these techniques it is not possible to achieve a high control of the polymer microstructure as in the case of the coordinative polymerization promoted by homogeneous catalysts based on transition metals. In analogy to the polymerization of 1,3-alkadienes, the microstructure of the resulting polymers, the molecular mass and thus the physical and chemical properties of the final material are heavily dependent on the polymerization technique and catalytic system employed. The nature of the metal center and the type of ancillary ligand play a crucial role in tuning and determining these properties as well as the range of application of the materials produced.

2.3 Stereoregular polymerization of acyclic terpenes: state of art

The stereoregular homo- and co-polymerizations of **M**, **O**, and **F** with various comonomers have been reported to be promoted by catalytic systems based on titanium, [59] group 3 and rare-earth metals, [60–63] iron,[64] and cobalt.[65,66] As we will see, for polymers deriving from these monomers containing double bonds along the polymer chain it's possible not only to have polymers with different concatenation (chemoisomerism 1,2, 1,4 or 3,4) and *cis-trans* geometric isomerism, but also stereoisomerism *iso-syndium* due to groups present along the polymer chain. Let's review the main advances in this research field.

2.3.1 Titanium

Titanium catalysts were the first systems used for the polymerization of 1,3-dienes, and the system $AlR_3/TiCl_4$ is still one of the most important for the preparation of *cis*-1,4-polyisoprene (**PI**). About terpenes, attempts to stereoregularly polymerize **M** dates back to 1960 by employing heterogeneous Ziegler-Natta type catalysts, using approximately 3 mol% of Al^iBu_3 and $TiCl_4$ ([Al]/[Ti] = 2–2.5). At low temperatures (0 °C), the highest molecular weights polymers were reported, observing a monomer conversion of ~80 %. However, the inherent viscosity (η_{inh} = 0.3-1) indicated relatively low M_n and a structure consisting of 1,4 units was assigned to polymers. 1,4-**PM**s with higher molecular weights (η_{inh} = 2–5.5) were reached with Al^iBu_3 and VCl_3 ([Al]/[V] = 5–8.5) in heptane solution, obtaining conversions almost quantitative, but batches usually contained considerable amounts of insoluble products (15-20 % or even more).[67] Surprisingly, after these initial studies, monomers such as **M** were forgotten and only recently "rediscovered".

In 2017, Capacchione *et al.* described stereoregular polymers of **M** and **O** and their copolymerizations with styrene (**S**),[68] by using homogeneous [OSSO]-type bis(phenolate) titanium complexes **1**-**2**[69] and catalyst **3** (Figure 11), activated by methylaluminoxane (**MAO**).

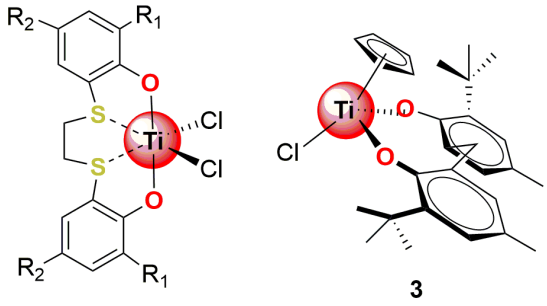

1 R_1=^{t}Bu, R_2=^{t}Bu
2 R_1=Cumyl, R_2=Cumyl

Figure 11 – Ti-based complexes 1, 2 and 3.

The nature of the ancillary ligand on the metal center had a strong influence on stereoselectivity. Indeed, in **O** polymerization ([**O**]/[Ti] = 500, [Al]/[Ti] = 500, 24 h, 0-70 °C, toluene), **1** and **2** provided a polymer (M_n up to 33.7 kg mol^{-1}, $Đ$ = 1.1-1.7, T_g from -17 to -29 °C) having mainly *trans*-1,4 fashion (70%) at 70 °C, while at lower temperature (0 °C) an isotactic 1,2-**PO** (>99%) was produced. In **M** polymerization, **1**/**MAO** system yielded a prevalently (92%) *trans*-1,4-**PM** (M_n up to 66.4 kg mol^{-1}, $Đ$ = 1.22-1.71, T_g from -58 to -62 °C). Instead, titanocene catalyst **3** showed a predominance of *cis*-1,4 microstructure (56-92 %) for both monomers.

Complexes **1** and **2** were also able to copolymerize **M** and **O** with **S** in a wide range of compositions (11–96% mol of **M** and 13–85% mol of **O**), giving copolymers with relatively narrow $Đ$ (1.1–1.9) and higher molecular weight (M_n up to 102 kg mol^{-1}). In particular, for **S**-**M** copolymerization, the reactions were performed at 70 °C ([Al]/[Ti] = 500, [**M** + **S**]/[Ti] = 1000,

24 h), producing the corresponding copolymers with **M** present as *trans*-1,4 units (62–89% mol) with isolated **S** units for copolymers with a lower **S** amount and short isotactic **PS** segments in polymers having a higher **S** content.[68]

2.3.2 Group 3 and rare-earth metals

Complexes based on group 3 or rare-earths elements have been widely used in the stereoselective polymerization of 1,3 alkadienes.[70] In particular, lanthanide-based catalysts are well-known to be highly *cis* specific in the polymerization not only of **B** but also of many other substituted butadienes. The serious problem, especially of rare-earths elements, is to implement their catalysts in industrial processes due to the high cost of these metals.

In 2016, Li and Zhang reported the first stereoregular **O** polymerization, employing half-sandwich rare-earth metal dialkyl complexes **4**-**10** (Figure 12), bearing chiral and achiral cyclopentadienyl ligands, in combination with $[Ph_3C][B(C_6F_5)_4]$ and Al^iBu_3.[71,72]

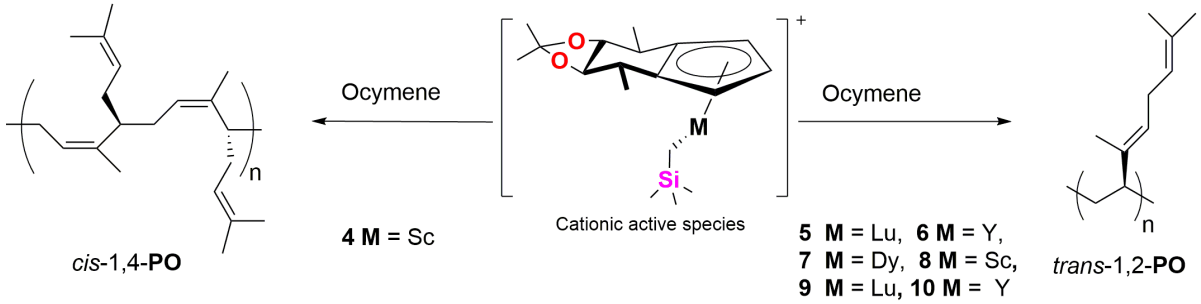

Figure 12 – Regio and stereo-controlled polymerization of **O** by complexes **4**–**10**.

Under mild experimental conditions ([**O**]/[Metal] = 450, [Al]/[Metal] = 5, 0.2-71 h, T = from -40 to 30°C, toluene), Sc complex **4** delivered syndiotactic *cis*-1,4-**PO** (selectivity up to 100%, *rrrr* = 100%), while the corresponding achiral cyclopentadienyl-ligated **8** afforded isotactic *trans*-1,2-**PO** (selectivity up to 78%, *mm* up to 54%), showing the highest catalytic activity (264 kg mol_{Sc}^{-1} h^{-1}). **PO**s obtained displayed M_n up to 446 kg mol^{-1} and narrow $Đ$ (1.38-1.79). The temperature strongly influenced the selectivity: *cis*-1,4 and syndiotactic (*rrrr*) selectivity progressively increased up to 100% as the polymerization temperature decreased from 30 to -40 °C. Albeit with lower activity, the same selectivity of **8** was observed for Lu **5** and **9**, Y **6** and **10**, Dy **7** complexes analogs (*trans*-1,2-selectivity = 36-100%, *mm* = 33-100%, M_n = 27-255 kg mol^{-1}, $Đ$ = 1.36-3.13).

Later on, Hou has successfully used half-sandwich Sc-based complexes **11**-**13** (Figure 13), in combination with an equimolar of $[Ph_3C][B(C_6F_5)_4$, for the copolymerization of **M** with ethylene

(**E**) and propylene (**P**).[73] Under mild conditions ([**M**]/[Sc] = 150-500, p**E** = 0.1 MPa, 0.08-1 h, 25 °C, toluene), **11** gave diblock poly(**M**-*b*-**E**) up to 97 % of **M** content (*cis*-1,4 = 93-94 %, M_n = 880-930 kg mol^{-1}, $Đ$ = 1.78-1.80), while **12** provided a multiblock **M-E** copolymers with 12-58 % of **M** contents (3,4 = 69-73 %). Depending on the amount of **M** used, **13** produced alternating (when **M** was abundant) or random **M–E** copolymers. The obtained copolymer possessed T_gs between -51 and -71 °C and melting temperatures (T_m) at 122 and 133 °C, relating to **PM** and **PE** blocks, respectively. More remarkably, the terpolymerization of **M**, **E** and **P** could also be achieved using **13** (*p***E** = 0.03-0.06 MPa, *p***P** = 0.17-0.38 MPa), yielding a new family of **E**–**P**–diene rubbers (**EPDM**) with controllable compositions, unimodal and narrow $Đ$ (M_n = 880-930 kg mol^{-1}, $Đ$ = 1.55-1.79). In addition, it was also possible to introduce various other polar groups (such as thioacetic acid, sulfoacid, epoxidized, hydroxylated–chlorinated, and furan) in the C=C double bonds of resulting **M**-based polymers.

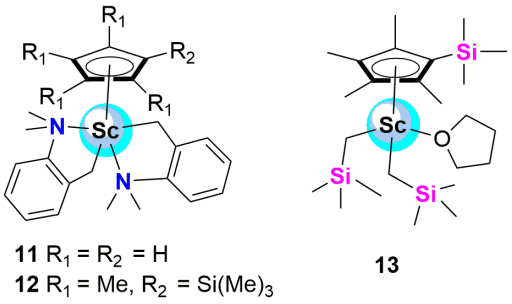

11 $R_1 = R_2 = H$
12 R_1 = Me, R_2 = Si(Me)$_3$

13

Figure 13 – Half-sandwich Sc dialkyl complexes **11–13**

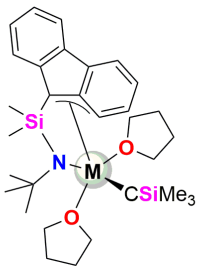

14 M = Sc
15 M = Lu
16 M = Y

Figure 14 – Flu-based complexes **14-16**

Zhang, Li, and Qiu synthesized a new fluorenyl-amide based constrained-geometry-configuration lanthanide alkyl complexes (η^3:η^1-FluSiMe$_2$NtBu)Mt(CH$_2$SiMe$_3$)(THF)$_2$, where Mt = Sc (**14**), Y (**15**), and Lu (**16**) (Figure 14).[74] These complexes, activated by different borate cocatalyst and in the presence of AlR$_3$ (R = Me$_3$, Et$_3$, ^{i}Bu$_3$), were used in the **M** polymerization ([**M**]/[Metal] = 250-4000, [Al]/[Metal] = 5-40, 1-48 h, 0-70°C, toluene, chlorobenzene or *ortho*-dichlorobenzene), affording **PM**s contained mainly *cis*-1,4-microstructure (76-100%) and a trace amount of 3,4 (M_n = 100-900 kg mol^{-1}, bimodal $Đ$ = 1.66-4.26, T_gs in the range from -60 to -67 °C). At 0 °C complete *cis*-1,4-selectivity (100%) and the narrowest $Đ$ (1.66) were obtained. The concentration of **M** affected positively the catalytic activity, which was found for **16** the highest (118 kg mol$_{Lu}^{-1}$ h^{-1}) and the lowest for **15** (0.002 kg mol$_Y^{-1}$ h^{-1}).

Zhang *et al.* reported on the living 3,4-polymerization of **M** and its living 3,4-copolymerization with **I** ($Đ$ = 1.06-1.20), catalyzed by binuclear Y complex **17**, bearing a bridged amidinate ligand (Figure 15).[75] Upon activation

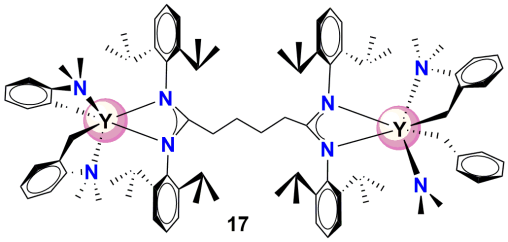

17

Figure 15 - Binuclear Y amidinate complexes **17**

with two equiv of $[Ph_3C][B(C_6F_5)_4]$, at the temperatures between -20 and 80° C, the catalyst **17** furnished **PM**s (M_n = 32-86 kg mol^{-1}), exhibiting *ultra*-high 3,4 selectivity (86-100%) and stereoselectivity (*mm* up to 100%, *mmmm* up to 95 %). At 80 °C, 3,4-selectivity dropped to 86% and the $Đ$ increased slightly (1.20). The copolymerization was also successfully carried in the range of -20 to 25 °C, providing a *di*-block 3,4-rich poly(**I**-*b*-**M**) (M_n = 79-91 kg mol^{-1}, $Đ$ = 1.10-1.22, 3,4-**PI** = 91-100%, 3,4-**PM** = 97-100%).

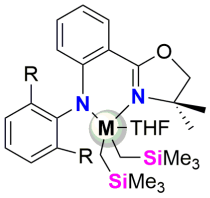

18 R = Me, **M** = Lu
19 R = ^{i}Pr, **M**= Lu
20 R = Me, **M** = Y
21 R = ^{i}Pr, **M** = Y

Figure 16 – Anilido-oxazoline supported Lu and Y complexes **18–21**

Subsequently, others complexes of Lu and Y (**18-21**) (Figure 16), supported by an anilido-oxazoline ligand and activated with one equiv of $[Ph_3C][B(C_6F_5)_4]$, were found to be active in **M** polymerization ([M]/[Lu or Y] = 1000, 0.5-2 h, 30 °C, toluene), offering high *cis*-1,4-selectivity (82.3–94.5 %), M_n = 69-152 kg mol^{-1} and $Đ$ = 1.87-2.05.[76]

Very recently, Shi *et al*. reported that rare-earth complexes **22-25** (Figure 17), containing rigid 4,5-(PR2)2–2,7,9,9-tetramethylacridane-based pincer ligands (acri-RPNP; R= ^{i}Pr and Ph), were found to be active in **M** polymerization ([**M**]/[Metal] = 500-1000, 0.08-2 h, 25-80°C, toluene).[77] Combined with $[Ph_3C][B(C_6F_5)_4]$ or $[PhMe_2NH][B(C_6F_5)_4]$, **22-25** produced **PM** with high M_n (up to 182 kg mol^{-1}) and very narrow $Đ$ (<1.08), that last data suggested that polymerizations proceeded in a living manner. At room temperature, **24**/$[Ph_3C][B(C_6F_5)_4]$ was able to convert 500 equiv of **M** with a yield of 73.4 % in 6 min (*cis*-1,4-**PM** = 98 %).

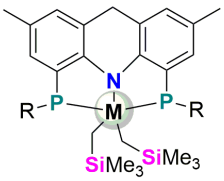

22 **M** = Lu, R= ^{i}Pr$_2$
23 **M** = Lu, R= Ph$_2$
24 **M** = Y, R= ^{i}Pr$_2$
25 **M** = Y, R= Ph$_2$

Figure 17 - PNP ligated rare-earth complexes **22–25**

By using a lanthanum catalyst **26** (Figure 18), Zinck and co-workers exploited the coordinative chain transfer polymerization (**CCTP**) of **M** and its statistical *co*- and *ter* polymerizations with **I** and **S**. The complex **26** was used in combination with *n*-butylethyl magnesium (Mg^{n}BuEt) and Al^{i}Bu$_3$.[78] **CCTP** involves a single transition metal-based catalyst and a metal alkyl of the main groups as chain transfer agent (**CTA**). In this kind of polymerization, the reversible chain transfer from the catalyst to the **CTA** allows the growth of several polymer chains per metal centre, improving the catalyst economy and the regioregularity of the final polymer.[79] Thus, highly *trans*-1,4 stereoregular poly(**M**-*co*-**S**), poly(**M**-*co*-**I**), and poly(**M**-*co*-**I**-*co*-**S**) copolymers were obtained ([Mg]/[Al]/[La] in different ratios, [Monomers]/[La] = 1000, 2-20 h, 70 °C, toluene) in a wide range of compositions and features (*trans*-1,4 selectivity up to 99%, M_n = 3-113 kg mol^{-1}; $Đ$ = 1.3-2,4; T_g in the range of -17 and -69 °C). By increasing the quantity of Mg^{n}BuEt, the increase of 3,4 enchainments (up to 87%) was observed in the microstructure of the *co*- and *ter*-polymers. Furthermore, the use of Al^{i}Bu$_3$, as a chain transfer agent, retained *trans*-1,4 stereospecific character of the polymerization.

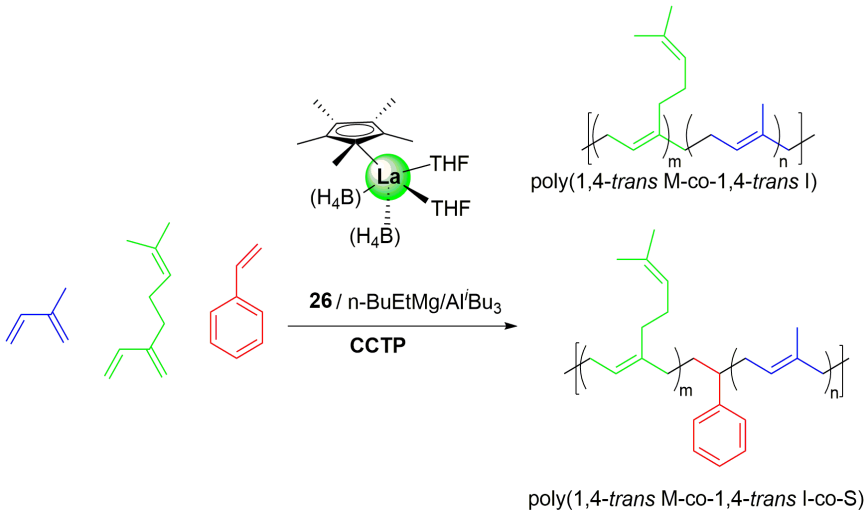

Figure 18 - CCTP of **M**, **I**, and **S** *co*- and *ter*-polymers obtained by using complex **26**

Later on, Li and Sun examined **M** polymerization and its copolymerization with **I** through a *β*-iminophosphonamide ligated lanthanum *bis*(benzyl) complex **27** (Figure 19), in combination with one equiv of [Ph$_3$C][B(C$_6$F$_5$)$_4$] and 5-40 equiv of AlR$_3$ (R = Me$_3$, Et$_3$, ^{i}Bu$_3$).[80] High *trans*-1,4 selectivity (64.9-97.9 %) in a living fashion was observed in almost all experiments ([**M**]/[La] = 500, 2-6 h, 0-60 °C, toluene). The resulting **PM** displayed low T_g values (usually below −60 °C) with moderate M_n (up to 62 kg mol^{-1}) and relatively narrow $Đ$ (1.17-1.83). In the copolymers, **M** incorporation rate varied from 10% to 80%, observing lower M_n (up to 39 kg mol^{-1}) and $Đ$ = 1.18-1.77. According to the Fineman-Ross method, **M** was found to be more reactive than **I** (r_M = 2.49 and r_I = 0.85). Furthermore, thanks to the living

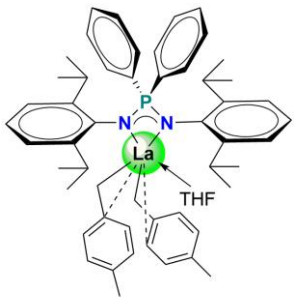

27

Figure 19 – Complex **27**

polymerization character, via sequential monomer addition, unprecedented poly(**I**-*b*-**M**-*b*-**I**) triblock copolymer was also reached (M_n = 48 kg mol^{-1}, $Đ$ = 1.22-1.24).

High *cis*-1,4 stereoselectivity of **M** was achieved by Visseaux *et al.* by means of neodymium borohydride-based complexes, $Nd(BH_4)_3(THF)_3$/Mg^{n}BuEt, Cp*$Nd(BH_4)_2(THF)_2$ (Cp* = C_5Me_5) and $Nd(BH_4)_3(THF)_3$/**BX**/Al^{i}Bu$_3$ (**BX** = $[CPh_3][B(C_6F_5)_4]$; $B(C_6F_5)_3$; $[HNMe_2Ph][B(C_6F_5)_4]$, in a 1:1 or 2:1 ratio with respect to [Nd]).[81] $Nd(BH_4)_3(THF)_3$/Mg^{n}BuEt was poorly efficient at room temperature, but the increase in temperature (80 °C) led to more than 80% polymer yield (~90% of *cis*-1,4) in 2 h for [Mg^{n}BuEt]/[Nd] = 1-2. **PM**s reached, under experimental conditions ([**M**]/[Nd] = 300, 22-80 °C, 0.5-240 h, toluene), showed M_n in good accordance with theoretical values expected (up to 71 kg mol^{-1}), and $Đ$ in the range of 1.29-2.02. When [Mg^{n}BuEt]/[Nd] = 3-20, a narrowing of $Đ$ (1.27) and a decrease in M_n (~3 kg mol^{-1}) were observed, while the 3,4-rate defects in the polymer increasingly appeared. These results were compatible with a **CCTP**, in which the propagation step takes place not exclusively on Nd, but also on Mg.[79] By using the Cp*$Nd(BH_4)_2(THF)_2$ half-sandwich complex generated in situ, **PM** synthesized was highly stereoregular (*cis*-1,4 = 98,5%). Further studies showed that $Nd(BH_4)_3(THF)_3$ combined to Al^{i}Bu$_3$ in the presence of a boron activator (**BX**) provided the highest activity (yield of 61 % in 10 minutes) and the highest M_n (49-91 kg mol^{-1}), but a less stereoregular, slightly soluble, crosslinked polymer with larger $Đ$ (2.18-3.26) was obtained.

Afterward, end-functionalized high *trans*-1,4-**PM** were prepared by means of $Nd(BH_4)_3$/Mg^{n}BuEt.[82] The living *trans*-1,4 stereoregular (>97 %) polymer chain was reacted with benzophenone afforded *trans*-1,4-**PM** up to 83 % CPh_2OH end-group.

In 2016, Gomez introduced two different Nd-based catalysts: $Nd(O^iPr)_3$ and NdV_3, for **M** polymerization (50-60 °C, 1.5 h, cyclohexane), affording high M_n (up to 300 kg mol^{-1}) with broad $Đ$ (2.4-8.8) and *cis*-1,4 selectivity of 92-96 %.[83] $Nd(O^iPr)_3$ was combined with $[HNMe_2Ph][B(C_6F_5)_4]$ (or $[CPh_3][B(C_6F_5)_4]$), and Al^{i}Bu$_3$ (or Al^{i}Bu$_2$H), and NdV_3 was activated by Al^{i}Bu$_3$ and $AlEt_2Cl$, showing first-order kinetics of monomer consumption. Features of bio-based polymeric products, especially in terms of M_n and $Đ$, were dependent on the nature and molar ratio of borane and alkyl aluminum *co*-catalysts. Indeed, the alkyl aluminum, on the one hand, in the formation of the active species was involved; on the other hand, it had the function of **CTA** by lowering the M_n. Dynamic mechanical analysis of **PM**s (T_g = from -66 to -62 °C) showed that the samples have properties similar to natural rubber, but the modulus values at its rubbery plateau were still low to be considered useful in applications at room temperature.

NdV_3 was also tested, in combination with Al^iBu_2H or ***m*-MAO** as cocatalyst, and $AlEt_2Cl$ as halogen source, in **O**, **M**, and **F** polymerization.[84] The catalyst system $NdV_3/Al^iBu_2H/AlEt_2Cl$ was employed for **O** polymerization ([O]/[Nd]=600, 50 °C, 4 h, cyclohexane), providing **PO** with *cis*-1,4 content (54-69%), M_n of 20-57 kg mol^{-1}, broad $Đ$ (3.8-8.2) and T_g in the range of -30 to -26 °C. NdV_3/***m*-MAO**/$AlEt_2Cl$ was able to polymerize **M** and **F** ([**M** or **F**]/[Nd] = 150-600, 55 °C, 2 h, cyclohexane) for [Al]/[Cl] ratio ≥ 35, since smaller ratios provided only traces of **PM**. For these copolymers, *cis*-1,4 content was >92%, M_n values were higher and the $Đ$ were narrower compared to **PO** results (M_n = 155-243 kg mol^{-1}, $Đ$ = 3.1-3.9).

Later, Stefan *et al*. described a halide-free complex of Nd, coordinated with three bidentate diethylphosphate (**DEP**) ligands ($[Nd(\mu\text{-}\mathbf{DEP})_3]_x$ and combined with Al^iBu_3, that was able to promote **M** polymerization at room temperature.[85] High *cis*-1,4 selectivity (≥95 %), M_n =13–48.5 kg mol^{-1}, and relatively narrow $Đ$ (1.8) were reached. Kinetics experiments demonstrated the pseudo-living character of polymerization, confirmed by the successful synthesis of block copolymer poly(**M**-*b*-**I**) (M_n = 15.5 kg mol^{-1}, $Đ$ = 3.1) through sequential monomer addition.

In 2017, Carpentier *et al.* reported on the copolymerization of **M** and **F** with **S** using an ansa-neodymocene catalyst (**28**) (Figure 20) in the presence of 10 equiv of $(^nBu)_2Mg$.[86] **M** and **F** were incorporated in the copolymers (**M** content = 5.6–30.8 mol %, **F** content = 1.5–9.8 mol %) depending on the initial feed, showing a microstructure consisting of 1,4- and 3,4-poly(terpene) units randomly distributed within syndiotactic **PS** segments. This distribution was also confirmed by the presence of a unique T_g (between -58 and 100 °C), whose value was a function of terpene content. A series of poly(**S**-*co*-**M**) and poly(**S**-*co*-**F**) (M_n = 14-37 kg mol^{-1}, $Đ$ = 1.3-3.9) were produced ([**S**]/[Nd] = 6000-16000, [Terpene]/[**S**] = 0.125-1, 60-120 °C, 2-22 h, cyclohexane or *n*-dodecane). The catalyst productivity, very low in homopolymerizations (0.28-5 kg mol_{Ne}^{-1} h^{-1}), reached up to 374 kg mol_{Ne}^{-1} h^{-1} in the case of **S-M** copolymerization. Terpolymers of **S** with **M** and **E** were also achieved (M_n up to 122 kg mol^{-1}, activity = 64-250 kg mol_{Ne}^{-1} h^{-1}). A narrow and monomodal dispersities ($Đ$ = 1.3–1.6) confirmed the formation of poly(**S**-*co*-**E**-*co*-**M**).

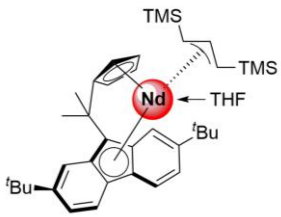

28

Figure 20 – Complex **28**

Li and Cui reported on the first example of high 3,4-selective polymerization of **M**, using a dialkyl Lu-based complex, bearing a NSN bidentate *β*-diimidosulfonate ligand (**29**) (Figure 21), activated by $[Ph_3C][B(C_6F_5)_4]$, and Al^iBu_3.[87] This system exhibited high activity in **M** and **I** polymerization with 3,4-regio- (> 99 %) and isospecific stereo-selectivity (*mmmm* > 99%). The 3,4-content was influenced by aluminum alkyls, decreasing passing from Al^iBu_3 to $AlEt_3$ and $AlMe_3$, and M_n dropped dramatically (from 461 to 28 kg mol^{-1}) due to the chain transfer to the Al center. *Iso*-**PM**s with a low T_g (-42°C) and narrow $Đ$ (1.41-2.43) under various experimental conditions ([Lu]/[B]/[AlR_3] = 1:1:5, 0.1-12 h, T between -30 and 60 °C, chlorobenzene or toluene) were obtained. Complex **29** was also active in random and block copolymerization of **M** and **I** (M_n = 143-253 kg mol^{-1}, $Đ$ = 1.46-1.63), by one-pot mixing or sequential addition of the two monomers.

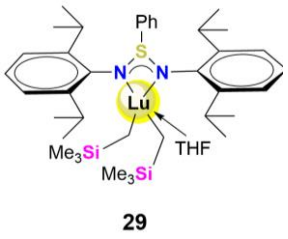

29

Figure 21 – Complex **29**

Soon after, Li and Cui observed that the use of NPN-ligand framework around metal and the variation of substituents on the N-aryl ring did not affect the catalytic activity, but changed the stereoselectivity.[88] Indeed, using catalysts **30**, **31**, and **32** (Figure 22), a shift from syndiotactic to moderate isotactic **PM** (*rr* up to 66 % and 33 % for 30 and 32, respectively; *mm* up to 95 % for 36) was achieved. Notably, this phenomenon was attributed to the polar solvent (chlorobenzene) and to the less steric space of complexes **30** and **32**, which increased the possibility of forming the *exo-endo* geometry, favoring thus isoselectivity. The *syndio*-3,4 **PM** showed a higher T_g (-30 °C) compared to that of *iso*-3,4 PM (-43 °C). The increase of the polymerization temperature (from -30 °C to 60 °C) had a slight influence on 3,4 selectivity (decreased from >99 % to 94 %), but a positive effect on catalytic activity.

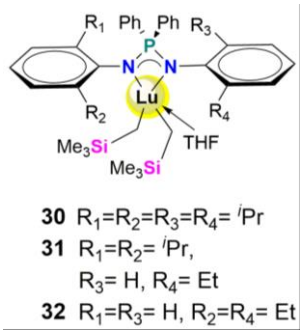

Figure 22 – Structures of complexes **30-32**

Lately, using the ternary catalytic system **31**/$[Ph_3C][B(C_6F_5)_4]$/Al^iBu_3 (6h, -30 °C, chlorobenzene), further work on the synthesis of random copolymers of 3-methylenehepta-1,6-diene (**MHD**) with **I** or **M** was carried out.[89] The resulting copolymers had high regio and stereoselectivities (1,2-selectivity >99%, *mm* triad >90%), as confirmed by **NMR** spectroscopy. Molecular weights were rather low (M_n = 9-13 kg mol^{-1}) with narrow $Đ$ (1.5-1.6). For random poly(**MHD**-*co*-**I**) and poly(**MHD**-*co*-**M**) an elastomeric thermal behavior was observed (single T_g values at -14.9 °C and -43 °C, respectively). Furthermore, these polymers were post-

functionalized via thiol-ene "click" reaction by use 2,2-dimethoxy-2-phenylacetophenone as photoinitiator, transforming all pendant vinyl groups into the corresponding -CH_2CH_2SR functionalities, allowing to preparation materials with tailored thermal and surface properties.

2.3.3 Iron

Despite iron-based catalysts having not been much studied in the past, the interest for these systems in the field of the stereospecific polymerization of conjugated dienes has grown enormously in recent years thanks to the fact that iron, being less toxic than many other transition metals, is characterized by greater sustainability and lower environmental impact.[70]

In 2012, Ritter *et al*. investigated the polymerization of **M** and **F** (only *β*-isomers) with very active iron(II) iminopyridine complexes **33**-**34** (Figure 23).[64] In particular, complex **33** ([Fe]/[Al]/[Ph_3C^+]/[M] = 1:5:1:20012 h, 23 °C) led mainly to *trans*-1,4 polymer, while complex **34** ([Fe]/[Al]/[Ph_3C^+]/[F] = 1:30:1:200, 24 h, 23 °C) led to *cis*-1,4 polymer. Both complexes were activated by [Ph_3C][$B(C_6F_5)_4$], trityl BArF and Al^iBu_3 or $AlEt_3$ in toluene. Although the origin of the high selectivity was not elucidated, the authors proposed that the higher electron density on the iron atom increases the *trans*-1,4 selectivity. Thus, alkyl-substituted imines (**33**) favored *trans*-1,4 insertion, whereas aryl-substituted imines (**34**) favored *cis*-1,4 insertion. The **PM** and **PF** obtained possessed high M_n (>70 kg mol^{-1}) and controlled *Đ* (1.4-2.1).

More recently, Wang and co-authors introduced for **M** and **F** polymerization a library of novel aminopyridine iron(II) chloride catalysts **35-38**, bearing different alkyl substituents (methyl, ethyl, benzyl, and isopropyl groups) on the amine moiety.[90] The catalytic activity was both influenced by the steric hindrance of the ligand and the Lewis acidity of the metal center. The isopropyl group of **38** appears to show the best compromise, facilitating coordination and insertion of monomers and providing the higher activity (13.7 kg mol_{Fe}^{-1} h^{-1} in the case of **PF**). Complex **38** had excellent thermal stability and, activated by **MAO**, was able to promote polymerization of terpenes ([Monomers]/[Fe] = 500-1000, 25 °C, 2 h, toluene), exhibiting 1,4-regularity (up to 59% and 75% for **PM** and **PF**, respectively) and a smaller amount of 3,4-units. Intriguingly, the inactivity of **O** was explained considering that the long alkyl chain hampers its coordination to the metal center (Figure 23, part II). **PM** and **PF** have been achieved with M_n = 310-490 kg mol^{-1} and $Đ$ = 1.9.

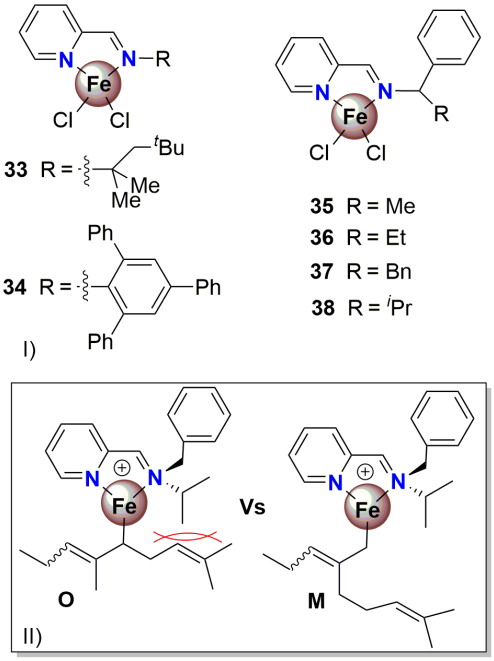

Figure 23 – I) Fe(II) iminopyridine complexes **33–34** and aminopyridine Fe(II) chloride catalysts **35–38**. II) Proposed mechanism of coordination and insertion for **O** and **M**.

2.3.4 Cobalt

Cobalt-based catalysts were intensively investigated for the stereoregular polymerization of 1,3 alkadienes, and therefore are also considered viable candidates for the terpene polymerization.[70]

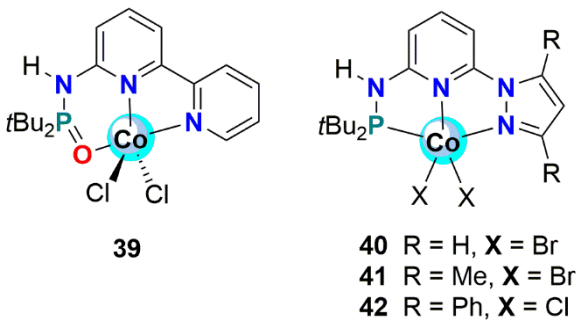

Figure 24 - Structures of Co(II)-based complexes **39–42**

Gong *et al.* reported the first example of Co(II) catalyst in the copolymerization of **M** with **I**, using **39** (Figure 24) combined with $AlEt_2Cl$ (30 °C, 1-2 h, toluene) in a living *cis*-1,4 fashion. After consumption of **I**, the sequential addition of **M** provided poly(**I**-*b*-**M**) with M_n up to 95.3 kg mol^{-1} and very narrow $Đ$ (1.05-1.09).[91] For **PM** blocks, **NMR** suggested mainly the presence of *cis*-1,4 microstructure (93.4 %), while two T_g values (-61.9 and -56.7 °C), relating to the two polymer blocks, were detected by DSC.

In 2019, the same authors synthesized new cobalt complexes **40**-**42** (Figure 24) , supported by PN^3 ligands and activated by $AlEt_2Cl$, for **M** polymerizations ([Al]/[Co] = 150-500, 1 h, 30-80 °C, toluene).[66] The microstructure of **PM**s (M_n = 121-289 kg mol^{-1}, $Đ$ = 1.2-2.6) was found from moderate to high *cis*-1,4 (66.1-99.4 %) with minor 3,4 units. Significantly, the increased steric hindrance for complexes **41** and **42** has a negative effect on the activity and selectivity if compared to **40**. Furthermore, complex **40** also allowed the preparation of random poly(I–*co*-M) (M_n = 103-156 kg mol^{-1}, $Đ$ = 1.6-1.9) with a broad range of compositions, by varying the monomer feed composition, with typical **M** content of 7.6-57.6 %. The copolymers showed *cis*-1,4 microstructure (69.4-73.4 % and 79.4-83.4 % for **I** and **M** units, respectively) and T_g in the range of -41.7 and -51.1°C.

Later on, Co(II) complexes **43**-**48** (Figure 25), bearing *bis*-chelated phenoxy (4,6-di-tert-butyl-2-phenol, naphthalen-2-ol)-imine ligands with pendant donor atoms (O, S, or P), were reported.[92] In combination with ***m*-MAO** or Al^iBu_3, these complexes were able to convert **M** into *cis*-1,4-**PM** (selectivity up to 97.2 %). For these catalysts, in the range of 0-100 °C ([Al]/[Co] = 300, 2 h, toluene), comparable specificity (*cis*-1,4 = 74.9-97.2 %) and activity were observed, proving **PM** with M_n of 272-312 kg mol^{-1} and $Đ$ of 1.8-3.2. Notably, the nature of the donor plays a fundamental role in stereocontrol and activity, influencing the insertion of the monomer. Indeed, the oxygen and sulfur atoms in **43**, **44**, **46**, and **47** are more prone to the metal-donor dissociation, favoring the coordination of the monomer with a consequent increase of selectivity.

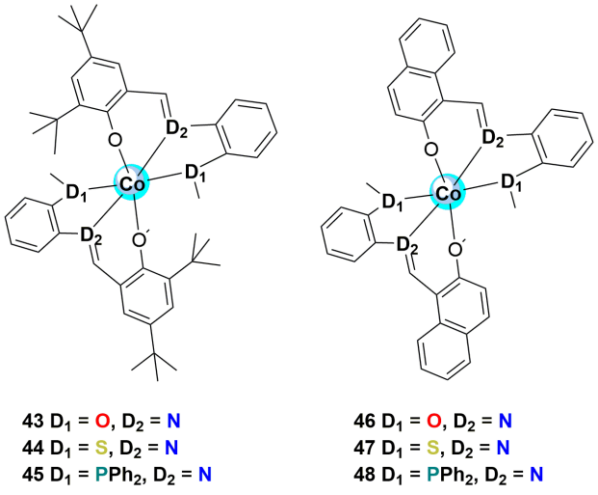

Figure 25 - Co(II) complexes **43–48**

Further investigations by the same research group on the synthesis of cobalt complexes **49** and **50**, supported by a 2-oxazoline-pyridine (N,N) ligand bearing a labile 6-(di-tert-butyl-phosphine oxide) moiety (Figure 26), and on their ability to copolymerize **I** with **M** derivative 2-methyl-6-methyleneoct-7-en-3-ol (**M-OH**) were disclosed.[93] In presence of an excess of $AlEt_2Cl$ and various masking agents such as **MAO**, $AlEt_3$, Al^iBu_3, Al^iBu_2H, $AlEt_2Cl$ or Al^iBu_2Cl, **49** and **50** ([$AlEt_2Cl$]/[Co] = 300, 1-3 h, 30 °C, toluene) allowed the synthesis of a poly(**I**-*co*-**M-OH**) with **M-OH** incorporation from 4.4 mol% to 31.5 mol%, M_n of 23-453 kg mol^{-1} and $Đ$ of 1.2-2.6.

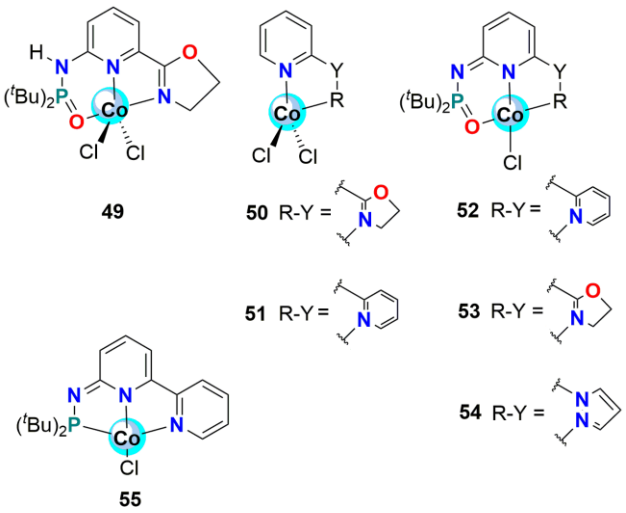

Figure 26 - Structures of Co(II)-based complexes **49–56**

The **DSC** thermograms of samples showed a single transition with T_g values (from -52.6 to 10.5 °C) increasing by increasing the incorporation of higher hydroxyl content. From these copolymers, it was possible to prepare SiO_2 filled vulcanizates in order to study the effect of the hydroxyl functionality in the compatibilization with the elastomeric matrix. The mechanical performances showed improvement of the tensile strength (9.6 ± 0.2 MPa) and elongation at break, an unusual stretchability (over 885.3 ± 2.0%), and improved hysteresis loss in comparison to standard **PI**/SiO_2 vulcanizates.

Recently, Gong *et al*. reported on a series of new Co-based complexes (**51**-**55**) (Figure 26) very active (yields in most cases above 90 % in about 1 h) in the polymerization of bifunctional monomers **M** derivatives (hydroxyl, furan, and pyridine group) and their controlled copolymerization with **I**.[94] Copolymerization followed a first-order kinetics dependence on monomer without obvious chain transfer and termination. The produced functional copolymers (M_n = 133-166 kg mol^{-1}, $Đ$ = 1.1-3.2) were mainly enchained with *cis*-1,4 fraction of 65.0%-74.1%, showing significantly improved hydrophilicity (proven by the reduced water contact angle), stable thermal property with a decomposition temperature exceeding 400 °C and good tolerance towards low temperature.

In order to develop more environmentally friendly polymer chemistry, the choice of natural building blocks (acyclic terpenes, in our case) is just the initial step. Indeed, the selection of catalytic systems that combine good performances, easy handling, and low costs would be highly desirable as well, allowing an improvement of the process's overall sustainability.
With the aim of synthesizing bio-based materials that could compete in properties with the typical petroleum-based elastomers, the stereoselective coordinative polymerization promoted by transition metal complexes seemed to be the best strategy to obtain materials with specific properties. Furthermore, some titanium-based catalysts (bearing [OSSO]-type bis(phenolato) ligands) developed at the University of Salerno have proved to be active and versatile in the synthesis of stereoregular polymers from conjugated dienes and in their

copolymerization with **S** and **E**. Therefore, these catalytic systems looked like the ideal candidates for the development of homogeneous catalysts for the polymerization of terpenes.

«Dans la vie, rien n'est à craindre, tout est à comprendre»

Marie Curie (1867-1934)

Chapter 3

Stereoselective (co)-polymerization of acyclic terpenes catalyzed by titanium-based complexes

3.1 Introduction

Titanium was the first transition metal to be used for the polymerization of dienes. In 1954, after the discovery of the remarkable activity in the polymerization of **E** and **P** by Karl Ziegler and Giulio Natta, $TiCl_4$ and $TiCl_3$ were used, in the presence of aluminum alkyls (AlR_3), to obtain polymers from different conjugated dienes.[95,96] These studies led to the first highly stereoregular *cis*-1,4 polyisoprene, observing for these material properties very similar to those of **NR**. Subsequently, the stereoselective polymerization of **B** (*cis*-1,4) was carried out with a system based on TiI_4 and AlR_3.[97]

The synthesis of polydienes catalyzed by transition metals has two significant advantages. The first is represented by the possibility of having well-defined regiochemistry polymerization, thus creating polymer chains with repetitive units of a single type; the second advantage linked to the use of these metals is that the polymerization mechanism, in addition to being regioselective, can also be stereoselective. A catalytic system able to synthesize stereoregular polymers allows producing materials with specific properties. The control of the microstructure of the polymers, as well as the control of their molecular masses, is fundamental to obtaining materials with interesting mechanical properties for industrial applications.

Titanium is the ninth-most abundant element in Earth's crust (0.63% by mass) and the seventh-most abundant known metal.[98] Its concentration is about 4 picomolar in the ocean. In addition, this metal is non-toxic and biocompatible. Thus, the synthesis of highly stereoselective Ti-based catalysts for the polymerization of olefins and dienes represents an attractive and economical target from an industrial point of view. In 2003 a considerable step towards the development of potentially versatile and useful Ti-based catalysts was represented by the synthesis of the first tetradentate [OSSO]-type bis(phenolato) ligands, reported by Okuda.[99] Indeed, the combination of the hard phenoxo-units with the two soft donors sulfur atoms imparts unique electronic properties to the metal center. The hemilabile nature of the interaction between the

sulfur atoms and the metal center has been shown to be crucial in modulating the reactivity and the selectivity, in many cases, allowing the obtaining of new polymeric materials.

In the first studies, the dichloro complex **1** (Figure 26) and the corresponding di(iso-propoxo) homolog were used, activated by **MAO**, in **S** polymerization, leading to isotactic **PS** with high molecular weight (up to 2 654 Kg mol^{-1}) and narrow dispersity ($Đ$ = 1.7–2.0). The isospecific **S** polymerization remained confined to the heterogeneous Ziegler-Natta catalysts until the discovery of these C(2)-bridged [OSSO]-titanium complexes. In the light of these results, it was decided to test these catalytic systems for the synthesis of polydienes.

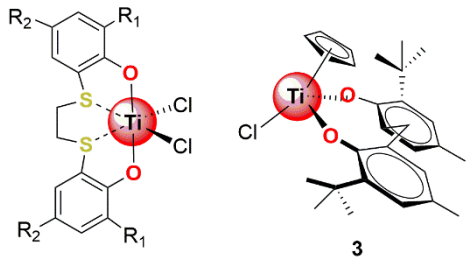

1 R_1=^{t}Bu, R_2=^{t}Bu
2 R_1=Cumyl, R_2=Cumyl
56 R_1=Cumyl, R_2= Me

Figure 26 - [OSSO]-titanium complexes

In 2007, Capacchione *et al*. observed that **1**/**MAO** system was active in the stereoselective polymerization of **B** and **I**, as well as in the copolymerization of **B** with **S**, giving mainly *trans*-1,4 polymers (80-96%).[100] Afterwards, complex **1** was also employed in the synthesis of alternating copolymers of **E** with **I**[101] and 4-methylpentadiene (**4MPD**)[102] and in the copolymerization of *p*-methylstyrene with **B** and **I**.[103]

Binary copolymerizations of **4MPD** with **S**, **B** and **I**, promoted by the titanium complex dichloro{1,4-dithiabutanediyl-2,2′-bis[4,6-bis(2-phenyl-2-propyl)phenoxy]}titanium (**2**) in combination with **MAO**, were also reported.[104]

In 2010, the dichloro complex {1,4-ditiabutanedil-2,2'-bis[4-methyl-6-(2-phenyl-2-propyl)phenoxy]} titanium (**56**) (Figure 26), activated by **MAO**, allowed to obtain, by living polymerization, an isotactic-**PS**-*block*-*trans*-1,4-**PB** copolymer, through sequential additions of monomers.[105]

Otherwise, Ti(η^5-C_5H_5)-(η^2-**MBMP**)Cl (**MBMP** = 2,2'methylen bis(6-tert-butyl-4-methylphenoxo) (Figure 26) (**3**) was found to be active in the polymerization of **S** and conjugated dienes such as **I** and **B**, showing a high *syndio*-selectivity and predominantly *cis*-1,4 microstructure (80-94%).

As described in 2.3.1 paragraph, in 2017, Capacchione's research group using homogeneous [OSSO]-type bis(phenolate) titanium complexes **1**-**2** and catalyst **3** achieved different stereoregular polymers of **M** and **O** and their copolymers with **S.**[68] Motivated by this recent encouraging results, we decided to investigate the *homo*, *co*- and *ter*-polymerization of **O**, **M** and **F** (Figure 27) with **B** and **S** in the presence of various [OSSO]-type titanium catalysts. Surprisingly, in spite of the importance of **B** in the industrial production of elastomers, its

copolymerization with acyclic terpenes had not yet been performed while I was conducting my investigations.

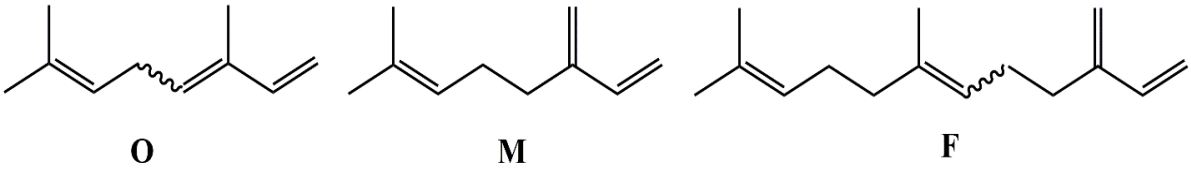

Figure 27 – Structure of **β**-ocimene (**O**), **β**-myrcene (**M**) and **β**-farnesene

3.2 Results and Discussion

3.2.1 Binary copolymerization of butadiene with ocimene and myrcene

Complex **2** has already been shown to promote the highly stereoselective **B** and **O** homopolymerization (95% of *trans*-1,4 and 92% of 1,2-stereoselectivity, respectively).[59] Therefore, we investigated its performances in the copolymerization of **B** and **O**, under mild experimental conditions (24 h, 30°C, and toluene).

Table 1 summarizes the main results. Due to the lower reactivity of **O** compared to **B**, an excess of **O** in the monomers feed was necessary. Using [**O**]/[**B**] = 1-9, it is possible to obtain copolymers in a wide range of compositions with the incorporation of the terpene up to 85% (run 1, **Table 1**). Probably due to the preferential incorporation as vinylic units ($\mathbf{O^V}$), T_gs are sensibly higher by increasing the amount of **O** (See Appendix 7, Figure 3S56). Yields and molecular weights increased by increasing the **B** feed content. For these materials, the narrow $Đ$ values confirmed a copolymeric nature.

Table 1. Copolymerization of *β*-ocimene (**O**) and butadiene (**B**) results.

Run[a]	O feed	B feed	Activity	M_w[b]	$Đ$[b]	Polymer Composition[c]					T_g[d]
						B	B structures %			O^T/O^V	
	(mol %)	*(mol %)*	*kg/(mol Ti)·h*	*(kDa)*		*(mol %)*	*1,2*	*1,4 cis*	*1,4 trans*	*(molar ratio)*	*(°C)*
1	90	10	0.3	15	1.3	15	-	5	95	8/92	- 24.3
2	80	20	0.7	23	1.3	40	-	5	95	11/89	- 38.1
3	70	30	1.4	29	1.3	68	4	5	91	12/88	- 53.0
4	50	50	5.2	101	1.8	80	4	6	90	9/91	- 61.6

[a] Reaction conditions: Catalyst = 9 mg (1 ·10^{-5} mol), [Al]/[Ti] = 800, [**O**] = 0.5 M (1.6 g), toluene, 30°C, 24 h. [b] Determined by SEC. [c] Determined by **NMR** (25 °C; $CDCl_3$), for further details see Appendix 7. [d] Determined by DSC.

According to the methods reported in Appendix 7 (Figures 3S1-3S4 and Equations 1-6), polymer compositions were determined by ^1H and $^{13}C\{^1H\}$ **NMR** spectroscopy in solution. Figure 28 shows $^{13}C\{^1H\}$ **NMR** spectra of the copolymers having different **O** content. The

evaluation of such spectra allows us to unequivocally assign the main signals of poly(ocimene-butadiene) copolymers (**POB**), whose complete assignments are reported in **Table 2**.

Spectroscopic data analysis allowed us to identify a multiblock microstructure that mainly consists of *trans*-1,4-**PB** and vinyl **O** segments. This last possesses an isotactic *trans*-1,2 tacticity, in analogy to homopolymers of **O** obtained using the same catalyst system.[59]

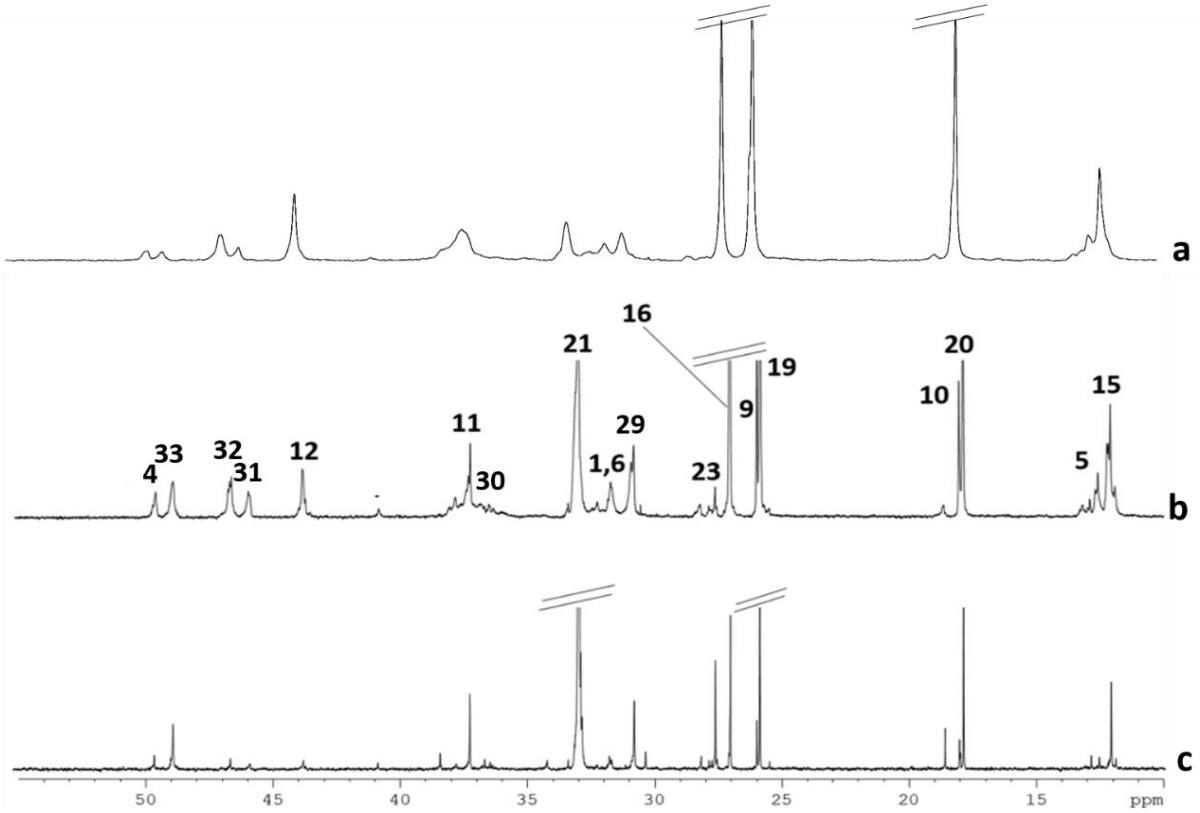

Figure 28. Aliphatic region of $^{13}C\{^{1}H\}$**NMR** spectrum of **POB** copolymers: (**a**) 15 % **B** (run 1, **Table 1**), (**b**) 40% **B** (run 2, **Table 1**), and (**c**) 80 % **B** (run 4, **Table 1**).

It was also possible to assign the signals reasonably associated with the junctions between blocks, through a deep study of 1D and 2D **NMR** techniques (lines 29-33 of Figure 28 and **Table 2**). An example of the reasoning made to identify the signals is the following: for the signal centred at 30.73 ppm (line 29 of **Table 2**, identified as a methylene through HSQC, Figure 3S15 of Appendix 7), analysis of the HMBC spectrum (Figure 3S16, Appendix 7) reveals correlations with protons at 5.40 and 1.33 ppm; these latter peaks were associated, by comparison with the literature data, with $\mathbf{B^{T}_{2}}$ and $\mathbf{O^{V}_{1}}$, thus identifying the signal as the $\mathbf{B^{T}_{4}}$ carbons linked with an ocimene vinylic unit ($\mathbf{B^{T}B^{T}_{4}O^{V}}$ and $\mathbf{O^{V}B^{T}_{4}O^{V}}$).

In addition, stereoerrors throughout the **O** segments were also detected ($\mathbf{O^{T}O^{V}_{2}O^{T}}$ at 46.51 ppm), similarly to previously reported **NMR** data for **PO** samples.[59]

Table 2. **NMR** assignments for **POB** synthesized with **2**/***m*-MAO** (runs 1-4, **Table 1**).

Unit [a]	Line	Atom	^{1}H [a] (ppm)	^{13}C [a] (ppm)
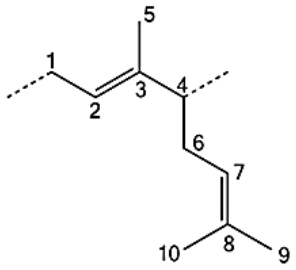	1	O^T_1	1.87-2.11	31.43-31.93
	2	O^T_2	5.05-5.12	123.74-125.02
	3	O^T_3	-	136.15-138.60
	4	$O^TO^T_4O^T$	1.92-2.02	49.48
	5	O^T_5	1.40-1.54	11.64-13.11
	6	O^T_6	1.87-2.11	31.43-31.93
	7	O^T_7	5.05-5.12	123.74-125.02
	8	O^T_8	-	130.05-131.95
	9	O^T_9	1.66	25.95
	10	O^T_{10}	1.57-1.59	18.02
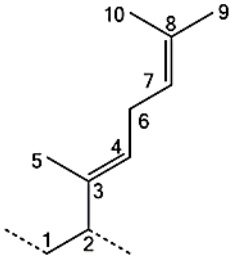	11	O^V_1	1.33	37.16
	12	O^V_2	1.94-1.98	43.66
	13	O^V_3	-	136.15-138.60
	14	O^V_4	5.05-5.12	123.74-125.02
	15	O^V_5	1.40-1.54	11.64-13.11
	16	O^V_6	2.67	26.98
	17	O^V_7	5.05-5.12	123.74-125.02
	18	O^V_8	-	129.00-131.60
	19	O^V_9	1.68	25.83
	20	O^V_{10}	1.62	17.88
C 	21	B^T_1	2.02	32.89
	22	B^T_2	5.40	130.18
	23	B^C_1	2.02	27.57
T 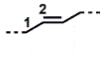	24	B^C_2	5.25-5.37	129.60
	25	B^V_1	4.88-4.99	114.36
	26	B^V_2	5.53-5.60	142.89
V 	27	B^V_3	1.86-1.98	-
	28	B^V_4	1.86-1.98	-
	29	$B^TB^T_4O^V$ / $O^VB^T_4O^V$	1.78-1.92	30.73
	30	$O^VB^T_1B^T$	2.02	36.57
	31	$B^TO^V_2O^V$	1.92-2.02	45.74
	32	$O^TO^V_2O^T$	1.92-2.02	46.51
	33	$O^VO^V_2B^T$	1.92-2.02	48.75

[a] $CDCl_3$, 25 °C, 600 MHz.

In the copolymerization of **M** with **B**, catalytic behavior of **2**/***m*-MAO** was also evaluated applying similar reaction conditions of **O-B** copolymerizations (different monomer ratios, 24 h, 30°C, and toluene as solvent). **Table 3** summarizes the results of the experiments performed.

Due to the sluggish reactivity of **M** compared to **B**, the incorporation of an appreciable amount of the terpene into the polymer chain (**M** content between 15 and 47 %) was possible only by using an excess of **M** with respect to **B**. In analogy with **POB** copolymers, yield and molecular weight increased by increasing the **B** in the alimentation feed.

Molecular weights distributions are monomodal and narrow $Đ$ (ranging from 1.4 to 2.0) confirmed that true copolymers were formed. The **DSC** curves of the copolymers showed T_g values in the range of application as elastomers.

Table 3. Copolymerization of *β*-myrcene (**M**) and butadiene (**B**).

Run[a]	M feed	B feed	Activity	M_w[b]	Đ[b]	Polymer Composition[c]					T_g[d]
						B	B structures %			M^T/M^V	
	(mol%)	*(mol%)*	*kg/(mol Ti)·h*	*(kDa)*		*(mol%)*	*1,2*	*1,4 cis*	*1,4 trans*	*(molar ratio)*	*(°C)*
5	90	10	0.1	26	1.5	53	3	7	90	71/29	- 65.5
6	80	20	0.5	32	1.4	70	2	8	90	69/31	- 68.8
7	70	30	0.9	45	1.5	77	3	8	89	68/32	- 71.1
8	50	50	3.2	76	2.0	85	4	8	88	67/33	- 69.7

[a] Reaction conditions: Catalyst = 9 mg (1 ·10^{-5} mol), [Al]/[Ti] = 800, [**M**] = 0.5 M (1.6 g), toluene, 30°C, 24 h. [b] Determined by SEC. [c] Determined by **NMR** (25 °C; $CDCl_3$), for further details see Appendix 7 . [d] Determined by DSC.

The microstructure of the synthesized poly(myrcene-butadiene) copolymers (**PMB**) was further examined by **NMR** characterization and the results of the complete assignments are summarized in **Table 4**. ^{1}H **NMR** spectra (See Appendix 7, Figures 3S5-3S8) clearly showed the presence of both monomers and the presence of the **M** units mainly enchained as *trans*-1,4 ($\mathbf{M^T}$) with a lower amount of 3,4 vinyl units ($\mathbf{M^V}$).

Moreover, the inspection of $^{13}C\{^1H\}$ **NMR** spectra (Figure 29) gave more detailed information on the distribution of the two repeating units along the polymeric chain, revealing a structure with prevalently isolated **M** units in the copolymers with higher **B** content ($\mathbf{B^TM^T_4B^T}$), and a multiblock microstructure for the polymers with a higher **M** content.

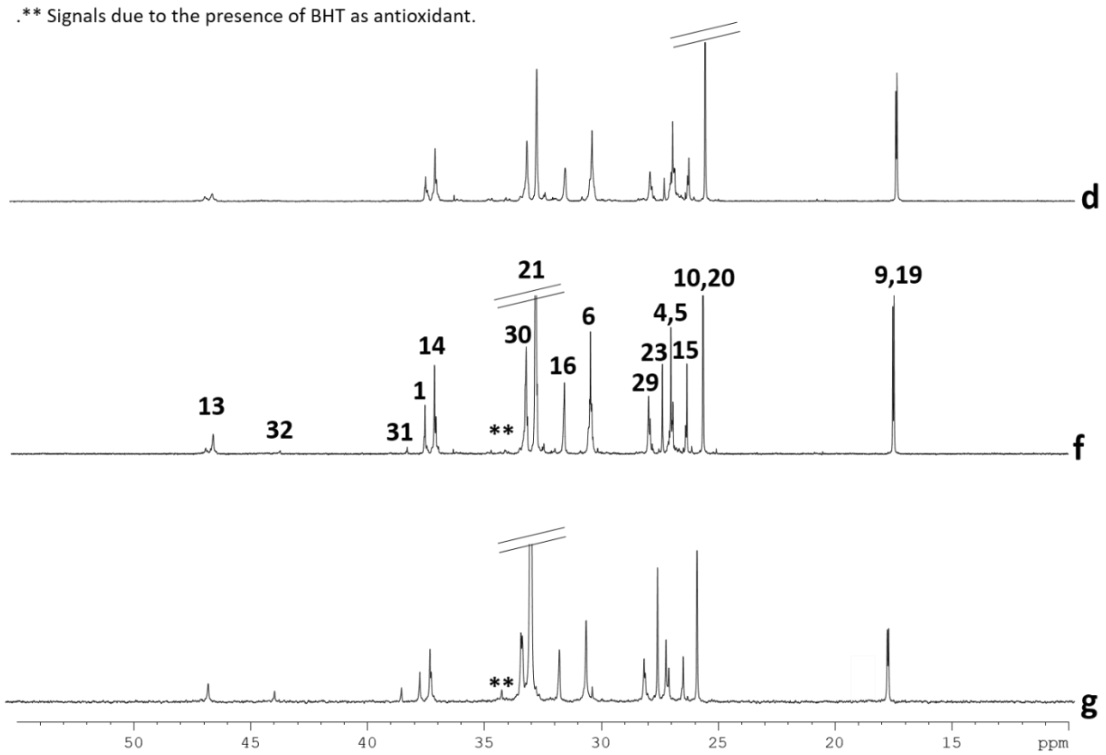

Figure 29. Aliphatic region of $^{13}C\{^1H\}$**NMR** spectrum of **PMB** copolymers: (**d**) 53 % **B** (run 5, **Table 3**), (**f**) 70 % **B** (run 6, **Table 3**) and (**g**) 85 % **B** (run 8, **Table 3**).

Also for **PMB**, several signals that arise from the junction between comonomers blocks have been reasonably assigned (lines 29-32, **Table 4**).

Table 4. NMR assignments for **PMB** synthesized with **2/*m*-MAO** (runs 5-8, **Table 3**).

Unit [a]	Line	Atom	^{1}H [a] (ppm)	^{13}C [a] (ppm)
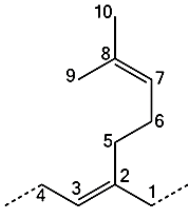	1	M^{T}_{1}	2.03	37.55
	2	M^{T}_{2}	-	139.04
	3	M^{T}_{3}	5.12	124.83
	4	M^{T}_{4}	2.03	27.08
	5	M^{T}_{5}	2.03	27.18
	6	M^{T}_{6}	2.03	30.55
	7	M^{T}_{7}	5.12	124.59-124.78
	8	M^{T}_{8}	-	131.58-131.64
	9	M^{T}_{9}	1.60	17.83
	10	M^{T}_{10}	1.66-1.69	25.88
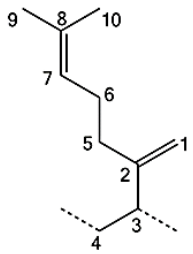	11	M^{V}_{1}	4.72, 4.79	109.38
	12	M^{V}_{2}	-	151.59
	13	M^{V}_{3}	2.03	46.46
	14	M^{V}_{4}	2.03	37.12
	15	M^{V}_{5}	2.03	26.47
	16	M^{V}_{6}	2.03	31.67
	17	M^{V}_{7}	5.12	124.59-124.78
	18	M^{V}_{8}	-	131.58-131.64
	19	M^{V}_{9}	1.60	17.88
	20	M^{V}_{10}	1.66-1.69	25.88
C 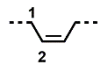	21	B^{T}_{1}	2.03	32.88
	22	B^{T}_{2}	5.41	130.18
	23	B^{C}_{1}	2.03	27.55
T 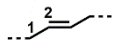	24	B^{C}_{2}	5.32-5.39	129.58
	25	B^{V}_{1}	4.91-4.98	114.39
	26	B^{V}_{2}	5.53-5.60	142.87
V 	27	B^{V}_{3}	1.86-1.98	-
	28	B^{V}_{4}	1.86-1.98	-
	29	$M^{T}M^{T}_{4}B^{T}$ $B^{T}M^{T}_{4}B^{T}$	2.03	28.06-28.12
	30	$M^{T}B^{T}_{1}B^{T}$	2.03	33.17-33.37
	31	$M^{V}B^{T}_{1}B^{T}$	2.03	38.31
	32	$M^{V}M^{V}_{3}B^{T}$	2.03	43.65

[a] $CDCl_3$, 25 °C, 600 MHz.

3.2.2 Homopolymerization of farnesene and its copolymerization with butadiene

The catalytic activity of the **2/*m*-MAO** system in the homopolymerization of **F** and its copolymerization with **B** was also investigated.

Homopolymerization attempt at 30°C was unsuccessful, reasonably due to the lower reactivity of **F**, compared to its predicted forenamed congeners **O** and **M**, towards our catalytic system.

Thus, a rise of the temperature to 50°C was necessary. Data relating to the experiments performed are shown in **Table 5**.

Table 5. Copolymerization of *β*-farnesene (**F**) and butadiene (**B**) results.

Run[a]	F feed	B feed	Activity	M_w[b]	$Đ$[b]	Polymer Composition[c]					T_g[d]
						B	B structures %			F^T/F^V	
	(mol %)	*(mol %)*	*kg/(mol Ti)·h*	*(kDa)*		*(mol %)*	*1,2*	*1,4 cis*	*1,4 trans*	*(molar ratio)*	*(°C)*
9	100	0	0.04	9	1.4	-	-	-	-	84/16	n.d.
10	90	10	0.07	20	1.1	48	-	9	91	79/21	- 58.0
11	80	20	0.2	41	1.3	66	4	7	88	83/17	- 65.9
12	70	30	0.4	56	2.0	77	4	8	87	86/14	- 67.0
13	50	50	2.0	90	1.4	81	5	7	87	77/23	- 68.6

[a] Reaction conditions: Catalyst **1** = 9 mg (1 ·10^{-5} mol), [Al]/[Ti] = 800, [**F**] = 0.5 M (2.4 g), toluene, 50°C, 24 h. [b] Determined by GPC. [c] Determined by **NMR** (25 °C; $CDCl_3$), for further details see supporting information. [d] Determined by DSC.

Poly(*β*-farnesene) (**PF**) was obtained with a molecular weight of 9 kDa and narrow $Đ$ of 1.4 with a prevalence of 1,4-insertions as revealed by the **NMR** data recorded, according to the literature.[106] In view of these results, the study was extended to the synthesis of poly(farnesene-butadiene) copolymers (**PFB**) (runs 10-13, **Table 5**).

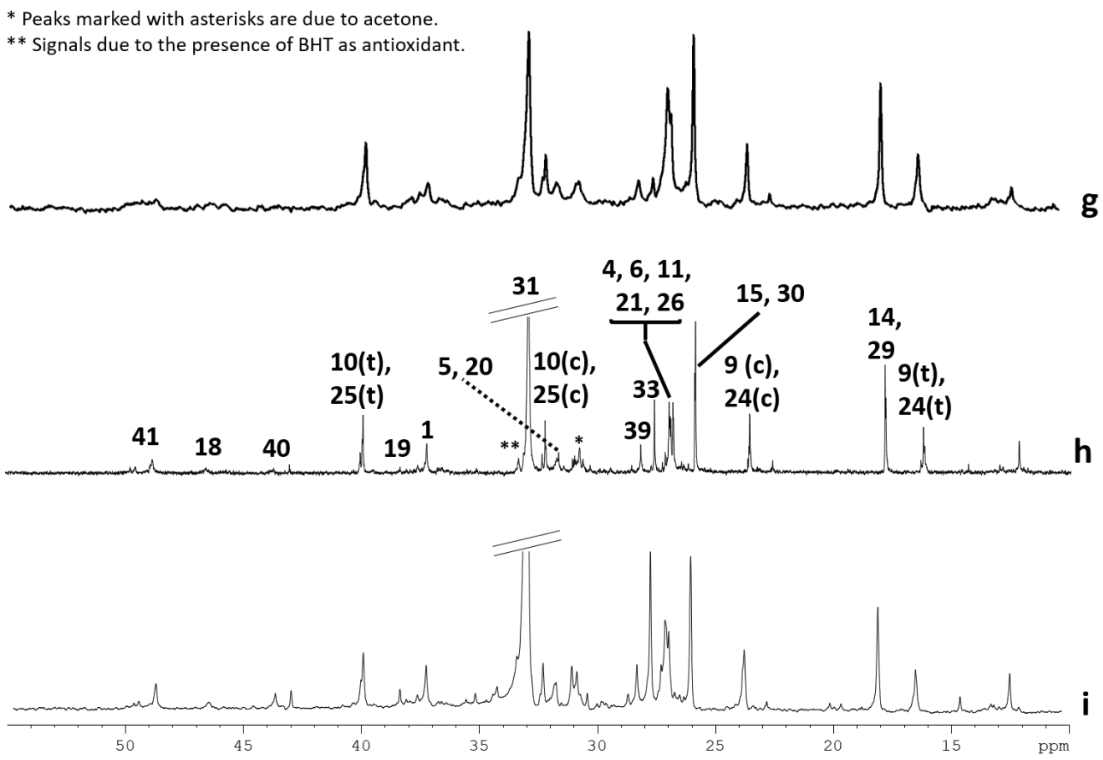

Figure 30. Aliphatic region of $^{13}C\{^1H\}$**NMR** spectrum of **PFB** copolymers: (**g**) 48 % **B** (run 10, **Table 5**), (**h**) 66 % **B** (run 11, **Table 5**) and (**i**) 81 % **B** (run 13, **Table 5**).

On the whole, copolymerization data were similar to those observed in the case of **PMB** (**M** incorporation in between 19 and 42%, considerable *trans*-1,4 stereoselectivity, molecular weight up to 90 kDa, $Đ$ = 1.1-2.0).

Table 6. NMR assignments for **PFB** synthesized with **2**/***m*-MAO** (runs 9-13, **Table 5**).

Unit [a]	Line	Atom	^{1}H [a] (ppm)	^{13}C [a] (ppm)
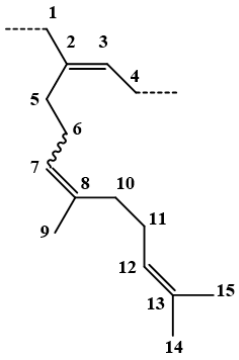	1	F^{T}_{1}	1.95-2.03	37.26
	2	F^{T}_{2}	-	138.72-139.59
	3	F^{T}_{3}	5.10	122.84-125.77
	4	F^{T}_{4}	1.97-2.16	26.63-27.40
	5	F^{T}_{5}	2.03	30.97
	6	$F^{T}_{6,}$	1.97-2.16	26.63-27.40
	7	$F^{T}_{7,}$	5.10	122.84-125.77
	8	$F^{T}_{8,}$	-	134.66-135.79
	9(t)	F^{T}_{9}	1.55-1.61	16.22
	9(c)	F^{T}_{9}	1.63-1.73	23.55
	10(t)	F^{T}_{10}	1.93-2.02	39.90
	10(c)	F^{T}_{10}	2.03	32.19
	11	F^{T}_{11}	1.97-2.16	26.63-27.40
	12	F^{T}_{12}	5.10	122.84-125.77
	13	F^{T}_{13}	-	131.13-131.89
	14	F^{T}_{14}	1.57-1.64	17.84
	15	F^{T}_{15}	1.69	25.84
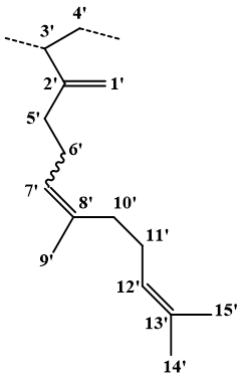	16	F^{V}_{1}	4.66-4.81	109.94
	17	F^{V}_{2}	-	154.46
	18	F^{V}_{3}	2.03	46.55
	19	F^{V}_{4}	1.99-2.03	38.37
	20	F^{V}_{5}	2.03	30.97
	21	F^{V}_{6}	1.97-2.16	26.63-27.40
	22	F^{V}_{7}	5.10	122.84-125.77
	23	F^{V}_{8}	-	134.66-135.79
	24(t)	F^{V}_{9}	1.55-1.61	16.22
	24(c)	F^{V}_{9}	1.63-1.73	23.55
	25(t)	F^{V}_{10}	1.93-2.03	39.90
	25(c)	F^{V}_{10}	2.03	32.19
	26	F^{V}_{11}	1.97-2.16	26.63-27.40
	27	F^{V}_{12}	5.10	122.84-125.77
	28	F^{V}_{13}	-	131.13-131.89
	29	F^{V}_{14}	1.57-1.64	17.84
	30	F^{V}_{15}	1.69	25.84
C 	31	B^{T}_{1}	2.03	32.89
	32	B^{T}_{2}	5.41	130.18
	33	B^{C}_{1}	2.03	27.58
T 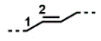	34	B^{C}_{2}	5.25-5.37	129.60
	35	B^{V}_{1}	4.88-4.99	114.36
	36	B^{V}_{2}	5.53-5.60	142.89
V 	37	B^{V}_{3}	1.86-1.98	-
	38	B^{V}_{4}	1.86-1.98	-
	39	$F^{T}F^{T}_{4}B^{T}$ $B^{T}F^{T}_{4}B^{T}$	2.03	28.19
	40	$F^{V}F^{V}_{4}B^{T}$	2.03	43.00-43.68
	41	$F^{V}F^{V}_{3}B^{T}$	1.91-1.99	48.77
	42	$F^{T}F^{T}_{4}B^{T}$	1.91-1.99	49.54

[a] $CDCl_3$, 25 °C, 600 MHz.

These outcomes, even if not surprising considering the structural similarity between **M** and **F** (see Fig. 27), are even so noteworthy. In fact, the outstanding industrial interest in the production of farnesene (due to its utilization as fuel, in agriculture and in cosmetics) pushed the development of advanced biotechnological processes (such as MegaBio).[107,108] This would encourage the intensification of the use of **F** as chemical building block which remains still unexploited.

Samples of **PFB** were characterized by 1D and 2D **NMR** spectroscopy and the main signals assignments are reported in Figure 30 and **Table 6**. A possible multiblock microstructure was detected with short homosequences of monomers, both mainly inserted as *trans*-1,4 units. It should be underlined that the long alkyl pendant groups of the **F** blocks, the methylene of the butadiene segments and the *cis*/*trans* isomerism of both make the ^{1}H **NMR** spectra, and thus correlations in COSY, HSQC and HMBC, particularly difficult to analyze (See Appendix 7, Figures 3S33-3S36).

3.2.3 Terpolymerization of ocimene with butadiene and styrene

With the aim of extending our study, a series of **O**/**B**/**S** terpolymerizations was also performed under mild conditions (different monomers ratios, 24 h, 50°C, and toluene as solvent), using [OSSO]-type titanium catalysts, **2** and **56** (Figure 26), activated by ***m*-MAO**. The introduction of **S** brings numerous advantages to elastomeric materials intended for tires in terms of breaking resistance, low rolling resistance in addition to wearing resistance.[109] The most relevant results are summarized in **Table 7**.

Table 7. Terpolymerization of *β*-ocimene (**O**) with butadiene (**B**) and styrene (**S**) results.

Run[a]	O feed	B feed	S feed	Activity	M_w[b]	$Đ$[b]	Polymer Composition[c]					T_g[d]
							B	B structures %		O^T/O^V (O %)	S	
		(mol %)		kg/(mol Ti)·h	(kDa)		(mol %)	1,4 cis	1,4 trans	(molar ratio)	(mol %)	(°C)
14	33.3	33.3	33.3	4.2	39.8	1.7	**41**	3	97	9/91 (**16**)	**44**	3.3
15	33.3	50.0	16.7	6.1	35.8	1.7	**60**	4	96	11/89 (**15**)	**25**	-29.8
16	32.9	45.2	21.9	6.2	38.3	1.5	**50**	7	93	9/91 (**17**)	**33**	-13.4
17	27.8	50.0	22.2	6.6	49.1	1.9	**55**	8	92	14/86 (**15**)	**30**	-20.7
18*	33.3	33.3	33.3	5.3	73.7	2.0	**43**	3	97	13/87 (**16**)	**43**	1.5
19*	27.8	50.0	22.2	7.9	67.2	2.1	**55**	8	92	18/82 (**13**)	**32**	-21.7
20*	20.0	54.0	26.0	8.1	70.7	2.2	**62**	7	93	9/91 (**6**)	**31**	-28.0

[a] Reaction conditions: Catalyst **2** = 9 mg (1 ·10^{-5} mol), Catalyst **56** (*) = 7 mg (1 ·10^{-5} mol), [Al]/[Ti] = 1200, [**O+B+S**] = 1.4 M, toluene (total solvent 25 ml), 50°C, 24 h. [b] Determined by GPC. [c] Determined by **NMR** (25 °C; $CDCl_3$ or TCDE), [d] Determined by DSC.

The biobased integral poly(**O**-*co*-**B**-*co*-**S**) terpolymers (**POBS**) were successfully synthesized in a wide range of compositions (the incorporation of the terpenes was up to 17 % mol) with M_w of 35.8-73.7 KDa, $Đ$ of 1.5–2.2 and T_gs between -28 and 3.3 °C. The process was *trans*-1,4 stereospecific for **B** (92-97%), while it provided mainly $\mathbf{O}^{\mathbf{V}}$ (82-91 %) in the case of **O.** Terpolymer compositions were determined by ^{1}H and ^{13}C NMR spectra (a typical example is provided in the Fig. 31): I) Ratio between **S** and **O+B** was calculated using ^{1}H NMR by integrating aromatic peaks of **S** (7.4-6.4 ppm) and methyne peaks of **B** and **O** (5.3-4.5) (**S** mol% = (Area$_{7.4\text{-}6.4}$/5)/[(Area$_{7.4\text{-}6.4}$/5)+((Area$_{5.6\text{-}4.5}$/8)*4)]*100; **B**+**O** mol% = 100 - **S** mol%; II) Ratio between **O** and **B** was determined by ^{13}C{^{1}H}NMR by integrating methylene signals at 32.9 ($\mathbf{B}^{\mathbf{T}}_1$ *trans*-1,4), 27.6 ($\mathbf{B}^{\mathbf{C}}_1$ *cis*-1,4), 31.7 ($\mathbf{O}^{\mathbf{T}}_1$ and $\mathbf{O}^{\mathbf{T}}_6$), and 27.0 ($\mathbf{O}^{\mathbf{V}}_6$) ppm.

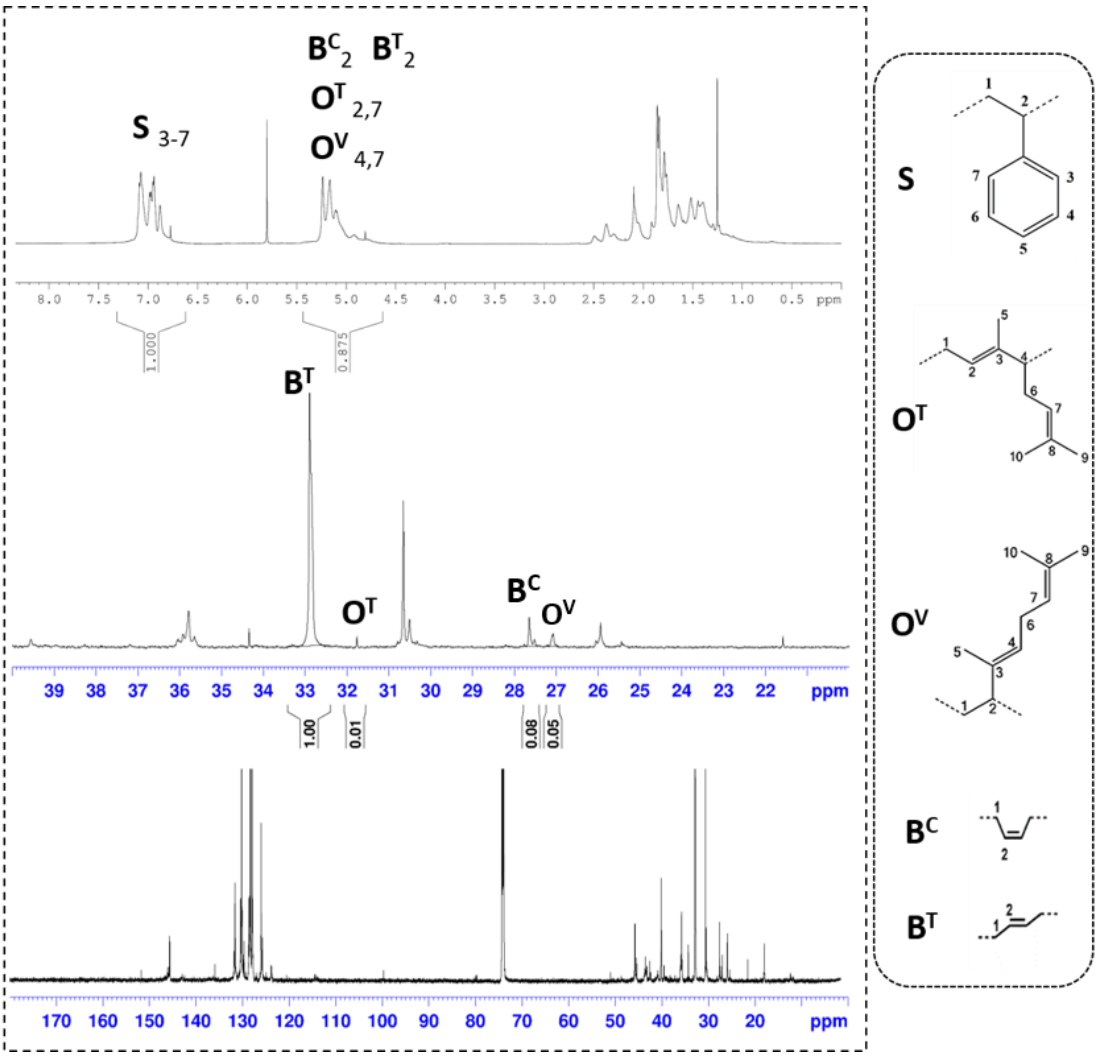

Figure 31. ^{1}H **NMR** spectrum (TCDE, 25 °C, 600 MHz) of **POBS** from run 20 of **Table 7** (top Figure); enlargement of aliphatic region of ^{13}C **NMR** spectrum of the previous sample (Figure in the middle); ^{13}C **NMR** spectrum (TCDE, 25 °C, 600 MHz) (lower Figure).

The composition of the alimentation feed was set in order to obtain a terpolymer with the lowest T_g containing about 5-20% mol of **O** in the polymer chain. Complex **57** was more active

than **2** and showed moderately productive for terpolymerizations (5.3–8.1 kg·mol^{-1}·h^{-1}). Its productivity increased with an increase in the [**B**]$_0$ +[**S**]$_0$ feed ratio. As shown in **Table 7**, the **POBS**s were fully characterized through **SEC**, **DSC**, and **NMR** analyses. As previously noted for copolymers, small **PS** sequences in the terpolymers were predominantly isotactic (identifying the diagnostic *ipso* carbon signal at δ 145.2 ppm in the carbon spectra).[110] Finally, from the **NMR** spectroscopic analyzes and the T_gs data, the microstructure of the terpolymers was reasonably random.

3.3 Materials and methods

General Procedures and Materials. Air- and moisture-sensitive compounds were manipulated under a nitrogen atmosphere using standard Schlenk techniques or an MBraun glovebox. All glassware was stored in an oven at 130 °C prior to use.

Commercial grade toluene (Sigma-Aldrich) was dried over calcium chloride, refluxed 48 h under a nitrogen atmosphere over sodium and distilled before use. Modified methylaluminoxane (***m*-MAO**; 7 wt% solution in heptane; AkzoNobel) was used as received. 1,3 butadiene, purchased from Società Ossigeno Napoli (S.O.N.), was dried by passing through a column filled with activated silica and molecular sieves (3-4 Å) and was slowly condensed in a Schlenk tube containing toluene at 0°C.

β-ocimene (≥ 90 %; mixture of *cis* and *trans* isomers), *β*-myrcene (≥ 95 %) and *β*-farnesene (mixture of isomers) were purchased from Sigma-Aldrich and were purified by overnight stirring over calcium hydride and distillation under reduced pressure. Dichloro{1,4-dithiabutanediyl-2,2'-bis[4,6-bis(2-phenyl-2propyl)phenoxy]}titanium complex was synthesized as reported in the literature.[111]

Instrumentation and Methods. ^{1}H and ^{13}C **NMR** spectra were recorded with Bruker spectrometers (300, 400 and 600 MHz) using 5 mm (o.d.) **NMR** tubes. 30 mg of samples were dissolved in $CDCl_3$ (0.5 mL) and were analyzed at room temperature. Chemical shifts were referenced to TMS and calculated by using the residual isotopic impurities of the deuterated solvent ($CDCl_3$: δ = 7.26 ppm in ^{1}H **NMR** and δ = 77.16 ppm in ^{13}C **NMR** experiments; TCDE: δ = 5.80 ppm in ^{1}H **NMR** and δ = 73.80 ppm in ^{13}C **NMR** experiments).

^{1}H **NMR** spectra were recorded using zg pulse program; pre-scan delay was 6.0 μs, and the relaxation delay between scans was 1 s; spectrum width was 12.0 ppm; 64 scans were accumulated.

^{13}C **NMR** spectra were recorded using zgpg30 pulse program; pre-scan delay was 6.0 μs, and relaxation delay between pulses was 2 s; spectrum width was set to 220.0 ppm; number of scans was 32000.

Exponential digital filter with the lb parameter of 2 Hz was applied prior to Fourier transformation. All the **NMR** spectra were integrated after baseline correction (a mean of minimum three integration values has been taken for each calculation).

Diffusion-ordered spectroscopy (**DOSY**) experiments were performed at room temperature on a Bruker Avance 600 spectrometer equipped with a 5 mm PABBO 600S3 BBF-H-D-OS-Z-SP probe. The standard Bruker pulse program, ledbpgp2s, employing a double stimulated echo sequence and LED, bipolar gradient pulses for diffusion, and two spoil gradients was utilized. The pulse gradients were increased from 5% up to 95% of the maximum gradient strength in a linear ramp with a total experiment time of 25 min. Diffusion times were 2500 ms, the eddy current delay was 5 ms, the gradient recovery delay was 0.2 ms, and the gradient pulse was 1000 ms. Individual rows of the quasi-2D diffusion databases were phased and baseline corrected. After Fourier transformation and baseline correction, the diffusion dimension was processed with the software Topspin3.2 and Diffusion from Bruker. Diffusion coefficients were calculated by Gaussian fits with the T1/T2 software of Topspin3.2.

The average molecular weights and molecular weights distributions of the samples were determined with a 150 C Waters GPC equipped with a RI detector, a JASCO 875-UV (254 nm) detector and a set of four columns from PSS (pore size of 106, 105, 104, and 103 Å, particle size of 5 μm). Tetrahydrofuran was used as carrier solvent with a flow rate of 1.0 mL/min at 25 °C. Calibration curve was established with commercial polystyrene standards. Thermal analysis (differential scanning calorimetry, DSC) was carried out on a **DSC** Q20 from TA Instruments, using a heating rate of 10 °C/min.

General copolymerization procedure (runs 1-13, **Tables 1, 3, 5**). In a round-bottomed flask, equipped with a magnetic stirrer, toluene, the linear terpene (*β*-ocimene, *β*-mircene or *β*-farnesene), ***m*-MAO** and a solution of butadiene (0,11 g/mL in toluene) were sequentially introduced. The mixture was stirred for few minutes at room temperature before adding complex **2** ($1{,}0 \cdot 10^{-5}$ mol) and warming to the desired temperature (30°C or 50°C). The polymerization was quenched by adding ethanol and then poured in acidified ethanol solution containing butylated hydroxytoluene (**BHT**). The polymer was recovered by filtration and then dried under vacuum at room temperature.

General terpolymerization procedure (runs 14-20, **Table 7**). In a round-bottomed flask, equipped with a magnetic stirrer, toluene, *β*-ocimene, styrene, ***m*-MAO** and a solution of butadiene (0,11 g/mL in toluene) were sequentially introduced. The mixture was stirred for few minutes at room temperature before adding complex **2** or **57** ($1{,}0 \cdot 10^{-5}$ mol) and warming to 50°C. The polymerization was quenched by adding ethanol and then poured in acidified ethanol solution containing butylated hydroxytoluene (BHT). The polymer was recovered by filtration and then dried under vacuum at room temperature.

3.4 Conclusion

In this chapter, the homopolymerization of **F** and, for the first time, the copolymerizations of **O**, **M**, and **F** with **B** catalysed by the [OSSO]-type titanium complex **2** activated by ***m*-MAO**, under mild reaction conditions, were achieved. The final polymers were characterized through **SEC**, **DSC**, and 1D and 2D **NMR** techniques. Thus, full assignment of the main signals and, in the case of copolymers, of the junctions between comonomer units were performed. In addition, the terpene content in the copolymers was found to be easily adjustable through judicious modifications of the alimentation feed. **POB** materials were obtained in a high degree of stereoselectivity (up to 95% of *trans*-1,4 for **B** and 92% of 1,2 insertions in the case of **O**), incorporating up to 85% mol of the terpene amount. T_gs of the samples were found to be strongly dependent on the **O** content. Likewise, **PMB** copolymers were obtained with a good stereoselectivity (up to 90% and 71% of *trans*-1,4 insertion for **B** and **M**, respectively) and the content of **M** incorporated was in the range of 15-47%. **F** showed a behavior similar to that of **M** and **PF** was achieved mainly as a 1,4-*trans* polymer, in the reaction of copolymerization with **B**. This first explorative study encouraged also the investigation of **O**, **B**, and **S** terpolymers, leading to obtaining polymers in a wide range of compositions with elastomeric properties (T_gs between -28 and 3.3 °C) containing 5-20% mol of **O**. Two catalytic systems, **2** and **56** (the latter was the most active) activated by ***m*-MAO** and under mild experimental conditions (different monomers ratios, 24 h, 50°C, toluene), in this type of synthesis were tested. The catalysts were found to be moderately productive for stereospecific terpolymerizations, providing *trans*-1,4 units for **B** (92-97%), mainly $\mathbf{O^V}$ (82-91 %) in the case of **O**, and predominantly isotactic **PS** sequences.

« Wenn du es nicht einfach erklaeren kannst,
hast du es nicht gut genug verstanden»
Albert Eistein (1879 – 1955)

Chapter 4

Stereoselective (*co*)-polymerization of acyclic terpenes catalyzed by a cobalt complex with phospane ligands

4.1 Introduction

In order to enlarge the number of stereoregular polymers obtained from linear terpenes, our attention has turned to catalytic systems based on transition metals capable of providing stereocontrol different from titanium-based systems previously tested. In particular, cobalt-based catalysts have shown a unique behavior in the polymerization of 1,3-dienes giving, on the base of the ligand framework, highly stereoregular *cis*-1,4- or 1,2- polybutadienes (see paragraph 2.3.4).[70,112,113]

In this context, an interesting class of cobalt catalysts for the polymerization of dienes is those of the bis(phosphane) complexes of general formula $CoCl_2(PRPh_2)_2$ (R = methyl, normal-propyl, ethyl, allyl, *iso*-propyl, cyclohexyl), activated by ***m*-MAO**.[113,114] The peculiarity of this family of complexes consists in the fact that they allow obtaining **PB** with a controlled microstructure (*cis*-1,4; 1,2; mixed *cis*-1,4/1,2 structure) simply by varying the nature of the phosphane framework coordinated to the cobalt atom. **PB** with a high *cis* content was obtained in the case of bulky aliphatic phosphines (e.g., P^tBu_3 and P^iPr_3), while **PB** with a *cis*-1,4/1,2 mixed structure was reached with aliphatic phosphines with a smaller steric hindrance (e.g., PEt_3 and P^nPr_3). On the contrary, the use of catalysts based on complexes with aromatic phosphines led to the insertion of essentially 1,2- units of **B** (**B^V**), showing an increase of the syndiotactic degree with increasing the phosphine steric hindrance.[113,114] Especially, by means $CoCl_2(PCyPh_2)_2$, (**57**, Figure 32, Cy = cyclohexyl), Ricci and co-workers observed a higher **B** polymerization rate (75% yield in 5 min), reaching stereoregular polymers (up to 88% mol of **B^V** and a syndiotactic index up to 78 %) in hydrocarbon solvents such as heptane at 20 °C.

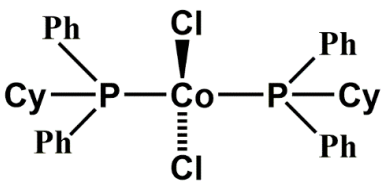

Figure 32. Complex $CoCl_2(PCyPh_2)_2$ (**57**)

These results prompted us to investigate for the first time the behavior of this catalytic system towards the stereoselective polymerization of **O**, **M**, and **F** and their copolymerization with **B**.

4.2 Results and discussion

4.2.1 Homopolymerization of ocimene, myrcene, and farnesene

The performance of the catalysts **57**, activated by ***m*-MAO**, was explored under mild experimental conditions (24 h, 25 °C, and hexane) in the polymerization of acyclic terpenes: **Table 8** summarizes the main results.

Homopolymerizations were carried on at room temperature in hexane because aromatic solvents were avoided for two main reasons: firstly, they can coordinate to the cobalt atom influencing the catalyst geometry and competing with the incoming monomer;[115] moreover, they tend to be more toxic and dangerous compared to aliphatic solvents and thus not convenient in industrial processes.[116]

In the case of **PO** (**Table 8**, run 21), the catalyst **57** produced a polymer with a molecular weight of 10.8 KDa, narrow polydispersity ($Đ$ = 1.4) and T_g of -31.3 °C. ^{1}H and ^{13}C {^{1}H} **NMR** spectra and methods used for determining polymer composition are reported in Appendix 7 (See Figs. 4S1, 4S4-5, and Equations 15-16). A deeper understanding of the microstructure arose from the solution **NMR** characterization. A prevalence of 1,2-insertions (72 % mol) was revealed and the polymer tacticity was determined by analyzing the ^{1}H **NMR** spectrum on the basis of the similar microstructure of 1,2-poly(3-methyl-1,3-pentadiene):[117] the two peaks at 0.90-1.35 ppm, attributed to the methylene protons of O^V_1, (See Fig. 4S1, Appendix 7) evidenced mainly 1,2 syndiotactic structure.

The system **57/*m*-MAO** was also active in the polymerization of **M** (**Table 8**, run 22). Analogously in the case of **PO**, polymer composition was determined by ^{1}H **NMR** spectroscopy (see Equations 17-18 in Appendix 7). The^{1}H **NMR** (Fig. 4S2) clearly showed the presence of the **M** units mainly (84 %) enchained as *cis*-1,4 units (**M^C**) and a lower amount (16 %) of 3,4 vinyl units (**M^V**). Reasonably, the different structure of **M** and **O** (see Fig. 27) exalts the steric effects governing the regiochemistry of monomer insertion, explaining a lower amount of vinyl units along the polymer backbone of **PM** compared to **PO**.[33]

An accurate inspection of the ^{13}C {^{1}H} **NMR** spectra demonstrated also the presence of signals related to head-to-head and tail-to-tail units along the polymer backbone (see Figure 4S6-7, Appendix 7).[118] The molecular weight characteristics of the synthesized elastomer was studied

by SEC, showing that the resulting **PM** had an M_w of 13.8 KDa, monomodal and narrow $Đ$ (1.8). **DSC** analysis displayed a T_g of -62.5 °C, the typical value of elastomeric materials.

A similar approach was used to explore the homopolymerization of **F**. In the last case, the system **57**/***m*-MAO** showed a very low catalytic activity (**Table 8**, run 23).

Table 8. Polymerization of *β*-ocimene (**O**), *β*-myrcene (**M**), and *β*-farnesene (**F**) results

Run[a]	Monomer	Activity[b]	M_w[c]	$Đ$[c]	Polymer Composition[d]	*Tg*[e]
		kg/(mol h)	*(kDa)*		*(%, molar ratio)*	*(°C)*
21	**O**	1.0	10.8	1.4	$\mathbf{O}^{V}$ 72 / $\mathbf{O}^{C}$ 28	-31.3
22	**M**	0.3	13.8	1.8	$\mathbf{M}^{V}$ 16 / $\mathbf{M}^{C}$ 84	-62.5
23	**F**	0.1	8.5	1.5	$\mathbf{F}^{3,4}$ 33 / $\mathbf{F}^{1,4}$ 67	-72.5

[a] Reaction conditions: **57** = 7 mg (1.05 ·10^{-5} mol), [Al]/[**57**] = 300, Hexane (16 mL), **O** = **M** = **F** = 0.009 mol, 24h, 25 °C. [b] Activity = kg/(mol **57**·h) [c] Determined by SEC. [d] Determined by ^{13}C {^{1}H}**NMR** and ^{1}H **NMR** analysis of the polymer (25 °C; $CDCl_3$).[e] Determined by DSC.

PF obtained had a molecular weight of 8.5 kDa, unimodal and narrow $Đ$ (1.5). The microstructure of **PF** is predominantly constituted by 1,4 addition units (67% mol), as evidenced by the presence in the ^{1}H **NMR** spectrum of a broad peak at 5.10 ppm, related to olefinic protons (H3,H7,H12 of ═CH– units, see Figure 4S3, Appendix 7). It was not possible to assign insertion regiochemistry (*cis* or *trans*). The ^{13}C {^{1}H} **NMR** spectrum (Figure 4S8, Appendix 7) also showed characteristic signals corresponding mainly to 1,4-units and, to a lesser extent, to 3,4-regioinsertions (33 %). The catalytic system **57**/***m*-MAO** has been shown to be able to polymerize **O**, **M**, and **F**, but with lower activity with respect to the **B** polymerization, as reported in the literature.

4.2.2 Copolymerization of butadiene with ocimene

As shown in the previous chapter, copolymerizations of **O**, **M**, and **F** with **B** were for the first time investigated by our research group,[119] by using Ti-based complexes bearing an [OSSO]-bisphenolate ligands. [118] In order to enlarge the study on butadiene-terpene copolymerization, the efficiency of **57**/***m*-MAO** in these transformations was also evaluated (**Tables 9-10**).

Table 9. Copolymerization of *β*-ocimene (**O**) and butadiene (**B**) results

Run[a]	O feed	B feed	Activity[b]	M_w[c]	$Đ$[c]	Polymer Composition[d]				
						B	B structures *(%)*		$\mathbf{O}^{V}/\mathbf{O}^{C}$	*Tg*[e]
	(mol %)	*(mol %)*	*kg/(mol h)*	*(kDa)*		*(mol %)*	*1,2*	*1,4-cis*	*(%, molar ratio)*	*(°C)*
24	90	10	0.9	32	2.4	33	85	15	77/23	-23.4
25	70	30	1.4	73	1.9	54	81	19	80/20	-9.6
26	50	50	2.7	139	1.8	68	85	15	82/18	-5.7

[a] Reaction conditions: **57** = 7 mg (1 ·10^{-5} mol), [Al]/[**57**] = 300, Hexane (16 mL), **O**+**B** = 0.0120 mol , 24 h, 25 °C. [b] Activity = kg/(mol **57**·h) [c] Determined by SEC. [d] Determined by ^{13}C {^{1}H}**NMR** and ^{1}H **NMR** analysis of the polymer (25 °C; $CDCl_3$). [e] Determined by DSC.

The data relating to M_w, $Đ$, polymer composition (see Equations 15, 19, and 23, Appendix 7) and T_g for poly(ocimene-butadiene) copolymers (**POB**) have been collected in **Table 9**.

By using a [**O**]/[**B**] ratio of 9 in the alimentation feed, **POB** with an M_w of 32 KDa and a relatively narrow $Đ$ was gained (**Table 9**, run 24). Both M_w and activity (up to 139 kDa and 2.7 kg/(mol$_{Co}$ h), respectively) increased gradually by increasing the percentage of **B** in monomer feed (runs 25-26). Notably, a shift of the T_g values towards higher temperatures was also noticed, reasonably as a result of the reduction of the flexibility of the chain due to the introduction of comonomer **B**, mainly as 1,2 units.

The microstructure of copolymers was investigated by ^{1}H, ^{13}C {^{1}H} and 2D **NMR** experiments. A blocky microstructure and a clear tendency of both comonomers to preferably insert as 1,2-vinylic unit emerged (See 4S12, 4S14, 4S16-18, Appendix 7). The **NMR**-DOSY confirmed the existence of copolymer, excluding the presence of homopolymer contaminants (Fig. 4S40, Appendix 7). Fig. 33 reveals ^{13}C {^{1}H} **NMR** spectra of the **POB** samples with different **B** content (up to 68 %mol) and **Table 10** summarizes the complete assignation of the main signals for these copolymers.

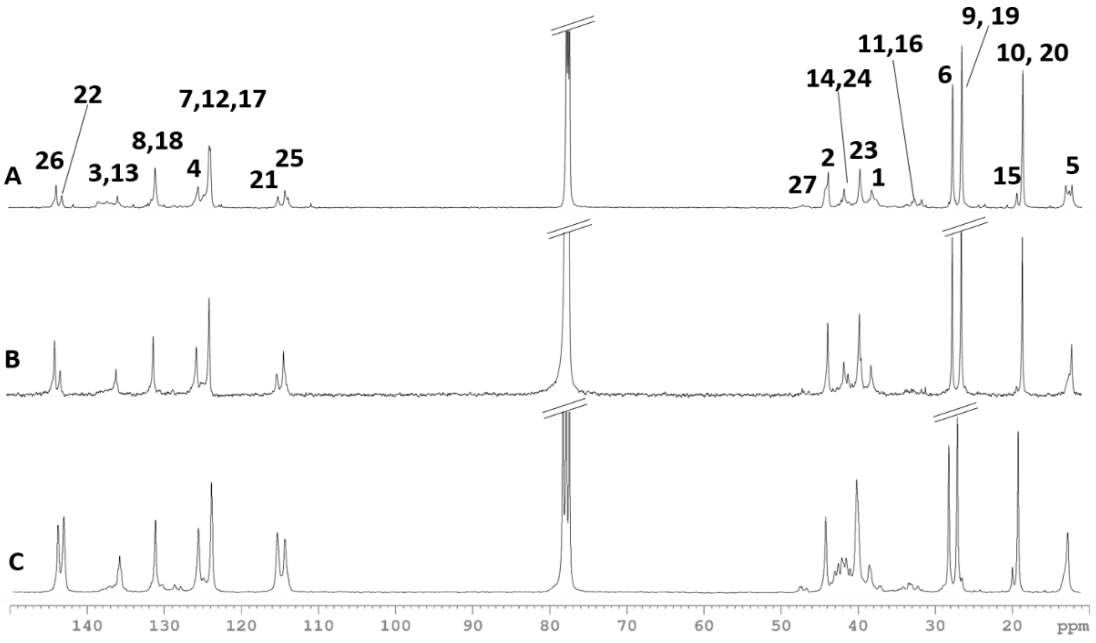

Figure 33. ^{13}C{^{1}H}**NMR** spectrum of **POB** copolymers: (A) 33 % of **B** (run 24, **Table 9**), (B) 54 % of **B** (run 25, **Table 9**) and (C) 68 % of **B** (run 26, **Table 9**).

Beyond the peaks attributable to homosequences, some signals reasonably related to junctions between blocks were also detected. For example, in the region between 110 to 150 ppm of the ^{13}C {^{1}H} **NMR** spectra it was observed that, as the content of **B** increases, the signals at 114.99 ppm (line 21, Fig. 33) and 143.13 ppm (line 22, Fig. 33) relative to $\mathbf{B^V_1}$ and $\mathbf{B^V_2}$ increase with

respect to the signals at 114.10 ppm (line 25) and 143.88 ppm (line 26). These last peaks can be assigned to butadiene vinyl carbons in $O^VB^V_1O^V$, $O^VB^V_1B^V$ or $B^VB^V_1O^V$ and $O^VB^V_2O^V$, $O^VB^V_2B^V$ or $B^VB^V_2O^V$ units. In addition, stereoerrors in the **O** and **B** segments (in particular $O^CO^V_2O^C$ and $B^CO^V_2B^C$ units between 45.40 to 46.65 ppm) were also detected, in analogy with **PO** samples reported in previous works.[118]

Table 10. NMR assignments for **POB** synthesized with **57**/***m*-MAO** (runs 25, **Table 9**).

Unit [a]	Line	Atom	^{1}H [a] (ppm)	^{13}C [a] (ppm)
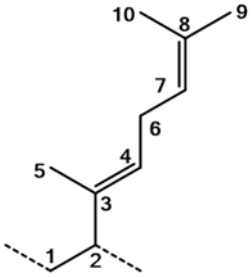	1	O^V_1	0.90-1.35	37.54
	2	O^V_2	2.07	43.23
	3	O^V_3	-	135.89
	4	O^V_4	5.08, 5.00	125.44
	5	O^V_5	1.35-1.48	11.30-12.30
	6	O^V_6	2.65	26.97
	7	O^V_7	5.08, 5.00	123.77
	8	O^V_8	-	131.08
	9	O^V_9	1.68	25.82
	10	O^V_{10}	1.61	17.84
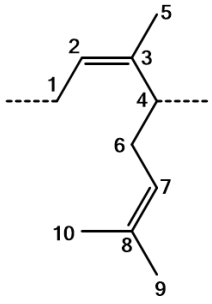	11	O^C_1	1.86-2.17	30.85-33.55
	12	O^C_2	5.08, 5.00	123.50-124.20
	13	O^C_3	-	135.60-136.40
	14	O^C_4	2.49	41.20
	15	O^C_5	1.53	18.60
	16	O^C_6	1.86-2.17	30.85-33.55
	17	O^C_7	5.08, 5.00	123.50-124.20
	18	O^C_8	-	130.80-131.60
	19	O^C_9	1.68	25.95
	20	O^C_{10}	1.61	17.98
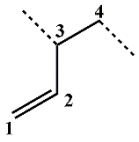	21	B^V_1	4.84-4.99	114.99
	22	B^V_2	5.32-5.39	143.13
	23	B^V_3	1.74-1.86	38.92
	24	B^V_4	1.02-1.28	39.70-42.60
	25	$O^VB^V_1O^V$	4.75-4.91	114.10
	"	$O^VB^V_1B^V$	"	"
	"	$B^VB^V_1O^V$	"	"
	26	$O^VB^V_2O^V$	5.38-5.43	143.88
	"	$O^VB^V_2B^V$	"	"
	"	$B^VB^V_2O^V$	"	"
	27	$O^CO^V_2O^C$	1.98-2.04	45.40-46.65
	"	$B^CO^V_2B^C$	"	"

[a] $CDCl_3$, 25 °C, 600 MHz.

4.2.3 Copolymerization of butadiene with myrcene

Experimental data related to copolymerizations of **M** and **B** promoted by the same catalytic system **57/*m*-MAO** are shown in **Table 11** (runs 27-29). This reaction was carried on in experimental conditions analogues to those of the **O** and **B** copolymerization (24 h, 25 °C, and hexane).

Table 11. Copolymerization of *β*-myrcene (**M**) and butadiene (**B**) results

Run[a]	M feed (mol%)	B feed (mol%)	Activity[b]	M_w[c] (kDa)	Đ[c]	Polymer Composition[d]				
						B (mol%)	B structures % 1,2	B structures % 1,4 cis	M^V/M^C (molar ratio)	T_g[e] (°C)
27	90	10	0.04	10	1.7	25	78	22	28/72	-55.1
28	70	30	0.1	14	2.1	39	75	25	47/53	-49.8
29	50	50	0.4	41	2.7	66	74	26	51/49	-37.1

[a] Reaction conditions: **57** = 7 mg (1 ·10^{-5} mol), [Al]/[**57**] = 300, Hexane (16 mL), **M**+**B** = 0.0120 mol , 24 h, 25 °C. [b] Activity = kg/(mol **57**·h) [c] Determined by SEC. [d] Determined by ^{13}C {^{1}H} **NMR** and ^{1}H **NMR** analysis of the polymer (25 °C; $CDCl_3$). [e] Determined by DSC.

However, the catalytic behavior was found to be dramatically influenced by the terpene nature. Indeed, the use of **M** as a comonomer resulted in an overall poorer catalytic activity (up to 0.4 kg mol_{57}^{-1}·h^{-1}). Moreover, lower M_w samples were obtained, even at relatively high content of butadiene. ^{13}C {^{1}H} **NMR** spectra of the **PMB** samples with increasing **B** content (up to 66 mol %) are reported in Fig. 34.

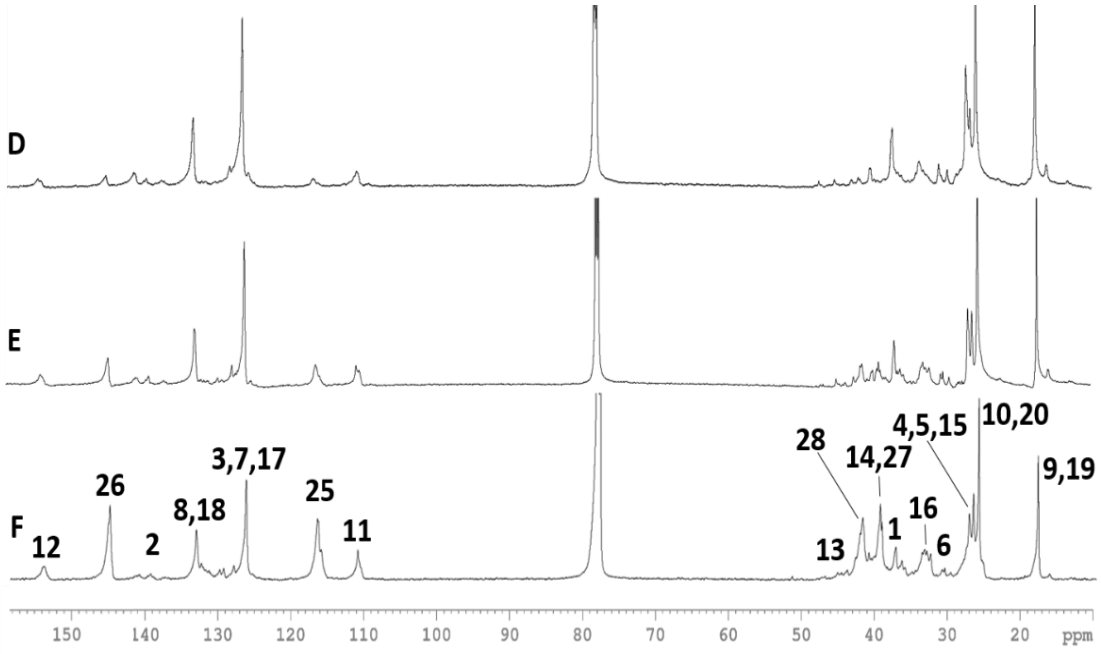

Figure 34. ^{13}C{^{1}H}**NMR** spectrum of **PMB** copolymers: (D) 25 % of **B** (run 27, **Table 9**), (E) 39 % of **B** (run 28, **Table 9**) and (F) 66 % of **B** (run 29, **Table 9**).

Interestingly, from the **NMR** analysis of **PMB** samples, a peculiar trend emerged. Indeed, differently from the case of **POB**, the molar percentage of terpene vinyl unit is not constant with the copolymer composition but sensitively increases by increasing the B content from 25 mol%

to 39 mol%. As a result of this tendency, in the **PMB** sample with the higher content of terpene, a clear prevalence of *cis* 1,4-unit was obtained.

Full 1D and 2D **NMR** characterization led to assignation of main peaks (**Table 12**) in accordance with the studies in the literature.

Table 12. NMR assignments for **PMB** synthesized with **57**/***m*-MAO** (runs 29, **Table 11**).

Unit [a]	Line	Atom	^{1}H [a] (ppm)	^{13}C [a] (ppm)
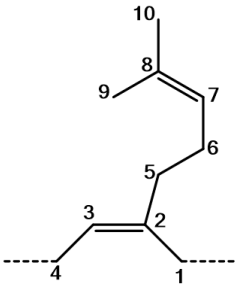	1	M^{C}_{1}	2.04	37.08
	2	M^{C}_{2}	-	139.38
	3	M^{C}_{3}	5.09-5.13	124.74
	4	M^{C}_{4}	1.99-2.30	26.98
	5	M^{C}_{5}	1.99-2.30	27.15
	6	M^{C}_{6}	2.04	30.81
	7	M^{C}_{7}	5.09-5.13	124.74
	8	M^{C}_{8}	-	131.48
	9	M^{C}_{9}	1.61	17.84
	10	M^{C}_{10}	1.69	25.83
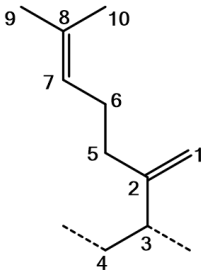	11	M^{V}_{1}	4.67-4.85	109.85
	12	M^{V}_{2}	-	152.14
	13	M^{V}_{3}	2.04	46.99
	14	M^{V}_{4}	2.00-2.31	39.90-40.45
	15	M^{V}_{5}	2.12	26.60
	16	M^{V}_{6}	1.83-2.15	31.80-34.18
	17	M^{V}_{7}	5.09-5.13	124.74
	18	M^{V}_{8}	-	131.48
	19	M^{V}_{9}	1.61	17.84
	20	M^{V}_{10}	1.69	25.83
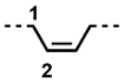	21	B^{C}_{1}	2.07	27.57
	22	$B^{V}_{4}B^{C}_{1}B^{V}$	-	25.23
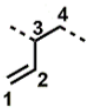	23	$B^{V}_{4}B^{C}_{2}B^{V}$	-	130.72
	24	$B^{V}B^{C}_{2}B^{V}_{3}$	-	127.82
	25	B^{V}_{1}	4.80-5.05	114.99
	26	B^{V}_{2}	5.30-5.48	143.12
	27	B^{V}_{3}	2.01-2.30	38.54-39.91
	28	B^{V}_{4}	1.12-1.43	41.00-43.17

[a] $CDCl_3$, 25 °C, 600 MHz.

Although the choice of Co-based catalyst **57** has led to stereopolymers different from those obtained by Ti complexes, low catalytic activity (especially in the case of **M**) limits its possible use on a larger scale. Furthermore, **57** was found to be inactive in the **S** polymerization and therefore it was not possible to obtain terpolymers. In Fig. 35 the differences in terms of stereoselectivity of the **POB** and **PMB** copolymers produced by using Ti- and Co-based complexes of this work are highlighted.

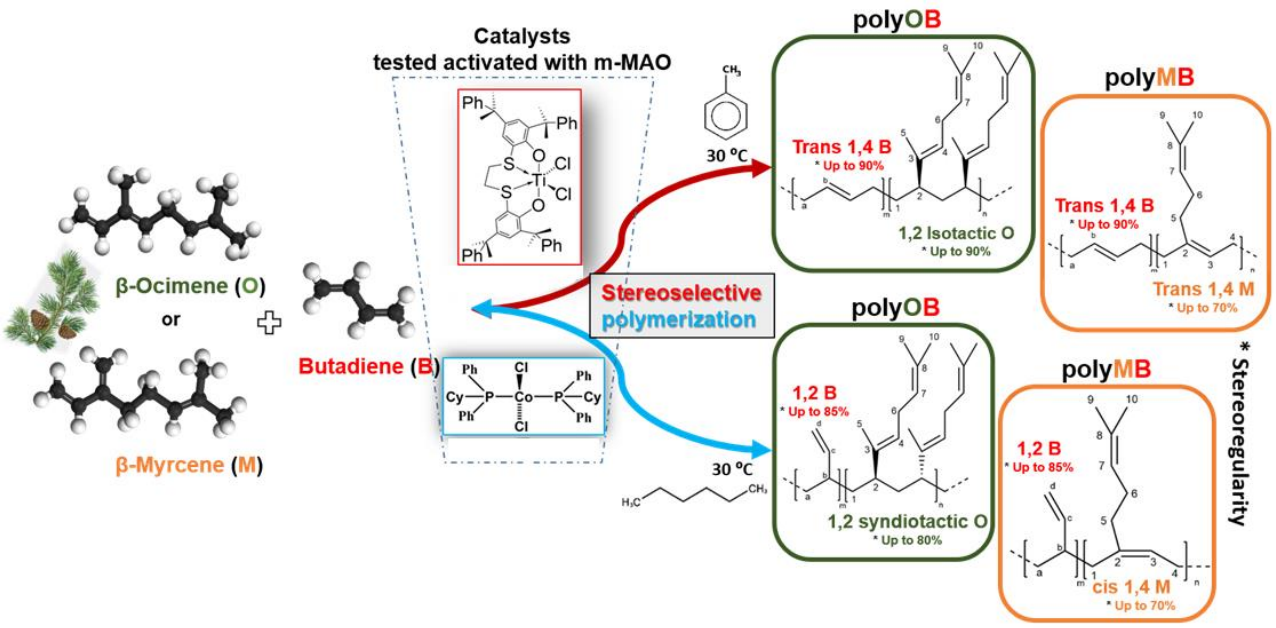

Figure 35. Stereoregularity of the **POB** and **PMB** copolymers obtained using the catalytic complexes **2** and **57** (Fig.s 26 and 32)

4.3 Materials and methods

General Procedures and Materials. All operations involving air- and moisture-sensitive compounds were carried on under a dry nitrogen atmosphere using an MBraun glovebox and Schlenk techniques. All glassware was stored overnight in an oven at 130 °C before use.

Hexane (Sigma-Aldrich) was dried over sodium/benzophenone and distilled prior to use. Modified methylaluminoxane (***m*-MAO**; 7 % wt solution in heptane; AkzoNobel) was used as received. 1,3 butadiene, purchased from Linde, was dried by passing through a column filled with silica and activated molecular sieves (3-4 Å) and was slowly condensed in a Schlenk tube containing hexane at 0 °C.

β-ocimene (≥ 90 %; mixture of cis and trans isomers), *β*-myrcene (≥ 95 %) and *β*-farnesene (mixture of isomers) were purchased from Sigma-Aldrich and were dried over calcium hydride and distilled under reduced pressure before use. $CoCl_2(PCyPh_2)_2$ was prepared as reported in the literature.[114]

Instrumentation and Methods. ^1H and $^{13}C\{^1H\}$, HSQC, COSY and HMBC spectra were recorded in $CDCl_3$ (0.7 mL) at 25 °C on a Bruker spectrometer (300, 400 and 600 MHz) calibrated relatively to the solvent peak in reference to tetramethylsilane (TMS).

Molecular weights distributions (M_w/M_n) and the polymers' number average molecular weights (M_n) were measured at 25 °C with a 150 C Waters GPC equipped with a RI detector, a JASCO 875-

UV (254 nm) detector and a set of four columns from PSS (pore size of 106, 105, 104, and 103 Å, particle size of 5 μm). Tetrahydrofuran was used as eluent at a flow rate of 1.0 mL/min. Calibration curve was established with commercial polystyrene standards.

Thermal analysis (differential scanning calorimetry, **DSC**) was carried out on a DSC Q20 from TA Instruments, with a heating and cooling rate of 10 °C min in the range −100 to 200 °C. Glass transition temperatures was reported for the second heating cycle.

General copolymerization procedure (runs 21-23, **Table 8**). In a round-bottomed flask, equipped with a magnetic stirrer, hexane, the linear terpene (**O**, **M** or **F**) and ***m*-MAO** were sequentially introduced. The mixture was stirred for few minutes at room temperature before adding complex **1** ($1{,}0*10^{-5}$ mol). The polymerization was quenched by adding ethanol and then poured in acidified ethanol solution containing butylated hydroxytoluene (**BHT**). The polymer was recovered by filtration and then dried overnight under in a vacuum oven at room temperature.

General copolymerization procedure (runs 24-29, **Tables 9**, **10**). In a round-bottomed flask equipped with a magnetic stirrer hexane, the linear terpene (**O**, **M** or **F**), ***m*-MAO** and a solution of butadiene (0,11 g/mL in hexane) were sequentially introduced. The mixture was stirred for few minutes at room temperature before adding complex **1** ($1{,}0 \times 10^{-5}$ mol). The copolymerization was quenched by adding ethanol and then poured in acidified ethanol solution containing butylated hydroxytoluene (**BHT**). The polymer was recovered by filtration and then dried overnight under in a vacuum oven at room temperature.

4.4 Conclusion

In this chapter, stereoselective polymerization **O**, **M** and **F** promoted by Co(II) complex **57** with phosphane ligands, activated by ***m*-MAO** at room temperature, were described. Homopolymerizzazions of **O**, **M** and **F** led to obtaining rubbers with a prevalent 1,2-vinylic microstructure in the case of **PO** (72%) and predominantly 1,4-units in the case of **PM** and **PF** (*cis*-1,4 = 84 % for **PM**, 1,4-addition = 67 % for **PF**). These polymerizations were carried on in hexane with a [terpene]/[Co] ratio of 850 in very mild conditions (24 h, 25° C). The system **57**/***m*-MAO** ([Al]/[**56**] = 300) showed a low catalytic activity for **F** (0,1 kg mol_{Co}^{-1} h^{-1}) and better activities for the other two terpenes (up to 1 kg mol_{Co}^{-1} h^{-1}).

The cobalt-based catalyst **57** was also able to promote binary copolymerization of **O** and **M** with **B**, providing copolymers (**POB** and **PMB**) in a wide range of compositions. For these samples, the catalytic activity increased by increasing **B** in the feed (up to 2.7 kg mol^{-1} h^{-1} for **POB**). Copolymers **POB** (M_n up to 77 kDa, $Đ$ = 1.8-2.4, 1,2-vinylic units = 77-82 %) and **PMB** (M_n up to 15 kDa, $Đ$ = 1.7-2.7, *cis*-1,4 units = 49-72 %) with blocky microstructure and elastomeric thermal properties (T_g from -5.7 °C to -72.5 °C) were obtained, having up to 67 % and 75% mol of **O** and **M**, respectively. Furthermore, the samples were fully characterized by **DSC**, **SEC** and **NMR**. In the latter case, an in-depth study of 1D and 2D **NMR** data allowed a reasonable assignation of main signals and the junctions between comonomers blocks.

«Somewhere, something incredible is waiting to be known»

Carl Sagan (1934-1996)

Chapter 5

Myrcene-Based elastomers via anionic polymerization

5.1 Introduction

During my PhD study, I spent seven months (from April to October 2019) at the Technische Universität München (TUM) in Germany. There, I also worked on another important polymerization technique: anionic polymerization.

The concept of anionic polymerization was first developed by Ziegler and Schlenk in early 1910.[120] Their pioneering work on the polymerization of diene initiated with sodium metal set the stage for the use of alkali metal-containing aromatic hydrocarbon complexes as initiators for various α-olefins. In 1936, Karl Ziegler proposed that anionic polymerization of **S** and **B** by consecutive addition of monomer to an alkyl lithium initiator occurred without chain transfer or termination. Twenty years later, living polymerization was demonstrated by Szwarc and coworkers, using sodium naphthalene as an initiator for the polymerization of **S** in THF.[121] In one of the breakthrough events in the field of polymer science, Szwarc showed unambiguously that electron transfer occurred from radical anion sodium naphthalene to **S**. This work provided the foundations for the synthesis of polymers with improved features.

More than 50 years later, anionic polymerization is still one of the most powerful synthetic tools for the preparation of well-defined polymers, allowing the control of the molecular architecture (molecular weight, low dispersity, composition and microstructure) depending on the chosen reaction conditions (temperature, counterion, additive and solvent).[34, 122]

Carbanions (or oxanions) with metallic counterions are mostly the active centres, highly sensitive to oxygen, moisture, functional groups and protic impurities in the chain propagation step. In the rubber industry, S-**SBR** is synthesized by an anionic polymerization process, which is initiated by organolithiums compounds, such as *sec*-BuLi or *n*-BuLi, soluble in common organic solvents.[9,10,16,123,124]

The key requirement for an aliphatic monomer to be suitable for living anionic polymerization is the existence of a 1,3-diene moiety in the monomer structure. Since **I** is the simplest alkyl-

substituted 1,3 diene monomer and terpenes formally consist of isoprene units, **M** and **F** have been reported as monomers for carboanionic polymerization.[125,126]

In the 1980s, pioneering anionic studies have shown that **M** can be polymerized using *sec*-BuLi in nonpolar solvents (e.g., benzene, cyclohexane), obtaining **PM** with a high amount of the preferable 1,4-units. In particular, anionic polymerization of **M** by means *sec*-BuLi in cyclohexane results in **PM** with 94% of the preferred 1,4-units and 6% of 3,4- units, while the polymerization in the more polar solvent THF, as reported by Bolton *et al.*, results in 30% of 1,4-units, 57% of 3,4-units, and 13% of 1,2-units.[127] In the 'green' ether solvents, like cyclopentyl methyl ether and 2-methyltetrahydrofuran, 1,2 and 3,4 units (36%–86%) were found enriched.[128]

Generally, high content of 1,4-units of polydienes is required for a low T_g and improved elasticity, when compared to polydienes with higher 3,4- or 1,2 content. Indeed, the slope of the linear correlation of the T_g strongly correlates with the polydiene architecture and diene monomer structure.[129] For example, a significant decrease of the slope in the order **PI** > **PM** > **PF** is observable (see Fig. 36), which is clearly related to the terpene side chain length. In the case of **PF**, a weak vinyl unit content T_g dependency can be attributed to its bottlebrush-like structure that results in a hindered tight packing of the polymer chains, resulting in a higher free volume and consequently in a lower T_g.

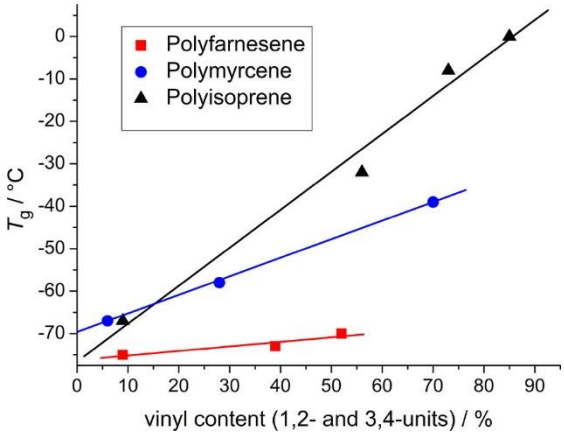

Figure 36. Glass transition temperature as a function of vinyl content for **PI**, **PM**, and **PF**.

In several recent works, copolymerization of **M** and **S** was also studied. In particular, the anionic copolymerization by *sec*-BuLi results in dependency of the polarity of the solvent in tapered copolymers (cyclohexane), random copolymers (cyclohexane and polar additives such as tetrahydrofurfuryl ether or tetramethylethylenediamine), and inverse block-like copolymers (THF; temperature-induced block copolymer).[34]

Very recently, a temperature-controlled one-pot anionic approach for the preparation of diblock copolymers consisting of **PS** and **PM** blocks has been described by Gallei *et al*. initiated by *sec*-BuLi.[130]

A viable alternative to organo-lithium compounds as anionic polymerization initiator is represented by alkali metal hydrides (LiH, NaH, and KH) that have been barely investigated due to their low solubility in organic solvents. They are compounds quickly available and stable

under an inert atmosphere in which one or more hydrogen centers have nucleophilic, basic, or reducing properties, commonly used as reducing agents in organic synthesis. However, in the literature, it is reported that the addition of Lewis acid (R_3Al, R_3B, R_2Zn, or R_2Mg) to LiH, NaH, and KH allows their solubilization in non-polar solvents by the formation of bimetallic complexes.[131–134]

In rare and limited cases, LiH, NaH and KH have been employed in polymerization.[135] Recently, systems based on their association with alkyl, alkoxide and hydride derivatives of Al, Mg and Zn in the retarded anionic polymerization (**RAP**) of **S** and dienes have been explored. Deffieux *et al.* reported that triisobutylaluminium (**TIBA**) in combination with NaH form soluble heterocomplexes (Al^iBu_3/NaH) able as initiating systems for the **RAP** of **S** at high temperature in concentrated monomer conditions.[136] The best performances were obtained at ratios 0.7< [Al]:[Na] <1, since for stoichiometric proportion or higher than 1 the system was found to be inactive. As depicted in Figure 37, at ratios [Al]:[Na] ≥1, only the 1:1 complex with an inactive site (s_1) was formed. Instead, in the presence of a slight excess of NaH with respect to **TIBA**, in addition to the 1:1 complex, the formation of the 1:2 complex with an active site (s_2) was postulated. Furthermore, the addition of tetrahydrofuran (**THF**) as a second polar additive increased the reactivity of the system and could lead to a mixture of complexes in which the formation of active Na-H bond (s_2) was favored.[134,137] Thus, the anionic *homo*-, *co*- and *ter*-polymerization of **M**, **S** and **I** by sodium hydride in combination with **TIBA**, as anionic initiator heterocomplexes, in highly concentrated monomer media at 100 °C were investigated. These initiating systems can represent a very useful and economical approach for the copolymerization of **M** with commodities such as **S** and **I**, enlarging the armory of techniques that allow the synthesis of more sustainable elastomers starting from terpenes.

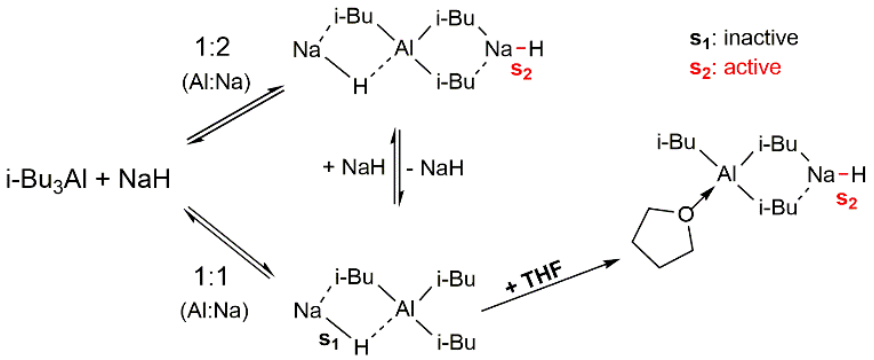

Figure 37. Formation of 1:2 and 1:1 [Al]/[Na] heterocomplexes of Al^iBu_3/NaH system and influence of THF on an inactive 1:1 complex, as suggested by Deffieux et al.

Table 13. Homopolymerizations of M, S and I, using Al^iBu_3/NaH as initiating systems at 100 °C

Run [a]	Monomers feed (M,S,I) [mol %]	$[NaH]$ *10^{-3}	$\frac{[mon]}{[NaH]}$	Time [h]	Yield [b] [%]	M_W[c] [KDa]	$Đ$[c]	T_g[f] [°C]	Polymer composition and microstructure [%] M (1,4/3,4/1,2)	S	I (1,4{*cis***}/3,4/1,2)
30*	100,0,0	6.0	500	24	-	-	-	-	-	-	-
31	100,0,0	6.0	500	24	58	50.2	1.7	-61.8	100 (46/52/2)	-	-
32[d]	100,0,0	6.0	500	24	7	264.9	1.7	n.d.	100	-	-
"	"	"	"	"	"	7.9	1.7	n.d.	"	"	"
33	100,0,0	3.0	1000	72	85	79.6	1.7	n.d.	100 (49/48/3)	-	-
34	100,0,0	2.2	1450	72	40	89.3	2.0	-76.5	100 (51/47/2)	-	-
35	0,100,0	6.0	500	8	100	151.2	1.4	105.5	-	100	-
36	0,100,0	2.2	1450	8	91	285.1	1.5	n.d.	-	100	-
37	0,0,100	6.0	500	12	40	24.9	1.5	n.d.	-	-	100 (30{53}/56/14)
38	0,0,100	6.0	500	24	74	33.4	1.5	-11.4	-	-	100 (32{52}/55/13)
39	0,0,100	3.0	1000	24	55	59.1	1.6	-14.9	-	-	100 (35{53}/54/11)

[a] Reactions were performed in toluene; [monomers] = 3.0; [Al]/[Na] = 0.8; [THF]/[Na] = 50. [b] Conversion was determined by gravimetry. [c] Determined by SEC in THF at 40°C, calibrated with polystyrene standards. [d] [THF]/[Na] = 0.
[e] Successive monomer additions (1st: styrene; 2nd: myrcene). [f] Determined by DSC. N.d. = not determined.
* No TIBA ** the complement to 100 is the percentage of the *trans* isomer

5.2 Results and discussions

PM, **PS**, and **PI** were synthesized (100 °C in degassed and dry toluene solutions) by anionic polymerization using the combination of **TIBA**/NaH as initiating systems (runs 31-39, **Table 13**). A blank experiment was performed with just NaH without **TIBA** and did not provide any polymer (run 30, **Table 1**). The effect in terms of efficiency and polymerization control of a second polar additive such as **THF** was observed in the **M** homopolymerizations. Its absence (run 32, **Table 13**) had negative effects on the polymerization yield (7%), by providing bimodal molecular weight distribution ($Đ$).

As already observed in previous studies, at ratios 0.7< [Al]:[Na] <1, THF reasonably increased the reactivity of the system, shifting the equilibrium of the complexes toward the formation of species with active sites (s_2) to which propagation reactions are restricted. According to ^{1}H **NMR** analysis of the vinylic proton signals at δ 4.7–5.2 ppm (see Fig. 5S1 and equations 27-28 of Appendix 7), **PM** consisted of an almost equimolar mixture of 1,4 *cis*/*trans* and 3,4 units with a small percentage (2-3%) of 1,2 units. In detail, the signals between 5.00-5.20 ppm were found assignable to the olefinic protons of *cis*-*trans* 1,4-units, whereas the doublets at 4.73–4.76 ppm belonged to 3,4-units. The determination of the *cis* and *trans* geometric isomers for 1,4 units was not possible to determine due to structural irregularity of **PM** and the overlap of some diagnostic signals in ^{13}C {^{1}H} **NMR** spectra (See Fig. 5S2, Appendix 7). However, a deeper analysis of the aliphatic portion of ^{13}C **NMR** spectrum (See Fig. 5S3, Appendix 7) permitted to detect, in accordance with literature data, the presence of many peaks (28.55, 29.89 and 37.23

ppm) related to head-to-head and tail-to-tail regio-irregular 1,4 units along the polymer backbone.[118,138] Furthermore, as evidenced by Sarkar *et al*., the presence of a higher percentage of 3,4-addition microstructures (47-52%, in our case), could make **PM** samples more susceptible toward sulfur vulcanization.[139,140] Size exclusion chromatography (**SEC**) analysis of synthesized **PM**s (runs 31-34, **Table 13**) revealed M_w in the range of 50.2–89.3 KDa and a monomodal $Đ$ = 1.7-2.0. The broader distribution of $Đ$, compared to the narrower values generally obtained with anionic polymerizations, can be explained by several factors. Especially, the high operating temperature (100 °C) in experimental conditions could facilitate termination reactions, as well as the presence of a chain transfer agent such as **TIBA**. Yields increased prolonging the polymerization times from 24 h (58%) to 72 h (85%); M_ws increased, at the expense of yield, increasing the [Monomer]/[NaH] ratio. **PM**s showed low T_g values (usually below -60°C) comparable to conventional rubbers.

PS obtained by Al^{i}Bu$_3$/NaH system (runs 35-36, **Table 13**) had characteristic spectra of an atactic polymer (for ^{1}H and ^{13}C **NMR** see Fig.s 5S6-5S7 of Appendix 7).[110] This evidence was also confirmed by **DSC** analysis that displayed a T_g around 105 °C without any T_m. As the trend of molecular weights of **PM**s, M_w grew up in line with the increase of the [monomer]/[NaH] ratio. For [**S**]/[NaH] = 1450, M_w was found to be 285.1 KDa with $Đ$ =1.5 and yield of over 90% in 8 h. The **I** homopolymerization has been reached using similar ternary initiating systems based on alkali metal hydride, trialkylaluminium and alkoxides in cyclohexane at different temperatures (80-120 °C), achieving mainly a mixture of 1,4 and 3,4 isoprene units (94-97%) and a small amount of 1,2 units (3-6%).[141] Data relating to **I** polymerizations (runs 37-39) are shown in **Table 13**. The best monomer conversion (74%) was achieved in 24 h, starting from [NaH] = 6.0*10^{-3} mol/L and [**I**]/[NaH] = 500. In Appendix 7 (Fig. 5S8) was reported a typical ^{1}H **NMR** spectrum, in which the peaks between 4.50 and 6 ppm were attributed to olefinic protons of 3,4- addition (4.65–4.72 ppm), 1,2- addition (4.80–4.90 ppm), 1,4- (*cis* and *trans*) addition (5.02 ppm) and 1,2- addition (5.70 ppm). The polymer compositions were determined by ^{1}H and ^{13}C {^{1}H} **NMR** spectroscopy in solution according to equations 31-35 (see Appendix 7). The contents of 1,4, 3,4-, and 1,2- units in the **PI** were in the ranges of 30-35%, 54-56% and 11-14%, respectively. The SEC analyses revealed that **PI** copolymers have M_w ranging from 24.9 to 59.1 KDa with $Đ$ of 1.5–1.6. The influence of the polydiene architecture on the thermal behavior was investigated by **DSC** measurements, showing T_g for polymers in the range between −14.9 and -11.4 °C. **TGA** curves of **PM**, **PS** and **PI** in argon atmosphere are also reported in Appendix 7 (Fig.s 5S38-40). From the **TGA** curve, it can be clearly seen that below 300 °C there is no

noticeable weight loss underling the thermal stability of the obtained materials. Moreover, plots for **M** and **I** conversions versus polymerization time (linear dependence) and evolution of M_w and $Đ$ versus conversion are shown in section 5.11 of Appendix 7.

5.2.1 Synthesis and characterization of poly(M–co-S), poly(M–b-S), poly(M–co-I) copolymers and poly(M-co-S-co-I) terpolymers

Copolymerization of various monomers is a powerful strategy to modify the properties of manufactured polymers satisfying specific needs, for example modifying T_g, reducing crystallinity, or changing the molecular architecture of polymer backbone chains in order to obtain new materials with better properties.

So, copolymerizations of **M** with **S** and **I** were performed in toluene, at 100 °C, using a [monomers]/[NaH] = 500-1450. The **Table 14** summarizes the main results of the experiments performed. Polymer compositions were fully elucidated by ^{1}H **NMR** and ^{13}C {^{1}H} **NMR**

Table 14. *Co*- and *ter*-polymerizations of M, S and I, using Al^iBu_3/NaH as initiating systems at 100 °C

Run [a]	Monomers feed (M,S,I) [mol %]	$[NaH]$ *10^{-3}	$\frac{[mon]}{[NaH]}$	Time [h]	Yield [b] [%]	M_w[c] [KDa]	Đ[c]	T_g[f] [°C]	Polymer composition and microstructure [%] M (1,4/3,4)	S	I
40	90,10,0	6.0	500	72	82	48.1	1.8	-47.7	87 (48/52)	13	-
41	90,10,0	2.2	1450	72	45	97.1	1.8	-52.2	89 (52/48)	11	-
42	70,30,0	2.2	1450	72	54	142.9	2.1	-42.4	65 (55/45)	35	-
43	50,50,0	2.2	1450	72	75	151.2	2.1	-4.9	38 (49/51)	62	-
44	30,70,0	2.2	1450	72	91	159.8	1.9	21.3	17 (56/44)	83	-
45	70,0,30	3.0	1000	72	78	71.3	1.7	-46.1	55 (59/41)	-	45
46	50,0,50	3.0	1000	72	85	66.5	1.9	-37.5	31 (58/42)	-	69
47	30,0,70	3.0	1000	72	80	62.9	1.8	-33.0	19 (53/47)	-	81
48	33,33,34	3.0	1000	72	83	98.7	2.7	-8.2	17	52	31
49	50,40,10	3.0	1000	72	81	145.2	2.2	-5.1	33	54	13
50	10,40,50	3.0	1000	72	80	90.9	1.7	11	8	45	47
51	50,50, 0	3.0	1000	8+72	88	60.2	1.8	98.9 -52.5	36 (46/54)	64	-
"	"	"	"	"	"	"	"		"	"	"

spectroscopy according to the methods reported in the Appendix 7 (See equations 27-30 and

[a] Reactions were performed in toluene; [monomers] = 3.0; [Al]/[Na] = 0.8; [THF]/[Na] = 50. [b] Conversion was determined by gravimetry. [c] Determined by **SEC** in THF at 40°C, calibrated with polystyrene standards. [d] [THF]/[Na] = 0.
[e] Successive monomer additions (1st: styrene; 2nd: myrcene). [f] Determined by DSC.
* The complement to 100 is the percentage of the *trans* isomer.

34-39,). The **NMR** spectra were recorded in $CDCl_3$ and 1,1,2,2 tetrachloroethane-d2 (**TCDE**) in order to have all the diagnostic signals free from the deuterated solvent peak. In all copolymers, 1,2 addition of **M** were not diagnosed. Complete assignments of ^{13}C {^{1}H} **NMR** spectra (see Fig.35) of synthesized poly(**M**–*co*-**S**) copolymers (**PMS**) are in agreement with data given in the literature. [68,142,143]

The direct comparison of carbon spectra of **PMS** copolymers (A, B, and C, Fig 38) and those of **PM** (not reported for simplification) and **PS** homopolymers (D, Fig. 38) pointed to the presence of additional signals that corresponded to the **M**-**S** dyads, already identified by Hulnik *et al.* in the emulsion cationic polymerization of **M** and **S** using a water-dispersible Lewis acid surfactant combined catalyst. [143]

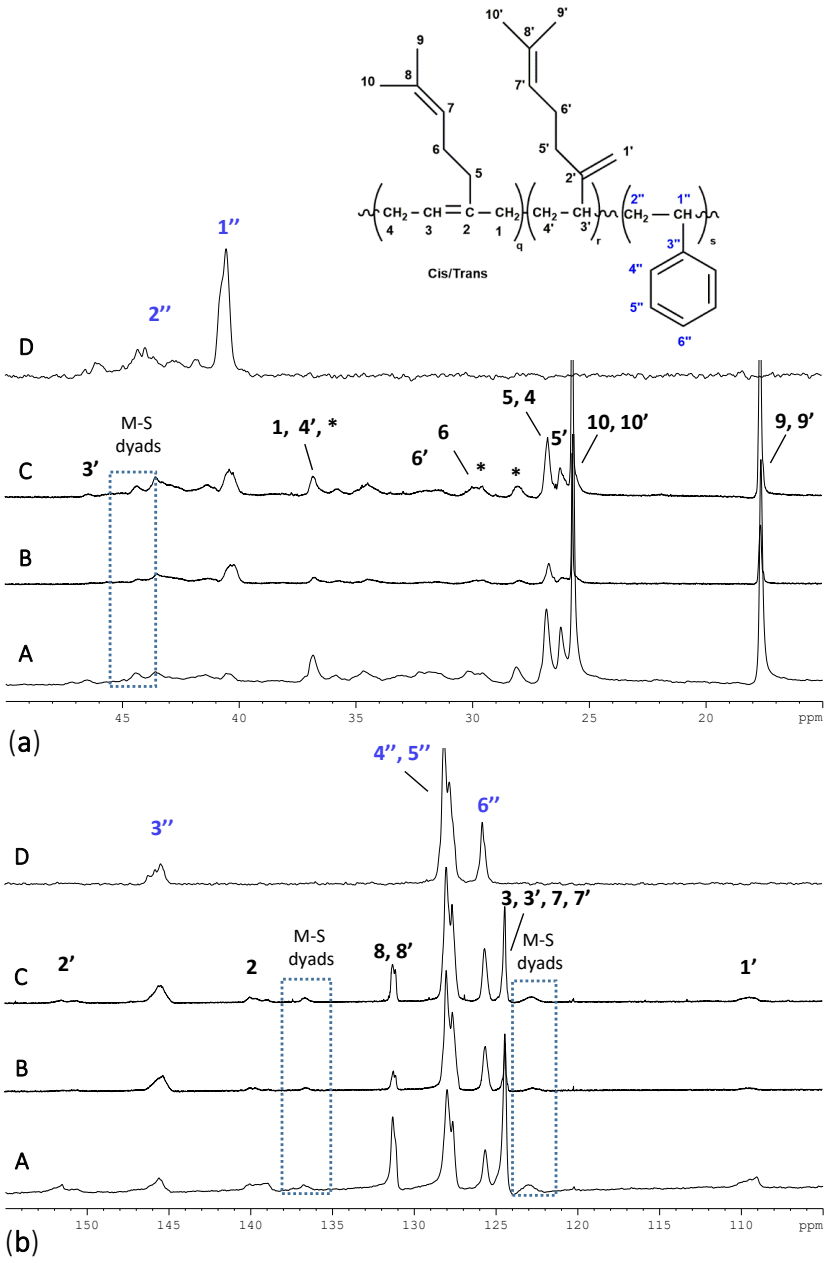

Figure 38. Aliphatic (a) and olefinic (b) regions of ^{13}C **NMR** spectra (TCDE, 25°C, 400 Mhz) of **PMS**, synthesized at different **M**:**S** ratios, and of **PS** homopolymer. A) **M**:**S** (mol/mol) = 70:30 (run 42, **Table 13**); B) **M**:**S** (mol/mol) = 50:50 (run 43, **Table 2**); C) **M**:**S** (mol/mol) = 30:70 (run 44, **Table 14**); **PS** (run 45, **Table 14**). *Signals attributed to head-to-head and tail-to-tail regioirregular 1,4 **M** units.

It was interesting to observe the C1'' and C2'' signals of the styrenic unit, at higher myrcene contents (A and B, Fig.38), almost disappeared simultaneously with the formation of the **M**-**S** dyads (highlighted).

Head-to-head and tail-to-tail enchainments bridge of *cis*-1,4 **M** additions (see Fig. 5S3 in detail, Appendix 7), were visible in all ^{13}C {^{1}H} spectra of **PMS** copolymers. The T_gs of these samples (runs 40-44, **Table 14**) lay between that of the homopolymers (−76.5 and 105.5 °C for **PM** and atactic **PS**, respectively). Exception of run 51 (diblock synthesis by sequential addition of monomers), were detected for copolymers a single T_g value, which decreased with an increasing amount of **M** incorporated in the polymer chain. Reasonably, this is due to the decrease in the comonomer content of **S** having a rigid

benzene ring. For comparison purposes, the Fox equation was applied for the calculation of T_g values, showing a good correlation between experimental and theoretical data (Fig. 39):

$$\frac{1}{T_g} = \sum \frac{W_i}{T_{g_i}}$$

where W_i is the weight fraction of i component and T_g and T_{gi} are the glass transition temperatures of the copolymer and i homopolymer, respectively.

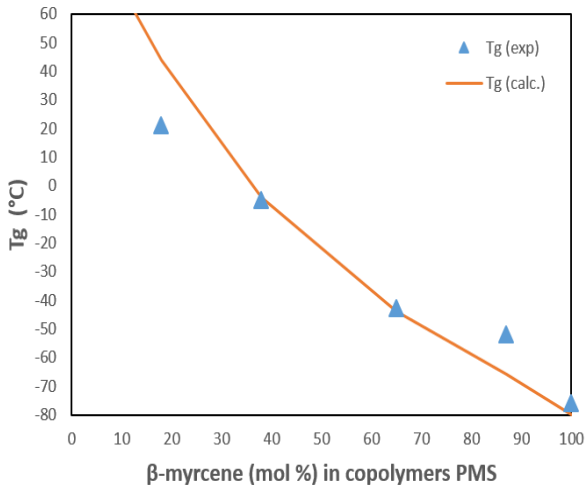

Figure 39. Glass transition temperatures (T_g) at different β-myrcene content (mol %) incorporated in copolymers.

Monomer reactivity ratios (r values) for **M**-**S** copolymerization were calculated by the Kelen-Tudos (**KT**) method (See paragraph 5.2 and **Table T3**, Appendix 7), considering the monomer feed ratios and the copolymer compositions (see **Table T1**, Appendix 7). To minimize the composition drift, the copolymerization reactions were stopped after 30 min (monomers conversion of 5-9%). The **KT** plots are shown in Fig. 5A2 (Appendix 7). The difference in reactivity between **M** and **S** (r_{myr} = 0.12 ± 0.003 and r_{sty}= 3.18 ± 0.65) indicated that **S** is more reactive than **M**. The product of the reactivity ratios, r_{myr} and r_{sty}, was less than the unity (r_{myr} x r_{sty} = 0.38). To evaluate the reactivity ratios it was also used a modified version of Kelen-Tudos called extended Kelen-Tudos method (**exKT**). In this method was included a new parameter called Z, by redefining η and ξ using the partial molar conversion of the monomers (see paragraph 5.2, Appendix 7). The **exKT** parameters were shown in the **Table T4** of Appendix 7. The reactivity of the monomers were found to be r_{myr} = 0.10 ± 0.004 and r_{sty} = 3.32 ± 0.68 with r_{myr} x r_{sty} = 0.33. The two methods (**KT** and **exKT**) are in good agreement with each other, revealing that $r_{sty} > 1$ and $r_{myr} < 1$. Thus, the polymer chains are enriched in **S** in the initial stages of polymerization, forming short sequences of **S** units. When the polymerizations proceed to higher monomer conversion, the monomer feed is enriched in the less reactive **M** favoring its incorporation in the chains. These data suggested a tendency of **S** and **M** to form a tapered polymer, as also observed in other recent anionic polymerization works.[144]

With the aim of making different **PMS** architectures, consecutive addition of **S** and **M** (run 51, **Table 14**) produced a poly(**M**–*b*-**S**) diblock copolymer (AB type) due to the living anionic polymerization character. **GPC** analysis of synthesized sample revealed unimodal $Đ$ (1.8) and

M_w = 60.2 KDa. The marked difference in M_w among poly(**M**–*b*-**S**) and corresponding homopolymers (**PM** and **PS**), obtained under the same experimental conditions, led us to exclude the formation of a polymer blend. As expected, ^{13}C **NMR** spectrum of poly(**M**–*b*-**S**) (Fig. 5S14, Appendix 7) confirmed the absence of **M**-**S** dyads diagnosed for **PMS** copolymer, showing only the characteristic signals of **M** and **S** homosequences. Moreover, high M_w (60.2 KDa) of diblock copolymer did not allow detecting the junction between the two blocks. The **DOSY** experiment confirmed unambiguously the copolymeric nature of examined samples (Fig. 5S25-5S26, Appendix 7). The **DSC** curve of poly(**M**–*b*-**S**) s were obtained in the temperature range of -90 to 250 °C under the atmosphere of N_2, displaying two T_g values (-52.5°C and 98.9°C), relating to the two different long monomer sequences, very close to those of homopolymers. Anionic polymerization initiated by Al^{i}Bu$_3$/NaH was also applied to produce poly(**M**–*co*-**I**) (**PMI**). The copolymerization data are summarized in **Table 14** (runs 45-47). At ratio **M**:**I** = 50:50 mol/mol of alimentation feed with [NaH] = 3.0*10^{-3} mol/L and [**M**+**I**]/[NaH] = 1000, a conversion of 85% was obtained in 72 h. ^{1}H **NMR** spectrum of **PMI** copolymers is shown in Fig.s 5S15-5S16 of Appendix 7. From the comparison of the ^{1}H and ^{13}C {^{1}H} **NMR** spectra of **PM**, **PI** and **PMI** (Fig. 5S15, Appendix 7), due to the structural similarity between monomers and the polyisoprenes sequences that contain all possible region-insertions (1,4-*cis*,

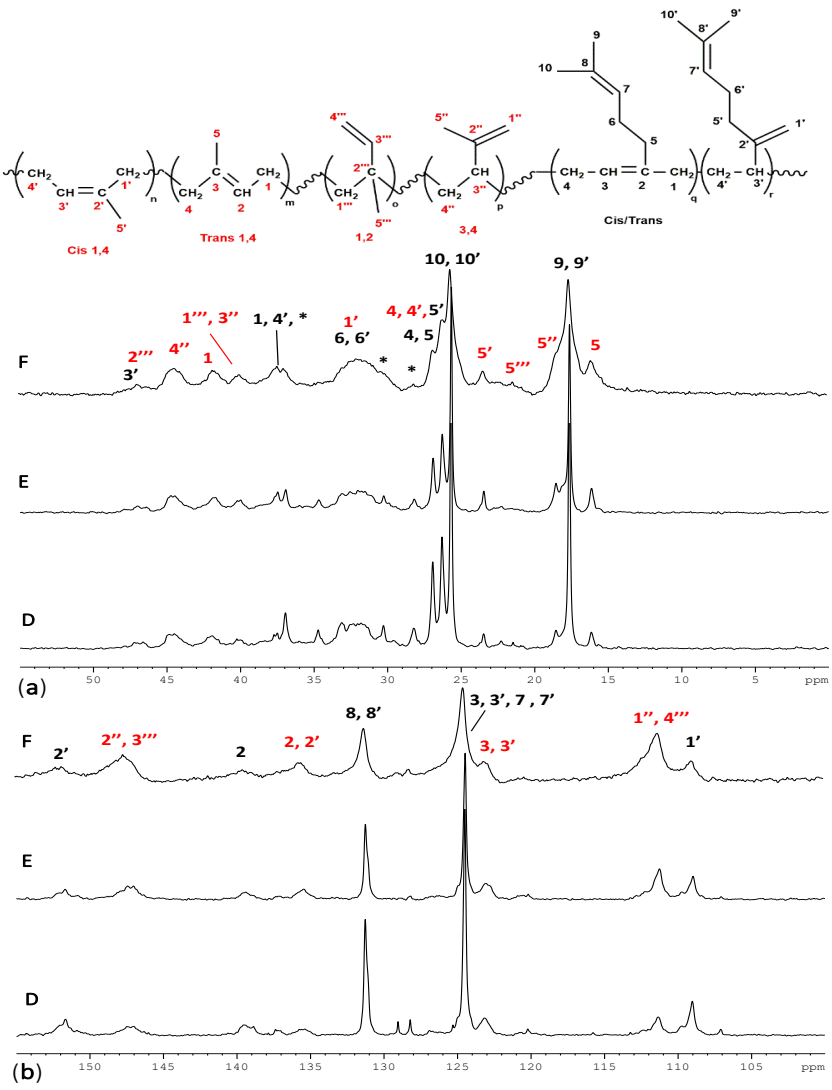

Figure 40. Aliphatic (a) and olefinic (b) regions of ^{13}C **NMR** spectra (TCDE, 25°C, 400 Mhz) of **PMI**, synthesized at different **M**:**I** ratios. D) **M**:**I** (mol/mol) = 70:30 (run 45, **Table 14**); E) **M**:**I** (mol/mol) = 50:50 (run 46, **Table 14**); F) **M**:**I** (mol/mol) = 30:70 (run 47, **Table 14**). *Signals attributed to head-to-head and tail-to-tail regioirregular 1,4 **M** units.

1,4-*trans*, 1,2 and 3,4 additions), it is observed that many peaks of different comonomeric units felt in the same region of spectra. Thus, the difficulty in the integration of significant signals involved an uncertainty in determining polymer compositions (see 5.1 of Appendix 7). In Fig.40 the ^{13}C **NMR** spectra of **PMI** copolymers with different **M**:**I** (mol/mol) ratios were reported. All the main peaks were assigned based on examples in the literature.[66,68,87,143,145] Furthermore, **PMI** copolymers showed a monomodal and $Đ$ = 1.7-1.9. Only one T_g was found for these copolymers, and no T_m were detected. Three experiments (**Table 14**, runs 48-50) were performed to test anionic initiator systems also in the terpolymerizations of **M**, **I** and **S**, resulting in M_w in the range of 90-145 KDa (yield on average 80%) and $Đ$ between 1.7 and 2.7 (**Table 14**, runs 48–50).

The structure of poly(**M**-*co*-**S**-*co*-**I**) (**PMSI**) with the assignments of the main peaks is exhibited in figure 5S21 of Appendix 7. In this case, the major complexity of **NMR** spectra reflects the microscopic structural irregularity, greatly limiting a depth microstructure study. **TGA** of **PMSI** copolymers revealed good thermal stability with a decomposition temperature close to 350 °C (see Figs. 5S41-5S47, Appendix 7).

We also performed some measurements related to the surface properties of the polymers. Indeed, the character of the surfaces is very important, since the surface properties are of great interest for some types of elastomers, especially tires and seals. Observing the variations in surface roughness and polarities and adjusting them (also with regard to lamellar structures) can help to develop more performing materials for such applications.

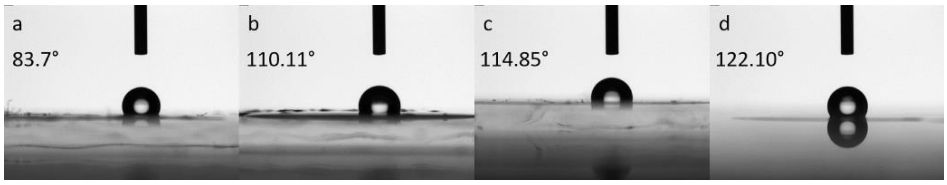

Figure 41. Water contact angles (**WCA**) measured for: **PMS** from run 44 of **Table 14** (a); **PMSI** from run 49 of **Table 14** (b); **PI** from run 37 of **Table 13** (c) **PMI** from run 47 of **Table 14** (d).

Water contact angle (**WCA**) is the most common method for determining the relative hydrophilicity of materials. Fig. 41 shows the contact angles for some **PMS** (a), **PMSI** (b), **PI** (c), and **PMI** (d), respectively (see **Table T7**, Appendix 7). The rise in contact angle from **PMS** (83.7°) to **PMI** (122.1°) is evident. Reasonably this trend could be explained by the effect of the greater quantity in the samples of **M** and **I** which introduce small side

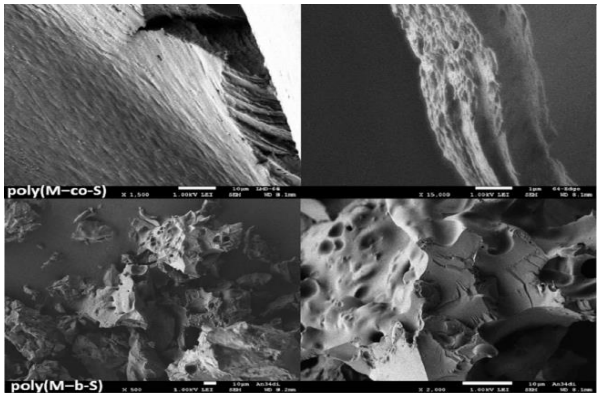

Figure 42. Scanning electron microscope (**SEM**) of poly(**M**–**co**-**S**) from run 44 of **Table 14** and poly(**M**–*b*--**S**) from run 51 of **Table 14**.

chains in the structure of the copolymers and by their microstructure (mainly 3,4 addition), factors that increase hydrophobicity. The possibility of modulating the surface structure and properties of the copolymers by adjusting the microstructure of the segments has been already observed in previous studies.

SEM is a type of electron microscope that allows to scanning of the surface of a sample with a high-energy beam of electrons. **SEM** has the potential to generate images with a few nanometres spatial resolution, and has a relatively large depth of field (up to 100 times that of an optical microscope).

This provides valuable information about the surface topography and composition of the scanned objects. The morphology of some samples, in particular poly(**M**–*co*-**S**) and poly(**M**–*b*-**S**) obtained, was subsequently investigated by **SEM**. Fig.42 shows the **SEM** images of runs 44 (upward) and 51 (below) collected in **Table 14**. These measurements show rough or wavy surface topographies of these polymers. Interestingly, edges and domains indicate the block structures present, and different dark areas in fine structures can show phase separation here (see section 8 of Appendix 7 for more images).

5.3 Materials and methods

General Procedures and Materials. All chemicals were stored and handled under an argon atmosphere using standard Schlenk techniques or an MBraun glovebox.

All glassware was stored overnight in an oven at 130 °C prior to use. *β*-myrcene (≥ 95 %), isoprene, and styrene (≥ 99 %) were all purchased from Sigma-Aldrich and were purified by overnight stirring over calcium hydride and distillation under reduced pressure. Monomers were stored on molecular sieves at 4 °C and before each set of experiments the amount of water was measured with a Mettler Toledo KF Coulometer DL36 Karl Fischer instrument (allowed max. 15 ppm H_2O).Toluene (Sigma-Aldrich) and tetrahydrofuran (Sigma-Aldrich) (THF) as solvents dried were obtained with an MBraun MBSPS-800 solvent purification system and were deoxygenized by three freeze-pump-thaw cycles, before storing on molecular sieves. Sodium hydride was stored under an argon atmosphere in a drybox. Triisobutylaluminum (Al^iBu_3, Sigma-Aldrich) (**TIBA**) was used as received.

Preparation of NaH/Al^iBu_3 initiator system. Under argon, NaH (0.096 g, $4*10^{-3}$ mol) was placed in a glass flask before adding 50 mL of dry and degassed toluene. Then, 3 ml of **TIBA** solution (25% wt in toluene) was added with a syringe to reach the ratio of [Al]/[Na] = 0.8. The final solution was let under vigorous stirring at 50 °C, until NaH was partially solubilized (4 h).

Typical Polymerization Procedure. Polymerizations were carried out under argon at 100 °C in a glass flask for 72 hours. 88 µl of Al^{i}Bu$_3$/NaH solutions (ratio [Al]/[Na] = 0.8) and 25 µl of THF were added with a syringe to dry and degassed toluene (0,5 ml). Finally, 0,5 mL of myrcene was added to the reaction mixture and the system was maintained under stirring after equilibration at the desired temperature. The polymerization was stopped by adding methanol containing a little amount of hydrochloric acid and 2,6-bis(1,1-dimethylethyl)-4-methylphenol (BHT) as stabilizing agent. The polymer was washed and dried under vacuum until constant weight. 230 mg polymer (58 % yield, M_w = 50.2 KDa, $Đ$ = 1.7).

Typical Co-polymerization Procedure. Co-Polymerizations were carried out under argon at 100 °C in glass flasks for 72 hours. 30 µl of Al^{i}Bu$_3$/NaH solutions (ratio [Al]/[Na] = 0.8) and 9 µl of THF were added with a syringe to dry and degassed toluene (0,5 ml). Finally, 0,28 mL of myrcene and 0,19 ml of styrene were sequentially added to the reaction mixture and the system was maintained under stirring after equilibration at the desired temperature. The co-polymerization was stopped by adding methanol containing a little amount of hydrochloric acid and 2,6-bis(1,1-dimethylethyl)-4-methylphenol (**BHT**) as stabilizing agent. The copolymer was washed and dried under vacuum until constant weight. 295 mg polymer (75 % yield, Mw = 151.2, $Đ$ = 2.1).

Preparation of diblock copolymer. In a glass flask equipped with magnetic stirrer 30 µl of Al^{i}Bu$_3$/NaH solutions (ratio [Al]/[Na] = 0.8) and 9 µl of THF were added with a syringe to dry and degassed toluene (0,5 ml). At 100°C, the polymerization starts after injection of 0,19 mL of styrene. After 8 hours, the glass flask was opened in a drybox and was quickly added 0,28 mL of myrcene. The polymer was coagulated after a further 72 h in methanol containing a little amount of hydrochloric acid and 2,6-bis(1,1-dimethylethyl)-4-methylphenol (**BHT**). The polymer was washed and dried under vacuum at room temperature until constant weight. 366 mg polymer (93 % yield, M_w = 60.2, $Đ$ = 1.8).

Polymer Characterizations. ^{1}H and ^{13}C **NMR** analysis were recorded Bruker AV III-300, AV HD-400 and AV III-500 spectrometer at room temperature. Chemical shifts δ are reported in ppm relative to tetramethylsilane and calibrated to the residual ^{1}H or ^{13}C signal of the deuterated solvent.

Diffusion-ordered spectroscopy (**DOSY**) experiments were carried out at 298 K on a Bruker Avance 600 spectrometer with the standard Bruker pulse program (ledbpgp2s). The latter used a double stimulated echo sequence and LED, bipolar gradient pulses for diffusion, and two spoil

gradients. For the duration of the experiment (about 25 min), the pulse gradients were increased from 5% up to 95% of the maximum gradient strength in a linear ramp. The parameters were set as follows: diffusion times were 2500 ms, the eddy current delay was 5 ms, the gradient recovery delay was 0.2 ms, and the gradient pulse was 1000 ms. Individual rows of the quasi-2D diffusion databases were phased and, after Fourier transformation and baseline correction, the diffusion dimension was processed with the Bruker software Topspin3.2 and Diffusion. By Gaussian fits diffusion coefficients were calculated, using T1/T2 software of Top-spin3.2.

Size exclusion chromatography (**SEC**) measurements were performed using a PolymerLaboratoriesGPC50 Plus chromatograph (calibrated with polystyrene standards) and equipped with Deflection RI detector at 40 °C with THF as the eluent (flow of 1 mL/min).

Differential scanning calorimetry (**DSC**) analysis was conducted on a **DSC** Q2000 instrument. 2-5 mg of polymer was sealed into a **DSC** aluminium pan and heated from -90 to 250 °C at 10 °C/min. The reported values are those determined in the second heating cycle.

Thermal gravimetric analysis (**TGA**) measurements were performed on a TA Instruments Q5000 SA. The heating and cooling rate was adjusted to 10 °C/min and the temperature range measured was 40-600 °C under inert atmosphere of Argon.

Water contact angle measurements (**WCA**) were performed on a Krüss DropShape Analyser. The evaluation was performed with the program ImageJ. The samples were applied via solvent casting on glass object carriers and measured several times. The average of these values represents the contact angle.

Scanning electron microscope (**SEM**) measurements were recorded on a JEOL field emission scanning electron microscope JSM-7500F. The secondary electrons produced by the electrons of the beam (primary electrons) in interaction with the atoms of the object under investigation served as informations source. The samples were examined at different magnifications.

5.4 Conclusion

Homo- and *co*-polymerizations of **M** with **S** and **I**, and *ter*-polymerization of all monomers have been reached using soluble heterocomplexes consisting of sodium hydride in combination with triisobutylaluminum as anionic initiating system at 100 °C in toluene. By adjusting the initial feed ratio, it was easily possible to obtain polymers in a wide range of compositions with

different architectures and various thermal properties. Molecular weights could be well controlled through the simple regulation of the [monomers]/[NaH] ratio. Materials exhibited an elastomeric behavior and good thermal stability with a decomposition temperature exceeding 300 °C. Moreover, all the samples were fully characterized by **SEC**, **GPC**, and **NMR** spectroscopy (^{1}H, ^{13}C and DOSY experiments). In some cases, to study the surface properties, **WCA** and **SEM** characterizations were also performed. A more complete study of **PMS** was carried out, highlighting their tapered microstructures with high molecular weights (ranging from 48.1 to 159.8 KDa) and a single T_g. Indeed, for **PMS** the reactivity constants were determined by Kelen–Tudos (r_{myr} = 0.12 ± 0.003 and r_{sty} =3.18 ± 0.65) and extended Kelen-Tudos (r_{myr} = 0.10 ± 0.004 and r_{sty} = 3.32 ± 0.68) methods from which the tendency of **S** and **M** to form a tapered polymer was supposed, in accordance with **NMR** studies.

«Occorre diffidare del quasi-uguale... Le differenze possono essere piccole,

ma portare a conseguenze radicalmente diverse»

Primo Levi (1919-1987)

Chapter 6

Preparation and characterization of innovative compounds for high performance tires

6.1 Introduction

With increasing global concern for fossil fuel consumption, the automotive industry moves toward more efficient and sustainable vehicles.[146,147] In this sector, tires are of great importance as the tire compound material in contact with the road surface, under cyclic deformation, dissipates energy due to its viscoelastic nature. On the other hand, the friction between the road and the tire surface of vehicles is required for safety and comfort. These two contrary characteristics of the tire need a compromise to deliver a secure and efficient ride. The tire designer is faced with the impossible task of trying to satisfy all the needs of the vehicle manufacturers and the consumers and is therefore forced to seek a compromise, often with an emphasis on safety and long tread life.

In the last years, the utilization of synthetic rubbers from natural sources in a huge market such as automotive tires has been extensively examined.[119,138,142,148,149] Indeed, many efforts have been devoted in respect to partial substitution of conventional synthetic polymers which, in a market still dominated by fossil commodities, would be a considerable sustainability improvement.[34,84,127,140,142,150] One of the goals of tire research is to increase driving safety along with increasing overall performance, hopefully by using more sustainable materials. In particular, high-performance tires (called **HP** and **UHP**, “High-Performances” and "Ultra High Performances") are designed to be used at high speeds, allowing high grip especially when vehicles are moving in road curves. In this context, a tire’s composition affects grip, but also fuel economy, and its lifetime. Currently, the elastomeric compositions used for the production of high tire treads are mainly based on styrene-butadiene copolymers (**SBR**), blended with butadiene rubber (**BR**) and natural rubber (**NR**).[7,9] These elastomers are characterized by low T_g values, generally above –50 ° C (**SBR** has T_g between -50 and - 10 ° C). It is believed that a

high T_g value allows a high adherence to the road surface of the tire tread but, at the same time, confers reduced resistance to abrasion and high rolling resistance. Conversely, a low T_g value provides high abrasion resistance and low rolling resistance but the grip of the tire is reduced. Since it is not possible to have all the best properties using a single elastomeric compound, to obtain tire treads with optimal characteristics, elastomeric compositions of tires have been industrially prepared which combine blends of elastomeric polymers and/or copolymers with different chemical-physical characteristics. Furthermore, the grip characteristics of the tread of high-performance tires, in particular in extreme driving conditions (at high speed and cornering) are positively influenced by the presence of high percentages of styrene in the elastomeric materials used for the preparation of the tire compounds compositions. Indeed, the use of polymers and copolymers with a high styrene content allows for increasing the hysteresis values of the finished tire tread. This chapter describes the study of the mechanical properties of the most promising elastomers, obtained in our previous investigations, about their use for the formulation of high-performance tires compounds. A scale-up process was developed to produce a quantity of polymer such as to be able to create a laboratory model tyre compound to test its characteristics. All the mechanical studies of the specimens were carried out in the laboratories of Pirelli (Milan), partner of this industrial project. Pirelli Tyre is one of the world leaders in this sector, being a group active in the design, development, production, and marketing of tires for various types of vehicles.

6.2 Results and discussions

6.2.1 Preparation of macrosamples for tires innovative compounds

To produce a series of tire compounds and test their mechanical properties, it was necessary to carry out appropriate specimens based on the new elastomeric materials synthesized during our research work and then compare them with commercial references. For this scope, elastomers obtained by using [OSSO]-type titanium catalysts (see Chapter 3) seemed to be the best candidates, due to their high stereoregular microstructures, properties (T_g, M_w, $Đ$), and better activity of Ti-based catalytic systems employed to synthesize them.[119] Furthermore, these catalytic systems thanks to the abundance and great availability of the titanium, in addition to the highly tailorable ligand framework, would guarantee a possible versatile industrial scale-up since they have already been used to produce high-performance tires tread, as demonstrated by some recent patents

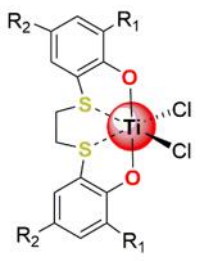

56 R_1=Cumyl, R_2= Me

Figure 43. [OSSO]-type titanium catalyst **56**

(WO2012069335A1, ITMI20102199A1, IT1404141B1, EP2643367B1, and EP2643367A1). In particular, by using the complex **56** (Figure 43) activated by ***m*-MAO** (the most active catalytic system in **O**, **S**, and **B** terpolymerizations, see 3.2.3 paragraph), four samples on a larger scale were produced (polybutadiene, **PB**; polyocimene-butadiene copolymers, **POB**; polyocimene-butadiene-styrene terpolymers, **POBS**; polybutadiene-styrene copolymer, **PBS**). The experimental synthesis procedures have been reported in the 6.3 section (Materials and Methods). The characteristics of synthesized materials, fully analyzed by **NMR**, **DSC**, and **SEC** (see Appendix 7, Fig. 6S1-6S10), have been summarized in **Table 15**.

Table 15. Samples A-D obtained by using **56/*m*-MAO** at room temperature (62 h)

				Polymer composition (wt %) [d]		
Samples [a]	M_w (kDa) [b]	$Đ$	T_g (°C) [c]	**B** (*trans*-1,4)	**S**	**O** (O^T/O^V)
A (***trans*-PB**)	226	2,0	-108,2	**100** (94)	-	-
B **(POB)**	86	1,6	-89,7	**80** (94)	-	**20** (14/86)
C **(POBS)**	132	1,7	-41,3	**52** (95)	**42**	**6** (10/90)
D **(PBS)**	199	2,6	-38,2	**60** (95)	**40**	-

[a] Reactions condition: for details, see 6.3.2; Yields (wt %): A = 98; B = 23; C = 64; D = 95. [b] Determined by **SEC** in THF at 40°C, calibrated with polystyrene standards. [c] Determined by **DSC**. [d] Determined by **NMR**.

The structures of the polymers were ascertained by spectroscopic measurements, revealing in accordance with previous experiments predominately *trans*-1,4 units for **B** (94-95% mol) in A-D samples, prevalent 1,2-**O** insertion (up to 90% mol) for B and C polymers, and small segments of *iso*-**PS** in the backbone chain of **POBS** terpolymer (sample C) and **PBS** copolymer (sample D). The T_gs were found in the range of -108.2 °C (***trans*-PB**) to -38.2 °C (**PBS**), values below 0 °C typical of elastomeric materials.

6.2.2 Silica-based composites with POB (sample B)

With the scope to explore a possible application of terpene-butadiene copolymers, model tread compounds in which *cis*-**BR** is in part replaced with **POB** were prepared according to recipes shown in **Table 16**. Considering the high *trans* content of **B** units in **POB** (sample B, **Table 15**), analogs treads in which *cis*-**BR** was partially substituted with *trans*-**BR** (obtained with the same catalytic system **56/*m*-MAO**)[100] were also considered as a comparison aid. For all samples, crosslinking was performed with a sulfur-based system.

Table 16. Recipes of **SSBR-BR** based compounds with *cis*-**BR**, *trans*-**BR** and **POB**

Run	Component	Reference	*trans*-PB (10) [a]	*trans*-PB (20) [a]	POB (10) [a]	POB (20) [a]
1	SSBR (NS 522)	100	100	100	100	100
2	*cis*-BR (BUNA CB25)	30	20	10	20	10
3	*trans*-PB (**A**)	-	10	20	-	-
4	POB (**B**)	-	-		10	20

[a] Quantities of ingredients are reported in parts per hundred of rubber (phr). Other ingredients: **TDAE** = 10-16 phr; **ZEOSIL 1165 MP** = 70 phr; **Kristalek F85** = 10 phr; **TESPT silane** = 6 phr; stearic acid = 2 phr; **6-PPD** = 3phr; **TBBS** = 3phr; sulfur = 1phr. For details on the abbreviations, see 6.3 section. [b] Numbers in brackets indicate the phr of *cis*-**BR** replaced in the sample.

In **Table 17**, data related to the mechanical properties of these treads, measured after curing at 170°C for 10 minutes, are reported. Rheometric curves do not reveal appreciable differences in the vulcanization kinetic (very similar t_{90} values, *i. e.* the time to achieve optimal vulcanization, were found) showing that the reactivity of the polymers in the different treads is comparable; on the other hand, lower levels of maximum torque (M_H) were observed using *trans*-**BR** and **POB** with respect to commercial *cis*-**BR**, likely reflecting the lower molecular weight of lab-prepared polymers (86 KDa).

Table 17. Properties of **SSBR-BR** based nanocomposites with *trans*-**PB** and **POB**

	Reference	*trans*-**PB** (10) [a]	*trans*-**PB** (20) [a]	**POB** (10) [a]	**POB** (20) [a]
t_{30} (*min*)	2.17	1.89	1.55	2.22	2.24
t_{90} (*min*)	6.9	6.94	7.08	7.52	7.82
RPA measurement (70 °C 10 Hz)					
ML (*dN m*)	4.37	4.57	5.53	4.09	4.29
MH (*dN m*)	18.84	15.69	15.33	14.6	14.39
d_G'(0.5-10) (MPa)	0.86	0.85	1.05	0.81	0.89
G' (9%) (MPa)	1.57	1.44	1.53	1.35	1.37
tan δ (9%)	0.127	0.168	0.185	0.152	0.16
Stress strain test (23 °C)					
Ca 0.1 (MPa)	0.49	0.51	0.6	0.44	0.47
Ca 0.5 (MPa)	1.05	1.23	1.35	1.07	1.06
Ca 1 (MPa)	1.58	1.84	1.92	1.68	1.66
Ca 3 (MPa)	5.92	5.73	5.07	6.15	6.19
Stress at break (MPa)	21.76	19.37	14.29	17.81	16.67
Elongation at break (%)	712.02	706.55	682.06	644.93	617.33

[a] Numbers in brackets indicate the phr of cis-BR replaced in the sample.

Dynamic-mechanical measurements, such as strain sweep tests performed in torsion mode, allowed us to determine the storage modulus G' and the loss factor tan δ, as a function of the strain amplitude. Storage modulus G' was similar in all cases, somehow lower with **POB**.

Hysteresis (tan δ) was significantly higher when *trans*-**BR** was used instead of *cis*-**BR**, reasonably for the lower mobility of the molecular chains and the higher crystallinity related to *trans* conformation. In the case of **POB**, the performance was closer to those of the reference rubber, despite the high content of *trans* units. The reason for such behavior lies in the fact that the renewable comonomer decreases the crystallinity of the *trans*-**B** polymer backbone, increasing its chances to build smaller domains and thus to better homogenize with **S-SBR**. Tensile measurements (stress-strain tests) were carried out on crosslinked nanocomposites by applying uniaxial stretching on Dumbell specimens. Tensile curves displayed that *trans*-**BR** gave higher rigidity if compared with *cis*-**BR** at low deformations (Ca 0.1-0.5, load at 10% and 50% elongation respectively) and lower values at high deformation, resulting in a worsening of the final properties. This could be interpreted as an effect of the less mobile polymer chains of *trans*-**BR** and its tendency to self-organize and thus to display lower compatibility with **S-SBR** with respect to the case of *cis*-**BR** utilization. Conversely, **POB** showed a tensile behaviour very close to that of reference *cis*-**BR**: at low strain (up to 50% deformation = Ca 0.5) moduli were fully in line or even lower than reference, at high strain were slightly higher than reference, thus showing an opposite trend vs the homopolymer *trans*-**BR**. These values are somehow unexpected in view of lower G' and MH and can be tentatively interpreted assuming that the copolymers with **O** could help dispersion of silica filler and/or favour reactivity with silane and thus effective binding between silica and polymer matrix. The ultimate properties were less affected than in the case of the compound containing *trans*-**BR**. Also in this case, this observation could be interpreted as an effect of the reduced crystallinity and better homogenization with **S-SBR** due to the unsaturated side chains introduced by the terpene monomer. In conclusion, the replacement of commercial high *cis*-**BR** with the corresponding *trans*-polymer, with or without **O** in polymer, results in compounds that tend to be more rigid and with worse breaking behavior. Conversely, **POB** showed better behavior in a model tread compound than butadiene homopolymer (*trans*), suggesting that they could be used as a substitute for commercial *cis*-**BR** in a tread without altering its mechanical properties too much.

6.2.3 Tire compounds with POBS (sample C)

As is known, the grip of the high-performance tire tread, in particular under extreme driving conditions, is influenced by the presence of high percentages of **S** in the elastomers used for the preparation of the compounds.[151,152] However, commercial **SBR** available on the market and mostly used for the tire formulation contain a maximum percentage of **S** equal to about 40% by weight. Indeed, traditional polymerization techniques do not allow to obtaining of **SB**

copolymers with higher percentages of **S** because this would promote the formation of block copolymers in which 10 or more consecutive **S** units (with high T_g), compromising the mechanical properties and abrasion resistance of the tire. To modulate the T_g of the compounds, it is possible to add resins and/or polymers with a low molecular weight (typically less than 2000 Da), generally with a high content of **S** (equal to at least 25% by weight). Due to their low molecular weight and high content of **S**, they are used to modulate the hysteresis of the tire tread and, as they dissolve at least partially in the elastomeric compositions, they also modulate the T_g. However, the resins have the disadvantage of not crosslinking with the elastomeric polymers of compounds. Therefore, tearing of the tire tread can occur, especially in the case of severe use, even after not prolonged use of the same. Alternatively or in association with the resins, low molecular weight polymeric materials (typically less than 10,000 Da) can be added to the tire compounds. Polymers with low molecular weight have the advantage of being able to crosslink with the other elastomers, but they do not considerably increase the hysteresis since they do not have a content of styrene as high as that of resins. In the case of the use of co-cross-linkable low molecular weight polymers, the finished tire tread will have better tear resistance but a reduced grip, when compared with tire treads in which resins are added. To try to simultaneously improve the grip and durability properties, low molecular weight resins and polymers are often used together. The combination of these materials does not allow the problem of tearing the tire tread to be completely solved. Pirelli has already provided a solution to the above problems in patent EP2643367 B1, producing a tire compound in which elastomeric composition comprises at least a random **SB** copolymer (with **B** in *trans* conformation and **S** in isotactic configuration) having an **S** content higher than 40% by weight with respect to the total weight of the copolymer.

Thus, with the idea based on the above reasons given, different compound formulations were produced by replacing common commercial resins (in our cases, Novares TT30 and Kristalek F-85) with our samples C and D (**Table 15**). These compounds were then compared with a well-known commercial compound. The elastomeric compositions were prepared according to the recipes reported in **Tables 18-19**. All quantities are expressed in parts per hundred of rubber (phr). All components, except sulfur and

Figure 44. Brabender® internal mixer

accelerator, were mixed together in an internal mixer with T set at 130 °C (Brabender®, Fig. 44) for about 5 minutes. The sulfur and the accelerator were then added in the second phase and the compound was discharged after a further two minutes. The composites were finally further homogenized by passing them 5 times through an open roller mixer.

Table 18. Recipes of a reference compound and others based on **PBS** and **POBS**

	Component [a]	**Reference 1**	Compound 1	**Compound 2**
1	Novares TT30	10	-	-
2	PBS (Sample D)	-	10	-
3	**POBS** (Sample C)	**-**	**-**	**10**
4	Novares TL 90	5	5	5
5	HP755B (**TDAE**)	137.5	137.5	137.5
6	Silane JH75S	2.8	2.8	2.8
7	Stearic acid	1.4	1.4	1.4
8	ZnO	2.1	2.1	2.1
9	CRX 1391	60.0	60.0	60.0
10	Vivatec 500	12.5	12.5	12.5
11	6-PPD	1.0	1.0	1.0
12	TMQ	1.0	1.0	1.0
13	IB TUADS	0.4	0.4	0.4
14	CBS	2.7	2.7	2.7
15	Sulfur	1.4	1.4	1.4

[a] Quantities of ingredients are reported in parts per hundred of rubber (phr)

Table 19. Recipes of a reference compound and others based on **PBS** and **POBS**

	Component [a]	**Reference 2**	Compound 3	**Compound 4**
1	Kristalek F-85	12	-	-
2	PBS (Sample D)	-	12	-
3	**POBS** (Sample C)	-	-	**12**
4	SIR 20 P91	12.5	12.5	12.5
5	BUNA CB 25	15	15	15
6	NS 522	99.7	99.7	99.7
7	SI 69	7.0	7.0	7.0
8	Zeosil 1165 MP	87.5	87.5	87.5
9	Stearic acid	2.0	2.0	2.0
10	Vivatec 500	10.0	10.0	10.0
11	Zinc octoate	2.5	2.5	2.5
12	Riowax BN01	2.0	2.0	2.0
13	CRX 1391 CB	5.0	5.0	5.0
14	6-PPD	3.5	3.5	3.5
15	TMQ	1.8	1.8	1.8
16	IB TUADS	0.5	0.5	0.5
17	TBBS	2.0	2.0	2.0
18	PVI	0.3	0.3	0.3
19	Sulfur	1.4	1.4	1.4

[a] Quantities of ingredients are reported in parts per hundred of rubber (phr).

The static mechanical properties (load at 50%, 100%, and 300% elongation, designated CA 05, CA 1, CA 3 respectively, tensile strength and elongation at break) and dynamic properties (E' and tan δ) of each elastomeric composition were evaluated and the results were summarized in Tables **20**-**21**.

Table 20. Properties of a **reference compound** and others based on **PBS** and **POBS**

	Reference 1	**Compound 1**	**Compound 2**
IRHD (23 °C) [a]	57.7	59.7	**60.9**
Ca 0.5 (MPa) [b]	0.78	0.84	**0.89**
Ca 1 (MPa) [b]	1.29	1.12	**1.48**
Ca 3 (MPa) [b]	6.36	7.24	**7.78**
Stress at break (MPa)	14.33	17.27	**18.04**
Elongation at break (%)	565.0	579.6	**576.8**
E' 0 °C 10 Hz (MPa)	9.36	9.13	**9.80**
E' 23°C 10 Hz (MPa)	7.21	7.86	**8.13**
E' 100 °C 10 Hz (MPa)	3.30	3.70	**3.87**
tan δ 0 °C 10 Hz	0.851	0.738	**0.765**
tan δ 23 °C 10 Hz	0.653	0.600	**0.613**
tan δ 100 °C 10 Hz	0.203	0.196	**0.202**

[a] Measured according to the ISO 48:2007 standard; [b] measured according to ISO 37:2005 standard

Table 21. Properties of a **reference compound** and others based on **PBS** and **POBS**

	Reference 2	**Compound 3**	**Compound 4**
IRHD (23 °C) [a]	75.1	75.6	**73.2**
Ca 0.5 (MPa) [b]	1.37	1.42	**1.32**
Ca 1 (MPa) [b]	2.35	2.36	**2.15**
Ca 3 (MPa) [b]	10.43	10.32	**9.28**
Stress at break (MPa)	17.77	19.44	**19.25**
Elongation at break (%)	500.8	528.7	**564.8**
E' 0 °C 10 Hz (MPa)	9.26	10.02	**10.00**
E' 23°C 10 Hz (MPa)	9.15	10.11	**9.93**
E' 100 °C 10 Hz (MPa)	5.42	6.22	**5.85**
tan δ 0 °C 10 Hz	0.480	0.410	**0.427**
tan δ 23 °C 10 Hz	0.403	0.350	**0.361**
tan δ 100 °C 10 Hz	0.107	0.120	**0.125**

[a] Measured according to the ISO 48:2007 standard; [b] measured according to ISO 37:2005 standard

The hardness in degrees IRHD was measured according to standard ISO 37:2005 on samples of elastomeric compositions vulcanized at 170°C for 10 minutes. The dynamic mechanical properties were measured with an Instron dynamic tester in tension-compression by the following methods. A sample of the elastomeric composition (crosslinked at 170°C for 10 min) of cylindrical shape (length = 25 mm; diameter = 12 mm), preloaded by compression to 25% of

longitudinal deformation with respect to the initial length, and maintained at the specified temperature (0 °C, 23 °C, 100°C) throughout the test, was submitted to dynamic sinusoidal stretching having an amplitude of ±3.5% relative to the length in pre-load conditions, with a frequency of 10 Hz.

The dynamic mechanical properties are expressed in terms of dynamic elastic modulus (E') and values of the loss factor (tan δ). The value of tan δ is calculated as the ratio of the viscous modulus (E") to the elastic modulus (E'). The properties of compounds 1 and 2 (see **Table 20**) in comparison with a reference (Fig. 45) showed that: I) the static mechanical properties (Ca 0.5, Ca 1, Ca 3, elongation and stress at break) of compound 2, containing **POBS** (sample C, **Table 15**), was better than those of the reference 1 (compound present on the market) and compound 1 (compound according to Pirelli patent EP2643367 B1, containing **PBS**). In particular it is remarkable that while the introduction of **POBS** led to higher moduli at all deformations, such stiffening was accompanied by higher modulus and elongation at break, while in general a stiffening goes with a reduction of the properties at break; II) the modulus E' value of compound 2 was constantly higher than the values obtained with the compound 1 and, at the same time, the tan δ in the full temperature range, and in particular at 100°C, were higher for compound 2 than for compound 1 and closer to the reference. These data demonstrated that

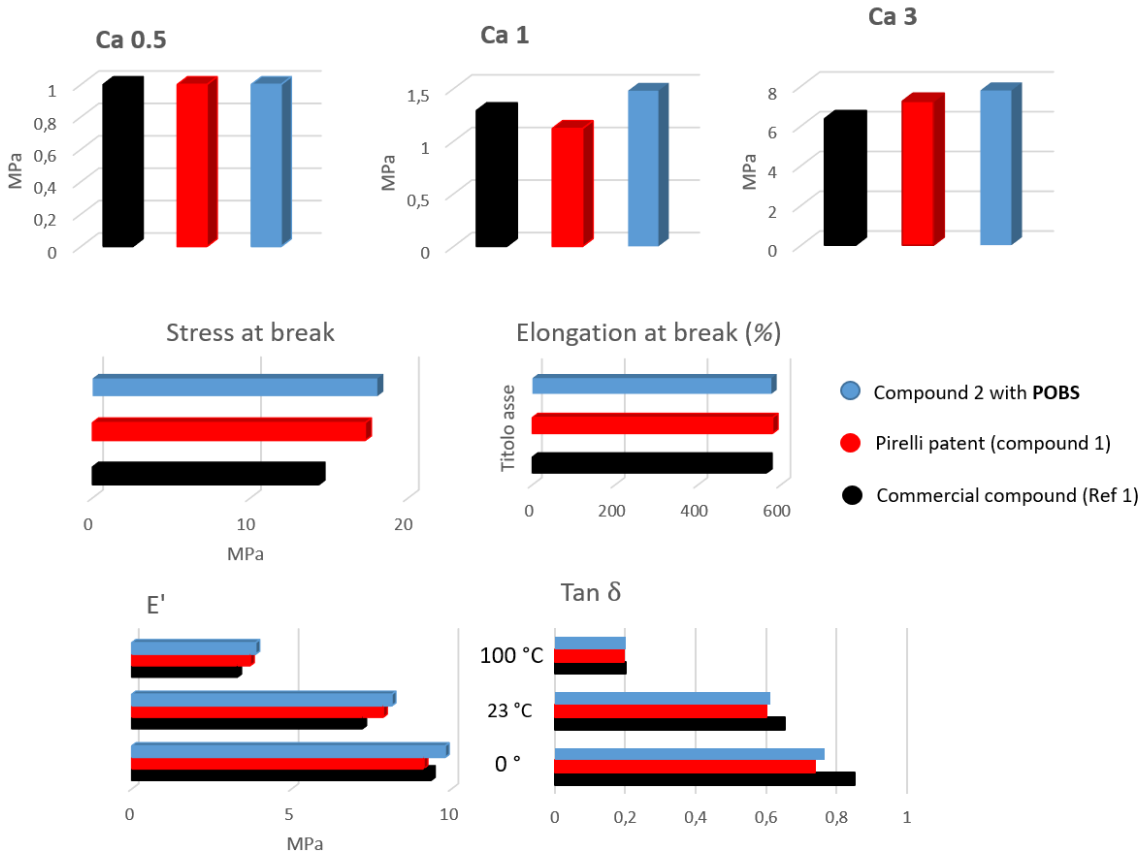

Figure 45. Comparison between the properties of the compounds in **Table 20**

a tire tread containing **POBS** simultaneously exhibited greater stiffness and mechanical strength accompanied by improved performance under severe use.

In the second series of compounds (see **Table 21**) the results obtained pointed out that: III) the load and elongation at break of the compound 4 with **POBS** were better than those of reference compound 2 and even better (in the elongation) than that of compound 3 (according to Pirelli patent with **PBS**); IV) the values of modulus E' of compound 4 were constantly higher than the value obtained with the reference 2 and comparable to that of compound 3; moreover, at the same time, the tan δ (hysteresis) at all temperatures was higher than those obtained with compound 3 and at 100 ° C also higher than the reference 2. The hysteresis at 100 °C is considered predictive of grip in extreme driving conditions: obtaining an increase in this value compared to known compounds by improving or maintaining the properties at breakage is an unexpected result of particular interest.[153] The results obtained showed that a tire tread containing **POBS** terpolymer in its formulation simultaneously presented greater mechanical strength, increasing the resistance to breaking/ tearing, accompanied by better performance in the event of severe use, improving adherence at all temperatures than the previous Pirelli patent invention (EP2643367 B1).

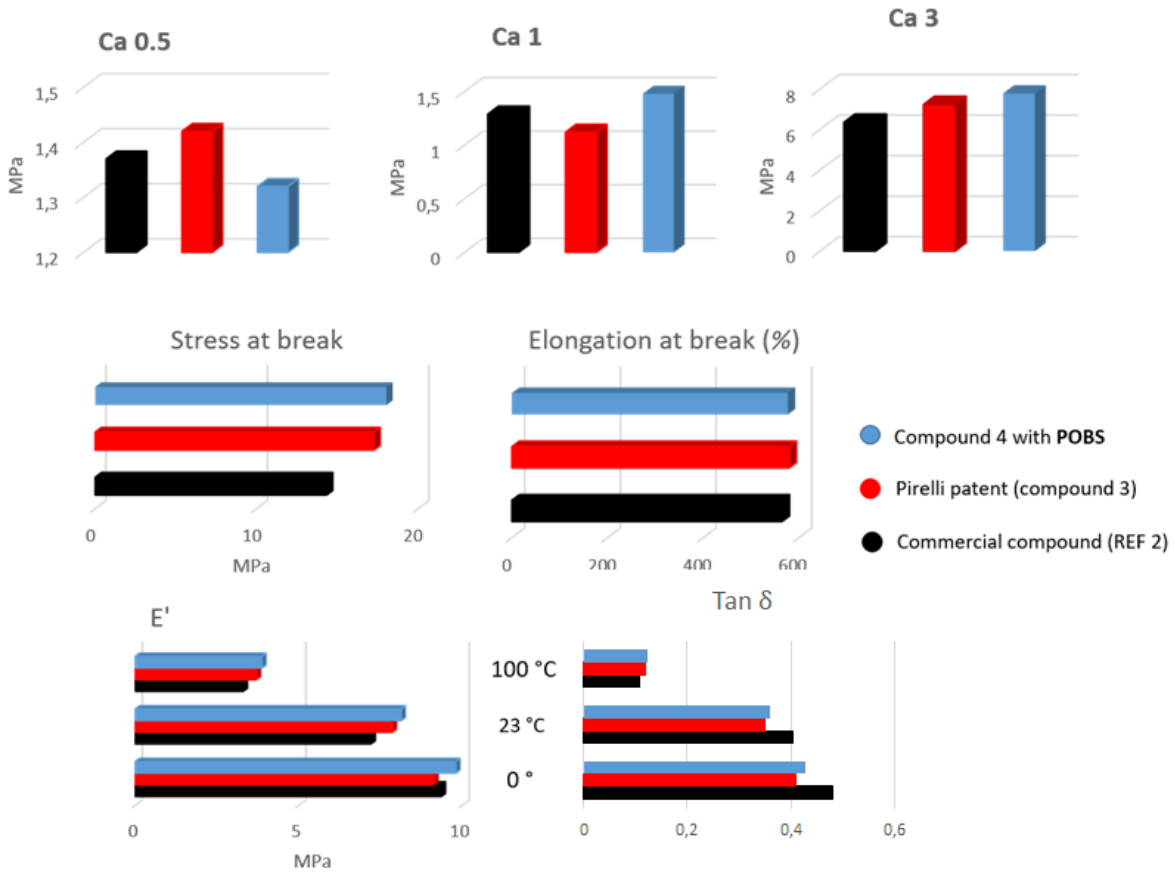

Figure 46. Comparison between the properties of the compounds in **Table 21**

All these results have led to the filing of a patent (Pneumatico ad elevate prestazioni - 2020P00004 IT), in collaboration with Pirelli, claiming very briefly the invention of a tire for vehicle wheels (in particular cars) in which the composition of tire compound includes at least one random terpolymer consisting of iso-**S**/*trans*-**B**/terpene.

6.3 Materials and methods

6.3.1. General Information

All reactions were performed under nitrogen using standard Schlenk or glovebox techniques. Toluene, ocimene (**O**), and styrene (**S**) were purchased from Sigma Aldrich and distilled before use. 1,3 Butadiene (B), purchased from Societa` Ossigeno Napoli (S.O.N.), was dried by passing through a column filled with activated silica and molecular sieves (3-4 Å) and was slowly condensed in a Schlenk tube containing toluene at 0°C.

NMR spectra were recorded on Bruker Bruker AVANCE 400 spectrometer (400 MHz for ^{1}H; 100 MHz for ^{13}C) and Bruker ASCEND 600 spectrometer (600 MHz for 1H; 150 MHz for 13C). NMR samples were prepared dissolving about 10 mg of compounds in 0.5 mL of deuterated solvent. ^{1}H and ^{13}C chemical shifts are listed in parts per million (ppm) downfield from TMS and are referenced from the solvent peaks or TMS.

The **DSC** measurements were carried out in nitrogen on a TA Instrument DSC Q20 calorimeter (heating and cooling rate of 10 °C/min).

The average molecular weights and molecular weights distributions of the samples were determined with a 150 C Waters GPC equipped with a RI detector, a JASCO 875-UV (254 nm) detector and a set of four columns from PSS (pore size of 106, 105, 104, and 103 Å, particle size of 5 μm). Tetrahydrofuran was used as a carrier solvent with a flow rate of 1.0 mL/min at 25 °C. The calibration curve was established with commercial polystyrene standards.

6.3.2 General polymerization procedure

In a round-bottomed flask, toluene and ***m*-MAO** were introduced. After 20 minutes, catalyst **56** (Figure 1) was dissolved in a portion of the solution and stirred for 45 minutes. Meanwhile, monomer(s) (**B**, sample A; **B** and **O**, sample B; **B**, **O** and **S**, sample C; **B** and **S**, sample D) was (were) added to the remaining solution and stirred at room temperature for 30 minutes. At this point, the catalyst solution was added and the reaction mixture was heated to 30°C for 62 hours. The polymerization was terminated by adding ethanol and pouring in an acidified ethanol solution containing butylated hydroxytoluene (**BHT**). The precipitated polymer was recovered

by filtration and dried in vacuum at 40°C. The quantities of the reagents used for the synthesis of the A-D samples are shown below:

Sample A: Homopolymer (*trans*-**PB**)

Reaction conditions (room temperature, 62 h): toluene 55 mL; **B** = 1.20 mol (533 mL of a 0.12 g/mL butadiene solution in toluene; catalyst **56** = 2.7 x 10^{-5} mol (18 mg), ***m*-MAO** = 1.6 x 10^{-2} mol (24 mL of 7 % wt solution in heptane). Yield: 98% wt

Sample B: Copolymer (Butadiene-Ocimene, **POB**)

Reaction conditions (room temperature, 62 h): toluene = 20 mL; **B** = 1.50 mol (593 mL of a 0.14 g/mL butadiene solution in toluene; **O** = 1.50 mol (260 mL), catalyst **56** = 9.1 x 10^{-5} mol (60 mg), ***m*-MAO** = 5.5 x 10^{-2} mol (82 mL of 7% wt solution in heptane). Yield: 23% wt.

Sample C: Terpolymer (Butadiene-Ocimene-Styrene, **POBS**)

Reaction conditions (room temperature, 62 h): toluene = 55 mL; **B** = 0.92 mol (333 mL of a 0.15 g/mL butadiene solution in toluene; **O** = 0.34 mol (57 mL); **S** = 0.44 mol (51 mL); catalyst **56** = 5.4 x 10^{-5} mol (36 mg), ***m*-MAO** = 3.2 x 10^{-2} mol (45 mL of 7% wt solution in heptane). Yield: 64% wt

Sample D: Copolymer (Butadiene-Styrene, **PBS**)

Reaction conditions (room temperature, 62 h): toluene = 20 mL; **B** = 1.50 mol (593 mL of a toluene solution containing 0.14 g/mL butadiene; **S** = 1.50 mol (172 mL), catalyst **56** = 9.1 x 10^{-5} mol (60 mg), ***m*-MAO** = 5.5 x 10^{-2} mol (82 mL of a 7% by weight solution in heptane). Yield: 95 % by weight.

6.3.3 Ingredients of the compounds

All of the following compound ingredients were used as received. **BUNA CB 25:** neodymium polybutadiene (high cis-BR) from Lanxess; **SBR** (**NS 522**): styrene-butadiene rubber Zeon; **TDAE**: treated distillate aromatic extract; **ZEOSIL 1165 MP**: precipitated synthetic amorphous silica from Solvay; **TESPT Silane**: Bis [3-(triethoxysilyl) propyl] liquid tetrasulfide from Evonik; **Kristalek F85:** hydrocarbon resin from y Eastman Chemical Co (USA); **6-PPD** (antioxidant): N-(1,3-Dimethylbutyl) N'-phenyl-p-phenylenediamine from Eastman; **TBSS:** N-tert-butyl-2-benzothiazyl-sulfenamide from Fisher Scientific; **Buna VSL 2438-2 HM**: solution of styrene-butadiene rubber in TDAE oil, comprising 38 wt.% of styrene, 24 wt.% of vinyl and 27 wt.% of oil, produced by Lanxess Deutschland GmbH, Germany; **Novares TT90**: hydrocarbon resin produced by Reutgers Germany GmbH, Germany; **Novares TT30**: hydrocarbon resin produced by Reutgers Germany GmbH, Germany; **Vivatec®** 500 (plasticizer) produced by Hansen &

Rosenthal, Germany; **CBS** (accelerant): N-cyclohexyl-2-benzothiazylsulphenamide, produced by Lanxess Deutschland GmbH, Germany; **Silane JH75S**: blend of Bis (triethoxysilylpropyl) tetrasulfide (**TESPT** 50%) supported on carbon black (50%), produced by Evonik Industries AG, Germany; **TMQ**: 2,2,4-Trimethyl-1,2-Dihydroquinoline produced by Synthos, Poland; **CRX 1391 CB**: carbon black manufactured by Cabot Corporation, USA; **HP755B** (**TDAE**): mixture of 100 parts by weight of styrene-butadiene rubber with 37.5 parts by weight of **TDAE** oil, comprising 39.6% by weight of styrene, 39.4% by weight of vinyl, produced by JSR Corporation, Japan; **IB TUADS**: isobutyl thiuram disulfide, produced by R.T.Vanderbilt; **SIR 20 P 91**: natural rubber, produced by Aneka Bumi Pratama, SED, Indonesia; **SI 69**: bis(3-triethoxysilylpropyl) tetrasulfide, produced by Degussa-Hüls; **Riowax BN01**: paraffin wax, produced by SER S.p.A.; **PVI**: N-cIclohexylthiophthalimide, produced by Brenntag Spa, Milan.

6.3.4 Characterization of the compounds

Crosslinking and dynamic mechanical characterization of rubber compounds

Crosslinking reaction was studied at 170°C with a Monsanto R.P.A 2000 rheometer, determining the minimum torque M_L, the maximum torque M_H at the end of crosslinking reaction, the time t_{30} (the time required to achieve 90% of the maximum torque M_H), the time t_{90} (the time required to achieve 90% of the maximum torque M_H). Dynamic shear moduli were then measured at 70°C, with a sinusoidal strain at 10 Hz of frequency, in a strain amplitude ranging from 0.5 % to 10%.

Stress-Strain tests

The stress-strain behavior of the cured composites was measured on a universal tensile testing machine (Zwick/Roll 2010) at a strain rate of 200 mm/min. S2 tensile specimens were prepared in accordance with DIN 53 504 from vulcanized flat sheets. Samples were fixed in pneumatic grips and stretched at constant speed until tensioned to failure. Ultimate tensile strength, modulus at 100% and 300% elongation, stress at break, and elongation at break were determined.

6.4 Conclusion

With the goal to develop innovative tire compounds, new elastomers have been synthesized using a [OSSO]-type titanium catalyst and tested in the formulation of tread compounds for high-performance tires. The **POB** copolymer showed better behavior in a model tread compound with respect to *trans*-butadiene homopolymer rubber. Indeed, the compound

characterizations suggested that the copolymers of butadiene and naturally derived monomers could in principle be used in substitution of standard *cis*-**BR** in a tread without major disruption of the compound properties. Continuing with the experimentation, the **POBS** terpolymer synthesized in the UNISA laboratories showed further improved static and dynamic mechanical properties in a tread compound. In particular, with higher values of the tensile strength (predictive of greater resistance to tearing), and of elongation load (predictive of lower compliance of the tire), and higher values of hysteresis (modulus E' and tanδ) at all temperatures (predictive of greater adhesion of the tire to the road surface, even in situations of severe use), this terpene-based elastomer is an excellent candidate to replace common resins in the formulations of tread compounds, being, on the one hand, a more sustainable material, on the other by significantly improving the mechanical properties of the tire.

Conclusions

The aim of this project was the synthesis of new elastomeric materials starting from terpene monomers, subsequently, the focus shifted to the study of the mechanical properties of the most promising materials in order to prepare new innovative compounds for more sustainable high-performance tires.

The main results here obtained are briefly reported:

- Synthesis of stereoregular homopolymers of **O**, **M**, and **F** by using [OSSO]-type titanium catalysts and a Co-based complex with a phosphine ligand;

- Synthesis of copolymers in a wide composition range of **O**, **M**, and **F** with other monomers (styrene and butadiene) through the above-mentioned complexes;

- Synthesis of **O** terpolymers with styrene and butadiene by means [OSSO]-type titanium catalysts;

- Synthesis of homo-, *co*-, and *ter*- polymers of **M** with styrene and isoprene through anionic polymerization, using NaH/TIBA as anionic initiator;

- Complete characterization of all new elastomeric materials by spectroscopic techniques (^{1}H, ^{13}C, and two-dimensional NMR), differential scanning calorimetry, gel permeation chromatography (GPC), and other types of characterizations in particular cases;

- A sample of **POB** copolymer was evaluated as a component in a model tread compound suggesting that it could be used as a substitute for commercial *cis*-**BR** in a tread without altering its mechanical properties too much;

- The synthesized **POBS** terpolymer showed further improved static and dynamic mechanical properties by replacing commercial resins in the formulation of a tread compound.

In conclusion, due to abundance in nature and interesting properties, there may be a great deal of interest more and more in the future in utilizing terpenes for producing polymers that could substitute, at least partially, for the fossil-based elastomers which are on the market today.

UNIONE EUROPEA
Fondo Sociale Europeo
Ministero dell'Università e della Ricerca
PON RICERCA E INNOVAZIONE 2014 - 2020

Acknowledgements

First of all, I am very grateful to my supervisor, Prof. Carmine Capacchione, for the help and sincere speeches during these years spent together. I also thank him for giving me the great opportunity to interact with really important academic and industrial environments such as the Technische Universität München and Pirelli Tyre S.p.A. Moreover, if he hadn't written this Ph.D. project, probably I think I would never have continued to do the thing I love most in the world: scientific research.

I also have to thank Prof. Leone Oliva for welcoming me into his laboratory at a very difficult moment in my life and for helping me grow as a man and researcher. I will always carry his teachings with me.

Great acknowledgments are for Prof. Bernhard Rieger, who hosted me in his laboratories at the TUM, Dr. Malte Winnacker (my tutor), and Dr. Sergei Vagin. The last two, in addition to being wonderful colleagues in my German period, I consider them really great friends as well as Dr. Andrea Causero.

I also thank Dr. Luca Giannini, Dr. Silvia Guerra, and Dr. Luciano Tadiello for making me feel totally at ease in Pirelli and to have supported this work with the mechanical tests of elastomeric specimens.

I dedicate a special thanks to my friend Veronica Paradiso for always giving me the right words and the best advice. I also thank all the laboratory colleagues, friends and other important people who have helped me directly or indirectly over the years: Nunzia, Vito, Simone, Giusy, Fabio, Francesco, Antonio, Giuseppe, Salvatore, Fatemeh, Yuri, Irene, Francesca, Daniele, Andrea, Luigi, Katiuscia, Gerardo, Raffaella, Arianna, Eleonora, Umberto, Romina, Simona, Roberto, Marco, and Cinzia.

Special thanks go to my family, in particular to my father Umberto, my mother Maddalena, my brothers Danae and Erwin, my uncle Sergio and my dear grandmother Maria, for their tireless encouragement and support. A dear memory also to my aunt Anna, Nonna Rosa and Nonno Alberto: you are always in my thoughts and in my heart!

Appendix 7

Chapter 3 – Supporting information

3.1 NMR Spectra

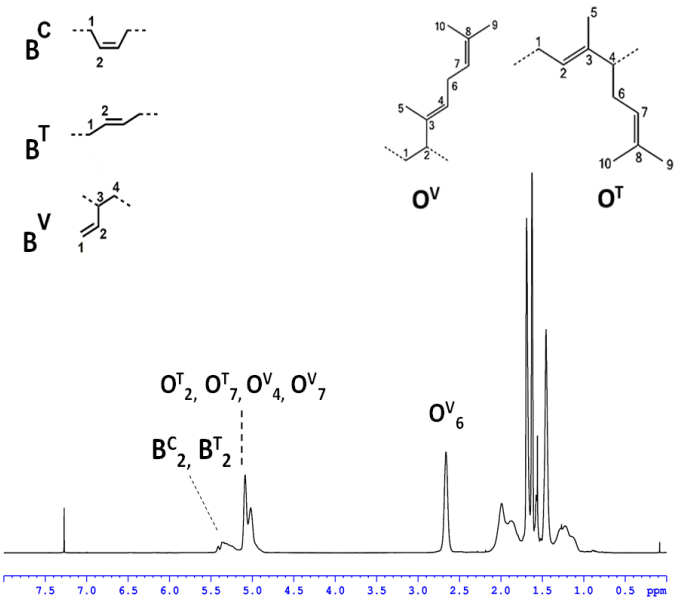

Fig. 3S1. ^{1}H **NMR** spectrum ($CDCl_3$, 25 °C, 600 MHz) of POB from run 1 of Table 1

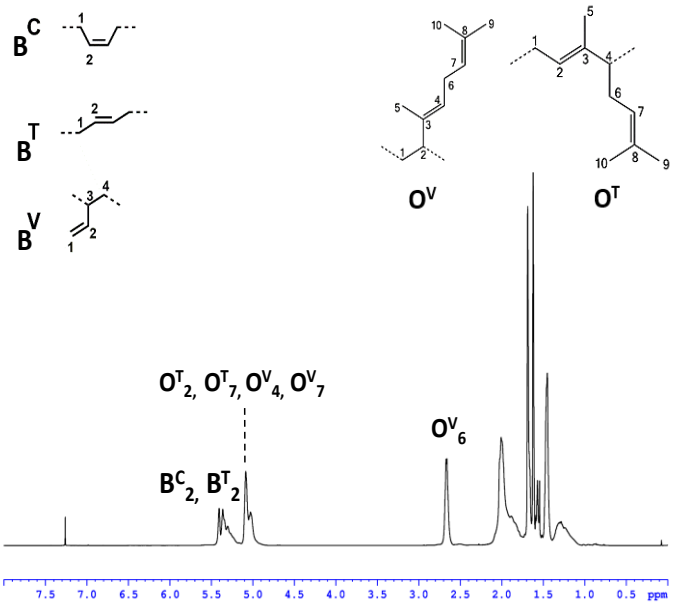

Fig. 3S2. ^{1}H **NMR** spectrum ($CDCl_3$, 25 °C, 600 MHz) of POB from run 2 of Table 1

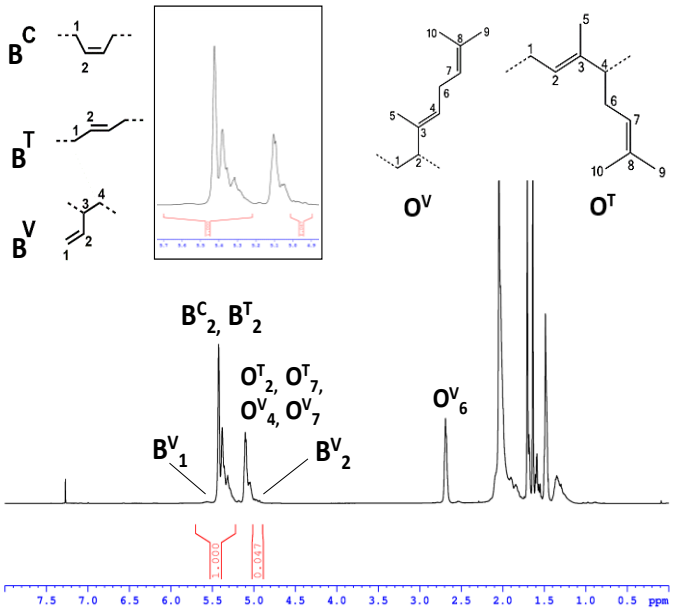

Figure 3S3. ^{1}H **NMR** spectrum ($CDCl_3$, 25 °C, 600 MHz) of POB from run 3 of Table 1

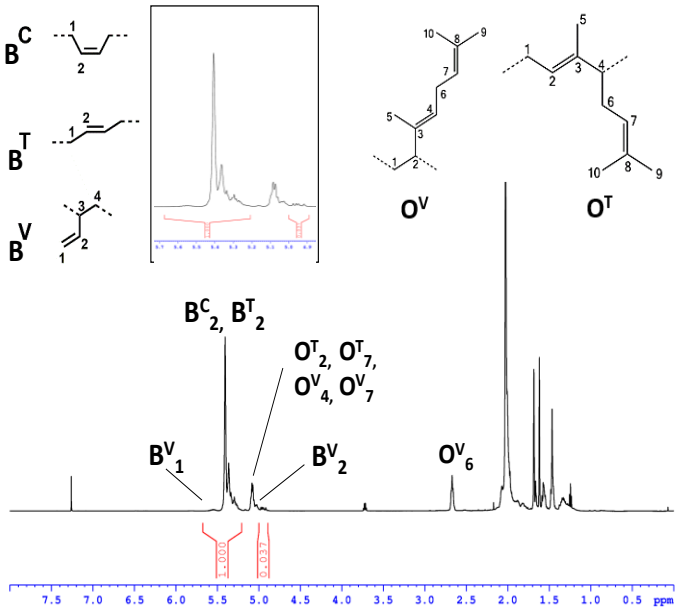

Figure 3S4. ^{1}H **NMR** spectrum ($CDCl_3$, 25 °C, 600 MHz) of POB from run 4 of Table 1

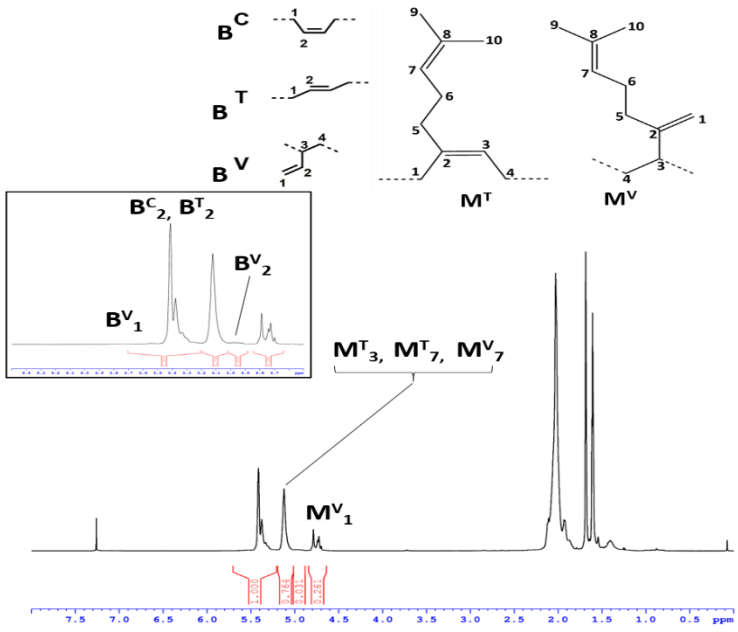

Figure 3S5. ^{1}H **NMR** spectrum ($CDCl_3$, 25 °C, 600 MHz) of PMB from run 5 of Table 3

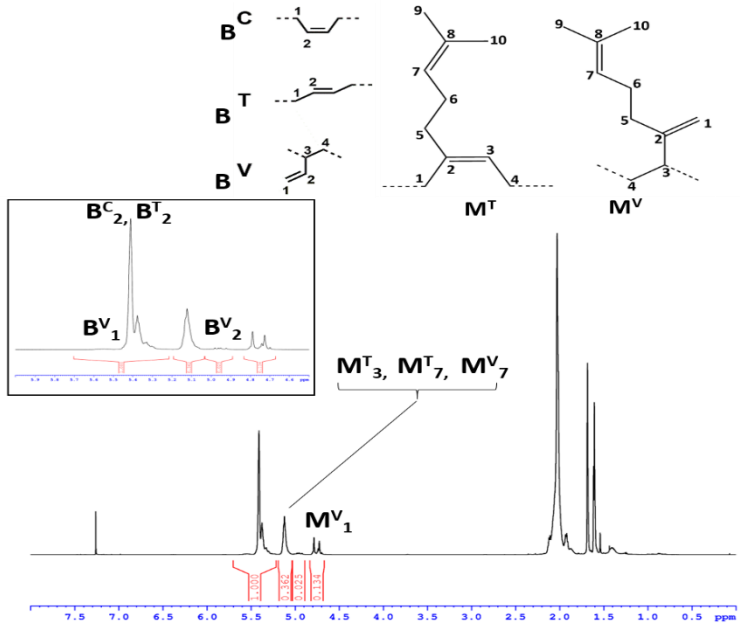

Figure 3S6. ^{1}H **NMR** spectrum ($CDCl_3$, 25 °C, 600 MHz) of PMB from run 6 of Table 3

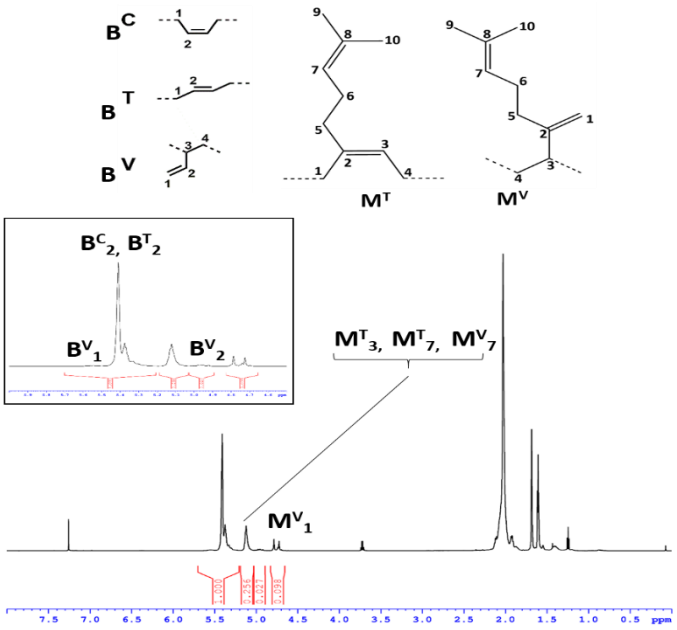

Figure 3S7. ^{1}H **NMR** spectrum ($CDCl_3$, 25 °C, 600 MHz) of PMB from run 7 of Table 3

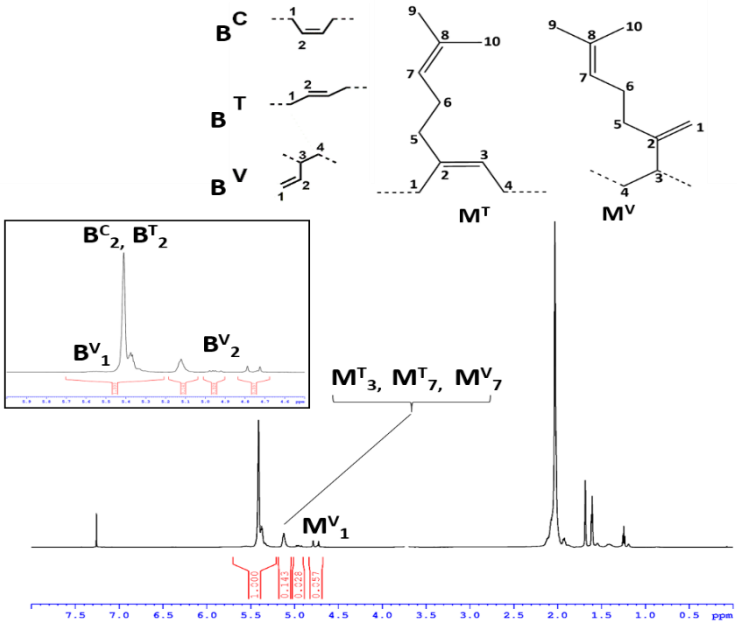

Figure 3S8. ^{1}H **NMR** spectrum ($CDCl_3$, 25 °C, 600 MHz) of PMB from run 8 of Table 3

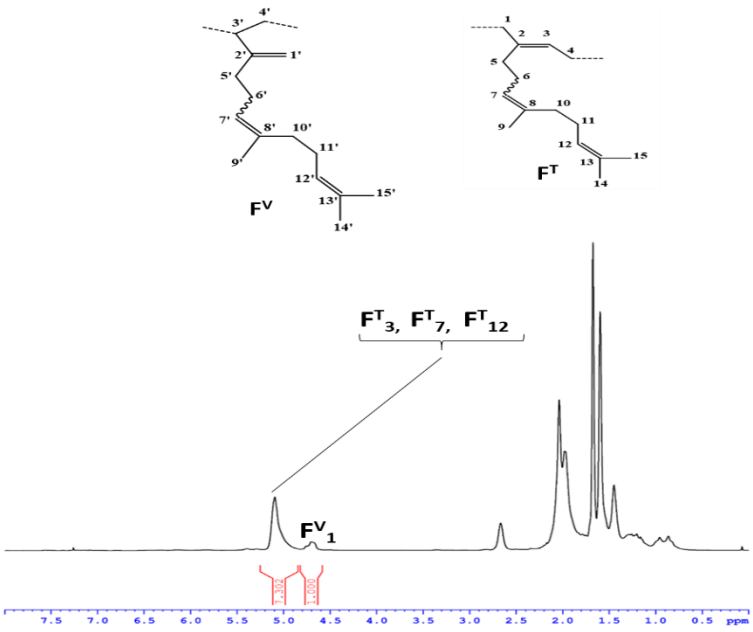

Figure 3S9. ^{1}H **NMR** spectrum ($CDCl_3$, 25 °C, 600 MHz) of PF from run 9 of Table 5

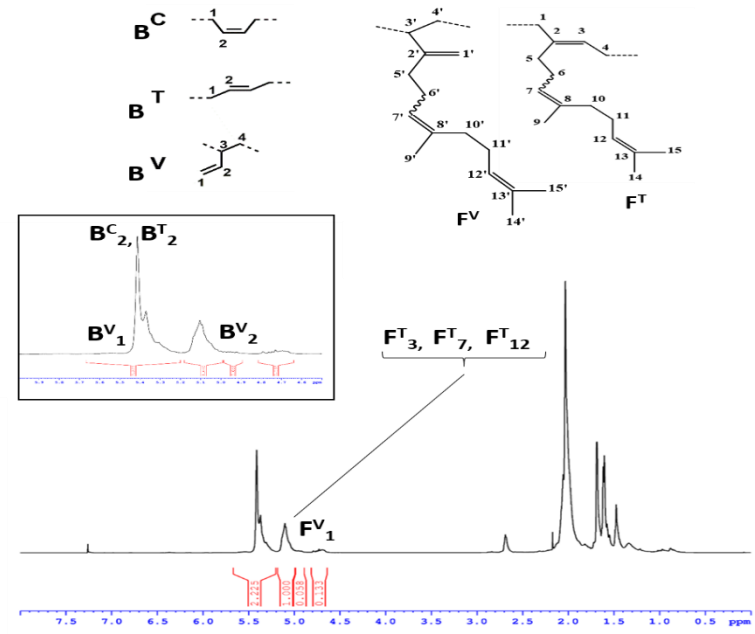

Figure 3S10. ^{1}H **NMR** spectrum ($CDCl_3$, 25 °C, 600 MHz) of PFB from run 11 of Table 5

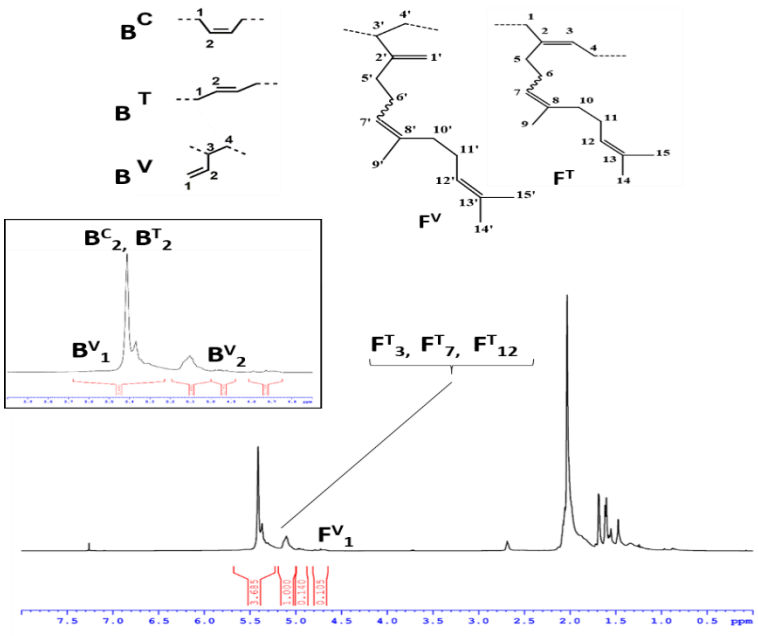

Figure 3S11. ^{1}H **NMR** spectrum ($CDCl_3$, 25 °C, 600 MHz) of PFB from run 12 of Table 5

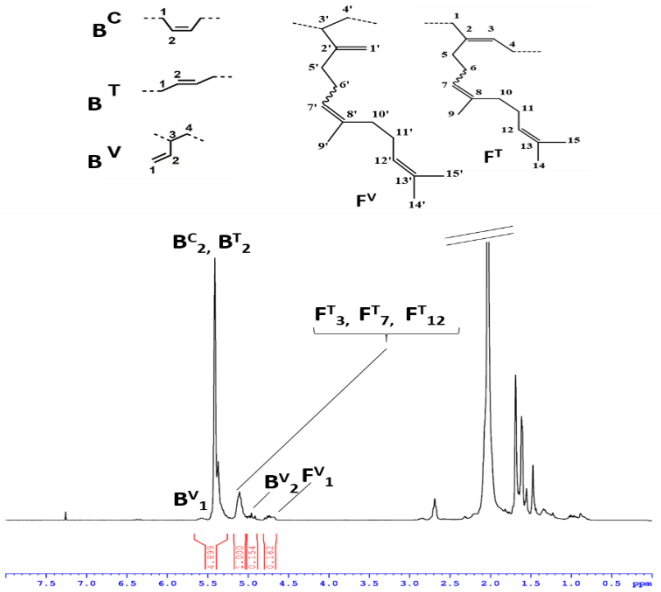

Figure 3S12. ^{1}H **NMR** spectrum ($CDCl_3$, 25 °C, 600 MHz) of PFB from run 13 of Table 5

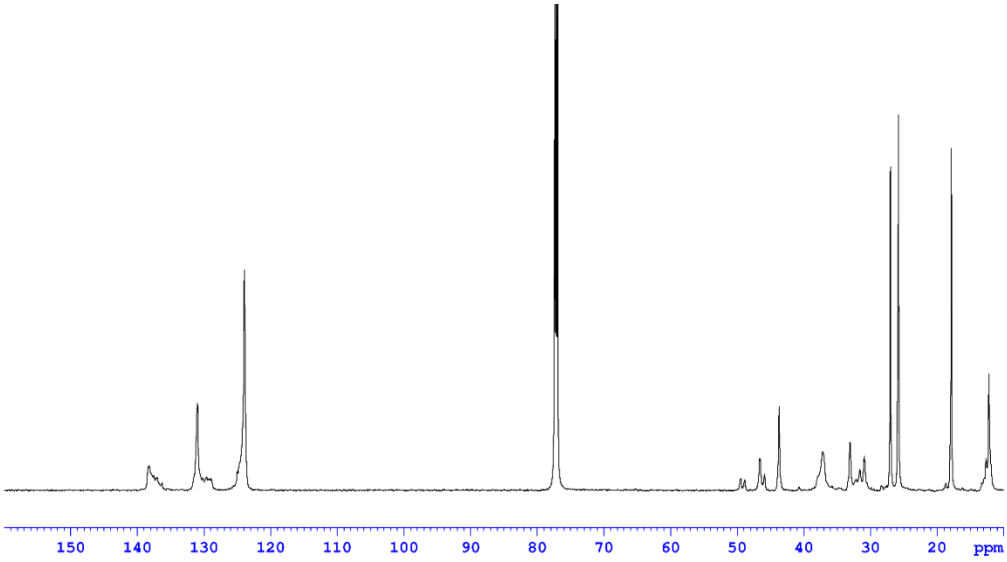

Figure 3S13. ^{13}C **NMR** spectrum ($CDCl_3$, 25 °C, 600 MHz) of POB copolymer from run 1 of Table 1.

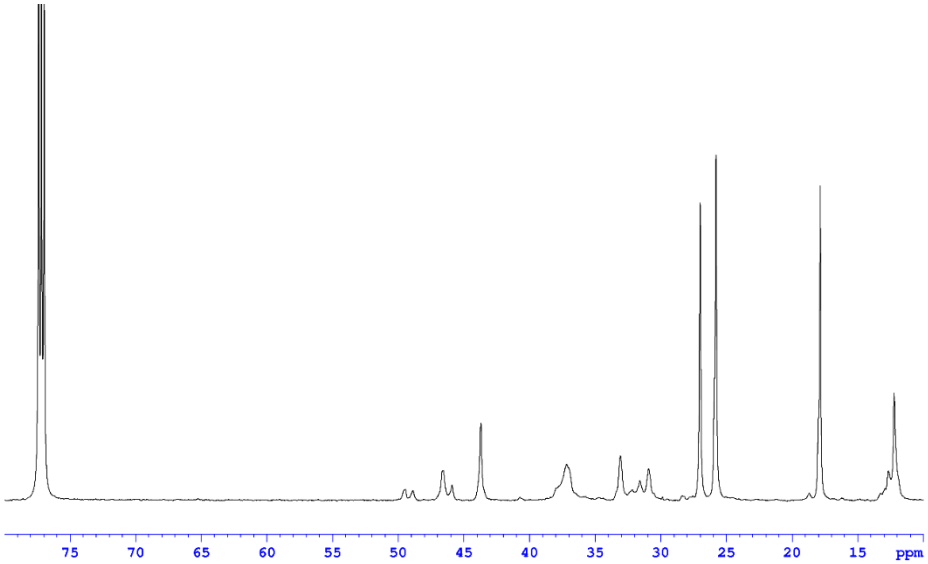

Figure 3S14. Enlargment of aliphatic region of ^{13}C **NMR** spectrum ($CDCl_3$, 25 °C, 600 MHz) of POB copolymer from run 1 of Table 1.

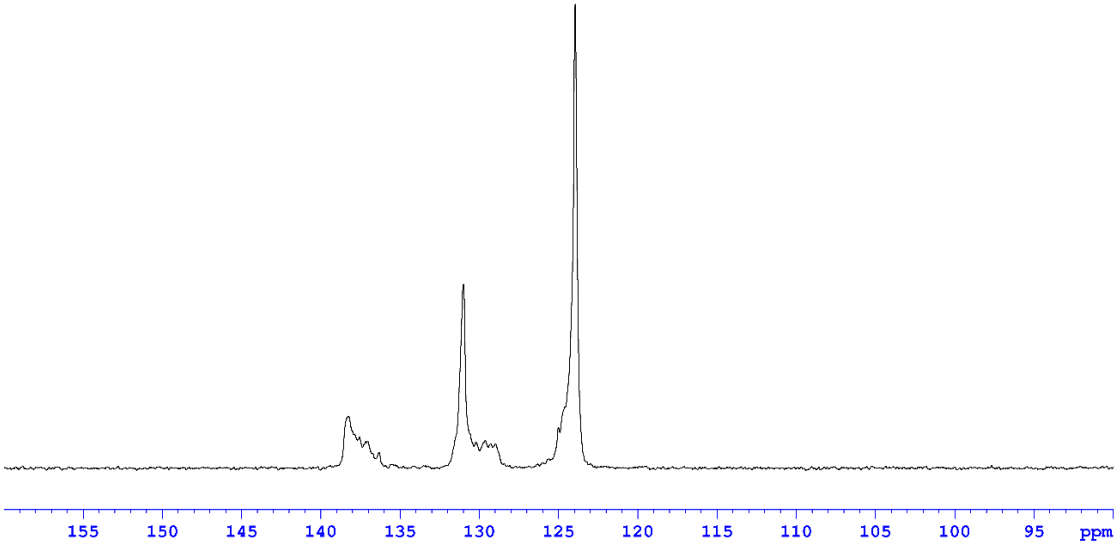

Figure 3S15. Enlargment of olefinic region of ^{13}C **NMR** spectrum ($CDCl_3$, 25 °C, 600 MHz) of POB copolymer from run 1 of Table 1.

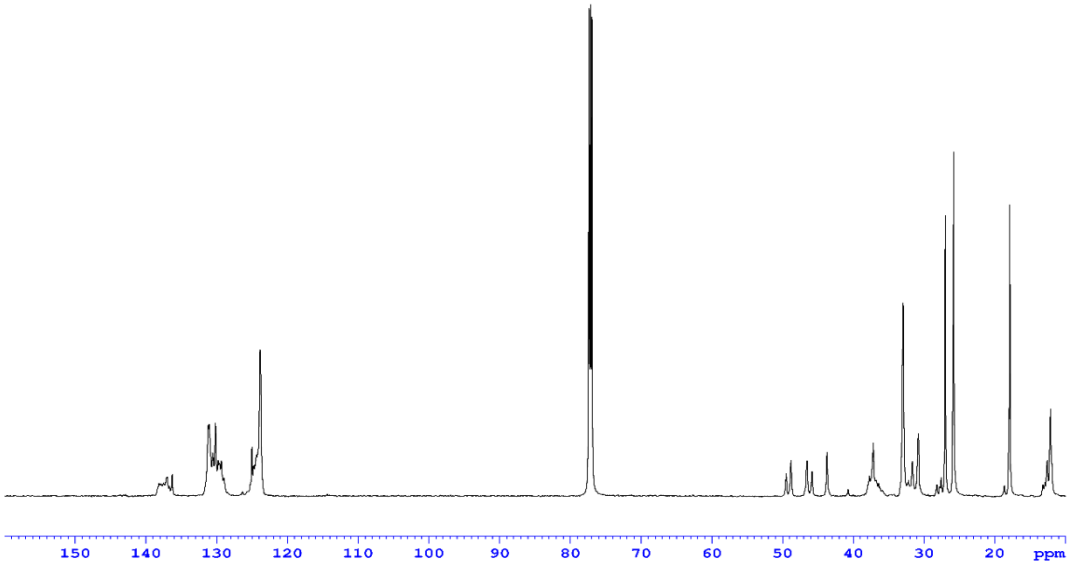

Figure 3S16. ^{13}C **NMR** spectrum ($CDCl_3$, 25 °C, 600 MHz) of POB copolymer from run 2 of Table 1.

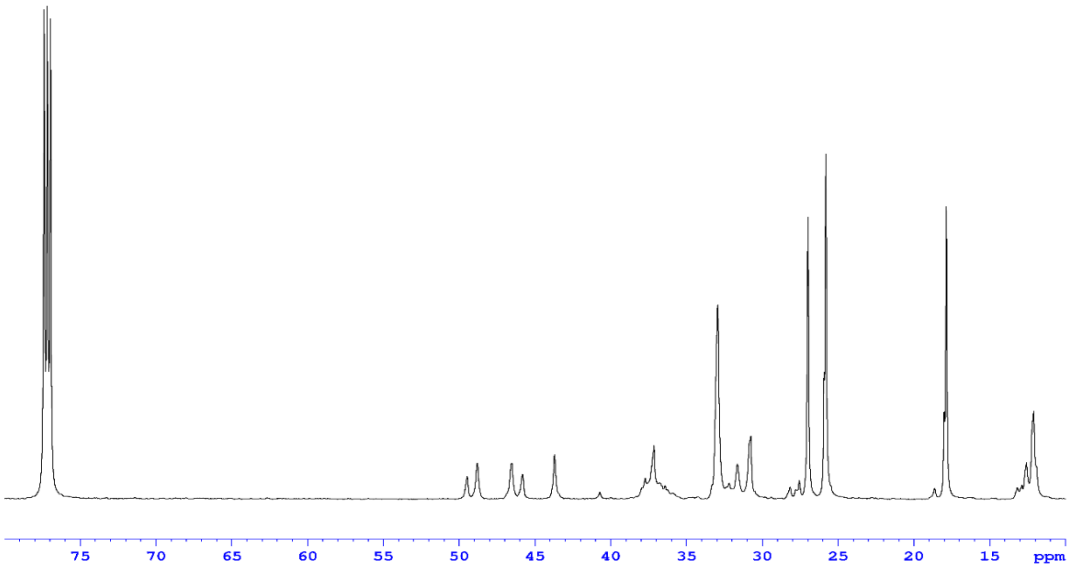

Figure 3S17. Enlargment of aliphatic region of ^{13}C **NMR** spectrum ($CDCl_3$, 25 °C, 600 MHz) of POB copolymer from run 2 of Table 1

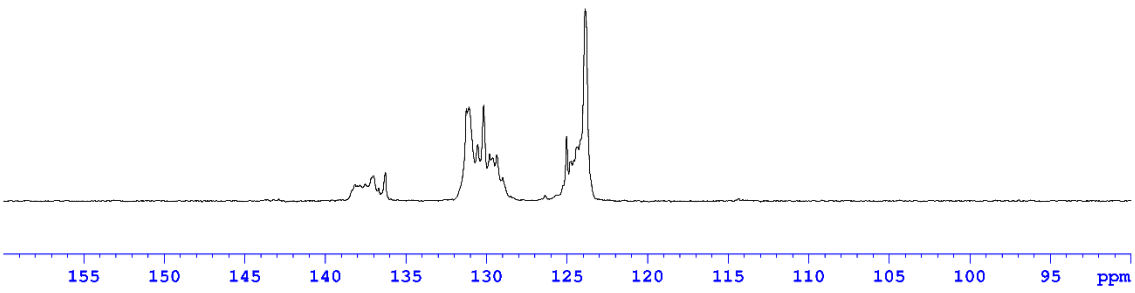

Figure 3S18. Enlargment of olefinic region of ^{13}C **NMR** spectrum ($CDCl_3$, 25 °C, 600 MHz) of POB copolymer from run 2 of Table 1.

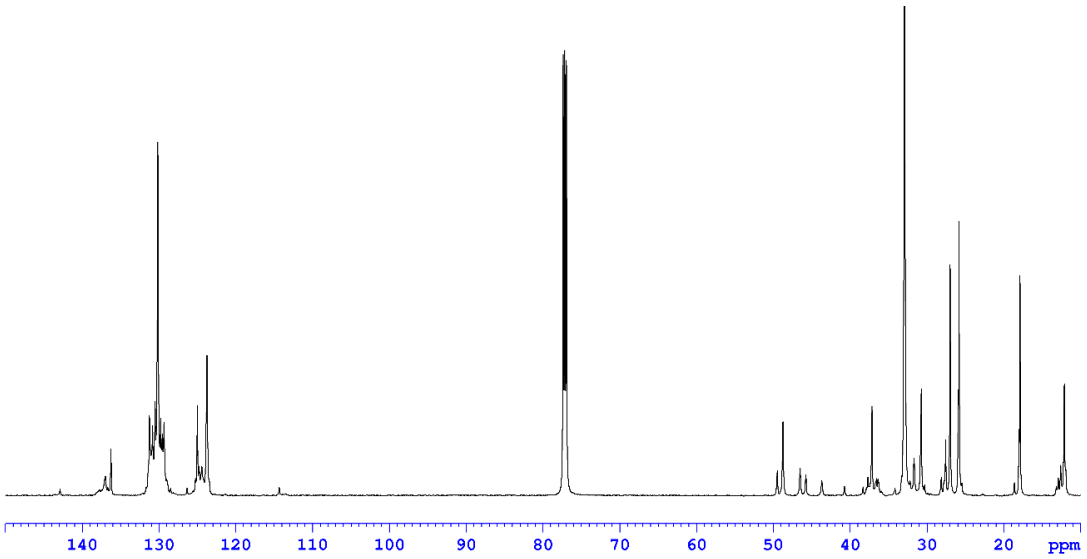

Figure 3S19. ^{13}C **NMR** spectrum ($CDCl_3$, 25 °C, 600 MHz) of POB copolymer from run 3 of Table 1.

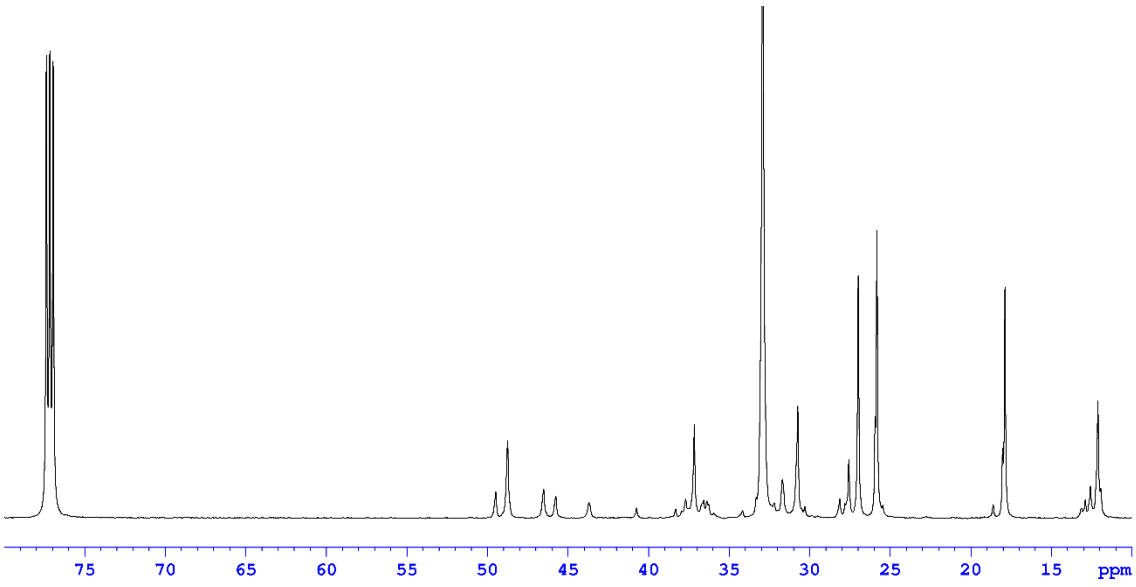

Figure 3S20. Enlargment of aliphatic region of ^{13}C **NMR** spectrum ($CDCl_3$, 25 °C, 600 MHz) of POB copolymer from run 3 of Table 1.

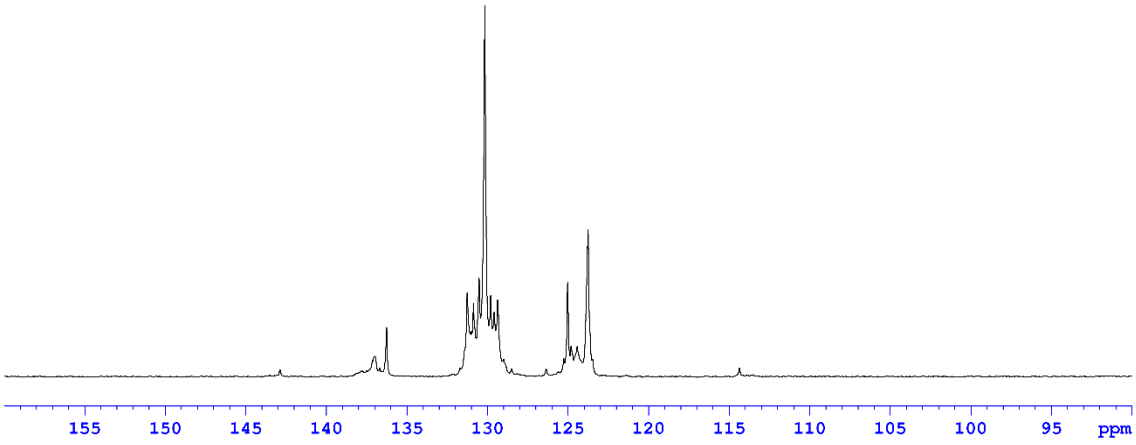

Figure 3S21. Enlargment of olefinic region of ^{13}C **NMR** spectrum ($CDCl_3$, 25 °C, 600 MHz) of POB copolymer from run 3 of Table 1.

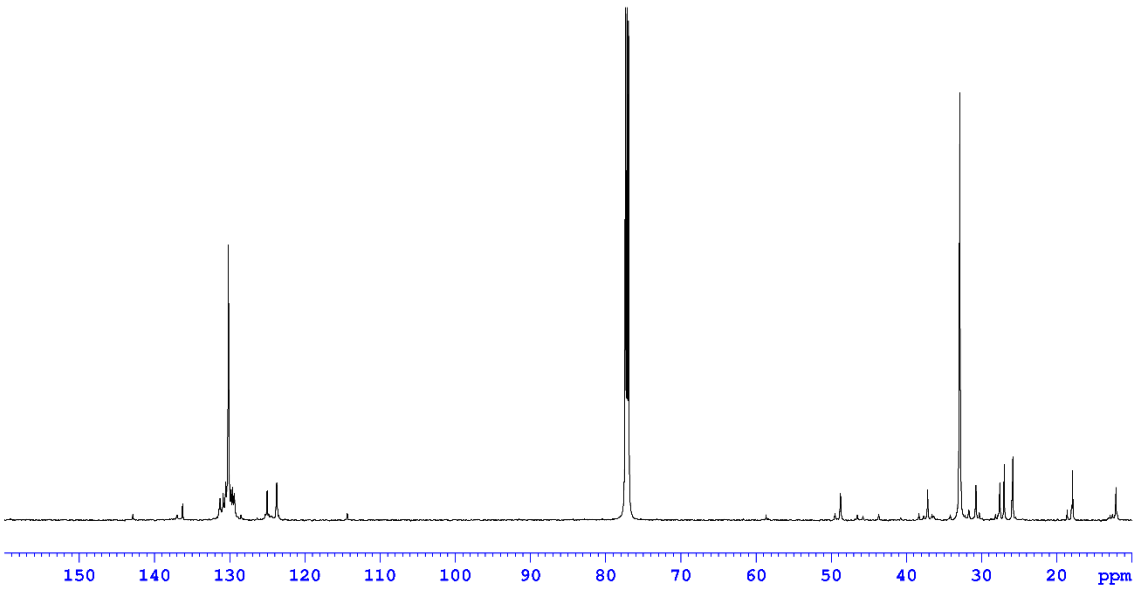

Figure 3S22. ^{13}C **NMR** spectrum ($CDCl_3$, 25 °C, 600 MHz) of POB copolymer from run 4 of Table 1.

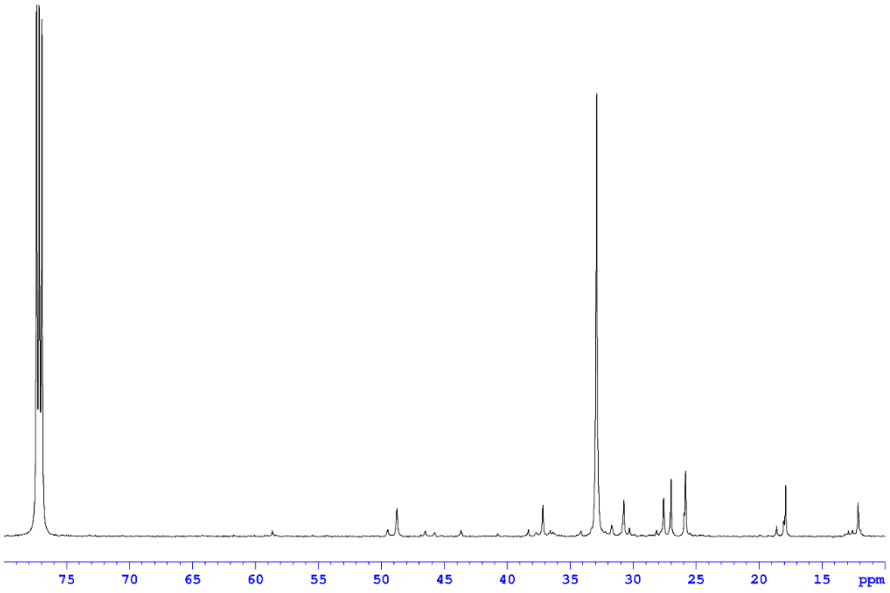

Figure 3S23. Enlargment of aliphatic region of ^{13}C **NMR** spectrum ($CDCl_3$, 25 °C, 600 MHz) of POB copolymer from run 4 of Table 1.

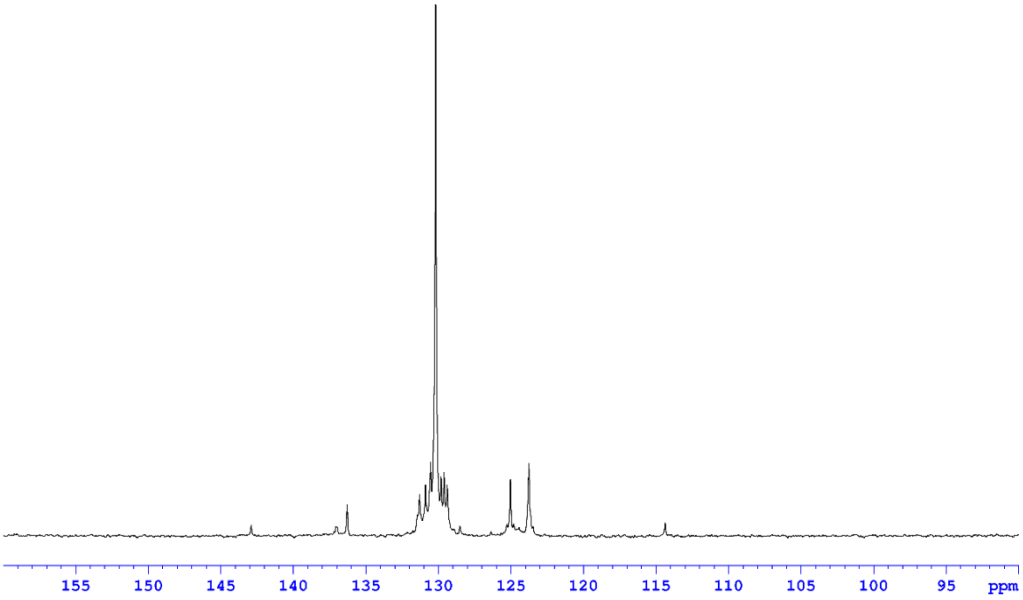

Figure 3S24. Enlargment of olefinic region of ^{13}C **NMR** spectrum ($CDCl_3$, 25 °C, 600 MHz) of POB copolymer from run 4 of Table 1.

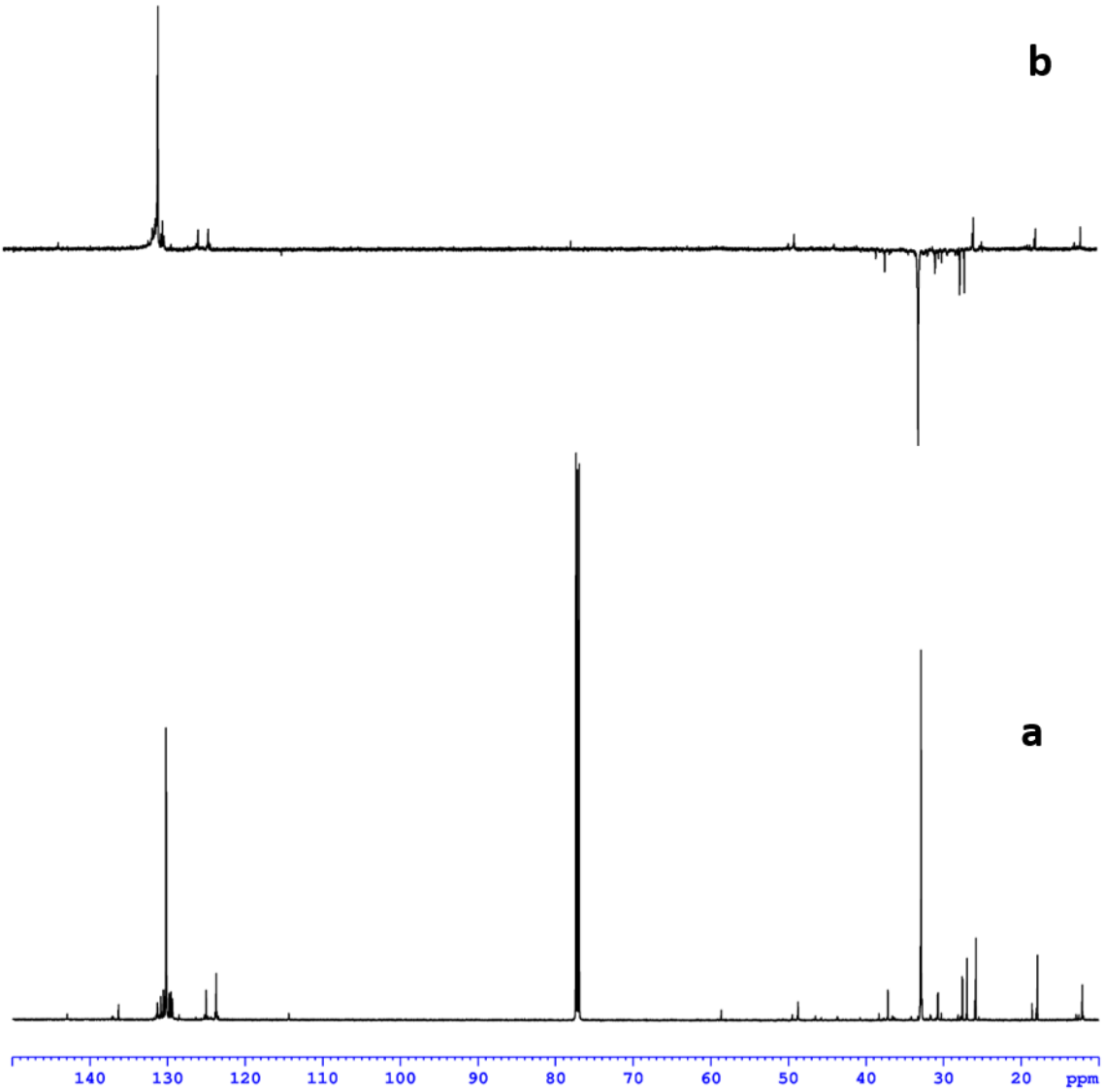

Figure 3S25. DEPT-135 (b) and ^{13}C **NMR** (a) spectra ($CDCl_3$, 25 °C, 600 MHz) of POB copolymer from run 3 of Table 1.

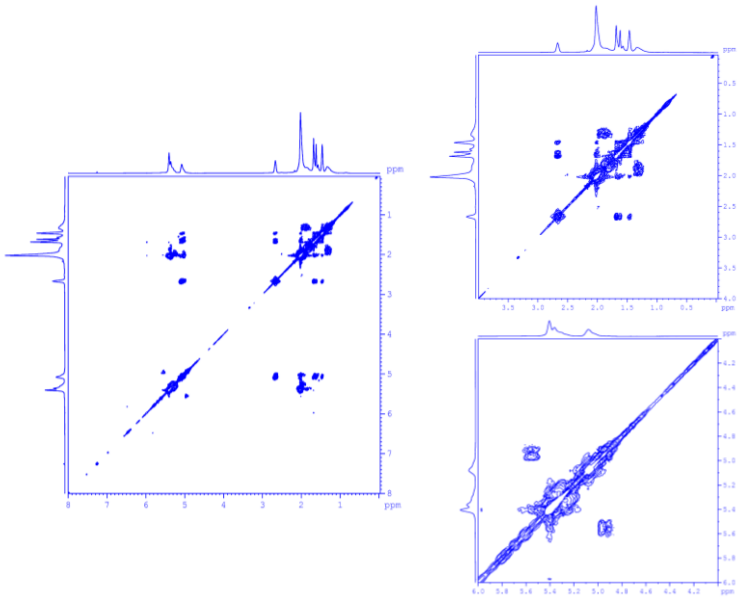

Figure 3S26. ^{1}H-^{1}H COSY spectrum ($CDCl_3$, 25 °C, 600 MHz) of POB copolymer from run 3 of Table 1.

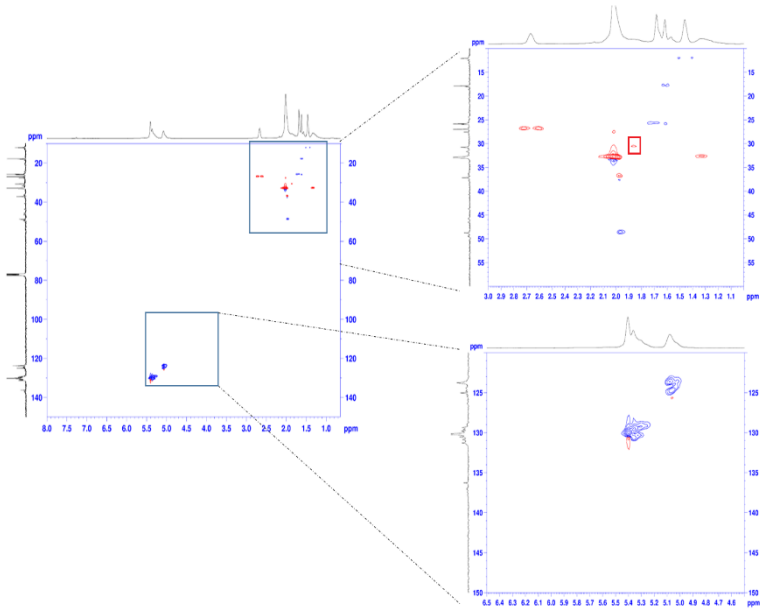

Figure 3S27. ^{13}C-^{1}H HSQC spectrum ($CDCl_3$, 25 °C, 600 MHz) of POB from run 3 of Table 1 with magnification of diagnostic regions. Methyl and methine signals are displayed in blue while methylenes in red.

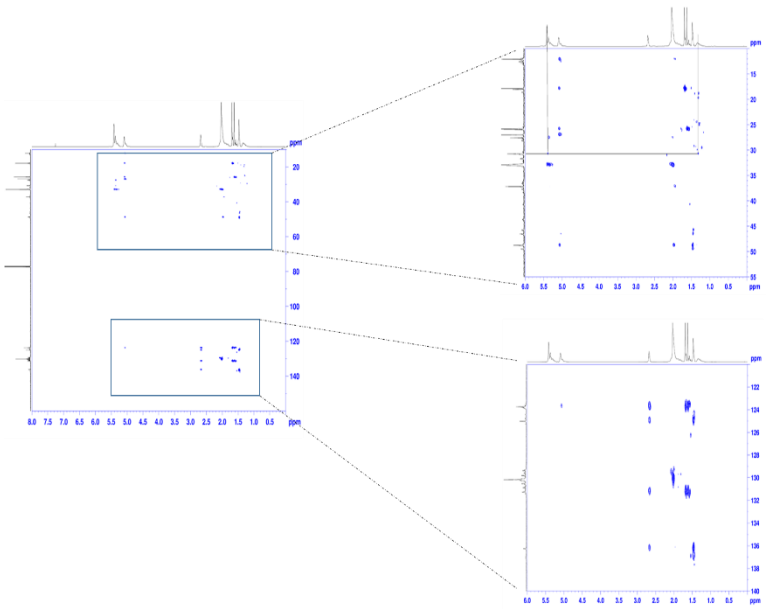

Figure 3S28. HMBC spectrum ($CDCl_3$, 25 °C, 600 MHz) of POB from run 3 of Table 1.

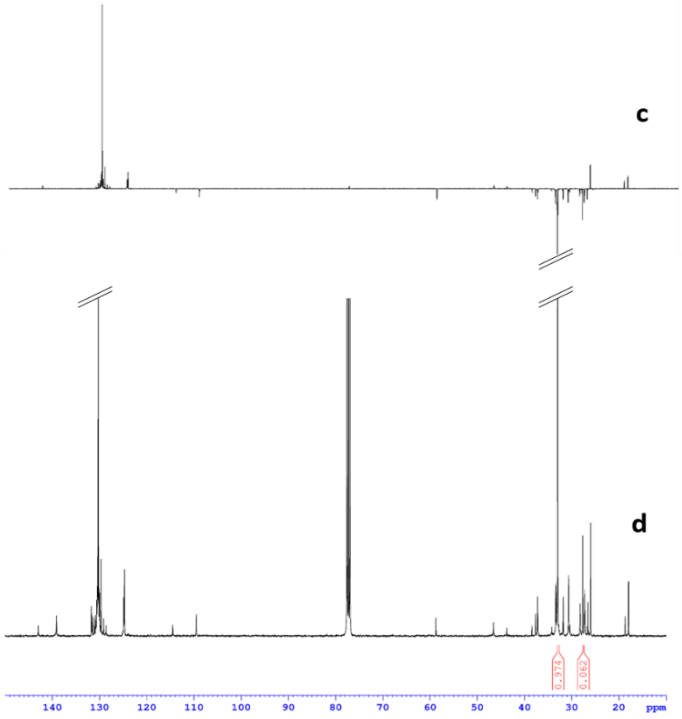

Figure 3S29. DEPT-135 (c) and ^{13}C **NMR** (d) spectra ($CDCl_3$, 25 °C, 600 MHz) of PMB copolymer from run 8 of Table 3.

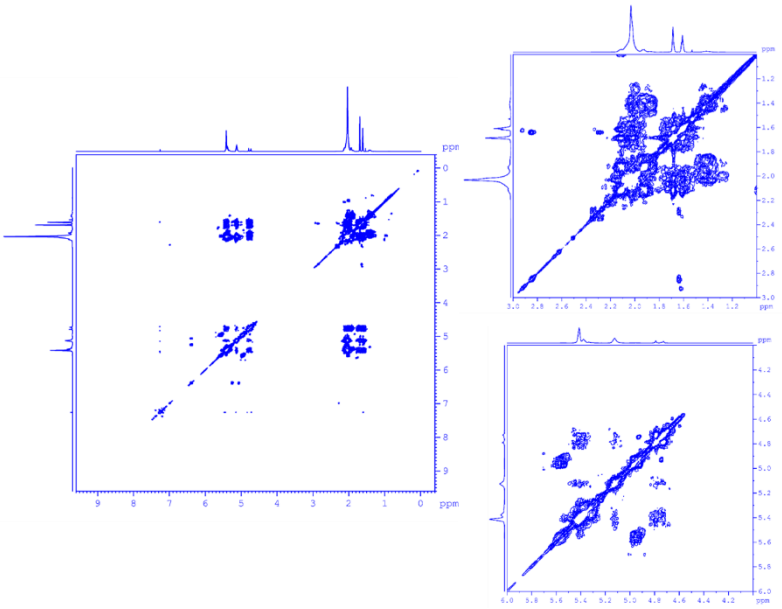

Figure 3S30. ^{1}H-^{1}H COSY spectrum ($CDCl_3$, 25 °C, 400 MHz) of PMB copolymer from run 6 of Table 3

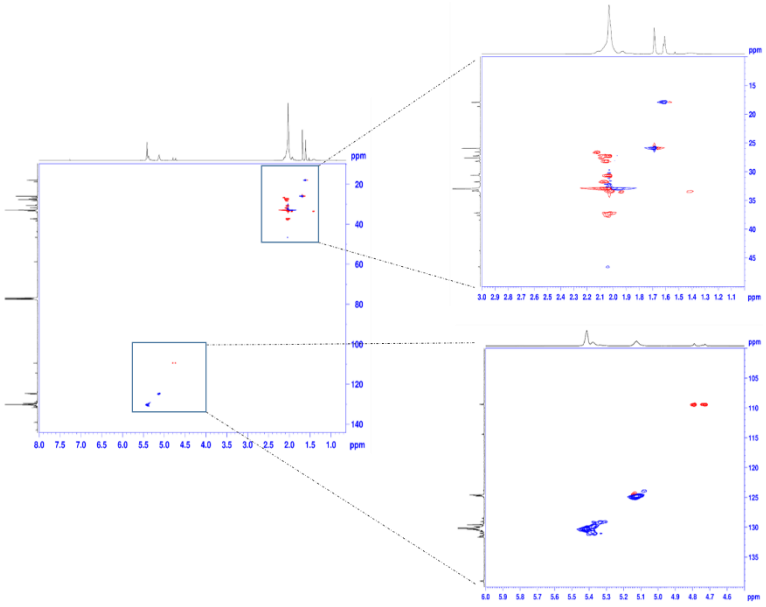

Figure 3S31. ^{13}C-^{1}H HSQC spectrum ($CDCl_3$, 25 °C, 400 MHz) of PMB from run 6 of Table 3 with magnification of diagnostic regions. Methyl and methine signals are displayed in blue while methylenes in red.

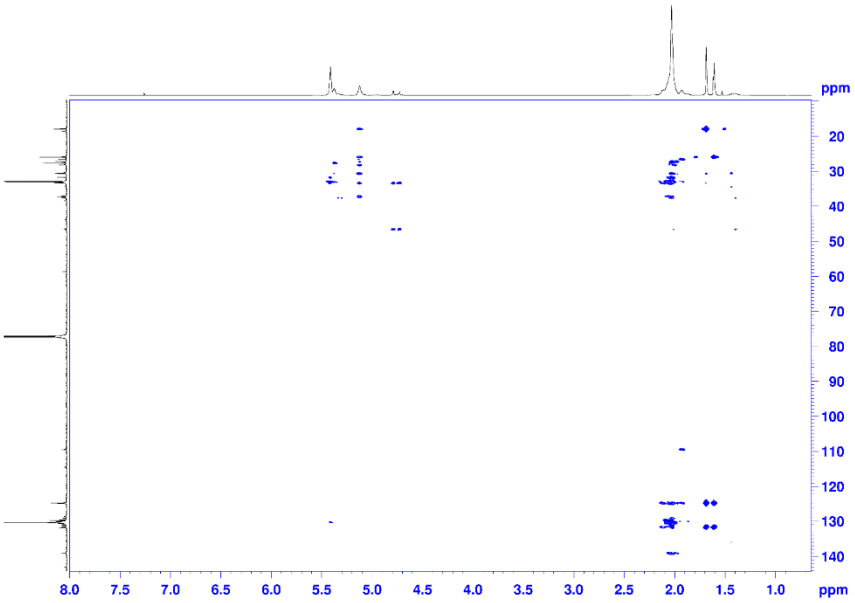

Figure 3S32. HMBC spectrum ($CDCl_3$, 25 °C, 400 MHz) of PMB from run 6 of Table 3.

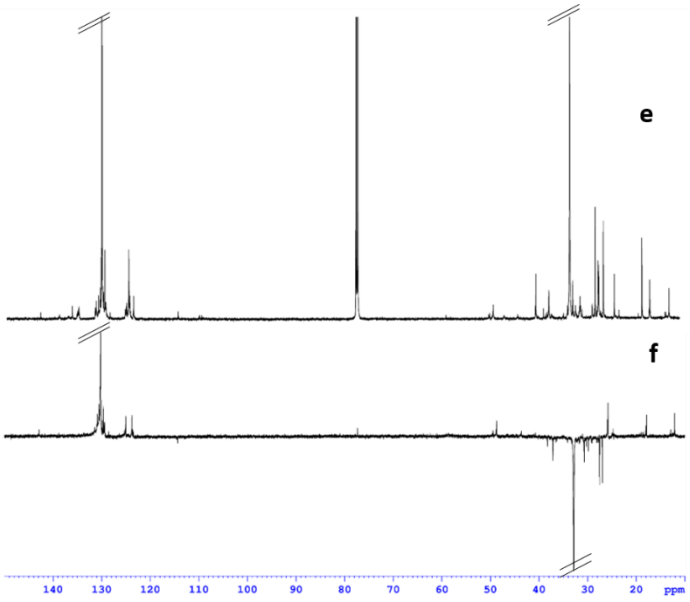

Figure 3S33. DEPT-135 (e) and DEPT-90 (f) spectra ($CDCl_3$, 25 °C, 600 MHz) of PFB copolymer from run 13 of Table 5.

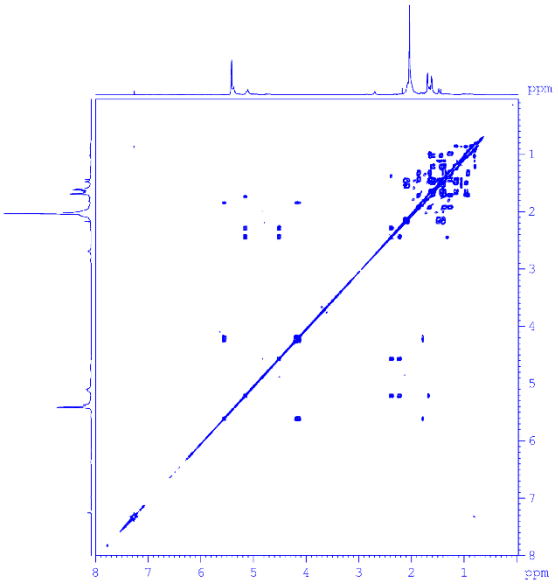

Figure 3S34. ^{1}H-^{1}H COSY spectrum ($CDCl_3$, 25 °C, 600 MHz) of PFB copolymer from run 13 of Table 5.

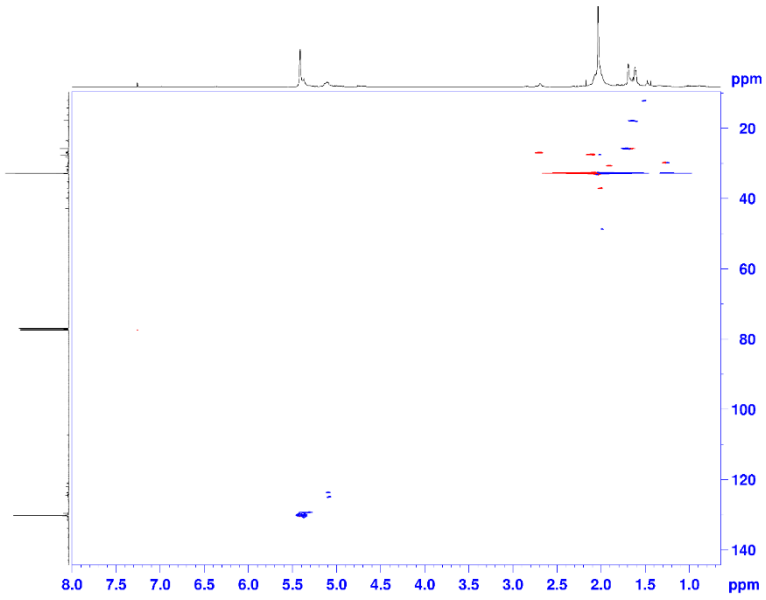

Figure 3S35. ^{13}C-^{1}H HSQC spectrum ($CDCl_3$, 25 °C, 600 MHz) of PFB from run 13 of Table 5. Methyl and methine signals are displayed in blue while methylenes in red.

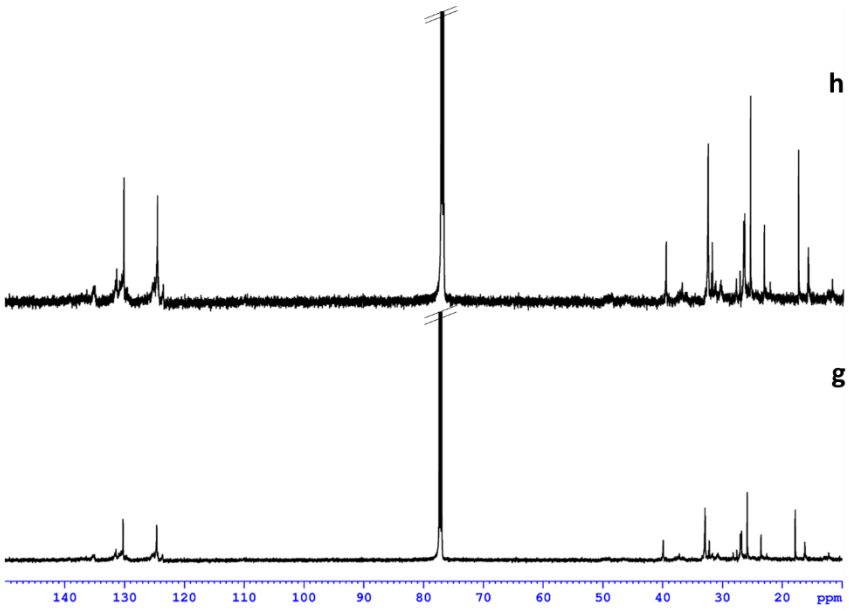

Figure 3S36. ^{13}C spectrum ($CDCl_3$, 25 °C, 600 MHz) of PFB from run 10 (g) of Table 5 and ^{13}C spectrum ($CDCl_3$, 25 °C, 600 MHz) of PFB from run 11 (h) of Table 5.

3.2 Determination of Polymer Compositions

2.1 Determination of $\mathbf{O^V}$ and $\mathbf{O^T}$ contents in POB copolymers by ^{13}C **NMR** ($CDCl_3$, 25 °C)

- $O^V(mol\%) = \frac{A_B}{A_B + \frac{A_A}{2}} \cdot 100$ **Equation 1**

Where $\boldsymbol{A_A}$ is the area of the signals $\mathbf{O^T_1}$ and $\mathbf{O^T_6}$ (δ=31.7 ppm) and $\boldsymbol{A_B}$ is the area of the signal $\mathbf{O^V_6}$ (δ=27.0 ppm).

- $O^T(mol\%) = 100 - O^V(mol\%)$ **Equation 2**

2.2 Determination of $\mathbf{B^C}$ and $\mathbf{B^T}$ contents in POB and PMB copolymers by ^{13}C **NMR** ($CDCl_3$, 25 °C)

- $B^C(mol\%) = \frac{\frac{A_k}{2}}{\frac{A_k}{2} + \frac{A_l}{2}} \cdot 100$ **Equation 3**

Where $\boldsymbol{A_K}$ is the area of the $\mathbf{B^C_1}$ and $\mathbf{B^C_4}$ carbons (δ=27.5 ppm) and $\boldsymbol{A_l}$ is the area of the $\mathbf{B^T_1}$ and $\mathbf{B^T_4}$ carbons (δ=32.9 ppm).

- $B^T(mol\%) = 100 - B^C(mol\%)$ **Equation 4**

2.3 Determination of 1, 2-structure and 1, 4-structure (cis and trans) of B contents in POB, PMB e PFB copolymers by ^{1}H **NMR** ($CDCl_3$, 25 °C)

- $B^{1,2}(mol\%) = \frac{A_d/_2}{\frac{A_{a+b+c} - A_d/2}{2} + A_d/_2} \cdot 100$ **Equation 5**

Where $\mathbf{A_{a+b+c}}$ represents the integrated area of $\mathbf{B^C_2}$, $\mathbf{B^T_2}$ and $\mathbf{B^V_2}$ (δ= 5.20-5.70 ppm), and $\mathbf{A_d}$ is the area of $\mathbf{B^V_1}$ (δ= 4.91-4.98 ppm).

- $B^{1,4}(mol\%) = 100 - B^{1,2}(mol\%)$ **Equation 6**

2.4 Determination of MV and MT contents in PMB copolymers by ^{1}H **NMR** ($CDCl_3$, 25 °C)

- $M^V(mol\%) = \frac{B_B}{B_A + \frac{B_B}{2}} \cdot 100$ **Equation 7**

Where $\boldsymbol{B_A}$ is the area of the signals $\mathbf{M^T_3}$, $\mathbf{M^T_7}$ and $\mathbf{M^V_7}$ (δ = 5.12 ppm) and $\boldsymbol{B_B}$ is the area of the signal $\mathbf{M^V_1}$ (δ = 4.72, 4.79 ppm).

- $M^T(mol\%) = 100 - M^V(mol\%)$ **Equation 8**

2.5 Determination of total B contents in POB copolymers by ^{13}C **NMR** ($CDCl_3$, 25 °C)

- $$B(mol\%) = \frac{\frac{A_k}{2}+\frac{A_l}{2}}{\frac{A_k}{2}+\frac{A_l}{2}+A_B+\frac{A_A}{2}}$$ **Equation 9**

Where $\boldsymbol{A_K}$ is the area of the $\mathbf{B^{C}_1}$ and $\mathbf{B^{C}_4}$ carbons (δ=27.5 ppm) and $\boldsymbol{A_I}$ is the area of the $\mathbf{B^{T}_1}$ and $\mathbf{B^{T}_4}$ carbons (δ=32.9 ppm); $\boldsymbol{A_A}$ is the area of the signals $\mathbf{O^{T}_1}$ and $\mathbf{O^{T}_6}$ (δ=31.7 ppm) and $\boldsymbol{A_B}$ is the area of the signal $\mathbf{O^{V}_6}$ (δ=27.0 ppm).

2.6 Determination of total B contents in PMB copolymers by ^{1}H **NMR** ($CDCl_3$, 25 °C)

- $$B(mol\%) = \frac{\frac{A_{a+b+c}-A_d/2}{2}+{A_d}/{2}}{\frac{A_{a+b+c}-A_d/2}{2}+{A_d}/{2}+\frac{B_A+{B_B}/{2}}{2}}$$ **Equation 10**

Where $\mathbf{A_{a+b+c}}$ represents the integrated area of polybutadiene $\mathbf{H_a}$, $\mathbf{H_b}$ and $\mathbf{H_c}$ (δ= 5.20-5.70 ppm), $\mathbf{A_d}$ is the area of $\mathbf{H_d}$ (δ= 4.91-4.98 ppm); $\boldsymbol{B_A}$ is the area of the myrcene signals $\mathbf{M^{T}_3}$, $\mathbf{M^{T}_7}$ and $\mathbf{M^{V}_7}$ (δ = 5.12 ppm) and $\boldsymbol{B_B}$ is the area of the myrcene signal $\mathbf{M^{V}_1}$ (δ = 4.72, 4.79 ppm).

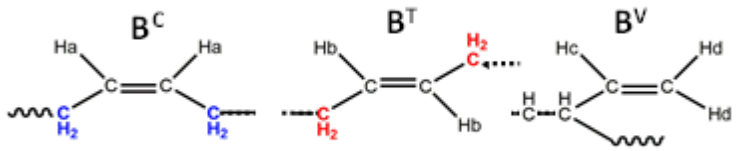

2.7 Determination of $\mathbf{F^{C}}$, $\mathbf{F^{T}}$ and $\mathbf{F^{V}}$ contents in PFB copolymers by ^{1}H **NMR** ($CDCl_3$, 25 °C)

- $$F^{T+C}(mol\%) = \frac{\frac{C_A}{3}}{\frac{C_A}{3}+\frac{C_B}{2}} \cdot 100$$ **Equation 11**

Where $\boldsymbol{C_A}$ is the integrated area of the signals $\mathbf{F^{T}_3}$, $\mathbf{F^{T}_7}$ and $\mathbf{F^{T}_{12}}$ (δ= 5.10 ppm) and $\boldsymbol{C_B}$ is the integrated area of the signal $\mathbf{F^{V}_1}$ (δ= 4.66-4.81ppm).

- $$F^{v}(mol\%) = 100 - F^{T+C}(mol\%)$$ **Equation 12**

2.8 Determination of total B contents in PFB copolymers by ^{1}H **NMR** ($CDCl_3$, 25 °C)

- $$B(mol\%) = \frac{\frac{A_{a+b+c}-A_d/2}{2}+{A_d}/{2}}{\frac{A_{a+b+c}-A_d/2}{2}+{A_d}/{2}+\frac{C_A}{3}+\frac{C_B}{2}}$$ **Equation 13**

- $$F(mol\%) = 100 - B(mol\%)$$ **Equation 14**

Where $\mathbf{A_{a+b+c}}$ represents the integrated area of polybutadiene $\mathbf{H_a}$, $\mathbf{H_b}$ and $\mathbf{H_c}$ (δ= 5.20-5.70 ppm), $\mathbf{A_d}$ is the area of $\mathbf{H_d}$ (δ= 4.91-4.98 ppm); C_A is the integrated area of the 1,4 polyfarnesene signals $\mathbf{F^T_3}$, $\mathbf{F^T_7}$ and $\mathbf{F^T_{12}}$ (δ= 5.10 ppm) and C_B is the integrated area of the 3,4 polyfarnesene signal $\mathbf{F^V_1}$ (δ= 4.66-4.81ppm).

3.3 DSC Thermal Analyses

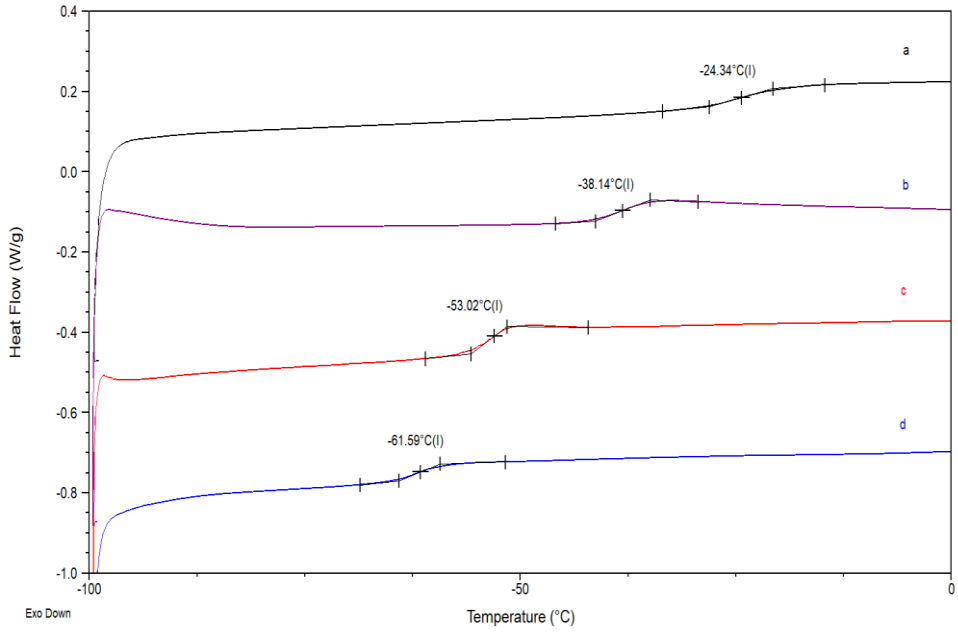

Figure 3S37. DSC thermograms of POB copolymer from run 1 (a), 2 (b), 3 (c) and 4 (d) of Table 1.

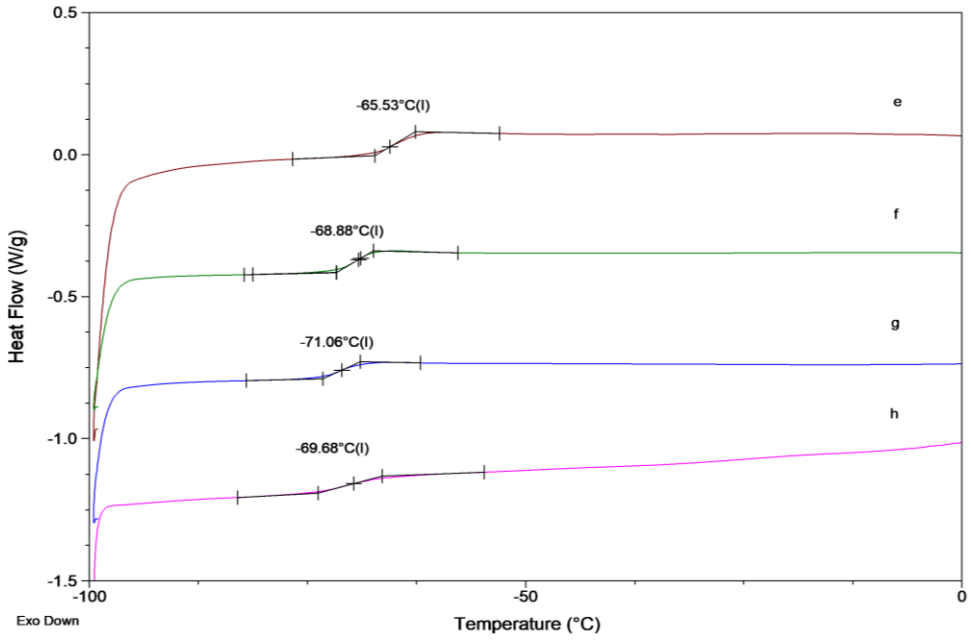

Figure 3S38. DSC thermograms of PMB copolymer from run 5 (e), 6 (f), 7 (g) and 8 (h) of Table 3.

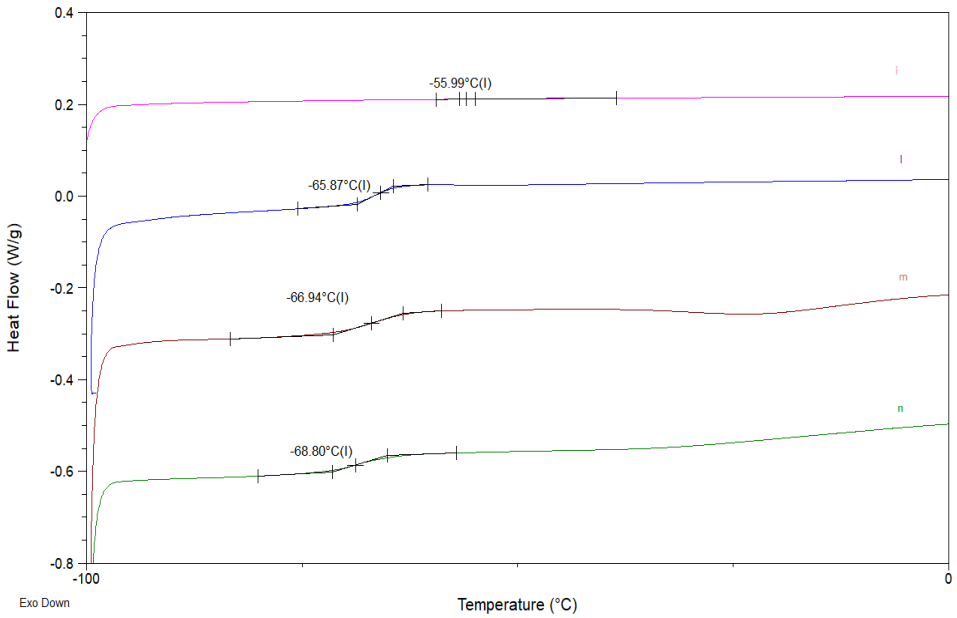

Figure 3S39. DSC thermograms of PFB copolymer from run 10 (i), 11 (l), 12 (m) and 13 (n) of Table 5.

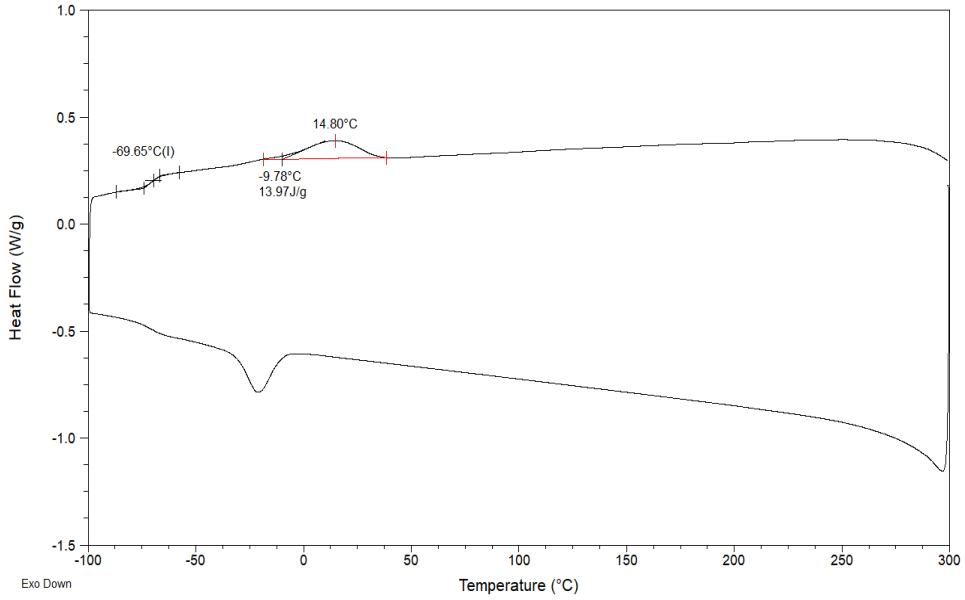

Figure 3S40. DSC thermograms of PFB copolymer from run 8 of Table 3.

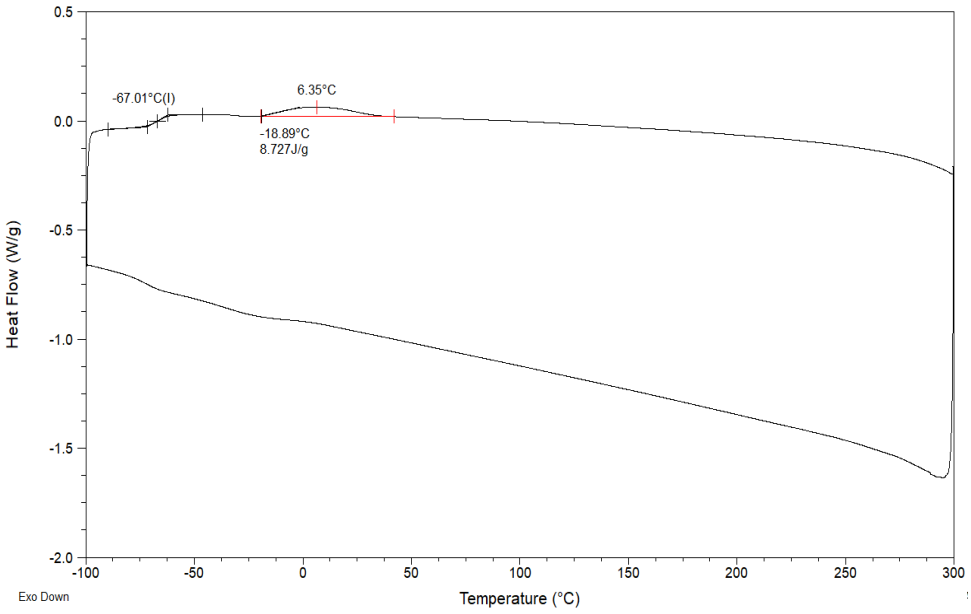

Figure 3S41. DSC thermograms of PFB copolymer from run 12 of Table 5.

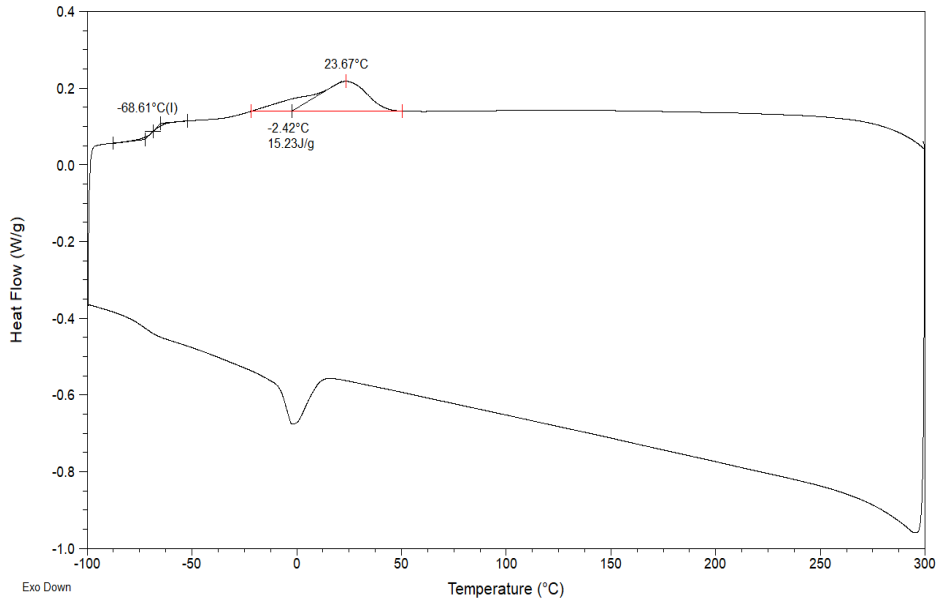

Figure 3S42. DSC thermograms of PFB copolymer from run 13 of Table 5.

3.4 GPC Analyses

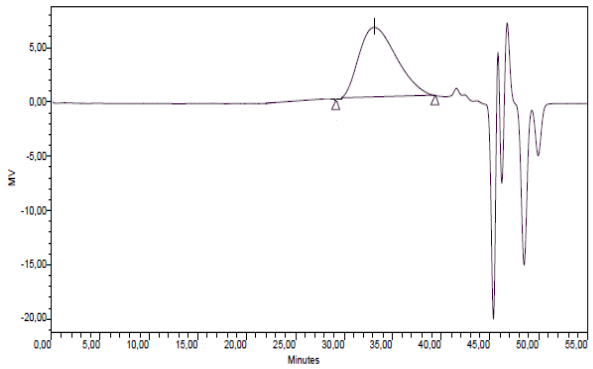

Figure 3S43. GPC curve of PMB copolymer from run 5 of Table 3.

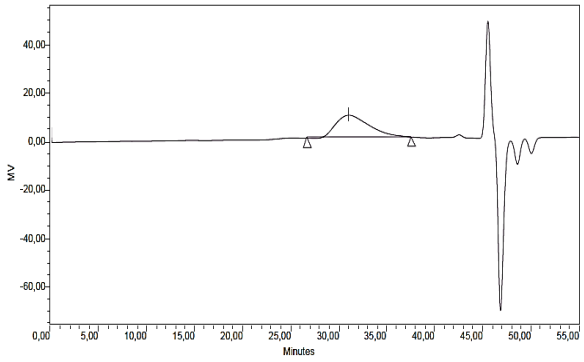

Figure 3S44. GPC curve of PMB copolymer from run 6 of Table 3.

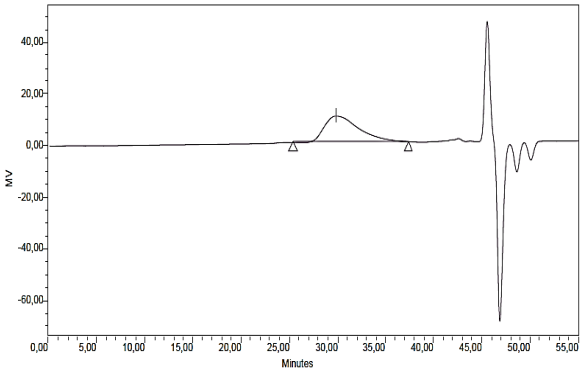

Figure 3S45. GPC curve of PMB copolymer from run 7 of Table 5.

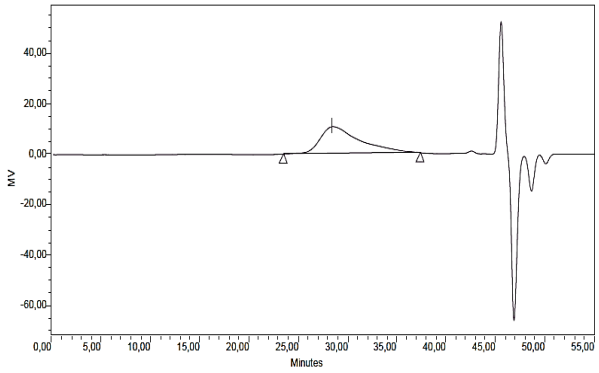

Figure 3S46. GPC curve of PMB copolymer from run 8 of Table 3.

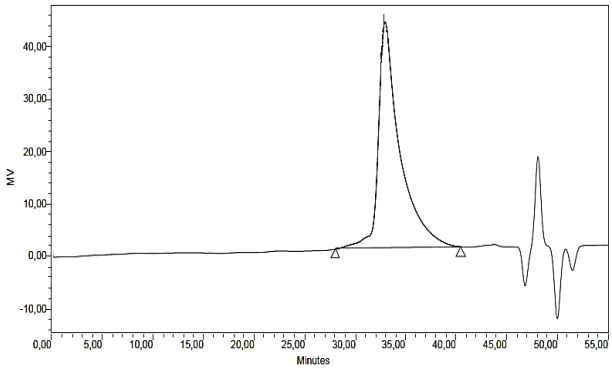

Figure 3S47. GPC curve of POB copolymer from run 1 of Table 1.

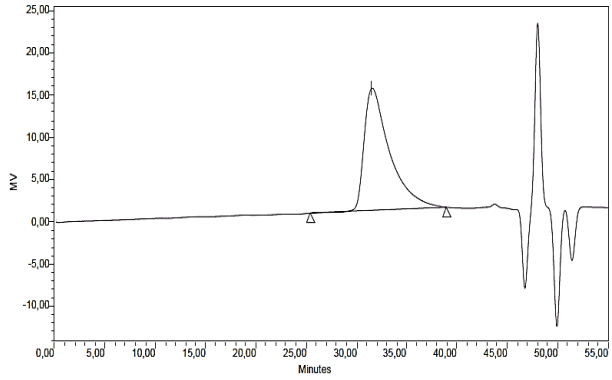

Figure 3S48. GPC curve of POB copolymer from run 2 of Table 1.

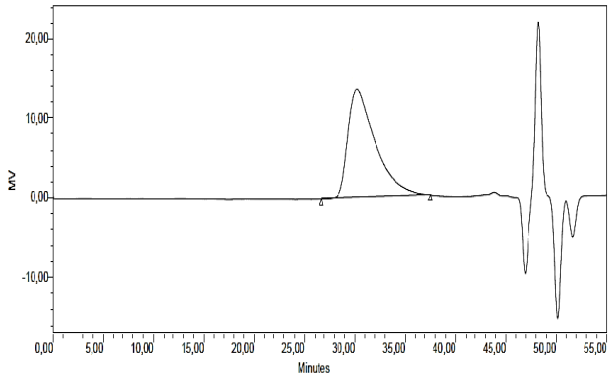

Figure 3S49. GPC curve of POB copolymer from run 3 of Table 1.

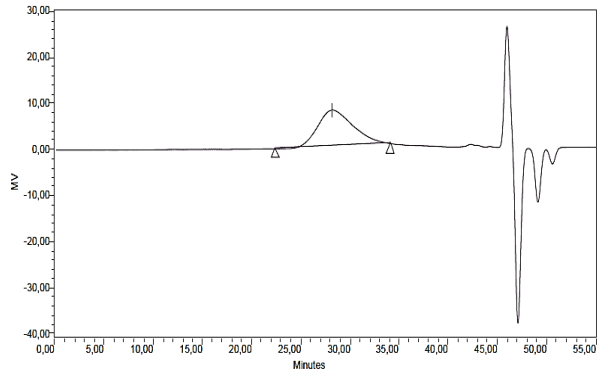

Figure 3S50. GPC curve of POB copolymer from run 4 of Table 1.

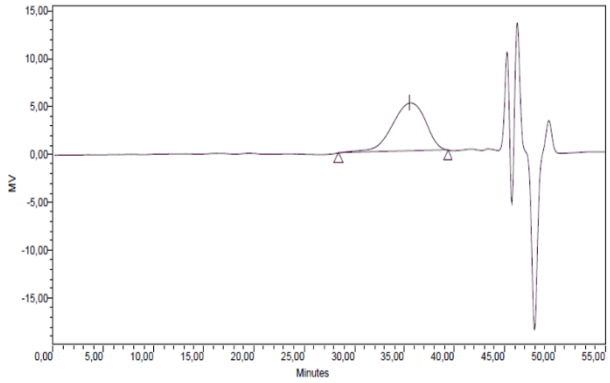

Figure 3S51. GPC curve of PF polymer from run 9 of Table 5.

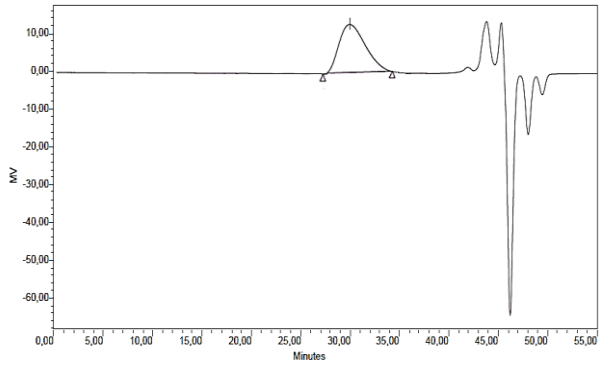

Figure 3S52. GPC curve of PFB copolymer from run 10 of Table 5.

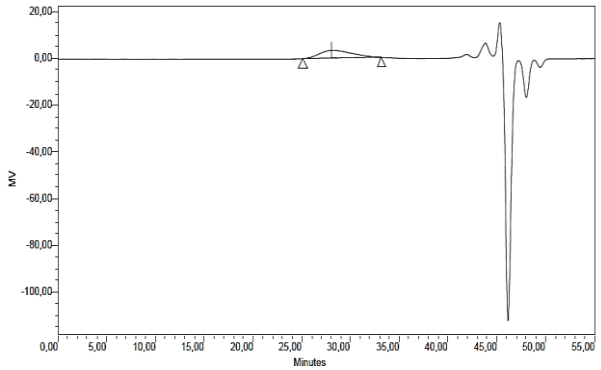

Figure 3S53. GPC curve of PFB copolymer from run 11 of Table 5.

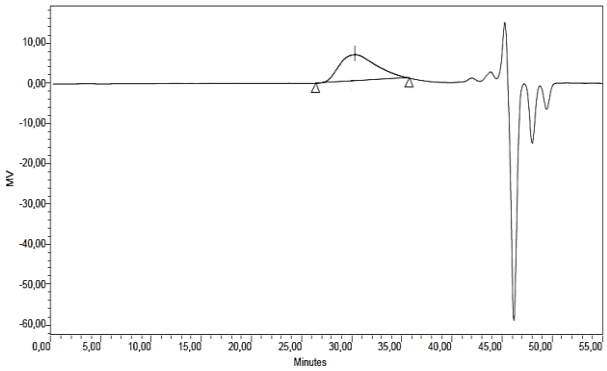

Figure 3S54. GPC curve of PFB copolymer from run 12 of Table 5.

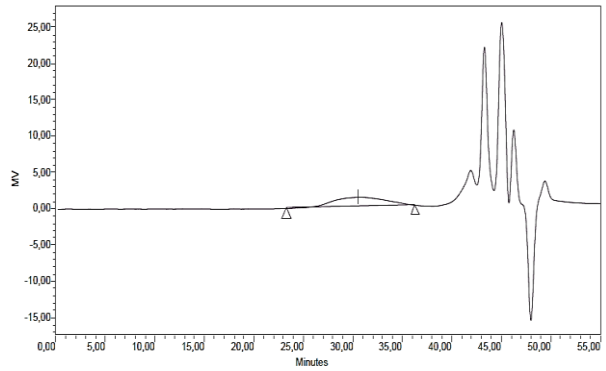

Figure 3S55. GPC curve of PFB copolymer from run 13 of Table 5.

3.5 Further investigations and graphs

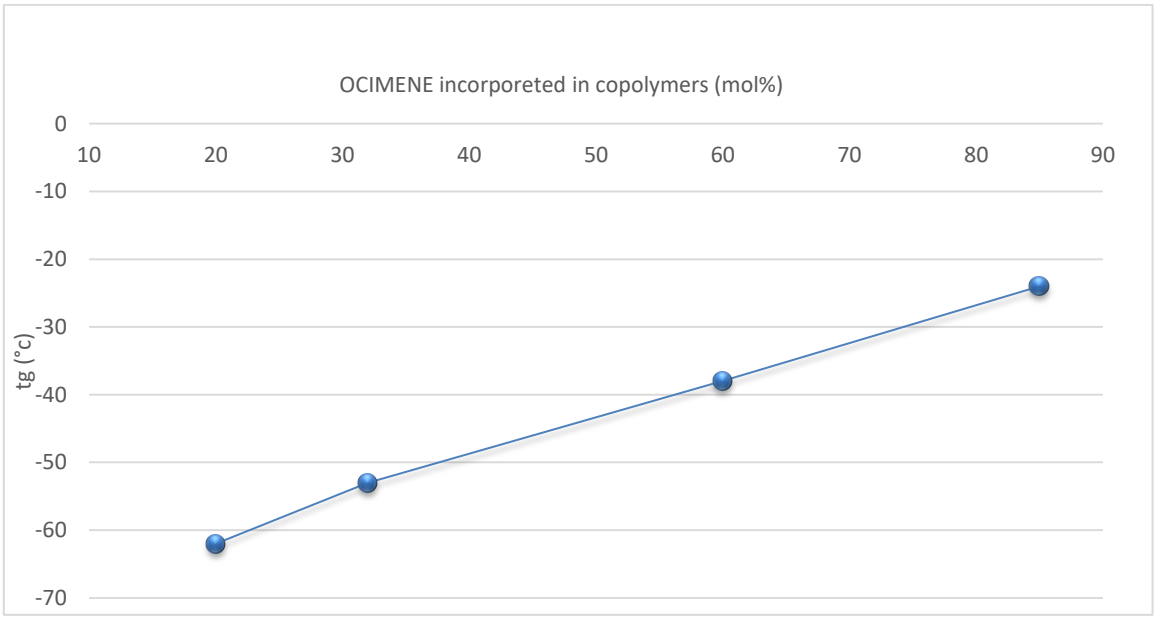

Figure 3S56. Variation of the glass transition temperature (T_g) of POB copolymers as a function of the ocimene content.

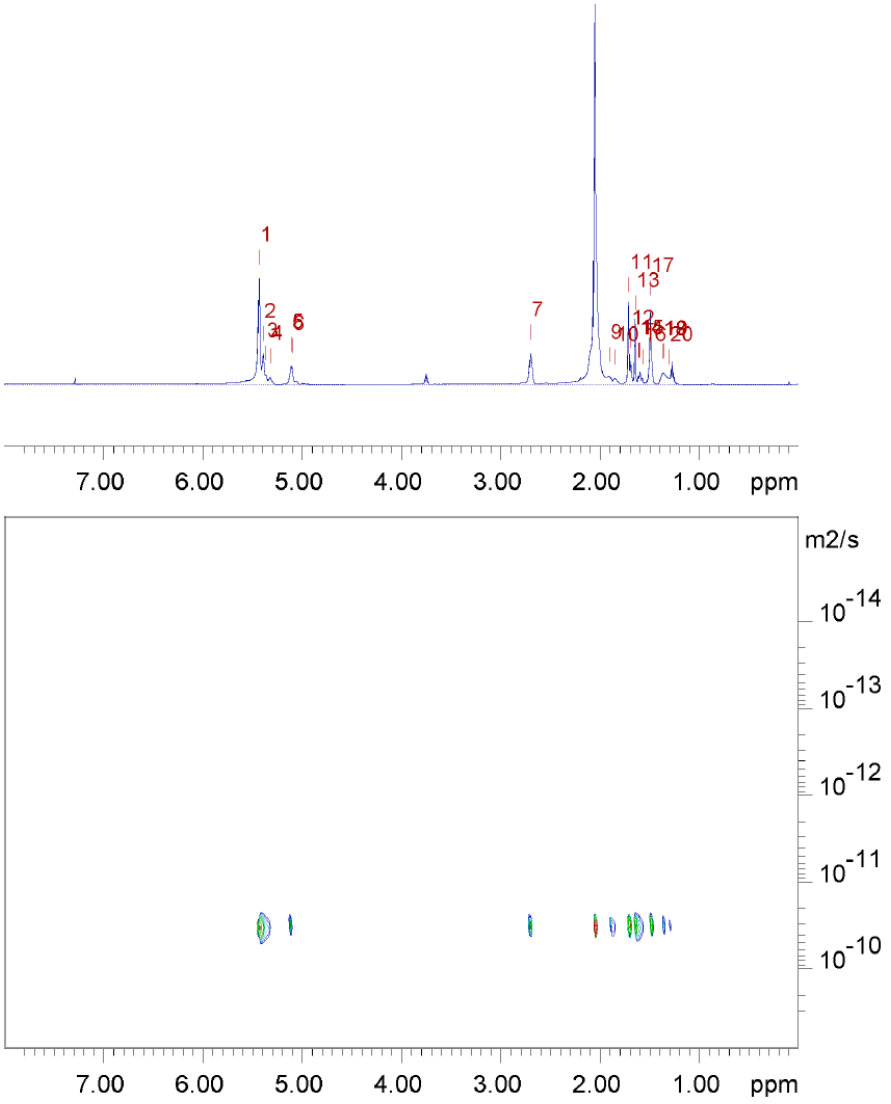

Peak name	F2 [ppm]	D [m2/s]	error
1	5.434	2.82e-11	1.736e-12
2	5.392	2.80e-11	1.738e-12
3	5.364	2.77e-11	1.808e-12
4	5.323	2.80e-11	1.770e-12
5	5.111	2.82e-11	1.784e-12
6	5.100	2.81e-11	1.713e-12
7	2.698	2.81e-11	1.711e-12
8	2.053	2.83e-11	1.754e-12
9	1.908	2.80e-11	2.362e-12
10	1.848	2.83e-11	2.042e-12
11	1.712	2.85e-11	1.794e-12
12	1.691	2.83e-11	2.013e-12
13	1.646	2.86e-11	1.795e-12
14	1.612	3.02e-11	3.826e-12
15	1.600	3.02e-11	3.031e-12
16	1.574	3.04e-11	3.498e-12
17	1.493	2.83e-11	1.756e-12
18	1.371	2.91e-11	2.693e-12
19	1.358	2.93e-11	2.708e-12
20	1.304	3.49e-11	6.889e-12

Figure 3S57. DOSY **NMR** spectrum ($CDCl_3$, 25 °C, 600 MHz) of POB copolymers from run 4 of Table 1.

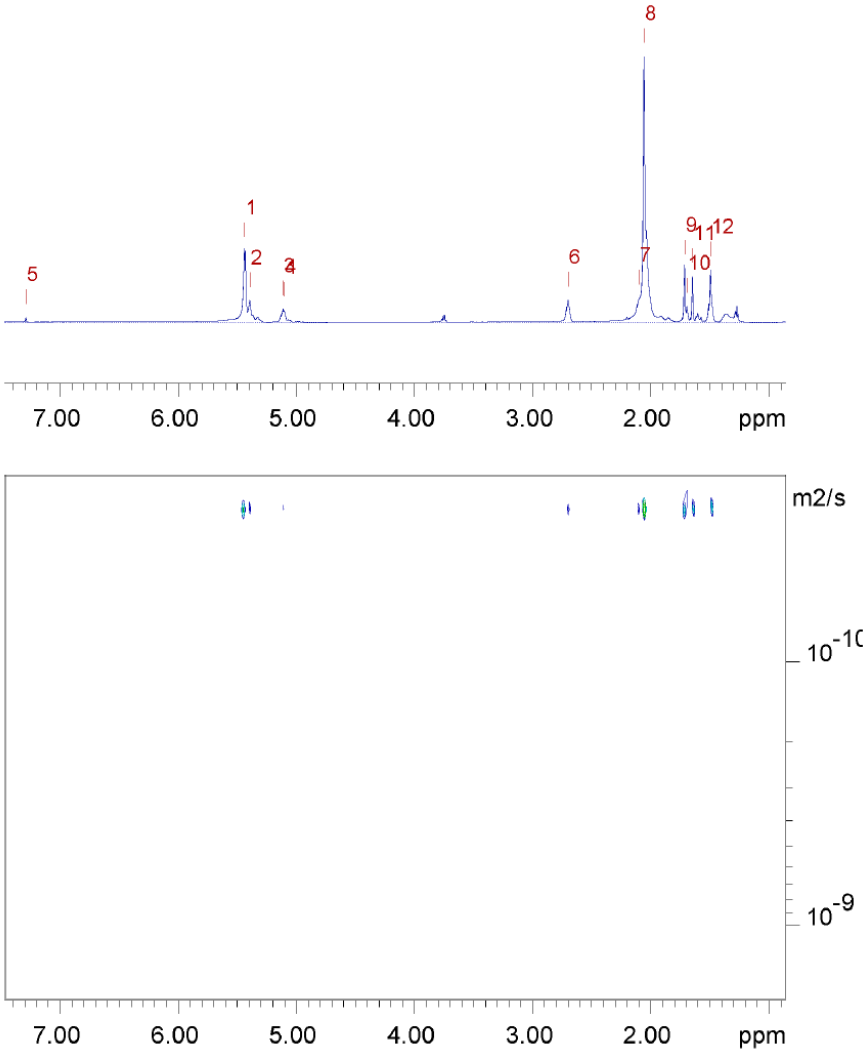

Peak name	F2 [ppm]	D [m2/s]	error
1	5.434	2.82e-11	1.732e-12
2	5.392	2.79e-11	1.725e-12
3	5.113	2.80e-11	1.773e-12
4	5.101	2.80e-11	1.696e-12
5	7.287	1.83e-09	2.876e-10
6	2.700	2.80e-11	1.678e-12
7	2.101	2.74e-11	2.036e-12
8	2.054	2.83e-11	1.748e-12
9	1.713	2.85e-11	1.761e-12
10	1.691	2.83e-11	2.028e-12
11	1.646	2.85e-11	1.760e-12
12	1.494	2.82e-11	1.708e-12

Figure 3S58. DOSY **NMR** spectrum ($CDCl_3$, 25 °C, 600 MHz) of PMB copolymers from run 8 of Table 3.

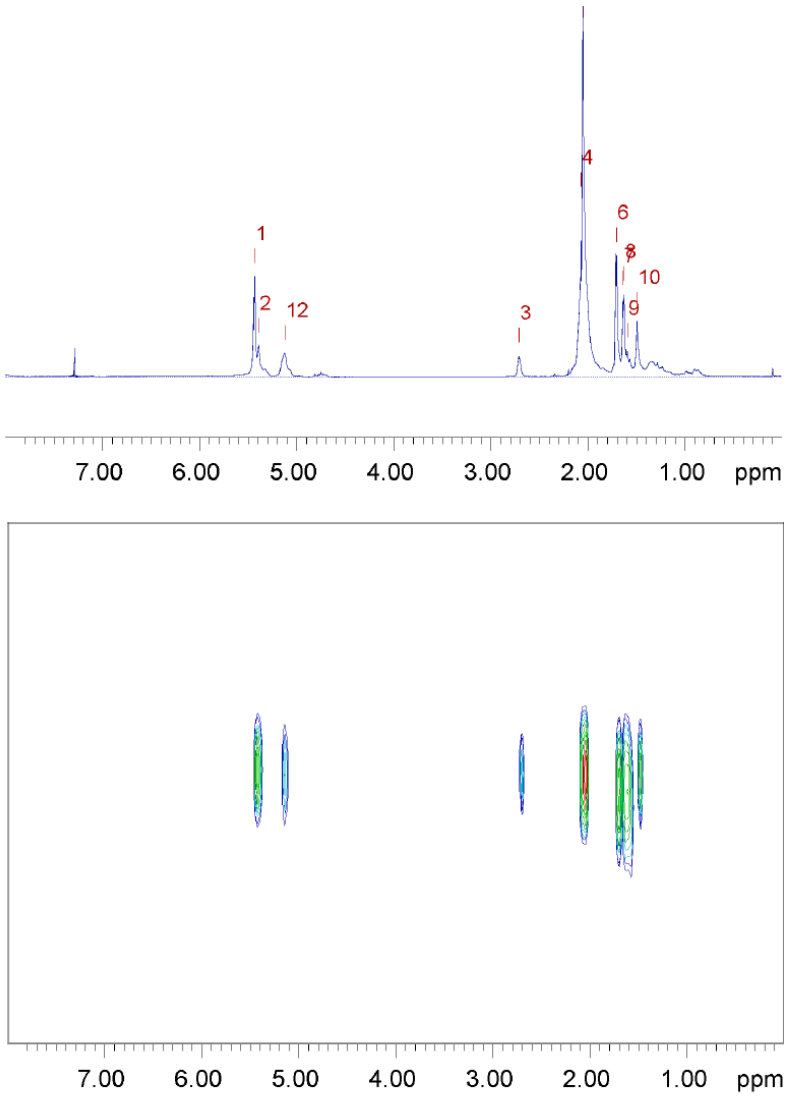

Peak name	F2 [ppm]	D [m2/s]	error
1	5.434	3.81e-11	4.970e-12
2	5.392	3.90e-11	5.498e-12
3	2.709	4.04e-11	5.957e-12
4	2.074	4.13e-11	6.425e-12
5	2.052	3.97e-11	5.215e-12
6	1.707	4.38e-11	7.520e-12
7	1.637	4.51e-11	8.801e-12
8	1.625	4.42e-11	7.716e-12
9	1.595	4.80e-11	1.038e-11
10	1.493	4.06e-11	5.873e-12
11	0.095	5.38e-11	3.753e-12
12	5.124	4.21e-11	6.713e-12

Figure 3S59. DOSY **NMR** spectrum ($CDCl_3$, 25 °C, 600 MHz) of PFB copolymers from run 11 of Table 5.

Chapter 4 – Supporting information

4.1 NMR Characterizations

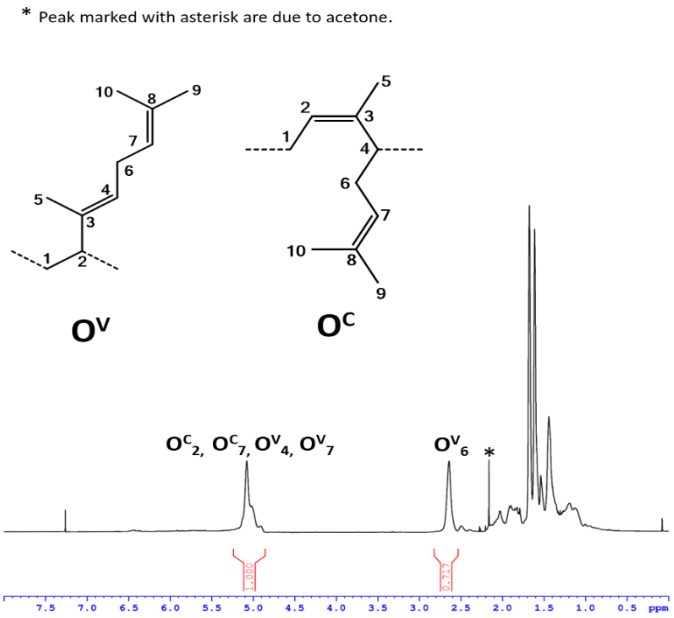

Figure 4S1. ^{1}H **NMR** spectrum ($CDCl_3$, 25 °C, 600 MHz) of PO from run 21 of Table 8.

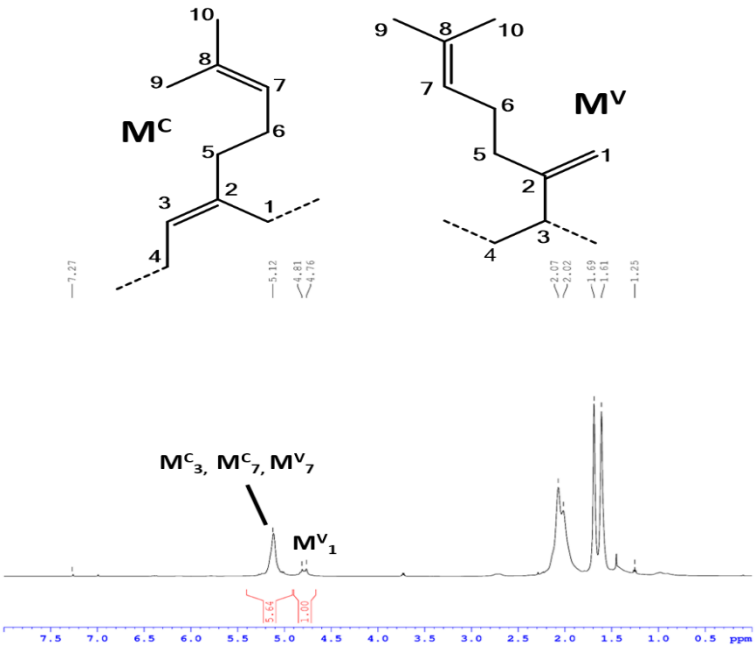

Figure 4S2. ^{1}H **NMR** spectrum ($CDCl_3$, 25 °C, 600 MHz) of PM from run 22 of Table 8.

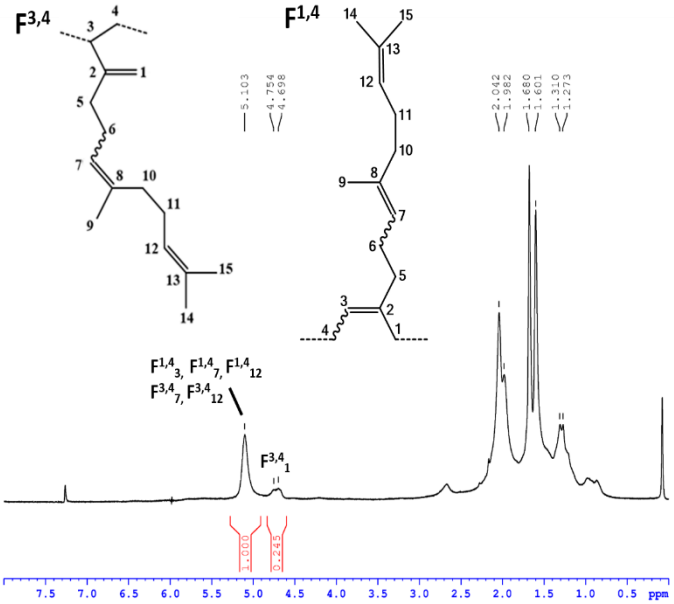

Figure 4S3. ^{1}H **NMR** spectrum ($CDCl_3$, 25 °C, 600 MHz) of PF from run 23 of Table 8.

Table 1A. **NMR** assignments for PO synthesized with **57**/***m*-MAO** (run 21, Table 8).

Unit [a]	Line	Atom	^{1}H [a] (ppm)	^{13}C [a] (ppm)
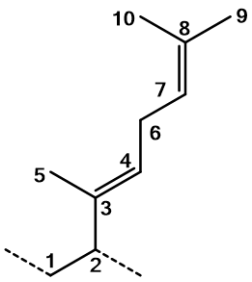	1	O^{V}_{1}	1.06-1.25	37.24
	2	O^{V}_{2}	1.76-1.94	43.86
	3	O^{V}_{3}	-	135.25-138.86
	4	O^{V}_{4}	5.08	123.69, 125.40
	5	O^{V}_{5}	1.44	12.41
	6	O^{V}_{6}	2.64	27.09
	7	O^{V}_{7}	5.08	123.69, 125.40
	8	O^{V}_{8}	-	130.47-131.78
	9	O^{V}_{9}	1.68	25.75
	10	O^{V}_{10}	1.61	17.84
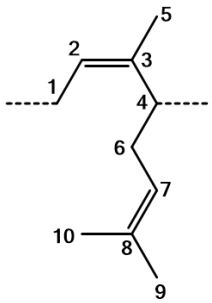	11	O^{C}_{1}	1.89-2.13	31.75-32.45
	12	O^{C}_{2}	5.08	123.69, 125.40
	13	O^{C}_{3}	-	135.25-138.86
	14	O^{C}_{4}	2.49	41.35
	15	O^{C}_{5}	1.50-1.55	18.66
	16	O^{C}_{6}	1.89-2.13	31.75-32.45
	17	O^{C}_{7}	5.08	123.69, 125.40
	18	O^{C}_{8}	-	130.47-131.78
	19	O^{C}_{9}	1.68	25.90
	20	O^{C}_{10}	1.61	17.96

[a] $CDCl_3$, 25 °C, 600 Mhz.

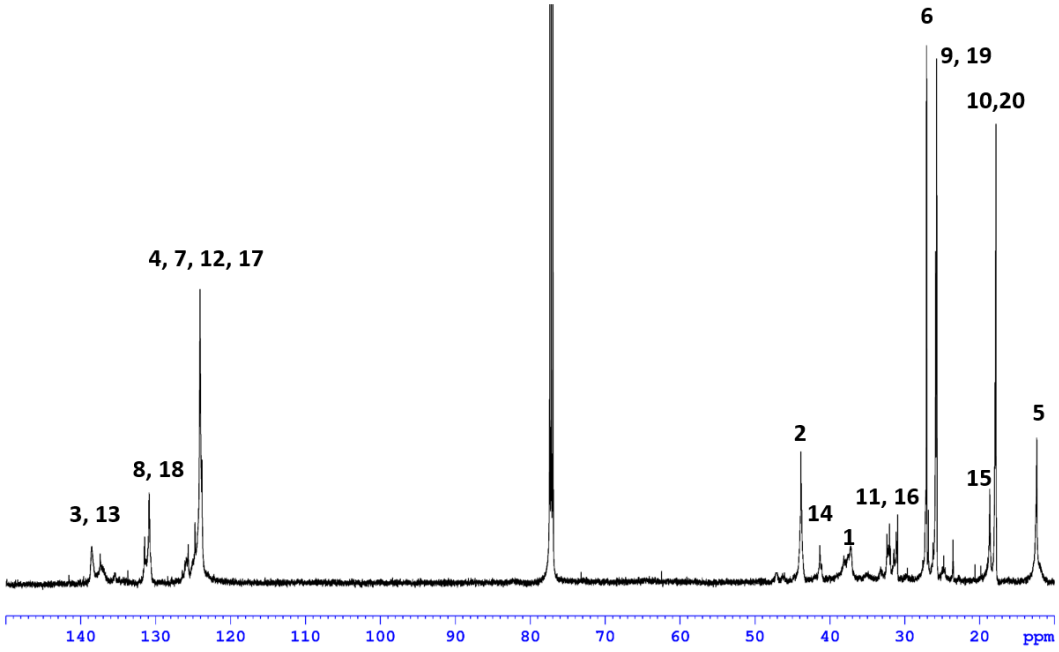

Figure 4S4. ^{13}C **NMR** spectrum ($CDCl_3$, 25 °C, 600 MHz) of PO from run 21 of Table 8.

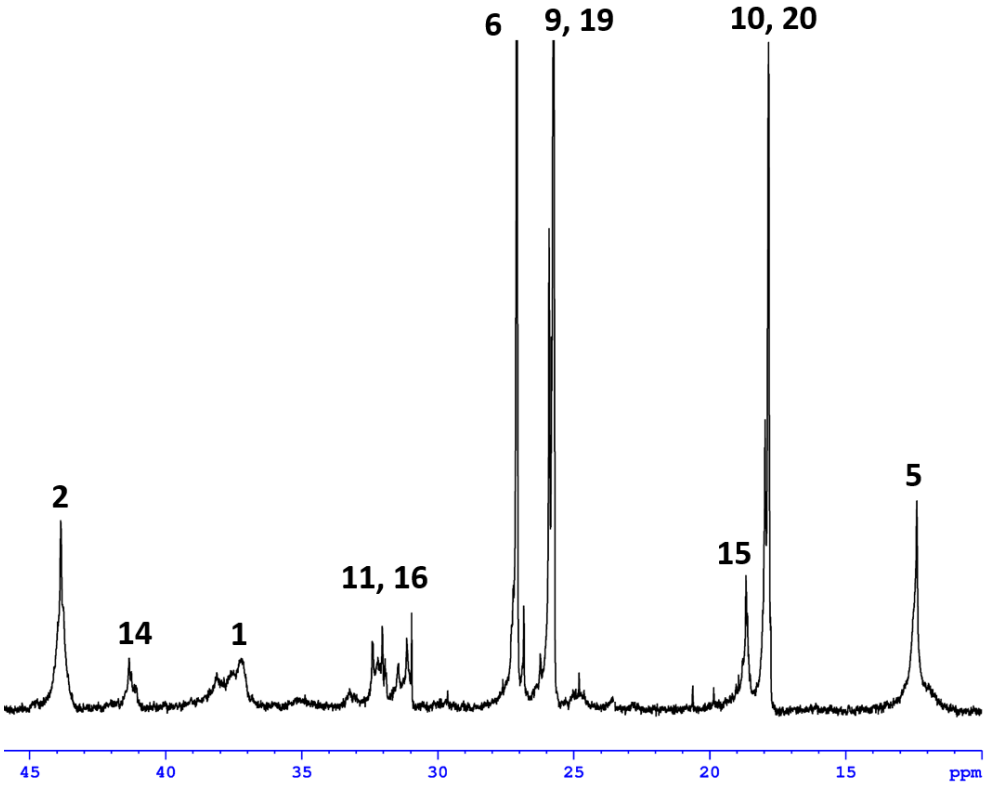

Figure 4S5. Aliphatic region of ^{13}C **NMR** spectrum ($CDCl_3$, 25 °C, 600 MHz) of PO from run 21 of Table 8.

Table 2A. **NMR** assignments for PM synthesized with 1/***m*-MAO** (run 22, Table 8).

Unit [a]	Line	Atom	^{1}H [a] (ppm)	^{13}C [a] (ppm)
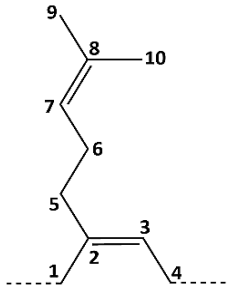	1	M^{C}_{1}	1.99-2.20	37.12
	2	M^{C}_{2}	-	139.18
	3	M^{C}_{3}	5.11	124.76
	4	M^{C}_{4}	1.99-2.20	26.95
	5	M^{C}_{5}	1.99-2.20	27.19
	6	M^{C}_{6}	2.06	30.86
	7	M^{C}_{7}	5.11	124.76
	8	M^{C}_{8}	-	131.28
	9	M^{C}_{9}	1.61	17.80
	10	M^{C}_{10}	1.68	25.80
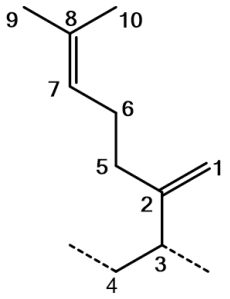	11	M^{V}_{1}	4.76-4.81	109.39
	12	M^{V}_{2}	-	151.82-152.36
	13	M^{V}_{3}	2.05	47.01
	14	M^{V}_{4}	1.95-2.05	39.89-40.44
	15	M^{V}_{5}	1.99-2.20	26.68
	16	M^{V}_{6}	1.99-2.20	32.70-34.44
	17	M^{V}_{7}	5.11	124.76
	18	M^{V}_{8}	-	131.28
	19	M^{V}_{9}	1.61	17.80
	20	M^{V}_{10}	1.68	25.80

[a] $CDCl_3$, 40 °C, 600 Mhz.

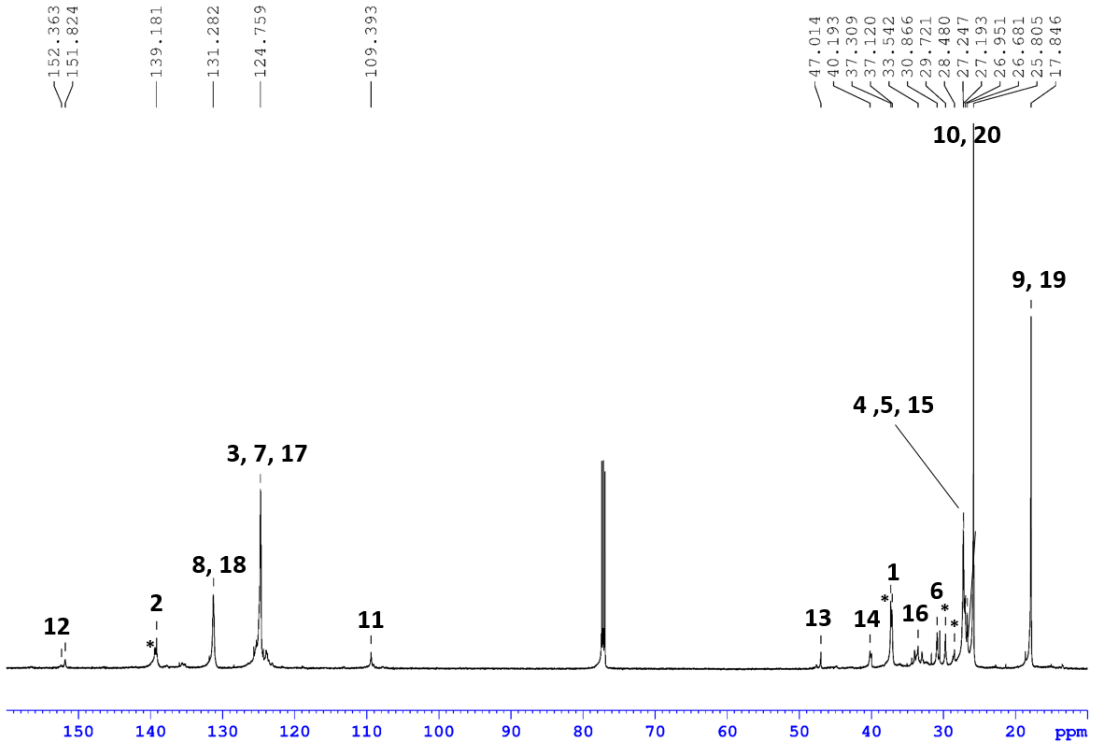

Figure 4S6. ^{13}C **NMR** spectrum ($CDCl_3$, 25 °C, 600 MHz) of PM from run 22 of Table 8.
* Signals attributed to cis-cis head-to-head and tail-to-tail junctions.

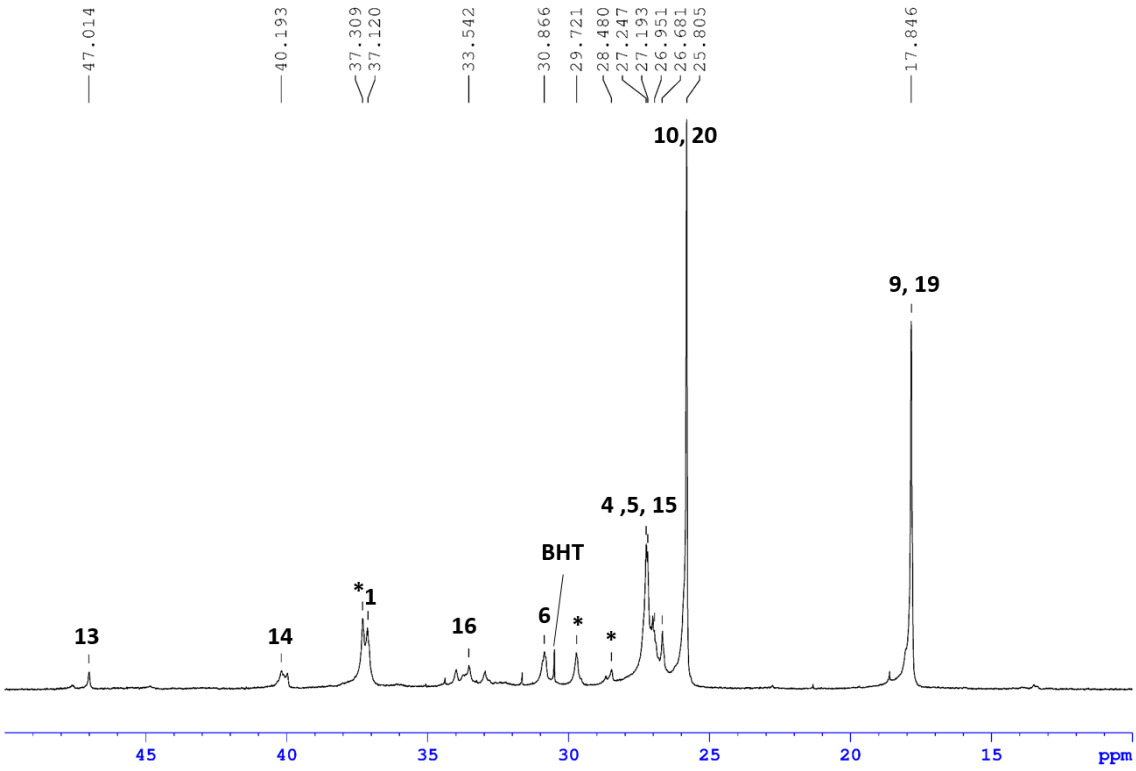

Figure 4S7. Aliphatic region of ^{13}C **NMR** spectra ($CDCl_3$, 25 °C, 600 MHz) of PM from run 22 of Table 8.
* Signals attributed to cis-cis head-to-head and tail-to-tail junctions.

Table 3A. **NMR** assignments for PF synthesized with 1/***m*-MAO** (runs 23, Table 8).

Unit [a]	Line	Atom	^{1}H [a] (ppm)	^{13}C [a] (ppm)
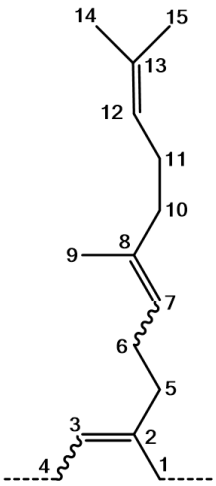	1	$F^{1,4}{}_1$	1.95-2.03	37.63
	2	$F^{1,4}{}_2$	-	138.72-139.59
	3	$F^{1,4}{}_3$	5.10	122.90-125.77
	4	$F^{1,4}{}_4$	1.97-2.16	26.63-27.40
	5	$F^{1,4}{}_5$	2.03	30.19
	6	$F^{1,4}{}_{6,}$	1.97-2.16	26.63-27.40
	7	$F^{1,4}{}_{7,}$	5.10	122.90-125.77
	8	$F^{1,4}{}_{8,}$	-	134.66-135.79
	9(t)	$F^{1,4}{}_9$	1.55-1.61	16.17
	9(c)	$F^{1,4}{}_9$	1.63-1.73	23.58
	10(t)	$F^{1,4}{}_{10}$	1.93-2.02	39.97
	10(c)	$F^{1,4}{}_{10}$	2.03	32.20
	11	$F^{1,4}{}_{11}$	1.97-2.16	26.63-27.40
	12	$F^{1,4}{}_{12}$	5.10	122.90-125.77
	13	$F^{1,4}{}_{13}$	-	131.13-131.89
	14	$F^{1,4}{}_{14}$	1.57-1.64	17.86
	15	$F^{1,4}{}_{15}$	1.69	25.92
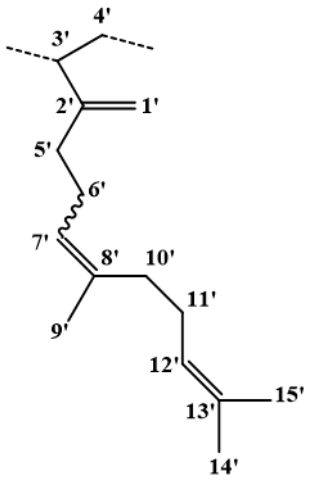	16	$F^{3,4}{}_1$	4.66-4.81	110.19
	17	$F^{3,4}{}_2$	-	154.58
	18	$F^{3,4}{}_3$	2.03	46.55
	19	$F^{3,4}{}_4$	1.99-2.03	38.37
	20	$F^{3,4}{}_5$	2.03	30.19
	21	$F^{3,4}{}_6$	1.97-2.16	26.63-27.40
	22	$F^{3,4}{}_7$	5.10	122.90-125.77
	23	$F^{3,4}{}_8$	-	134.66-135.79
	24(t)	$F^{3,4}{}_9$	1.55-1.61	16.17
	24(c)	$F^{3,4}{}_9$	1.63-1.73	23.58
	25(t)	$F^{3,4}{}_{10}$	1.93-2.03	39.97
	25(c)	$F^{3,4}{}_{10}$	2.03	32.20
	26	$F^{3,4}{}_{11}$	1.97-2.16	26.63-27.40
	27	$F^{3,4}{}_{12}$	5.10	122.90-125.77
	28	$F^{3,4}{}_{13}$	-	131.13-131.89
	29	$F^{3,4}{}_{14}$	1.57-1.64	17.86
	30	$F^{3,4}{}_{15}$	1.69	25.92

[a] $CDCl_3$, 25 °C, 600 MHz.

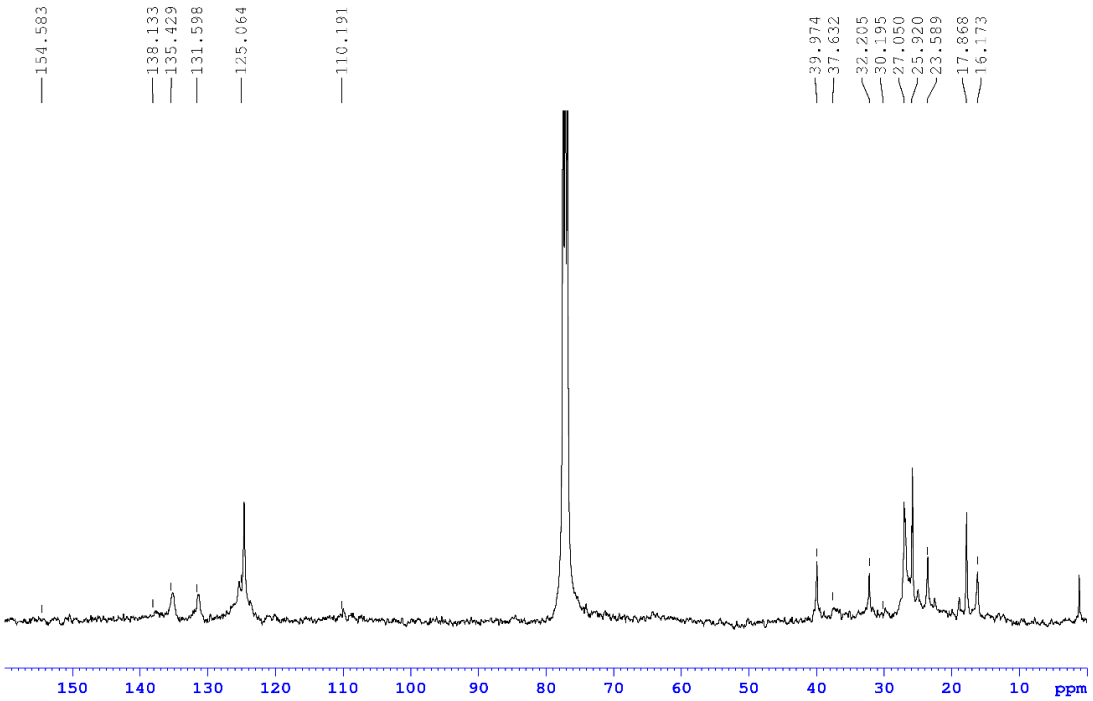

Figure 4S8. ^{13}C **NMR** spectrum ($CDCl_3$, 25 °C, 600 MHz) of PF from run 23 of Table 8.

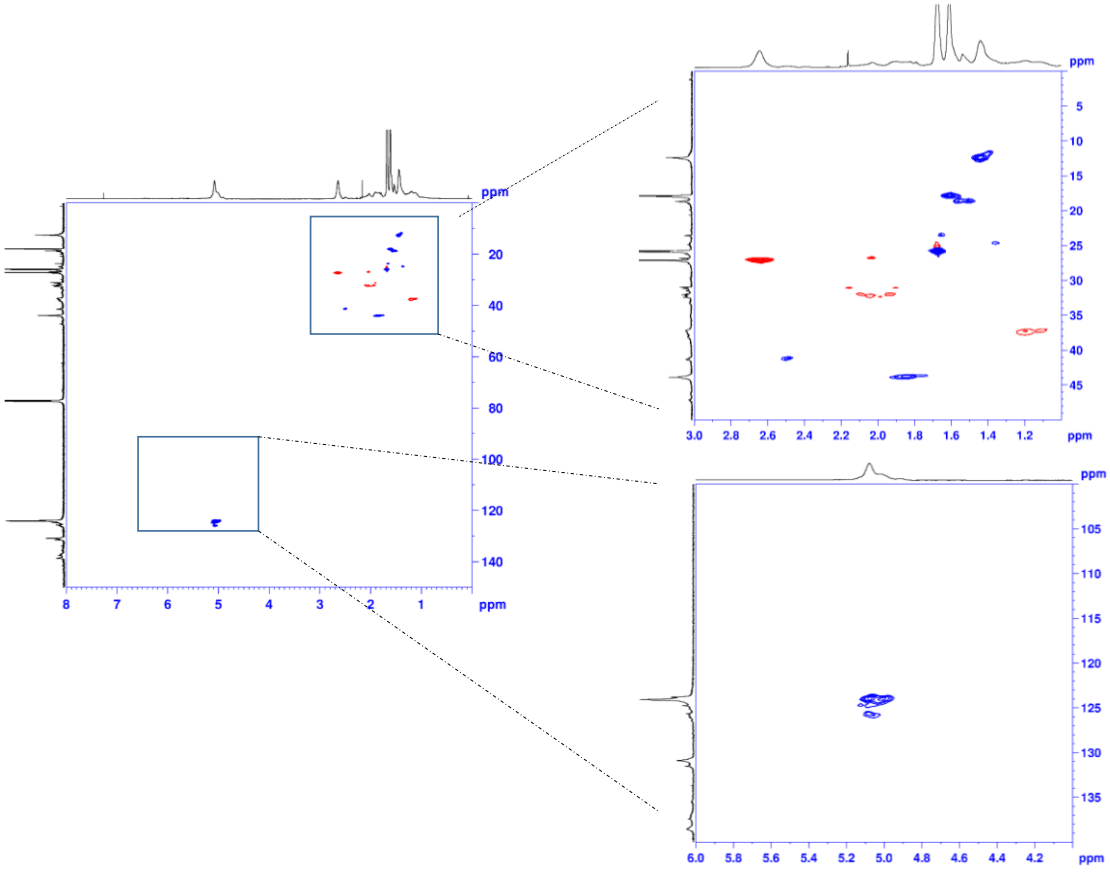

Figure 4S9. ^{13}C-^{1}H HSQC spectrum ($CDCl_3$, 25 °C, 600 MHz) of PO from run 21 of Table 8 with magnification of diagnostic regions. Methyl and methine signals are displayed in blue while methylenes in red.

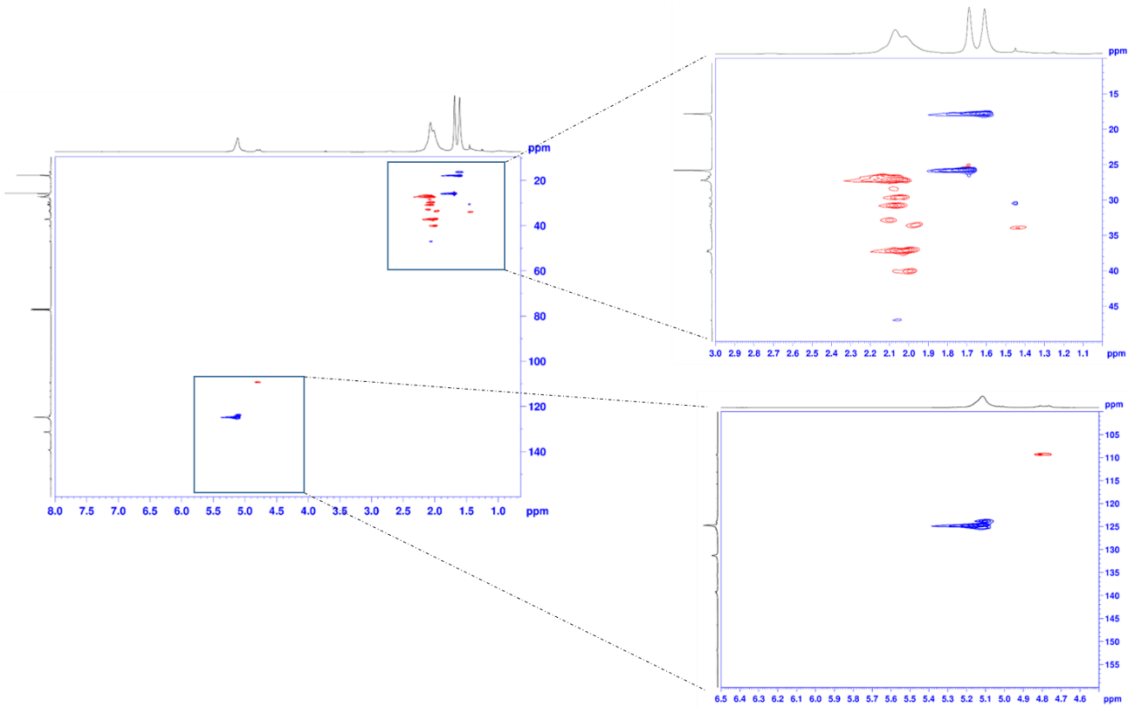

Figure 4S10. ^{13}C-^{1}H HSQC spectrum ($CDCl_3$, 25 °C, 600 MHz) of PM from run 22 of Table 8 with magnification of diagnostic regions. Methyl and methine signals are displayed in blue while methylenes in red.

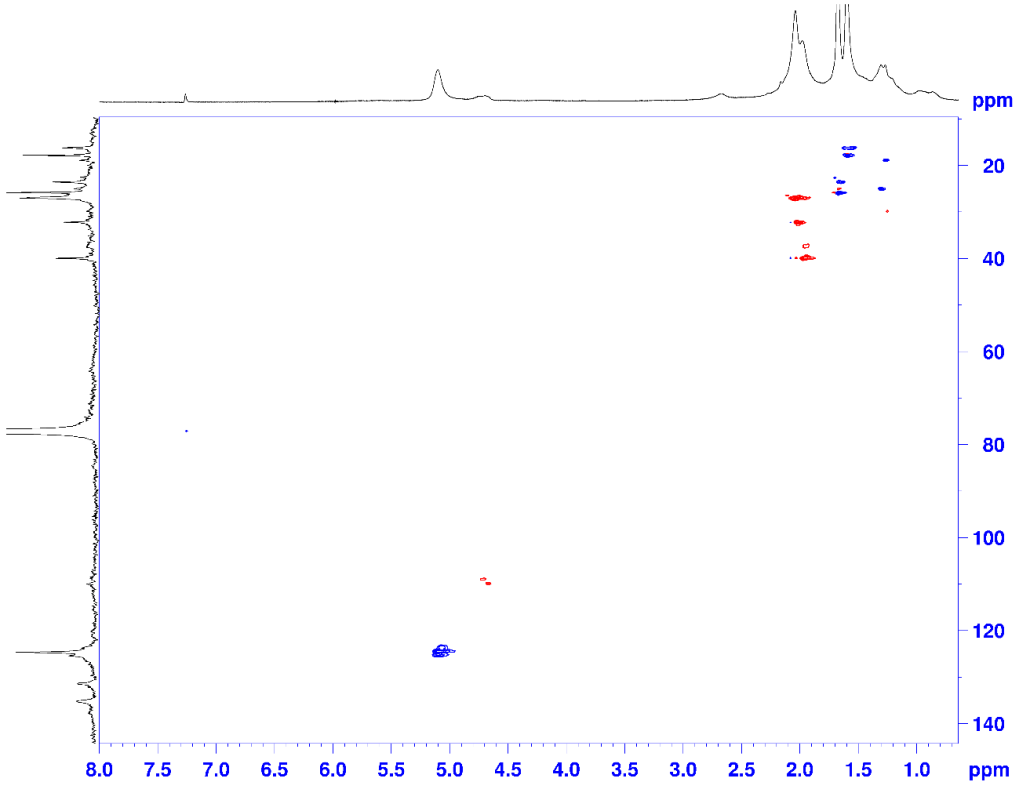

Figure 4S11. ^{13}C-^{1}H HSQC spectrum ($CDCl_3$, 25 °C, 600 MHz) of PF from run 23 of Table 8 with magnification of diagnostic regions. Methyl and methine signals are displayed in blue while methylenes in red.

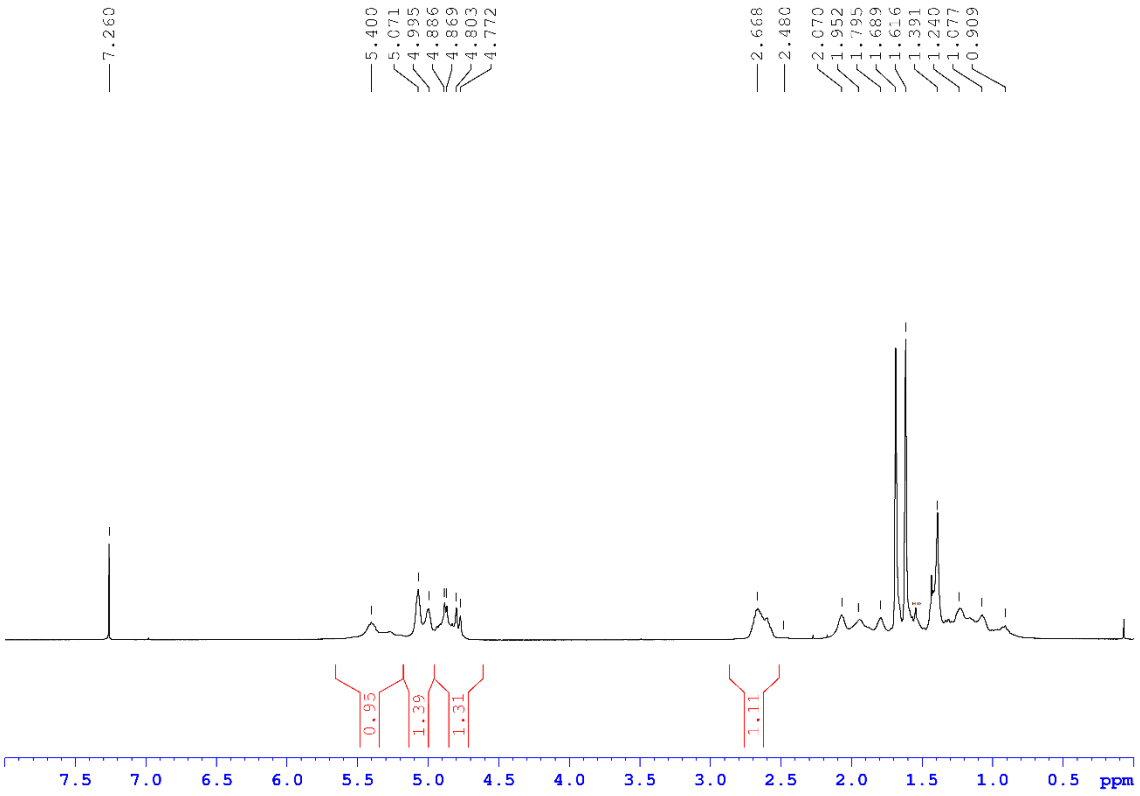

Figure 4S12. ^{1}H **NMR** spectrum ($CDCl_3$, 25 °C, 600 MHz) of POB from run 25 of Table 9

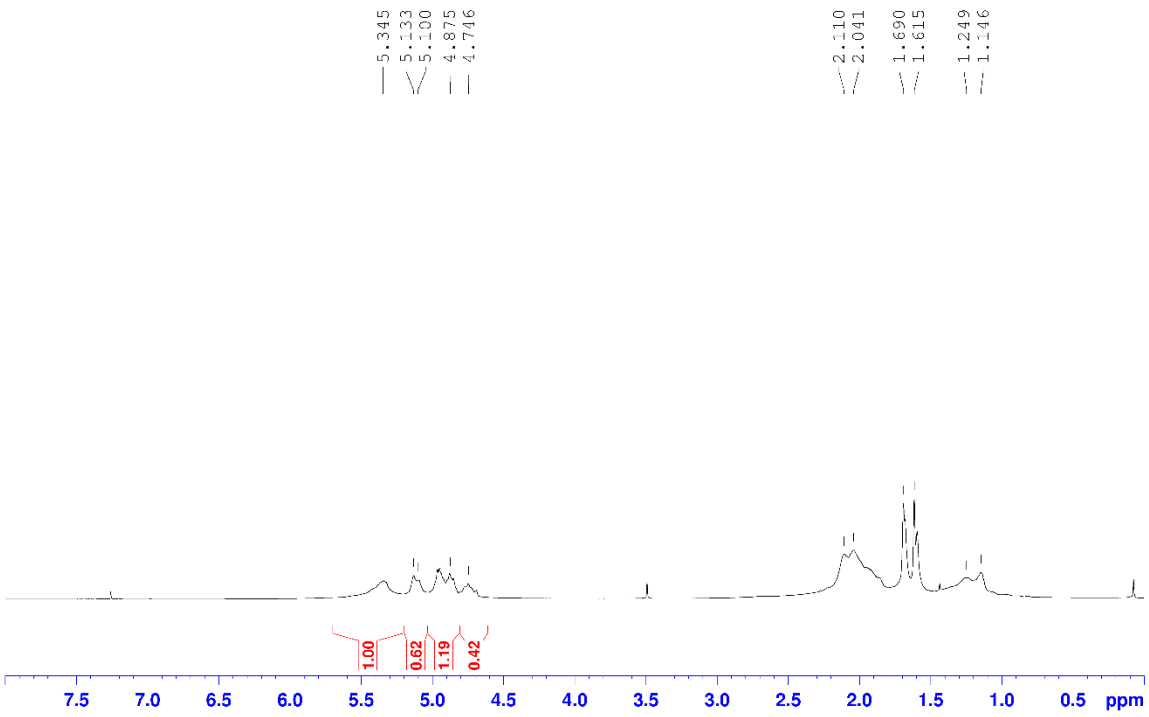

Figure 4S13. ^{1}H **NMR** spectrum ($CDCl_3$, 25 °C, 600 MHz) of PMB from run 29 of Table 11

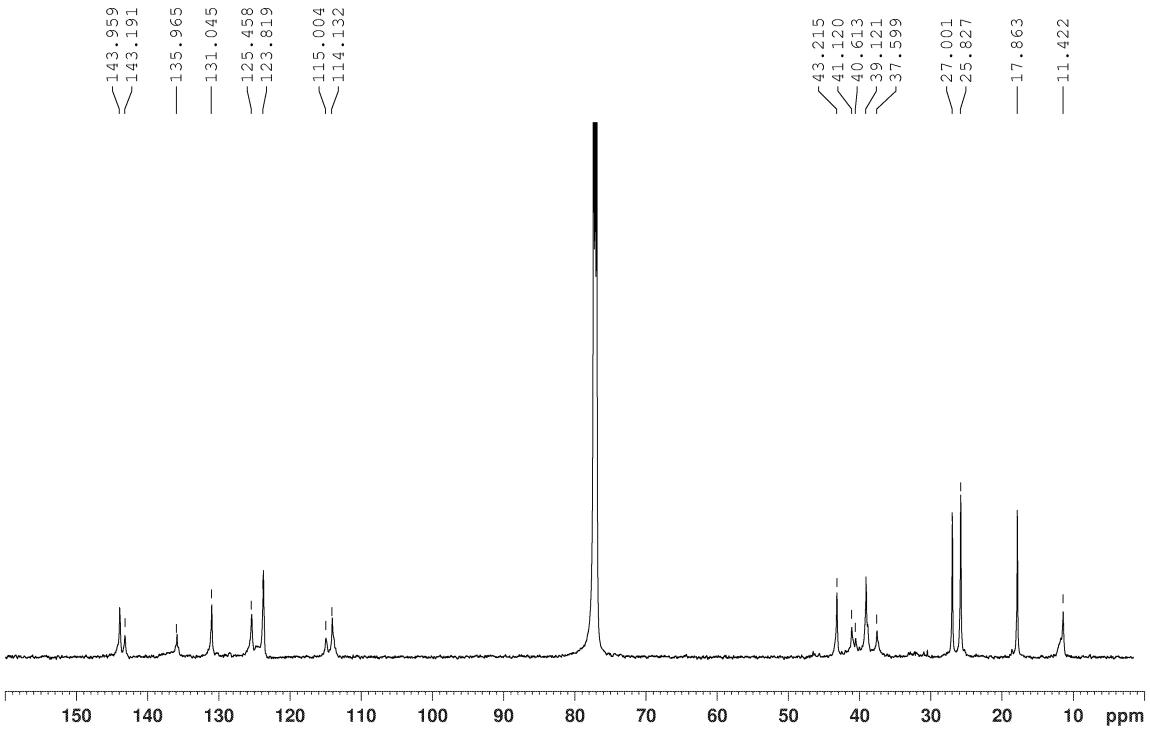

Figure 4S14. ^{13}C **NMR** spectrum ($CDCl_3$, 25 °C, 600 MHz) of POB from run 25 of Table 11.

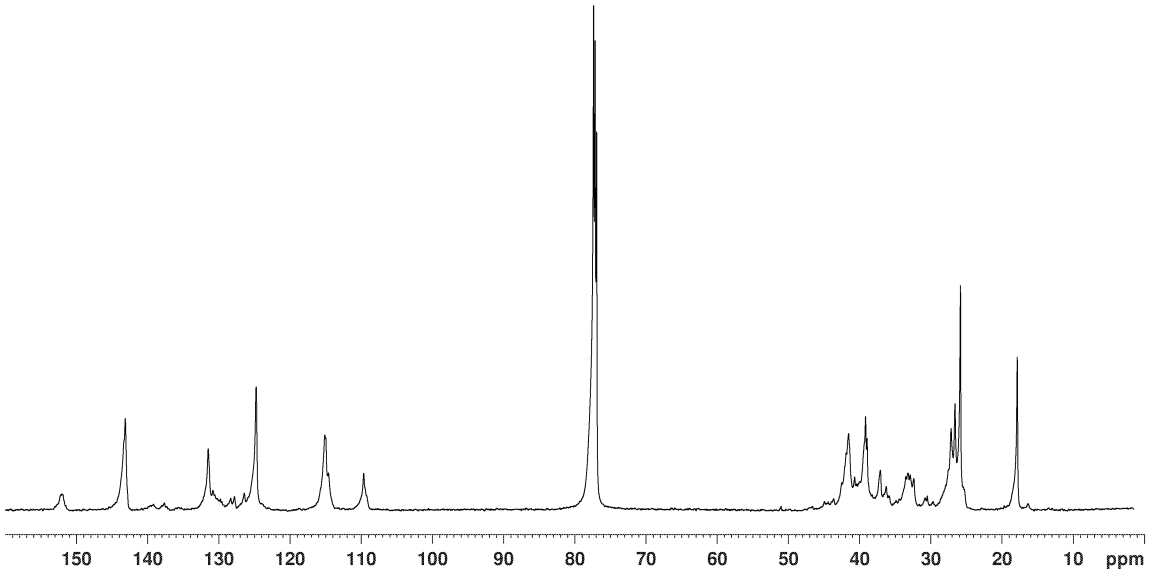

Figure 4S15. ^{13}C **NMR** spectrum ($CDCl_3$, 25 °C, 600 MHz) of PMB from run 29 of Table 11.

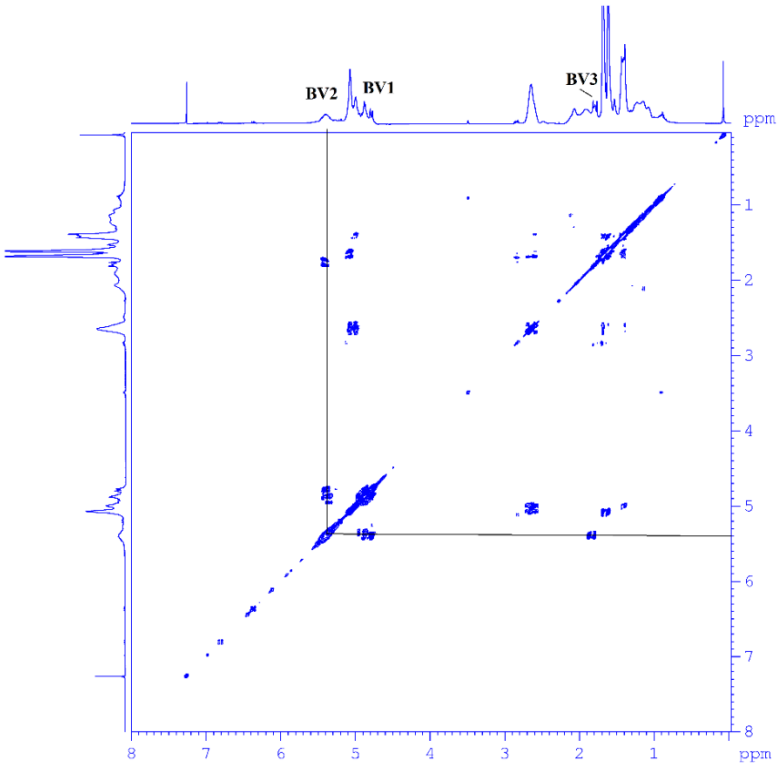

Figure 4S16. ^{1}H-^{1}H COSY spectrum ($CDCl_3$, 25 °C, 600 MHz) of POB copolymer from run 24 of Table 9.

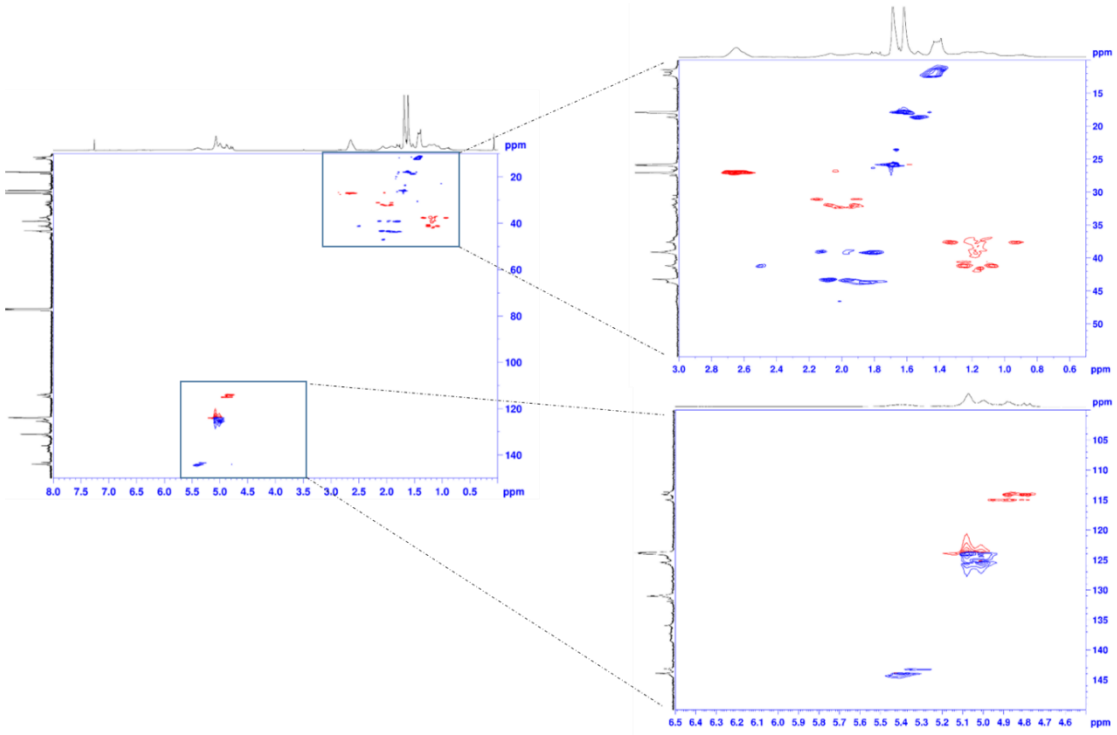

Figure 4S17. ^{13}C-^{1}H HSQC spectrum ($CDCl_3$, 25 °C, 600 MHz) of POB from run 24 of Table 9 with magnification of diagnostic regions. Methyl and methine signals are displayed in blue while methylenes in red.

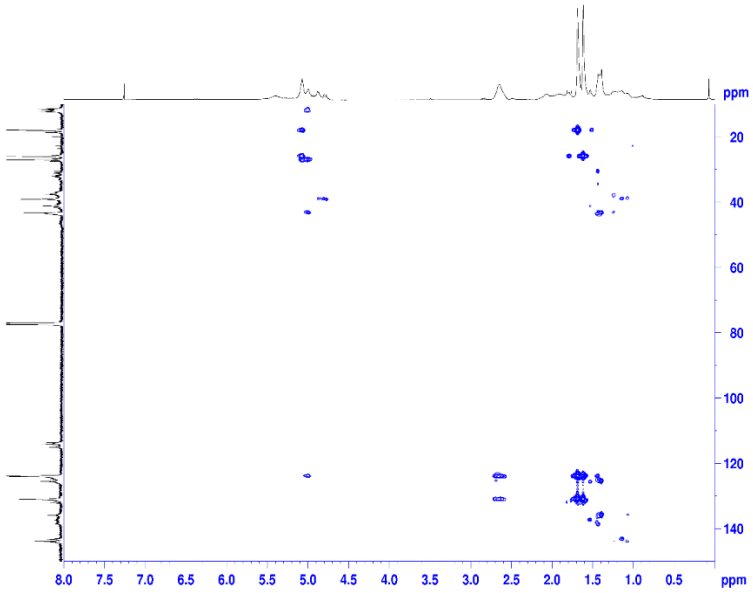

Figure 4S18. ^{13}C-^{1}H HMBC spectrum ($CDCl_3$, 25 °C, 600 MHz) of POB copolymer from run 24 of Table 9.

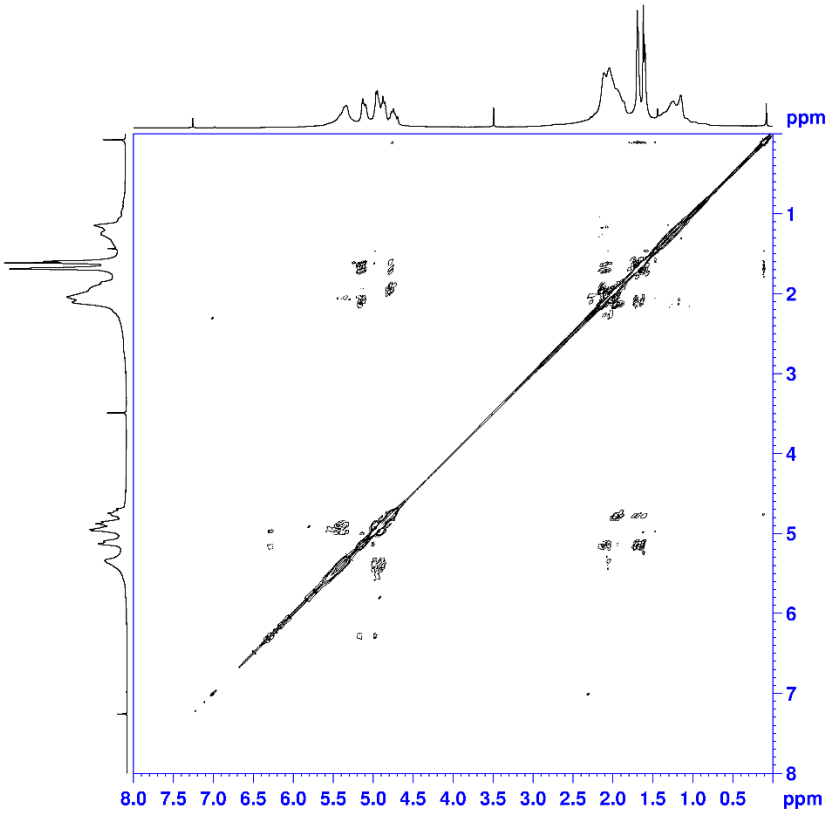

Figure 4S19. ^{1}H-^{1}H COSY spectrum ($CDCl_3$, 25 °C, 600 MHz) of PMB copolymer from run 24 of Table 9.

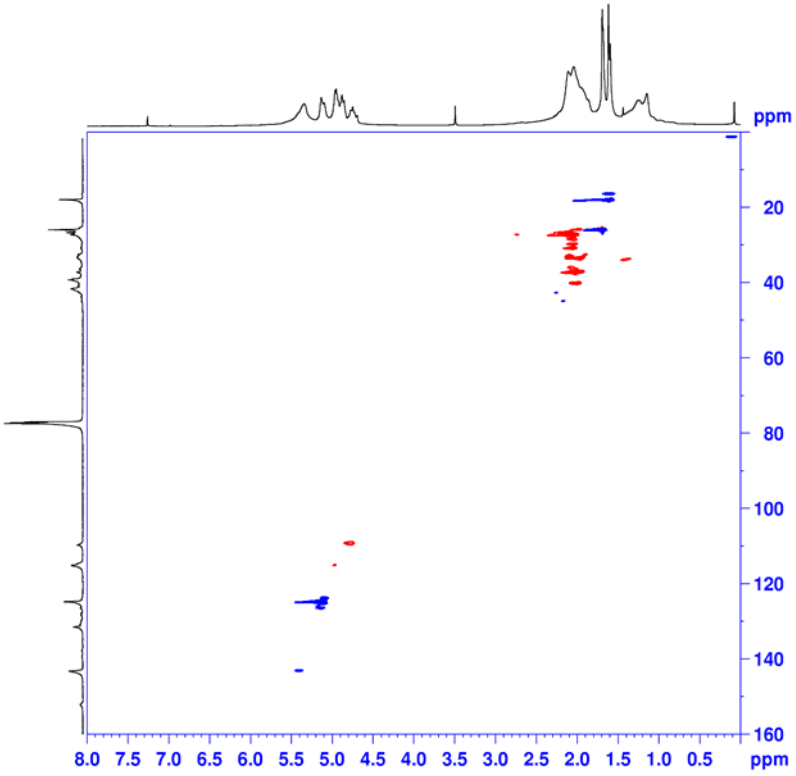

Figure 4S20. ^{13}C-^{1}H HSQC spectrum ($CDCl_3$, 25 °C, 600 MHz) of PMB from run 24 of Table 9 (methyl and methine signals are displayed in blue while methylenes in red).

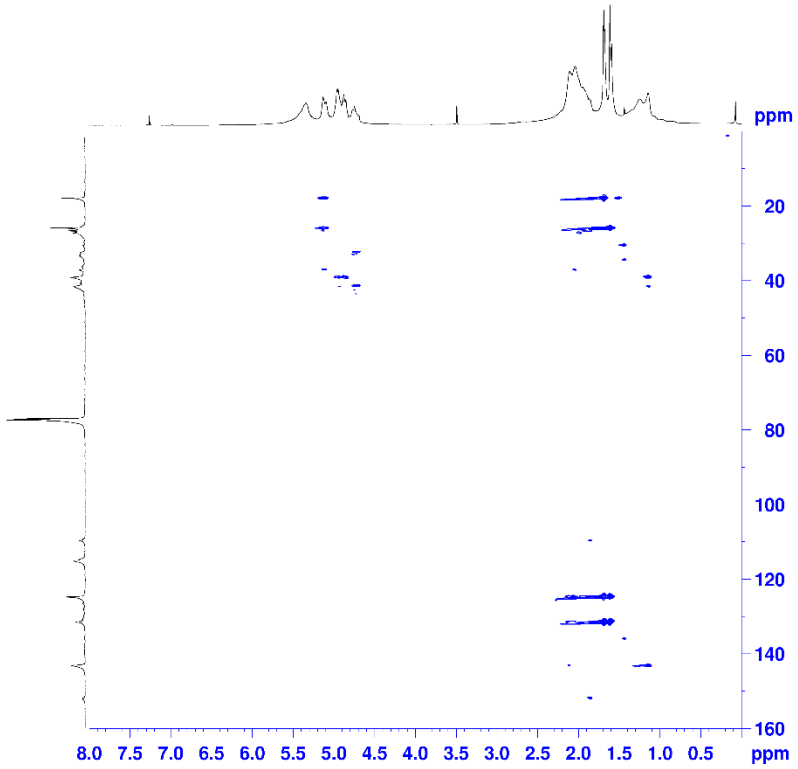

Figure 4S21. ^{13}C-^{1}H HMBC spectrum ($CDCl_3$, 25 °C, 600 MHz) of PMB copolymer from run 24 of Table 9.

4.2 Determination of Polymer Compositions

2.1 Determination of $\mathbf{O^V}$ and $\mathbf{O^C}$ contents in PO and POB polymers by ^{1}H **NMR** ($CDCl_3$, 25 °C)

- $O^V(mol\%) = \frac{A_A}{A_{A+(A_B-A_A)}} \cdot 100$ **Equation 15**

  Where $\boldsymbol{A_A}$ is the area of the signal $\mathbf{O^V_6}$ (δ=2.65 ppm) and $\boldsymbol{A_B}$ is the area of the signals $\mathbf{O^C_2}$, $\mathbf{O^C_7}$, $\mathbf{O^V_4}$ and $\mathbf{O^V_7}$ (δ=5.00-5.08 ppm).

- $O^C(mol\%) = 100 - O^V(mol\%)$ **Equation 16**

2.2 Determination of $\mathbf{M^V}$ and $\mathbf{M^C}$ contents in PM and PMB polymers by ^{1}H **NMR** ($CDCl_3$, 25 °C)

- $M^V(mol\%) = \frac{B_B}{B_A + \frac{B_B}{2}} \cdot 100$ **Equation 17**

  Where $\boldsymbol{B_A}$ is the area of the signals $\mathbf{M^C_3}$, $\mathbf{M^C_7}$ and $\mathbf{M^V_7}$ (δ = 5.12 ppm) and $\boldsymbol{B_B}$ is the area of the signal $\mathbf{M^V_1}$ (δ = 4.72, 4.79 ppm).

- $M^C(mol\%) = 100 - M^V(mol\%)$ **Equation 18**

2.3 Determination of total B contents in POB copolymers by ^{1}H **NMR** ($CDCl_3$, 25 °C)

- $B(mol\%) = \frac{C_A + \frac{C_B}{2}}{E_A + \frac{E_B}{2} + A_{A+(A_B-A_A)}}$ **Equation 19**

  Where $\boldsymbol{A_A}$ is the area of the signal $\mathbf{O^V_6}$ (δ=2.65 ppm), $\boldsymbol{A_B}$ is the area of the signals $\mathbf{O^C_2}$, $\mathbf{O^C_7}$, $\mathbf{O^V_4}$ and $\mathbf{O^V_7}$ (δ=5.00-5.08 ppm), $\mathbf{C_A}$ represents the integrated area of $\mathbf{B^C_2}$ and $\mathbf{B^V_2}$ (δ= 5.20-5.60 ppm) and $\mathbf{C_B}$ is the area of $\mathbf{B^V_1}$ (δ= 4.85-5.00 ppm).

- $O\ (mol\%) = 100 - B(mol\%)$ **Equation 20**

2.4 Determination of $\mathbf{F^{1,2}}$ and $\mathbf{F^{1,4}}$ contents in PF polymers by ^{1}H **NMR** ($CDCl_3$, 25 °C)

- $F^{1,4}(mol\%) = \frac{\frac{(D_A - D_B)}{3}}{\frac{(D_A - D_B)}{3} + \frac{D_B}{2}} \cdot 100$ **Equation 21**

  Where D_A is the integrated area of the signals $\mathbf{F^{1,4}_3}$, $\mathbf{F^{1,4}_7}$, $\mathbf{F^{1,4}_{12}}$, $\mathbf{F^{1,2}_7}$ and $\mathbf{F^{1,2}_{12}}$ (δ= 5.10 ppm) and D_B is the integrated area of the signal $\mathbf{F^{1,2}_1}$ (δ= 4.66-4.81ppm).

- $F^{1,2}(mol\%) = 100 - F^{1,4}(mol\%)$ **Equation 22**

2.5 Determination of $\mathbf{B^V}$ and $\mathbf{B^C}$ contents in POB and PMB copolymers by ^{1}H **NMR** ($CDCl_3$, 25 °C)

- $B^V(mol\%) = \frac{C_B}{C_A + \frac{C_B}{2}} \cdot 100$ **Equation 23**

Where $\mathbf{C_A}$ represents the integrated area of $\mathbf{B^{C}_2}$ and $\mathbf{B^{V}_2}$ (δ= 5.20-5.60 ppm), and $\mathbf{C_B}$ is the area of $\mathbf{B^{V}_1}$ (δ= 4.85-5.00 ppm).

- $B^{C}(mol\%) = 100 - B^{1,2}(mol\%)$ **Equation 24**

2.6 Determination of total B and M contents in PMB copolymers by ^{1}H **NMR** ($CDCl_3$, 25 °C)

- $B(mol\%) = \frac{C_A + \frac{C_B}{2}}{C_A + \frac{C_B}{2} + B_A + \frac{B_B}{2}}$ **Equation 25**

Where $\boldsymbol{B_A}$ is the area of the signals $\mathbf{M^{C}_3}$, $\mathbf{M^{C}_7}$ and $\mathbf{M^{V}_7}$ (δ = 5.12 ppm), $\boldsymbol{B_B}$ is the area of the signal $\mathbf{M^{V}_1}$ (δ = 4.72, 4.79 ppm), $\mathbf{C_A}$ represents the integrated area of $\mathbf{B^{C}_2}$ and $\mathbf{B^{V}_2}$ (δ= 5.20-5.60 ppm) and $\mathbf{C_B}$ is the area of $\mathbf{B^{V}_1}$ (δ= 4.85-5.00 ppm).

- $M\ (mol\%) = 100 - B(mol\%)$ **Equation 26**

4.3 DSC Thermal Analyses

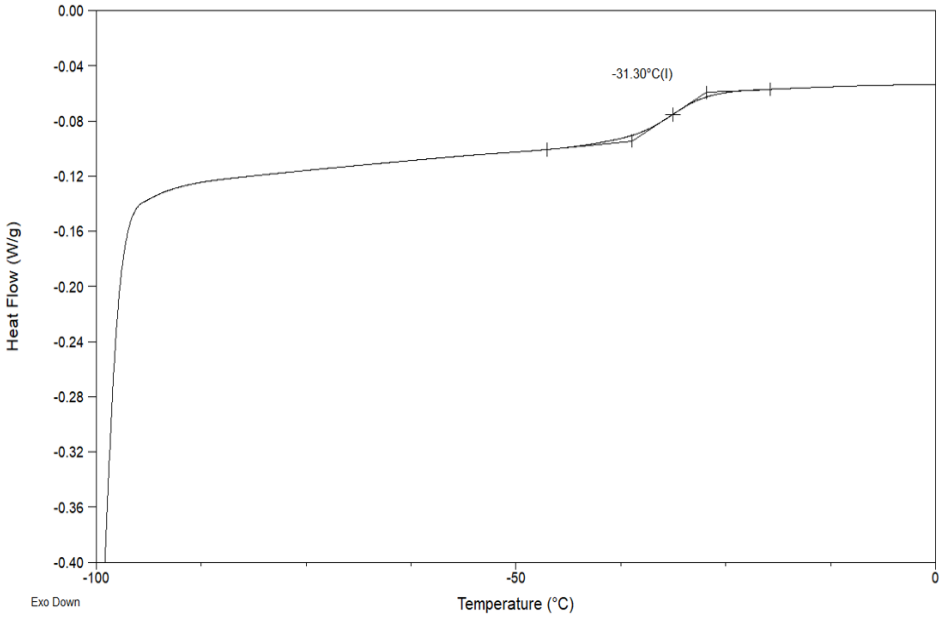

Figure 4S22. DSC thermograms of PO from runs 21 of Table 8.

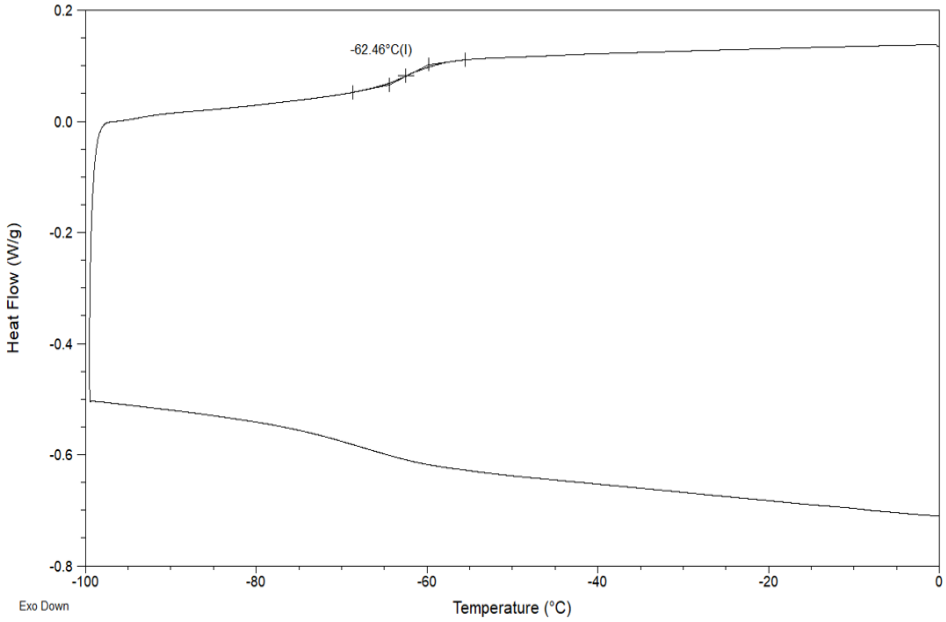

Figure 4S23. DSC thermograms of PM copolymer from run 22 of Table 8.

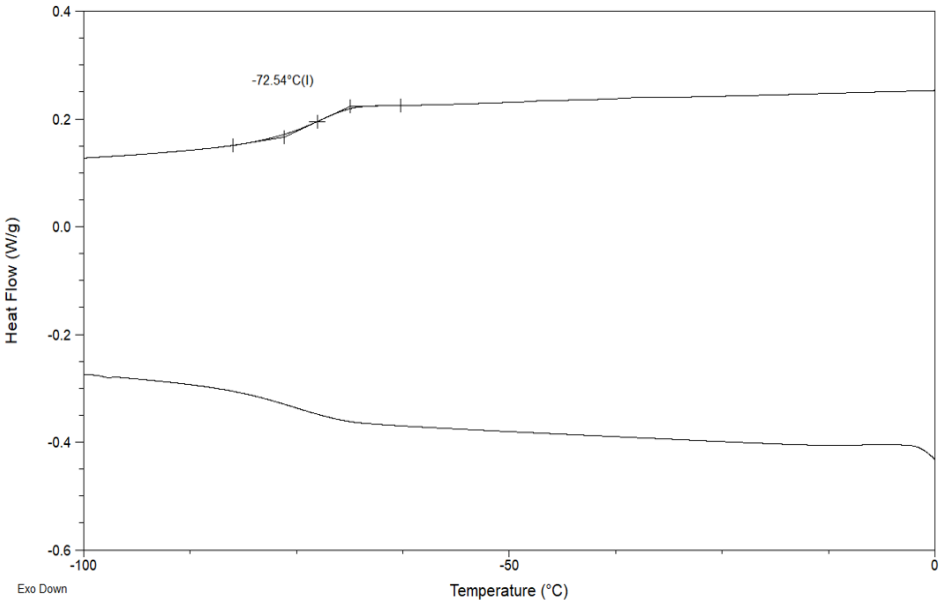

Figure 4S24. DSC thermograms of PF copolymer from run 23 of Table 8.

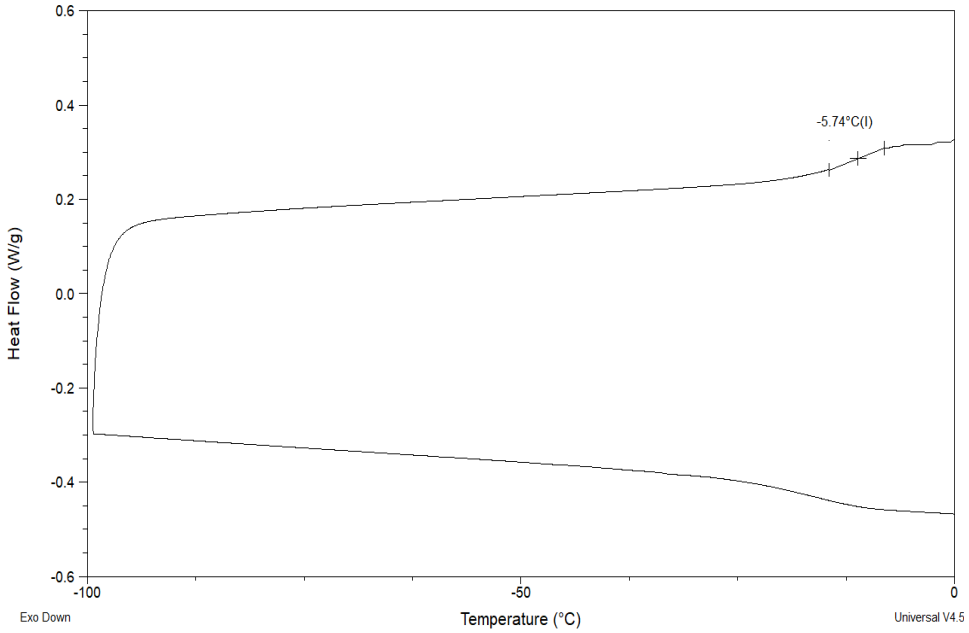

Figure 4S25. DSC thermograms of POB copolymer from run 24 of Table 8.

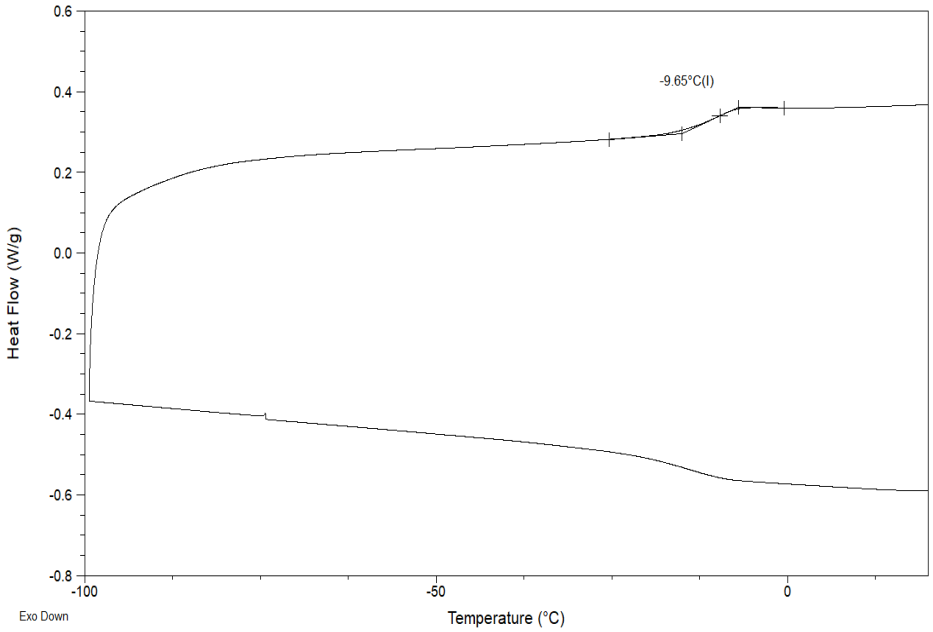

Figure 4S26. DSC thermograms of POB copolymer from run 25 of Table 9.

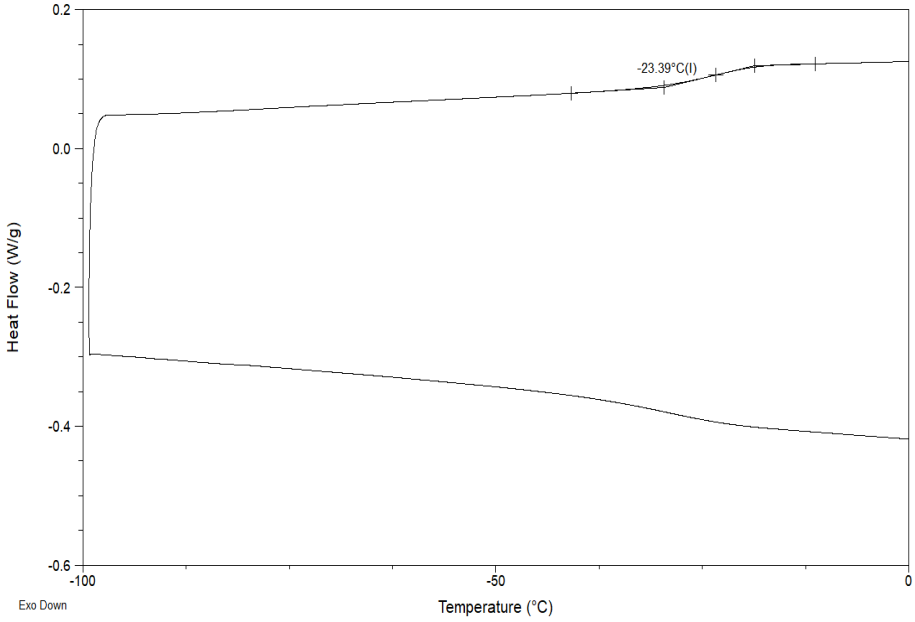

Figure 4S27. DSC thermograms of POB copolymer from run 26 of Table 9.

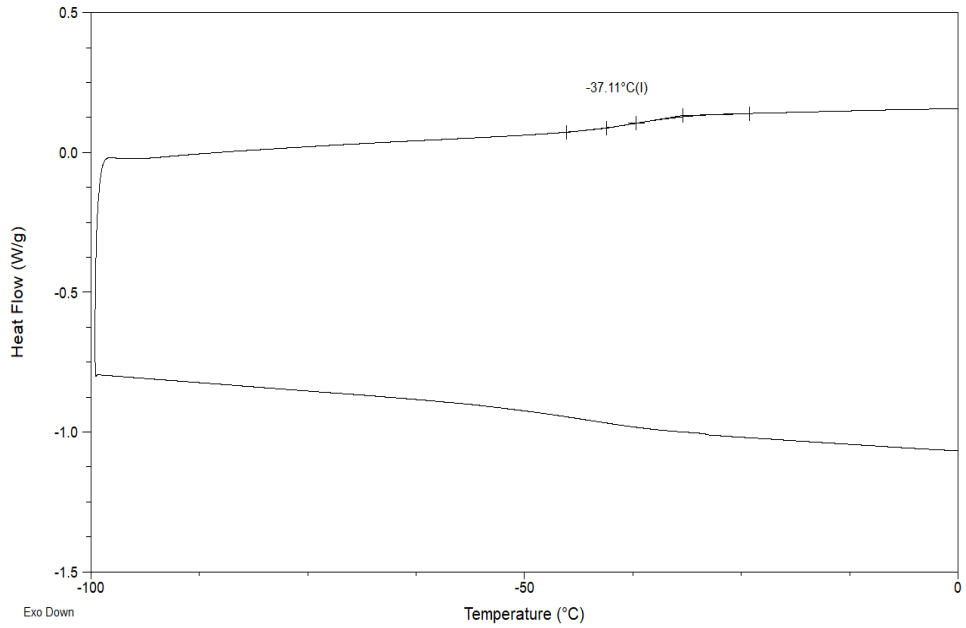

Figure 4S28. DSC thermograms of PMB copolymer from run 27 of Table 11.

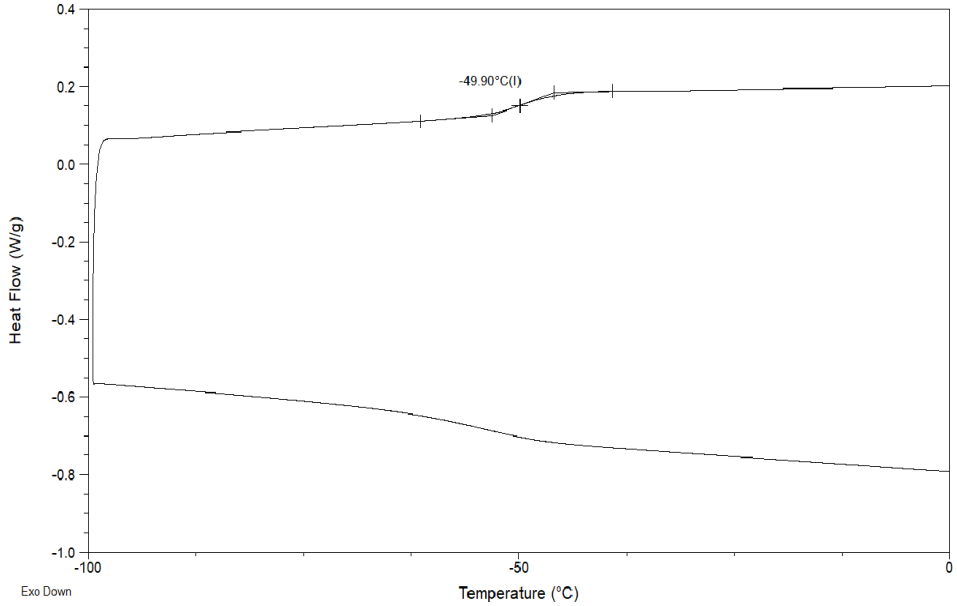

Figure 4S29. DSC thermograms of PMB copolymer from run 28 of Table 11.

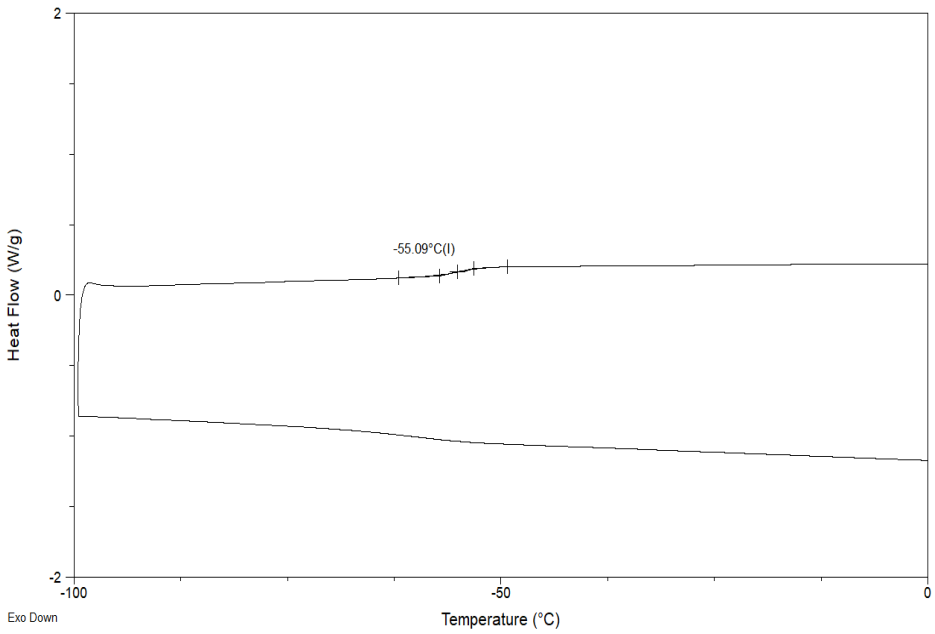

Figure 4S30. DSC thermograms of PMB copolymer from run 29 of Table 11.

4.4 GPC Analyses

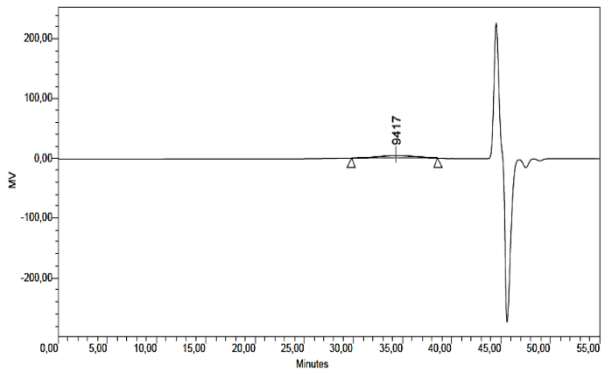

Figure 4S31. GPC curve of PO from run 21 of Table 8.

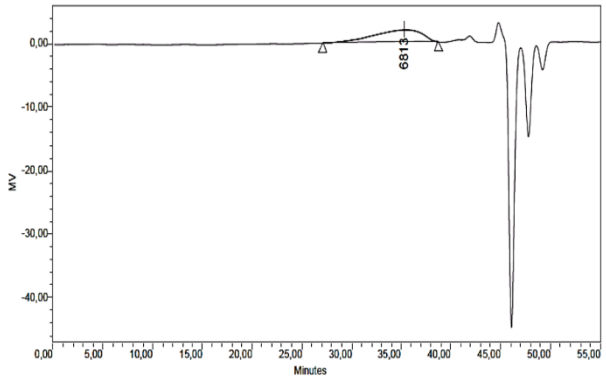

Figure 4S32. GPC curve of PM from run 22 of Table 8.

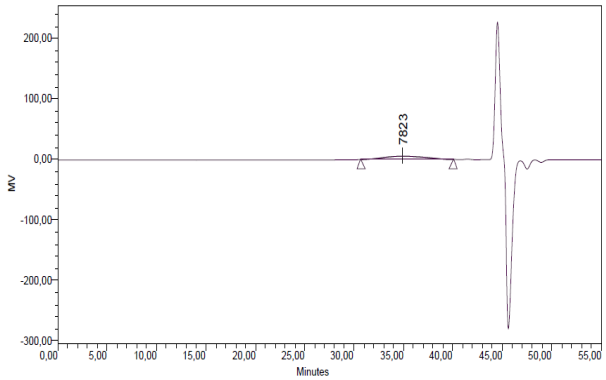

Figure 4S33. GPC curve of PF from run 23 of Table 8.

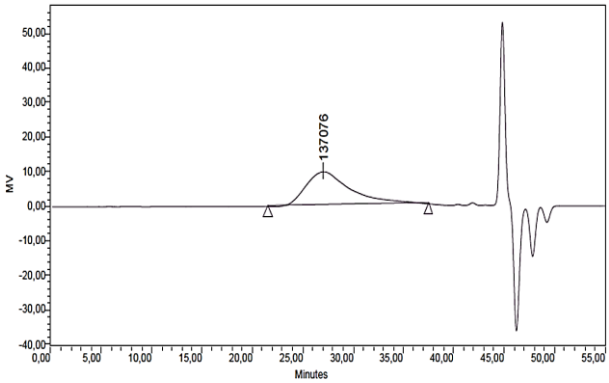

Figure 4S34. GPC curve of POB copolymer from run 24 of Table 9.

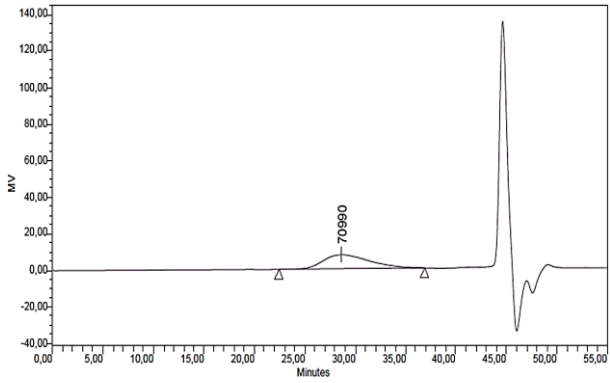

Figure 4S35. GPC curve of POB copolymer from run 25 of Table 9.

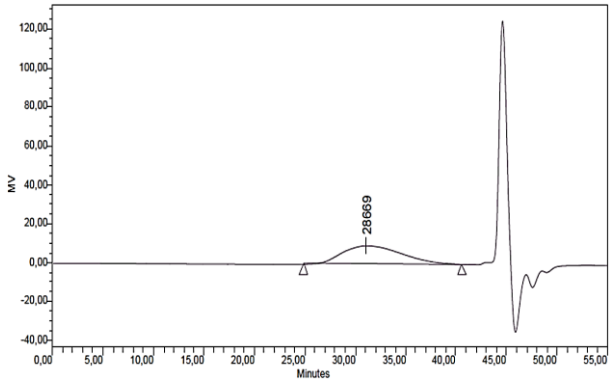

Figure 4S36. GPC curve of POB copolymer from run 26 of Table 9.

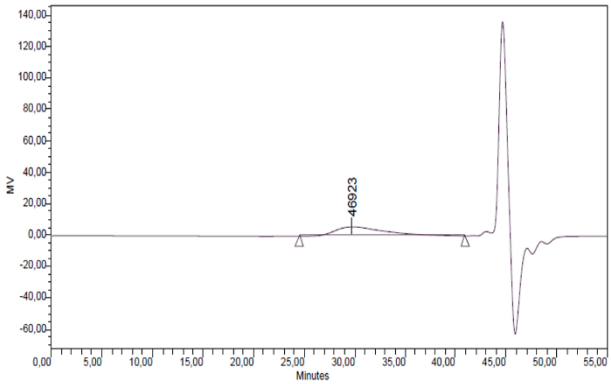

Figure 4S37. GPC curve of PMB copolymer from run 27 of Table 11.

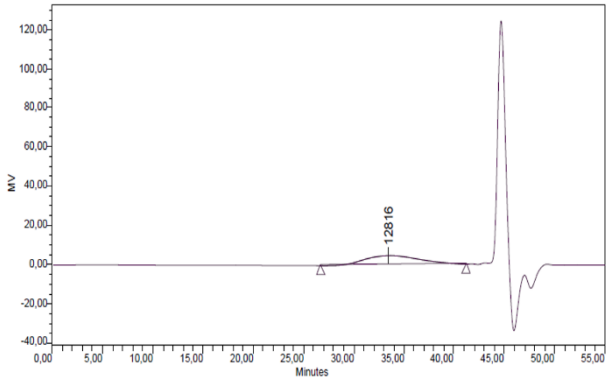

Figure 4S38. GPC curve of PMB copolymer from run 28 of Table 11.

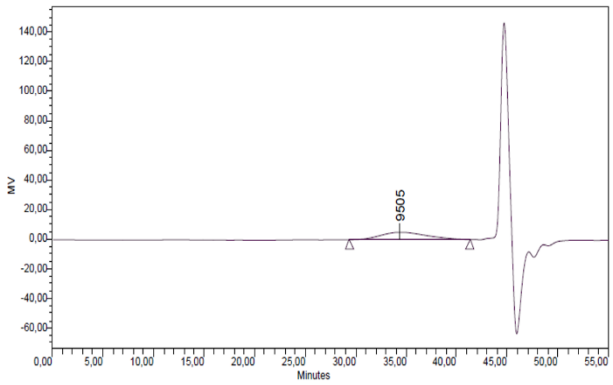

Figure 4S39. GPC curve of PMB copolymer from run 29 of Table 11.

4.5 Other Characterization

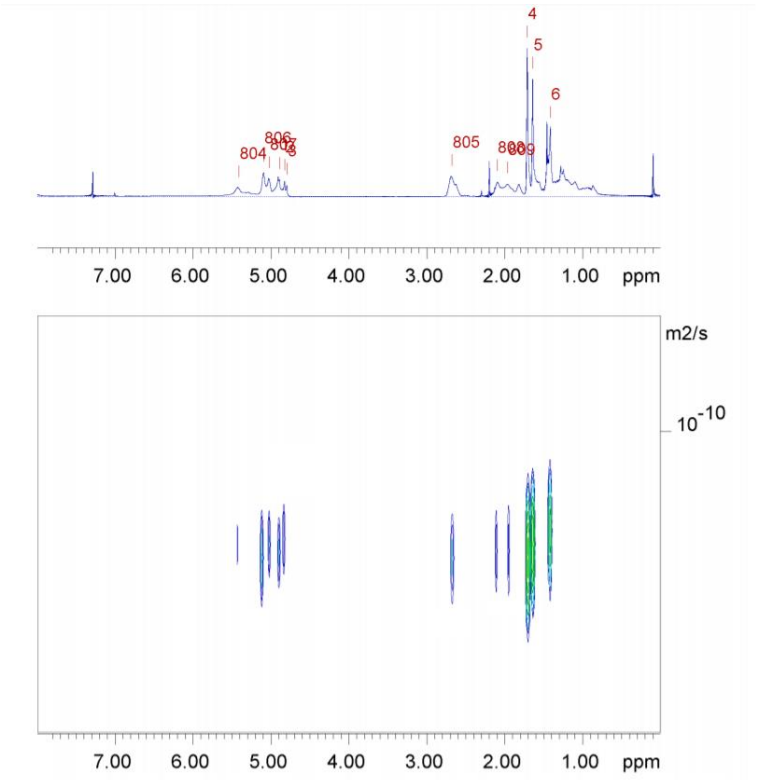

Peak name	F2 [ppm]	D [m2/s]	error
1	4.891	1.08e-10	4.891e-12
2	4.823	1.07e-10	5.092e-12
3	4.795	0.00	0.000
4	1.709	1.15e-10	6.103e-12
5	1.639	1.14e-10	5.936e-12
6	1.412	1.11e-10	5.813e-12
804	5.410	1.13e-10	7.129e-12
805	2.680	1.18e-10	5.930e-12
806	5.095	1.16e-10	5.998e-12
807	5.024	1.12e-10	4.845e-12
808	2.099	1.15e-10	6.346e-12
809	1.968	1.15e-10	8.126e-12

Figure 4S40. DOSY **NMR** spectrum ($CDCl_3$, 25 °C, 600 MHz) of POB copolymers from run 25 of Table 9.

Chapter 5 – Supporting information

5.1 Determination of Polymer Compositions

1.1 Determination of $M^{3,4}$ and $M^{1,4}$ contents in PM and PMS copolymers by ^1H NMR (TCE-d_2, 25 °C)

- $$M^{3,4}(mol\%) = \frac{A_B}{A_A+\frac{A_B}{2}+A_C} \cdot 100$$ **Equation 27**

Where: A_A is the area of the signals $\mathbf{M}^{1,4}{}_3$, $\mathbf{M}^{1,4}{}_7$, $\mathbf{M}^{1,2}{}_7$ and $\mathbf{M}^{3,4}{}_7$ (δ = 5.12 ppm); A_B is the area of the signal $\mathbf{M}^{3,4}{}_1$ (δ = 4.77 ppm); A_C is the area of the signal $\mathbf{M}^{1,2}{}_3$ (δ = 5.63 ppm);

- $$M^{1,4}(mol\%) = \frac{A_A-(\frac{A_B}{2}+A_C)}{A_A+\frac{A_B}{2}+A_C} \cdot 100$$ **Equation 28**

- $$M^{1,2}(mol\%) = 100 - (M^{3,4}(mol\%) + M^{1,4}(mol\%))$$

1.2 Determination of M and S contents in PSM copolymers by ^1H NMR (TCE-d_2, 25 °C)

- $$M(mol\%) = \frac{\frac{1}{2}\cdot(A_A+\frac{A_B}{2})}{\frac{1}{2}\cdot\left(A_A+\frac{A_B}{2}\right)+\frac{A_C}{5}} \cdot 100$$ **Equation 29**

Where: A_A is the area of the signals $\mathbf{M}^{1,4}{}_3$, $\mathbf{M}^{1,4}{}_7$ and $\mathbf{M}^{3,4}{}_7$ (δ=5.12 ppm); A_B is the area of the signal $\mathbf{M}^{3,4}{}_1$ (δ=4.77 ppm); A_C is the area of the signals S_4, S_5 and S_6 (δ=6.45-7.45 ppm)

- $$S\ (mol\%) = 100 - M(mol\%)$$ **Equation 30**

1.3 Determination of $I^{3,4}$, $I^{1,4}$ and $I^{1,2}$ contents in PI by ^1H NMR ($CDCl_3$ or TCE-$d2$, 25 °C)

- $$I^{3,4}(mol\%) = \frac{\frac{B_A}{2}}{\frac{B_A}{2}+(B_B-2B_C)+B_c} \cdot 100$$ **Equation 31**

Where: B_A is the area of the signals $\mathbf{I}^{3,4}{}_1$ (δ = 4.60-4.80 ppm); B_B is the area of the signal $\mathbf{I}^{1,2}{}_4$ and $\mathbf{I}^{1,4(cis+trans)}{}_3$ (δ = 4.80-5.40 ppm) and B_C is the area of the signal $I^{1,2}{}_3$ (δ = 5.75-5.90 ppm)

- $$I^{1,4}(mol\%) = \frac{(B_B-2B_C)}{\frac{B_A}{2}+(B_B-2B_C)+B_c} \cdot 100$$ **Equation 32**

- $$I^{1,2}(mol\%) = 100 - I^{3,4}(mol\%) - I^{1,4}(mol\%)$$ **Equation 33**

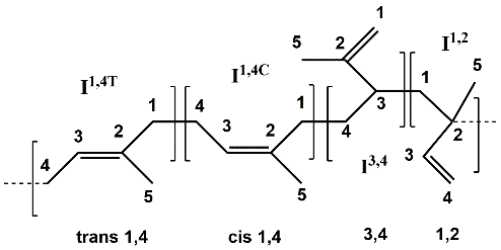

1.4 Determination of $\mathbf{I}^{1,4\ cis}$ and $\mathbf{I}^{1,4\ trans}$ contents in PI by ^{13}C NMR ($CDCl_3$, 25 °C)

- $I^{1,4}\,cis\ (mol\%) = \frac{C_A}{C_A+C_B} \cdot 100$ **Equation 34**

Where: C_A is the area of the signal $\mathbf{I}^{1,4\ cis}{}_5$ (δ=23.5 ppm); C_B is the area of the signal $\mathbf{I}^{1,4\ trans}{}_5$ (δ=16.3 ppm)

- $I^{1,4}\,trans\ (mol\%) = 100 - I^{1,4}\,cis\ (mol\%)$ **Equation 35**

1.5 Determination of M and I contents in PMI copolymers by ^{13}C NMR ($CDCl_3$, 25 °C)

- $M(mol\%) = \frac{C_A}{C_A+C_B+C_C} \cdot 100$ **Equation 36**

where: C_A is the sum of the areas related to the signals $\mathbf{M}^{1,4\ (cis+trans)}{}_2$ (δ=139.3 ppm) and $\mathbf{M}^{3,4}{}_{2'}$ (δ=151.6 ppm); C_B is the area of the signals $\mathbf{I}^{3,4}{}_1$ and $\mathbf{I}^{1,2}{}_4$ (δ=111.4 ppm); C_c is the area of the signals $\mathbf{I}^{1,4}{}_2$ (δ=135.6 ppm)

- $I(mol\%) = 100 - M(mol\%)$ **Equation 37**

1.6 Determination of $\mathbf{M}^{3,4}$ and $\mathbf{M}^{1,4}$ contents in PMI copolymers by ^{13}C NMR ($CDCl_3$, 25 °C)

- $M^{3,4}(mol\%) = \frac{C_D}{C_A} \cdot 100$ **Equation 38**

where: C_A is the sum of the areas related to the signals $\mathbf{M}^{1,4\ (cis+trans)}{}_2$ (δ=139.3 ppm) and $\mathbf{M}^{3,4}{}_{2'}$ (δ=151.6 ppm); C_D is the area of the signals $\mathbf{M}^{3,4}{}_{2'}$ (δ=151.6 ppm)

- $M^{1,4}(mol\%) = 100 - M^{3,4}(mol\%)$ **Equation 39**

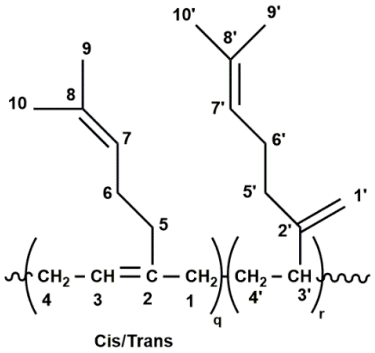

1.5 Determination of M and I contents in PMI copolymers by ^{13}C NMR (TCE-*d*2, 25 °C)

- $M(mol\%) = \frac{C_A}{C_A+C_B+C_C+C_E} \cdot 100$ **Equation 40**

where: C_A is the sum of the areas related to the signals $\mathbf{M}^{1,4\ (cis+trans)}{}_2$ (δ=139.3 ppm) and $\mathbf{M}^{3,4}{}_{2'}$ (δ=151.6 ppm); C_B is the area of the signals $\mathbf{I}^{3,4}{}_1$ and $\mathbf{I}^{1,2}{}_4$ (δ=111.4 ppm); C_c is the area of the signals $\mathbf{I}^{1,4}{}_2$ (δ=135.6 ppm); C_E is the area of the signals $\mathbf{S}_{3''}$ (δ=145.5 ppm) (see **Fig. S6**)

- $I(mol\%) = \frac{C_B+C_C}{C_A+C_B+C_C+C_E} \cdot 100$ **Equation 41**

- $S(mol\%) = \frac{C_E}{C_A+C_B+C_C+C_E} \cdot 100$ **Equation 42**

5.2 Determination of Reactivity Ratios

2.1 Fineman-Ross method

Fineman-Ross equation: $\mathbf{[(f-1)/f]F) = r_1 - r_2 F^2/f}$

where: f = myrcene/styrene molar ratios in the polymer (by ^{1}H **NMR** analysis)

F = myrcene/styrene molar ratios in the feed

r_1, r_2 = reactivity ratios

Table T1. Copolymerization of M and S with Al^{i}Bu$_3$/NaH.

Run [a]	Feed composition		Yield	Copolymer composition		M/S (molar ratio)		F^2/f	(f-1/f)F
	M (*mol*)	S (*mol*)	%	M (*mol*%)	S (*mol*%)	in feed (F)	in copolymer (f)		
1	0.42	0,42	9.1	21	79	1,00	0,26	3,76	-2,76
2	0.42	0,13	8,4	42	58	3,24	0,72	14,47	-1,23
3	0.42	0,11	9,5	45	55	3,81	0,82	17,72	-0,85
4	0.42	0,07	6,8	49	51	5,99	0,96	37,38	0,24
5	0.42	0,04	8,6	66	34	10,5	1,94	56,73	5,09

[a] Reaction conditions: 88 µL, toluene 0.5 mL, tetrahydrofuran 25 µL, 100 °C, 30 min.

Table T2. Reactivity ratio for copolymerization of M and S.

Iniziator	r_1	r_2	$r_1 \bullet r_1$
Al^{i}Bu$_3$/NaH	0.13 ± 0.002	3.47 ± 0.91	0.45

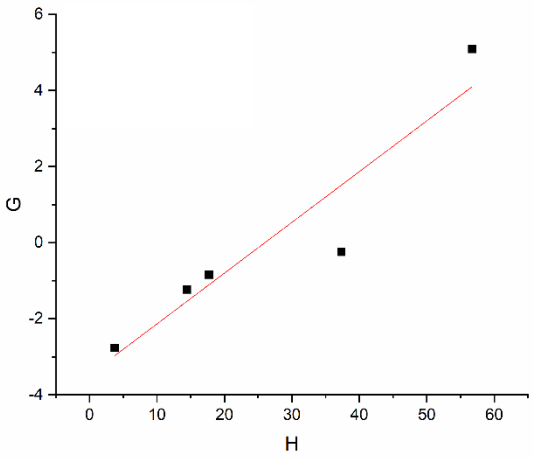

Figure 5SA1. Fineman-Ross plot for copolymerization of myrcene and styrene with Al^{i}Bu$_3$/NaH as initiating system at 100 °C in toluene and in the presence of THF (F = [Myr]/[Sty] in feed, f = [Myr]/[Sty] in copolymers, rMyr = 0.13 ± 0.002 and rSty = 3.47 ± 0.91).

5.3 Kelen-Tudos method

The reactivity ratio can also be estimated with Kelen-Tudos equation (**$\eta = (r_1+r_2/\alpha)\xi - r_2/\alpha$**) which variables are expressed as:

$G = (f-1/f)F$
$H = F^2/f$
$\eta = G/(\alpha+H)$
$\xi = H/(\alpha+H)$

Where η and ξ are the functions of the parameters G and H, and α is a constant equal to $(H_{max} \times H_{min})^{1/2}$, H_{max} and H_{min} being the lowest and highest H values, respectively.
The intercepts at ξ = 0 and ξ = 1 of the η versus ξ plot gives $-r_1/\alpha$ and r_2

Table T3. FR and KT parameters for PMS copolymers

Sample	$F = M_1/M_2$	$f = m_1/m_2$	H	G	ξ	η
RR1	1,00	0,26	3,76	-2,76	0,20	-0,150
RR2	3,24	0,72	14,4	-1,23	0,50	-0,042
RR3	3,81	0,82	17,7	-0,85	0,55	-0,026
RR4	5,99	0,96	37,4	-0,24	0,72	-0,004
RR5	10,4	1,94	56,7	5,09	0,80	0,071

$\alpha = (H_{min} \times H_{max})^{1/2} = 14,60$.

Table T4. Reactivity ratio for copolymerization of M and S.

Iniziator	r_1	r_2	$r_1 \bullet r_1$
Al^{i}Bu$_3$/NaH	0.12 ± 0.003	3.18 ± 0.65	0.38

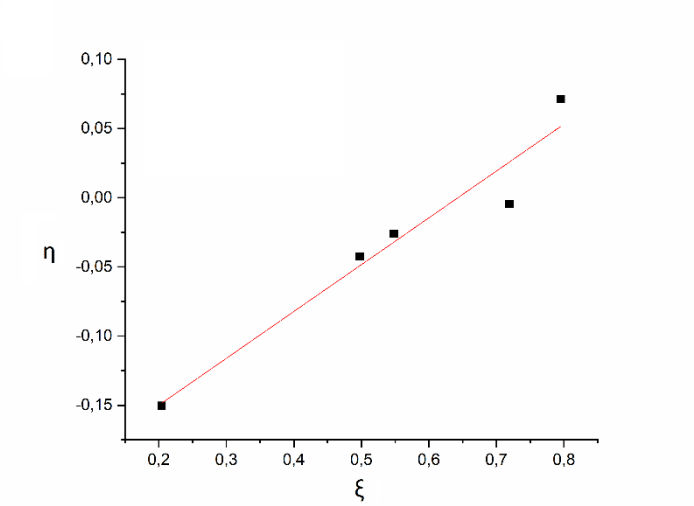

Figure 5SA2. Determination of reactivity ratios using Kelen-Tudos method for PMS copolymers (r_{Myr} = 0.12 ± 0.003 and r_{Sty} = 3.18 ± 0.65).

5.4 Extended Kelen-Tudos method

$Z = \log(1 - S_1)/\log(1 - S_2)$ where S_1 and S_2 are the partial molar conversions:

$S_2 = w(\mu + F)/(\mu + f) \times 100$, w = percentage of conversions, $\mu = M_{wt\,2}/M_{wt\,1}$
$S_1 = S_2 f/F$;

They derived an expression, $H = F2/f$ and $G = F(f - 1)/f$ In this method also, r2 and r1 can be readily obtained either graphically or computation using the least square methods by plotting 1 versus 0. The 1 versus 0 plot gives a straight line between 0 and 1 provided the system can be adequately described by the conventional copolymerization composition equation.

Table T5. exKT parameters for PMS copolymers

Sample	S_1	S_2	Z	H	G	ξ	η
RR1	0,041	0,155	0,249	4,26	-2,93	0,186	-0,129
RR2	0,050	0,225	0,202	17,6	-1,36	0,486	-0,038
RR3	0,059	0,274	0,189	22,8	-0,95	0,550	-0,023
RR4	0,043	0,266	0,140	48,4	-0,28	0,722	-0,004
RR5	0,066	0,358	0,154	81,2	6,09	0,814	0,061

$\alpha = (H_{min} \times H_{max})^{1/2} = 18{,}60$, $\mu = 0{,}765$.

Table T6. Reactivity ratio for copolymerization of M and S.

Iniziator	r_1	r_2	$r_1 \bullet r_1$
Al^{i}Bu$_3$/NaH	0.10 ± 0.004	3.32 ± 0.68	0.33

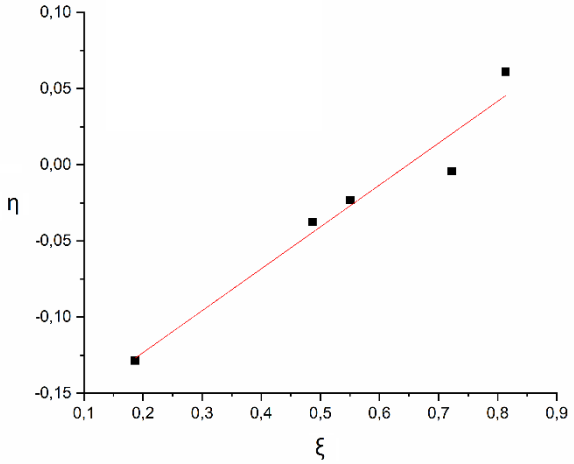

Figure 5SA3. Determination of reactivity ratios using extended Kelen-Tudos method for PMS copolymers (r_{Myr} = 0.10 ± 0.004 and r_{Sty} = 3.32 ± 0.68).

5.5 NMR Characterizations

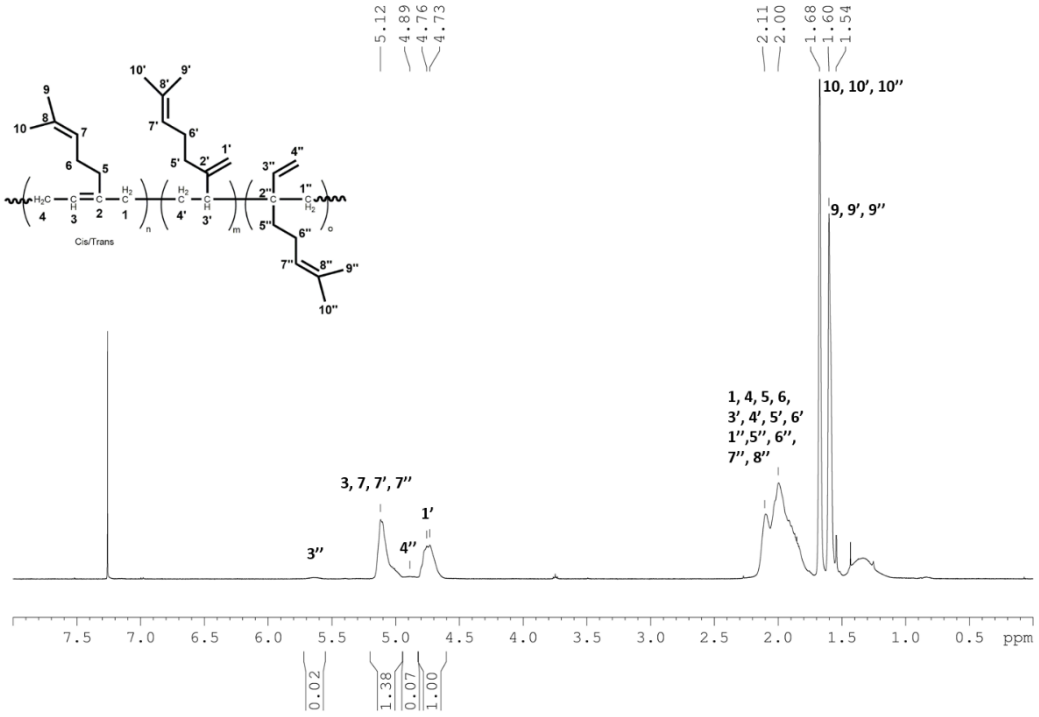

Figure 5S1. ^{1}H **NMR** spectrum ($CDCl_3$, 25 °C, 400 MHz) of PM from run 31 of Table 13.

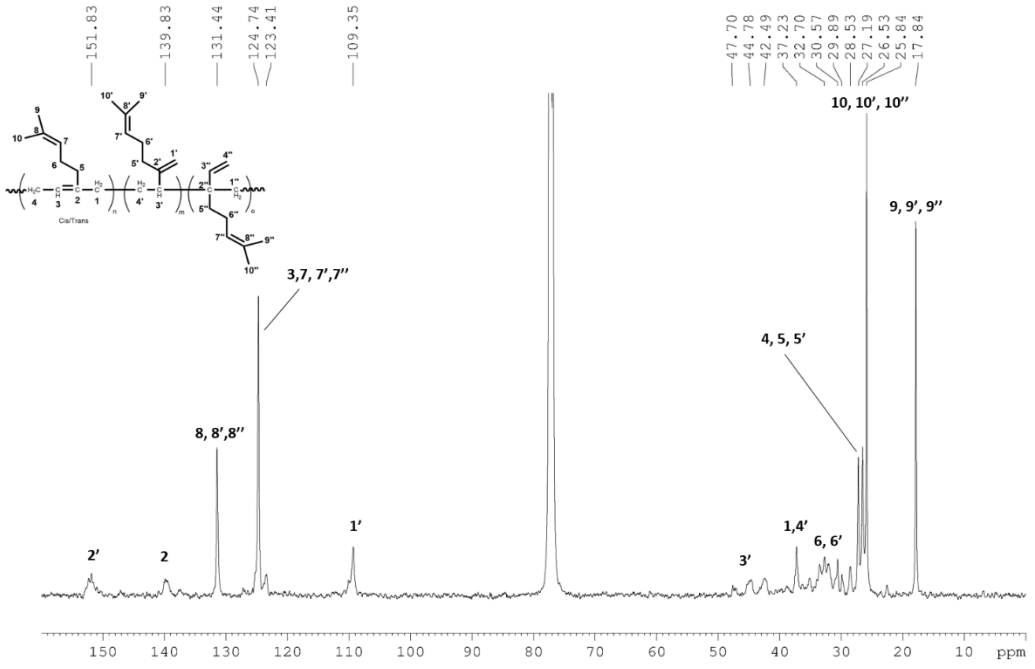

Figure 5S2. ^{13}C **NMR** spectrum ($CDCl_3$, 25 °C, 400 MHz) of PM from run 31 of Table 13.

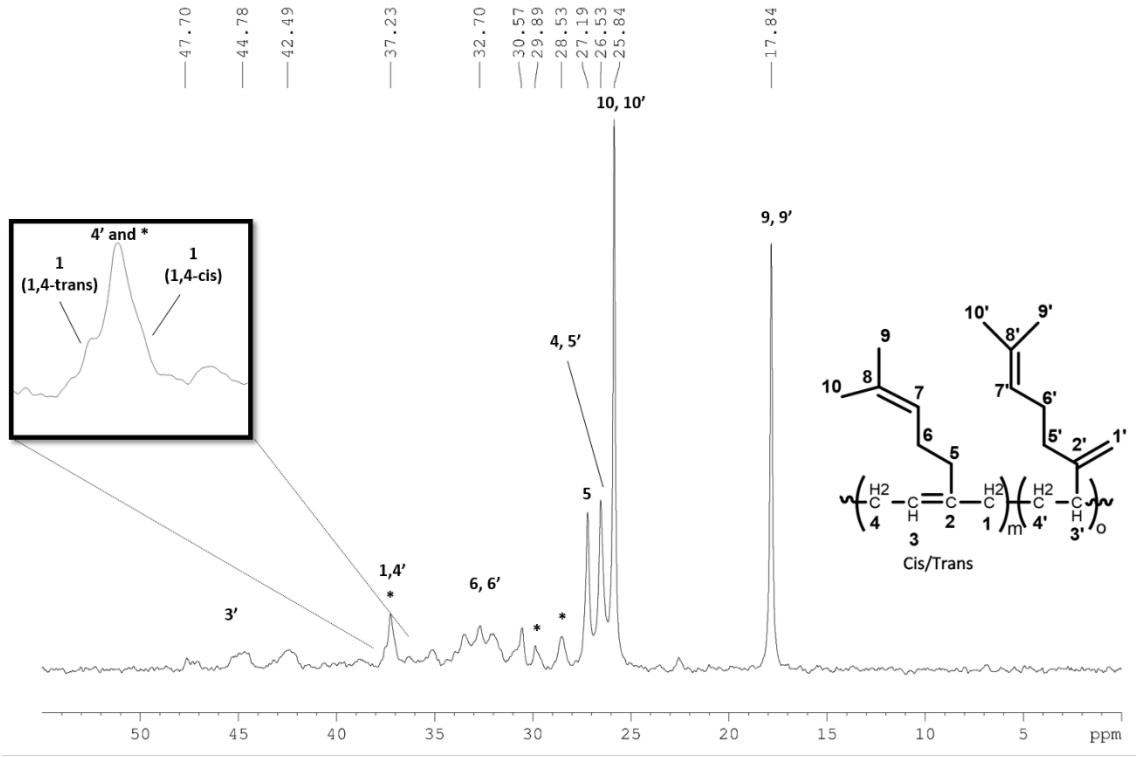

Figure 5S3. Enlargement of aliphatic region of ^{13}C **NMR** spectrum ($CDCl_3$, 25 °C, 400 MHz) of PM from run 31 of Table 13.

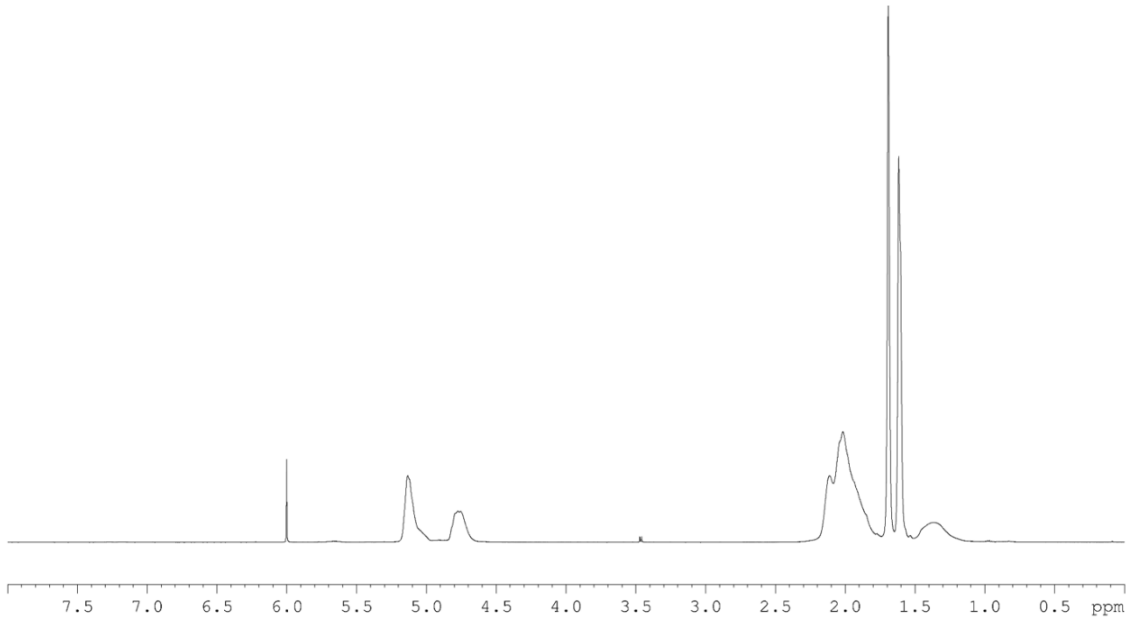

Figure 5S4. ^{1}H **NMR** spectrum (TCDE, 25 °C, 400 MHz) of PM from run 34 of Table 13.

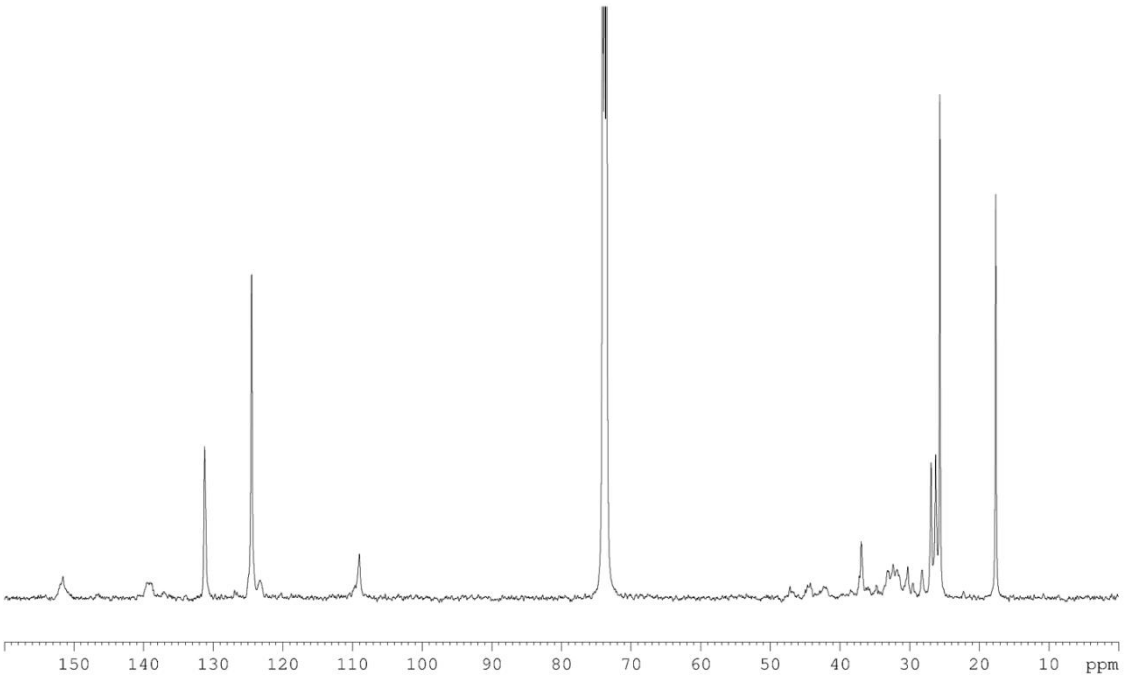

Figure 5S5. ^{13}C **NMR** spectrum (TCDE, 25 °C, 400 MHz) of PM from run 34 of Table 13.

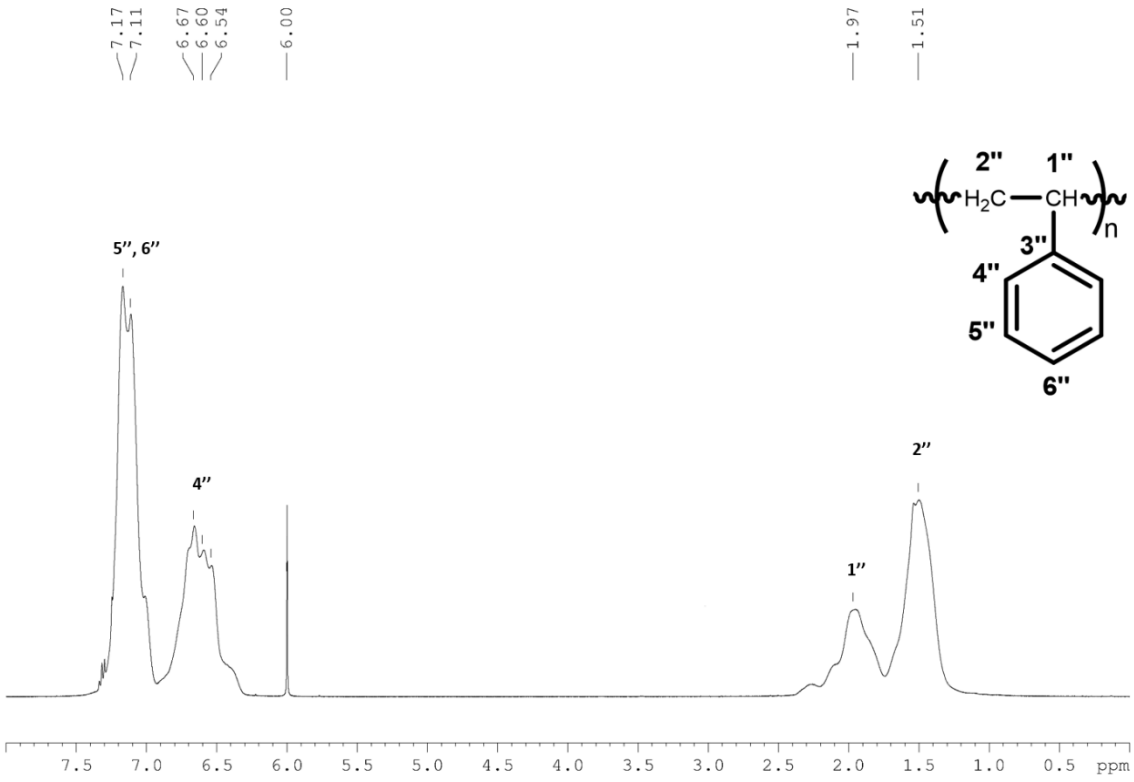

Figure 5S6. ^{1}H **NMR** spectrum (TCDE, 25 °C, 400 MHz) of PS from run 35 of Table 13.

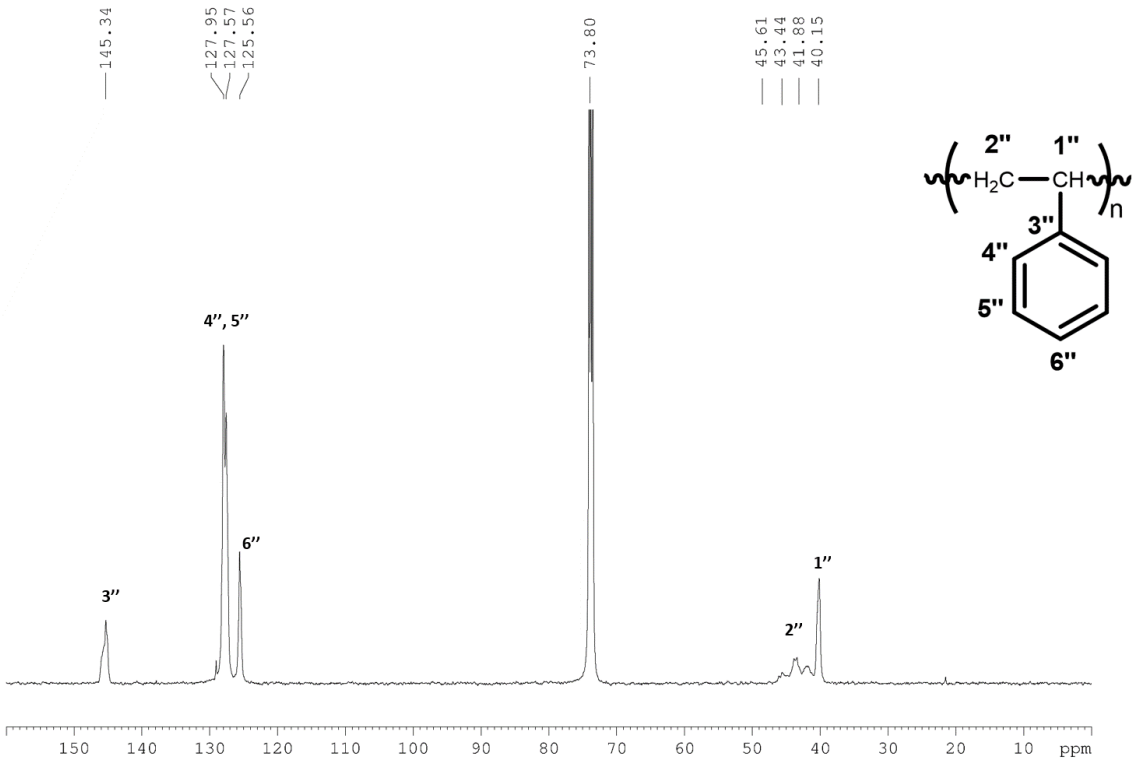

Figure 5S7. ^{13}C **NMR** spectrum (TCDE, 25 °C, 400 MHz) of PS from run 35 of Table 13.

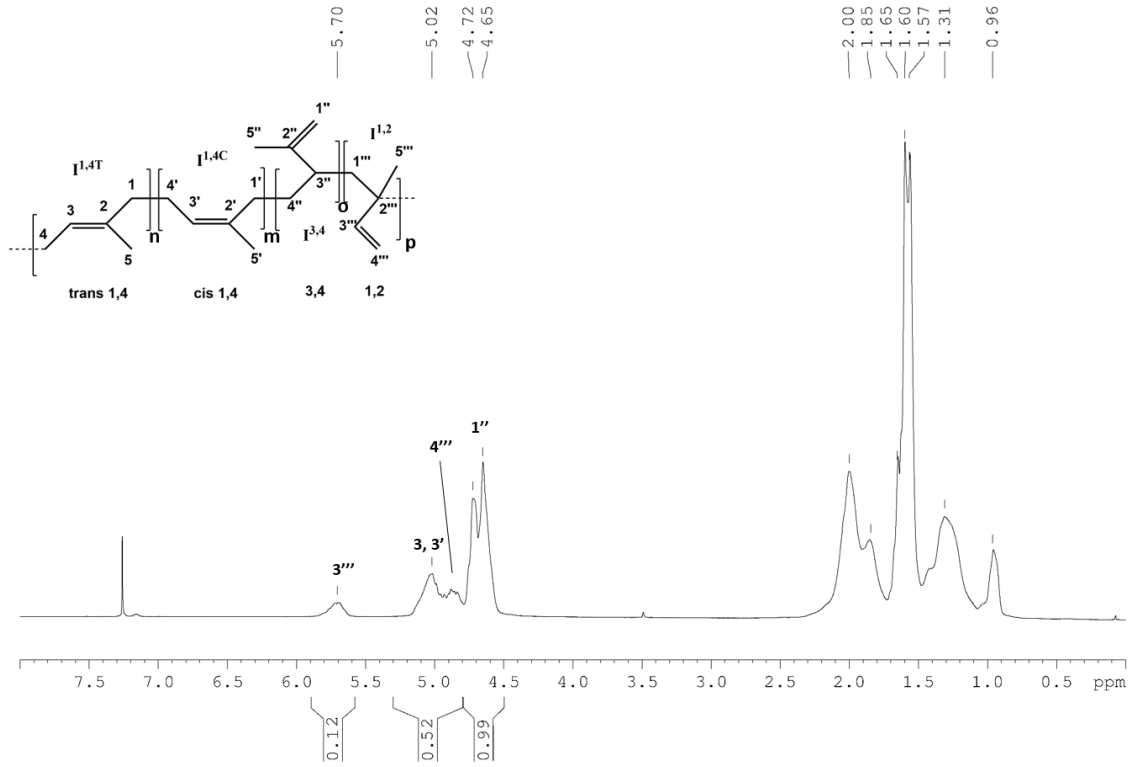

Figure 5S8. ^{1}H **NMR** spectrum (TCDE, 25 °C, 400 MHz) of PI from run 37 of Table 13.

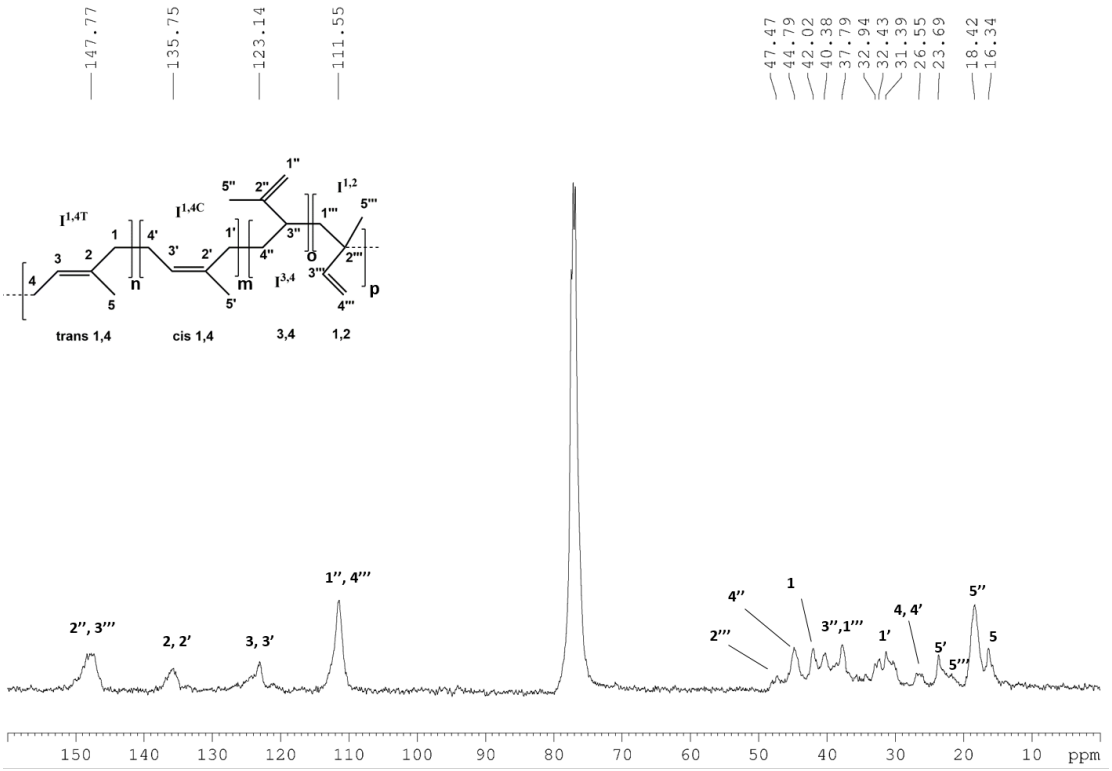

Figure 5S9. ^{13}C **NMR** spectrum (TCDE, 25 °C, 400 MHz) of PI from run 37 of Table 13.

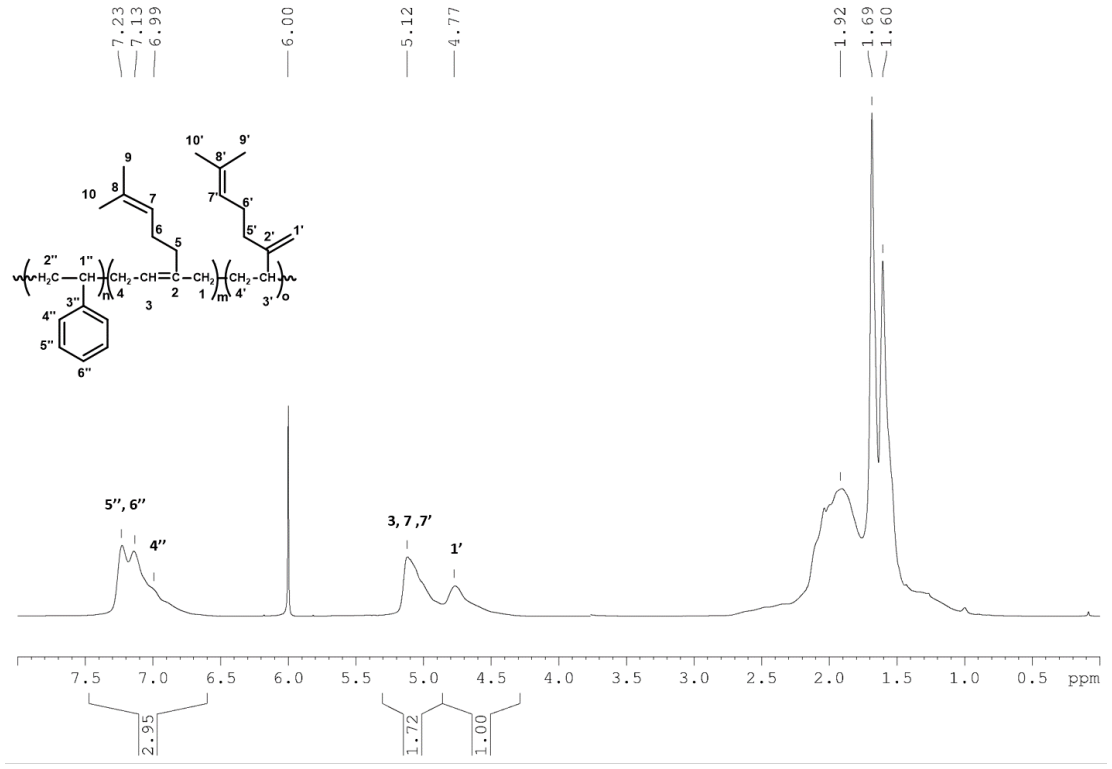

Figure 5S10. ^{1}H **NMR** spectrum (TCDE, 25 °C, 400 MHz) of PMS from run 42 of Table 14.

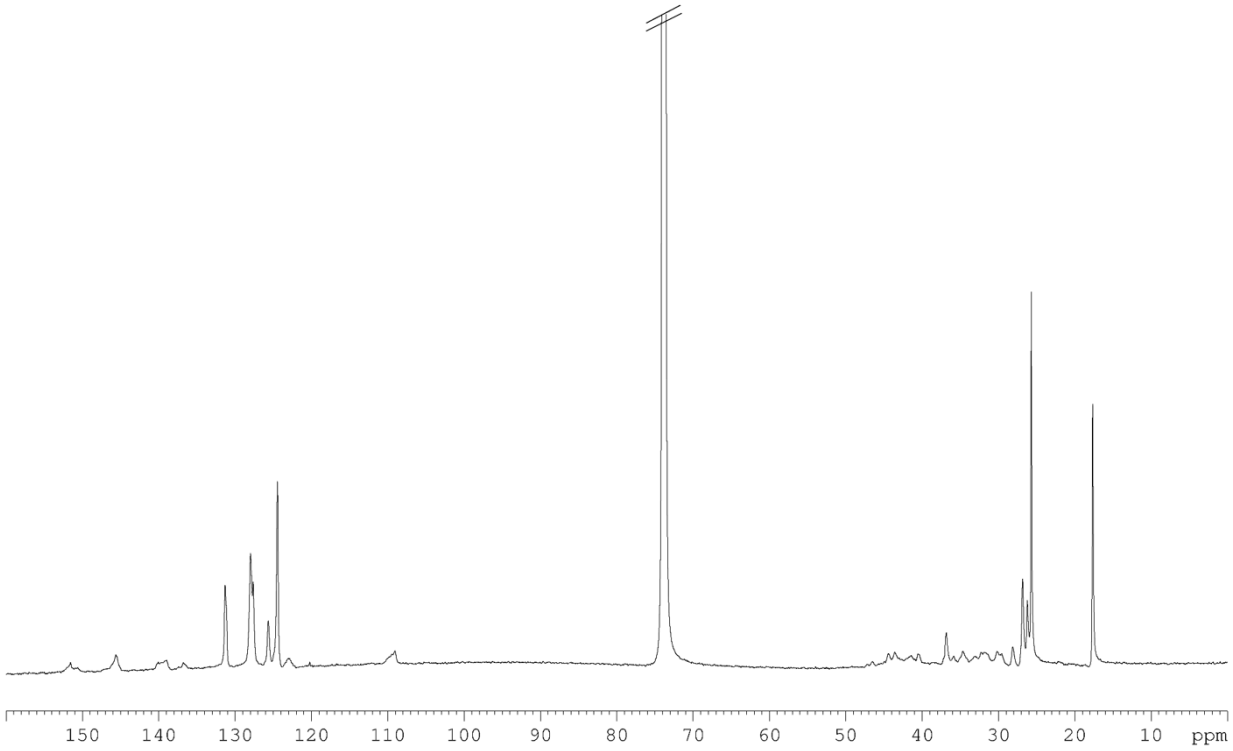

Figure 5S11. ^{13}C **NMR** spectrum (TCDE, 25 °C, 400 MHz) of PMS from run 42 of Table 14.

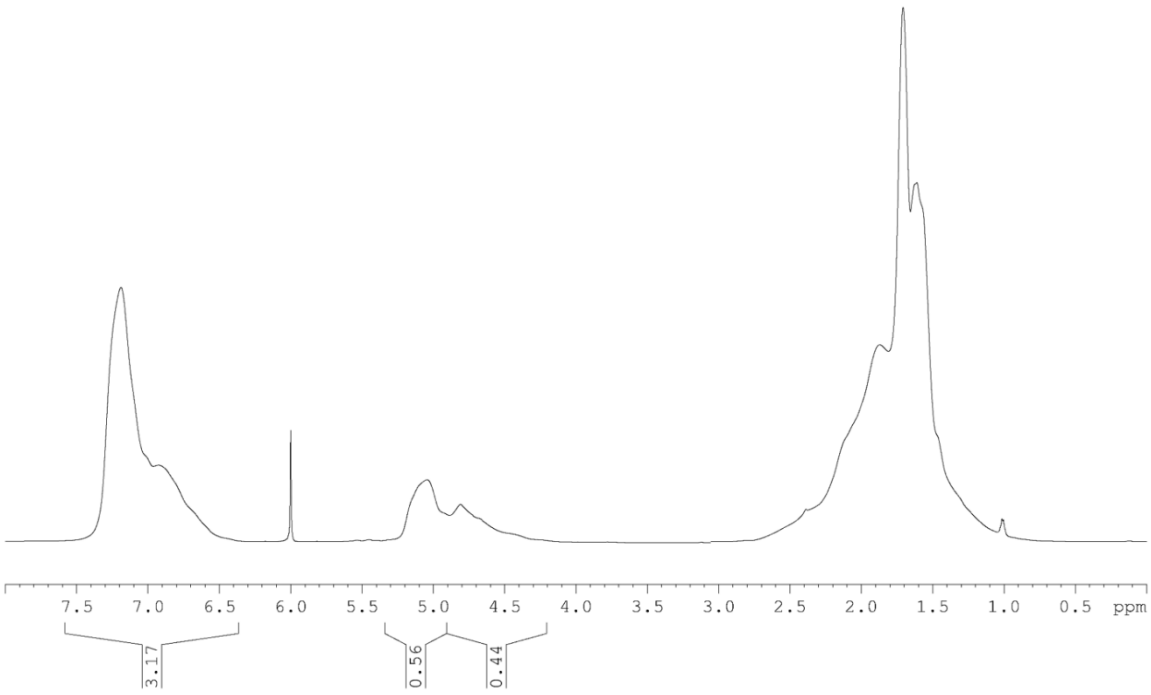

Figure 5S12. ^{1}H **NMR** spectrum (TCDE, 25 °C, 400 MHz) of PMS from run 43 of Table 14.

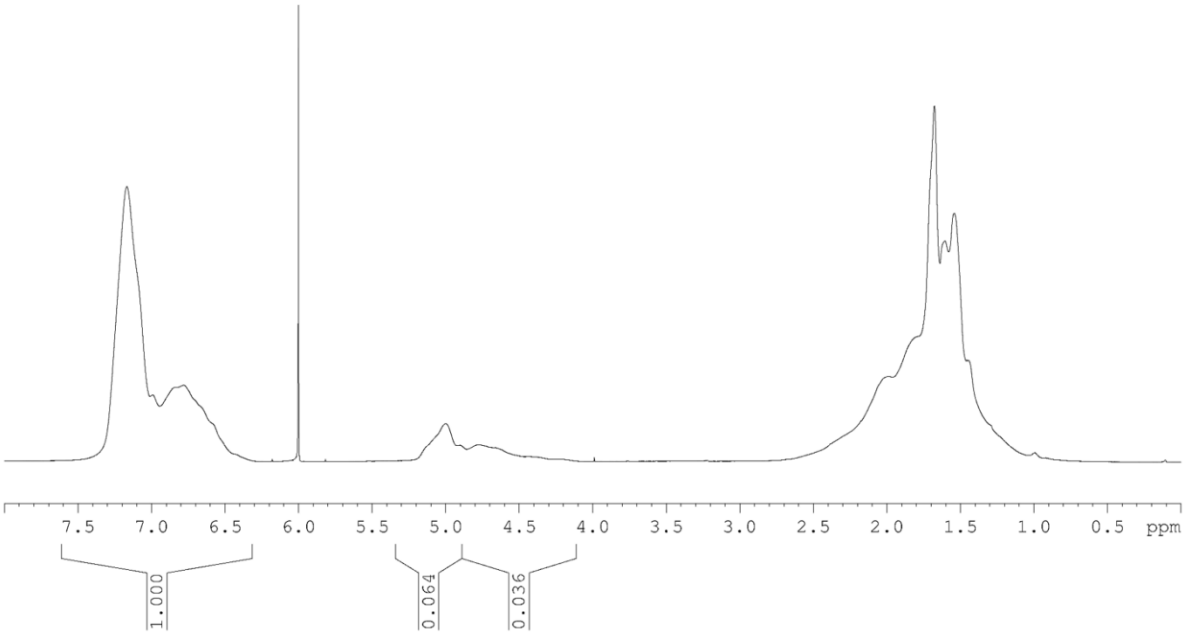

Figure 5S13. ^{1}H **NMR** spectrum (TCDE, 25 °C, 400 MHz) of PMS from run 44 of Table 14.

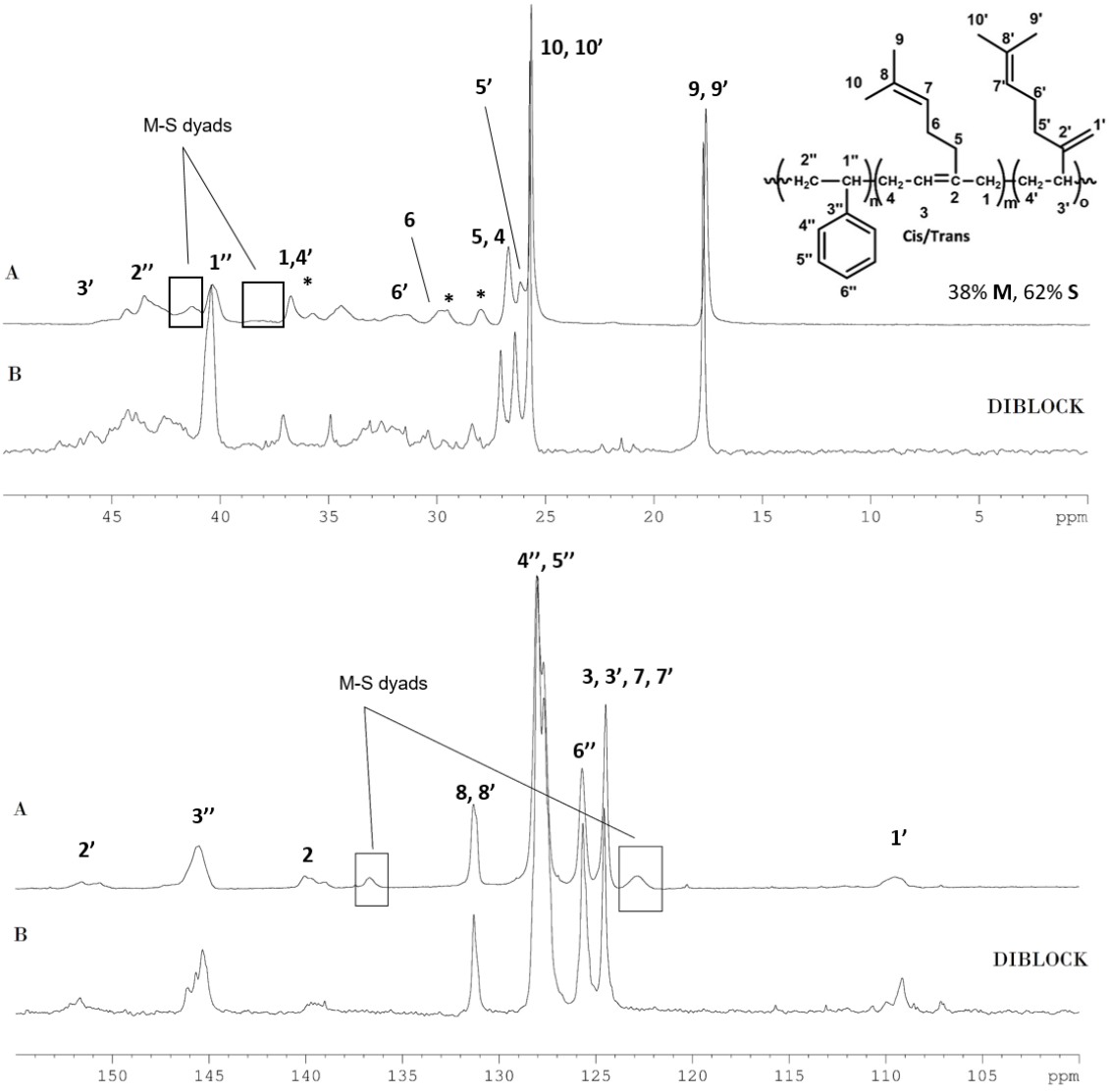

Figure 5S14. ^{13}C **NMR** spectra (TCDE, 25 °C, 400 MHz) of PMS copolymer from run 43 (a) and PMS diblock from run 51 (b) of Table 14.

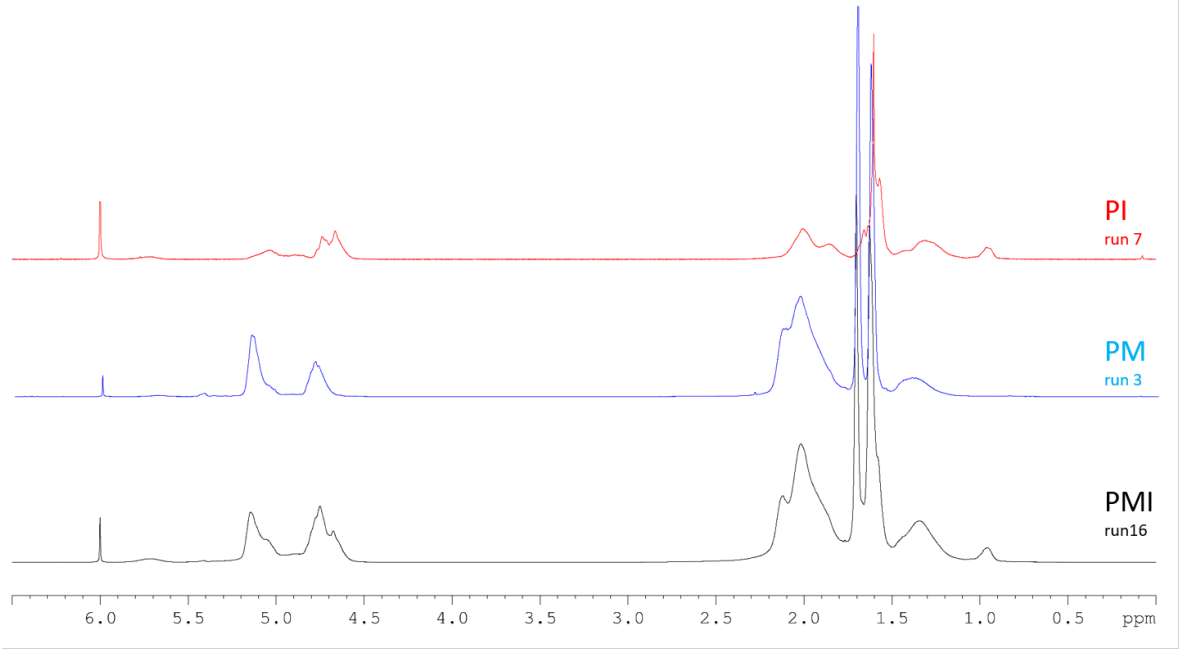

Figure 5S15. ^{1}H **NMR** spectra (TCDE, 25 °C, 400 MHz) of PM (run 33), PI (run 37) and PMI (run 46) from Table2 13-14.

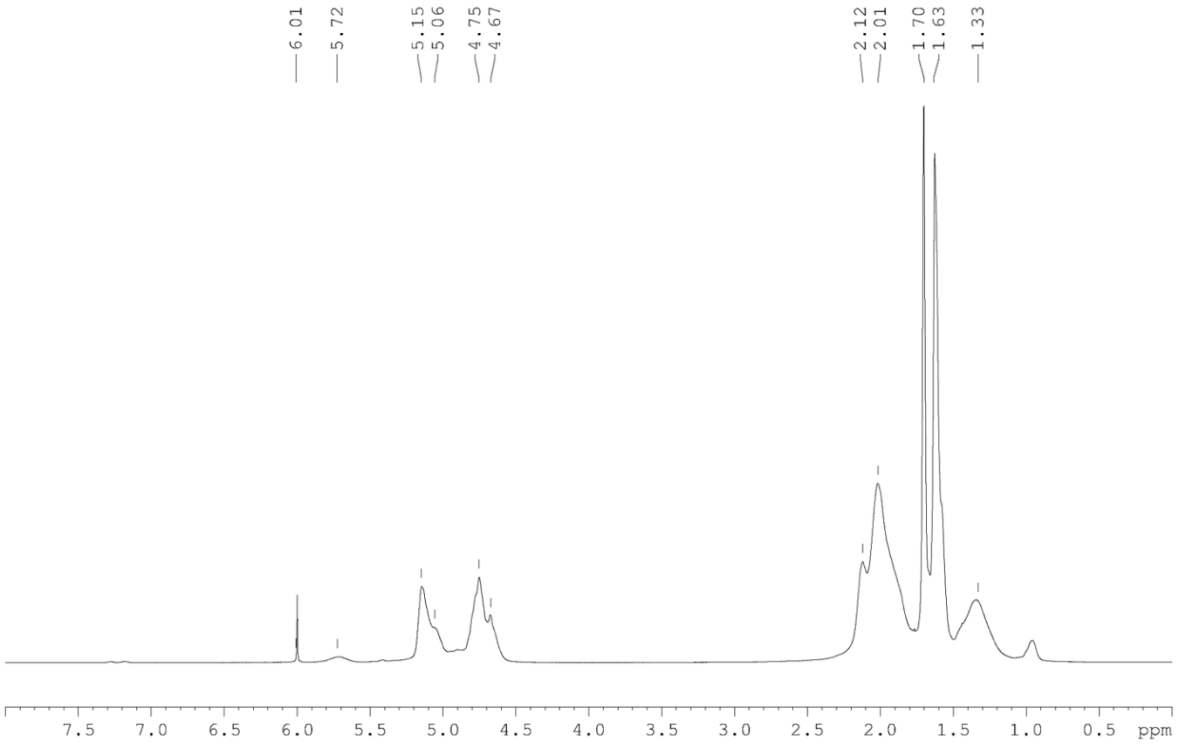

Figure 5S16. ^{1}H **NMR** spectrum (TCDE, 25 °C, 400 MHz) of PMI from run 46 of Table 14.

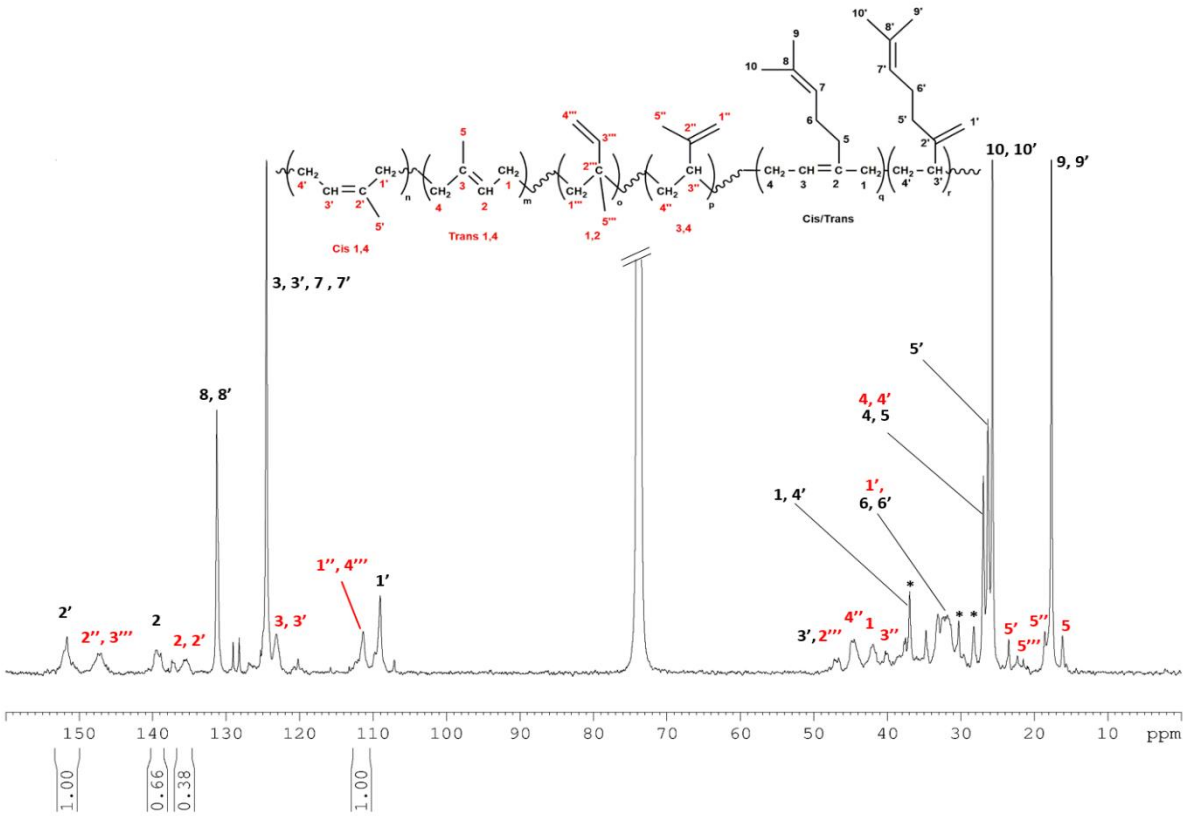

Figure 5S17. ^{13}C **NMR** spectrum (TCDE, 25 °C, 400 MHz) of PMI from run 46 of Table 14.

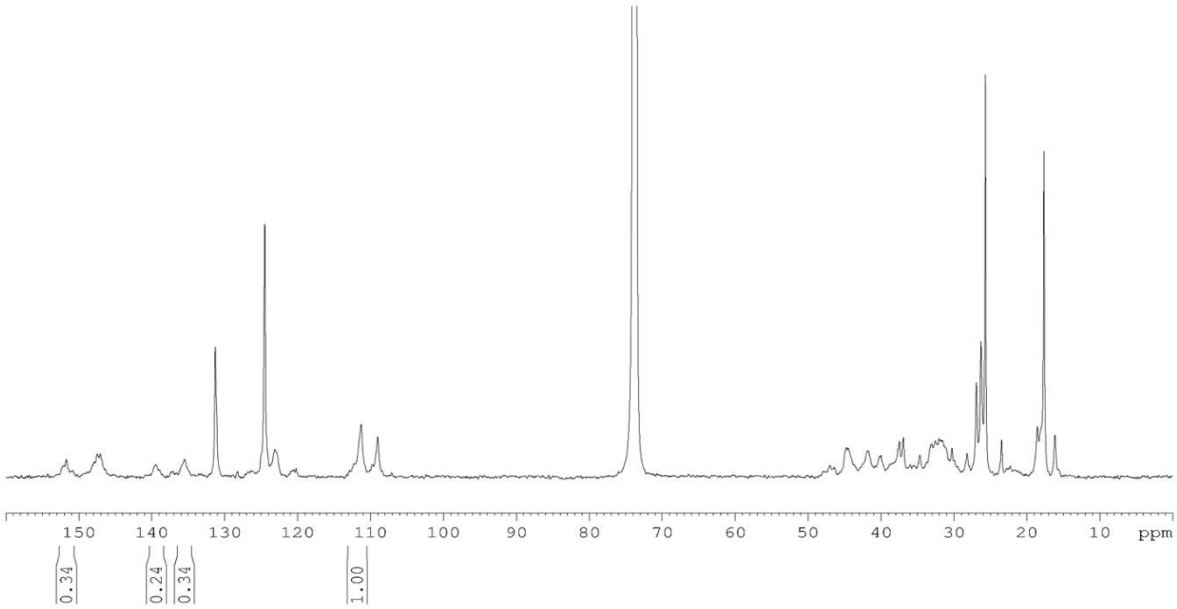

Figure 5S18. ^{13}C **NMR** spectrum (TCDE, 25 °C, 400 MHz) of PMI from run 47 of Table 14.

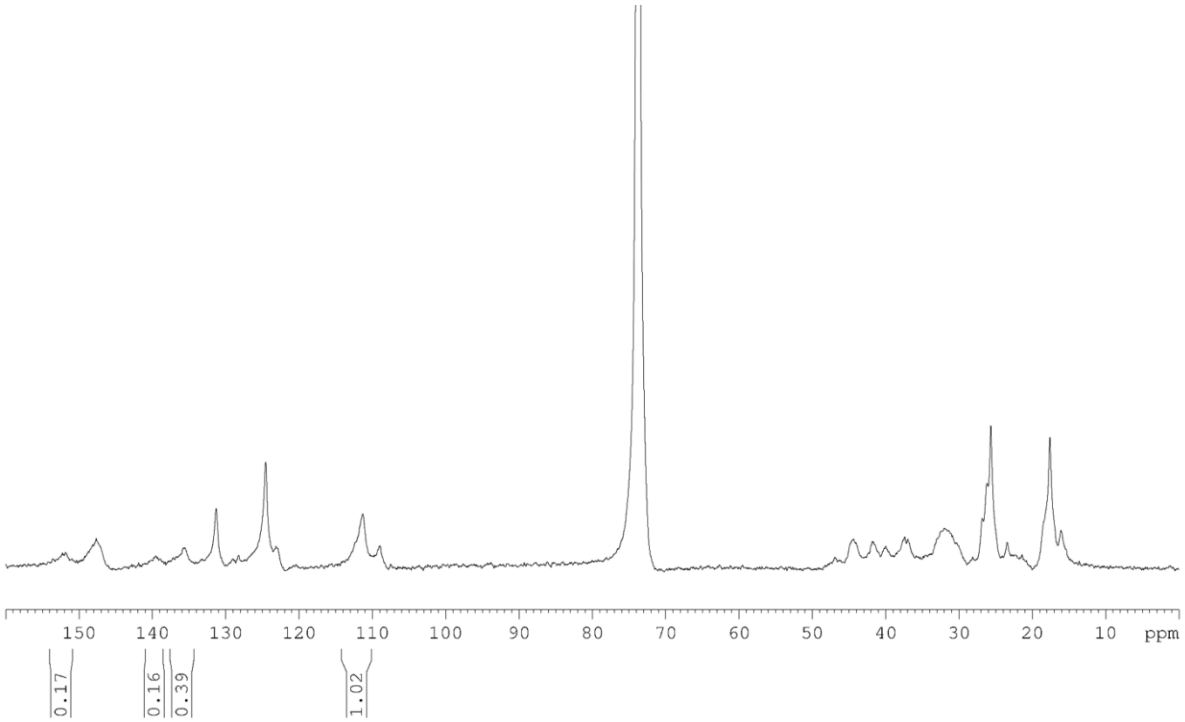

Figure 5S19. ^{13}C **NMR** spectrum (TCDE, 25 °C, 400 MHz) of PMI from run 48 of Table 14

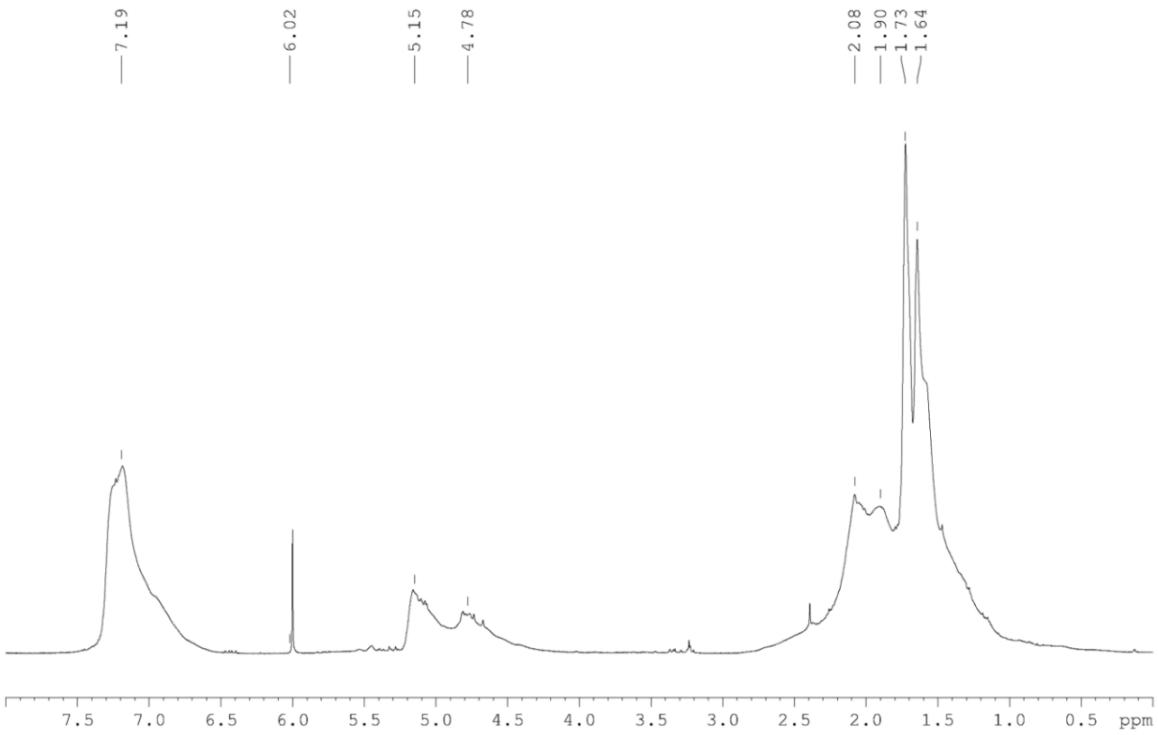

Figure 5S20. ^{1}H **NMR** spectrum (TCDE, 25 °C, 400 MHz) of PMSI from run 48 of Table 14

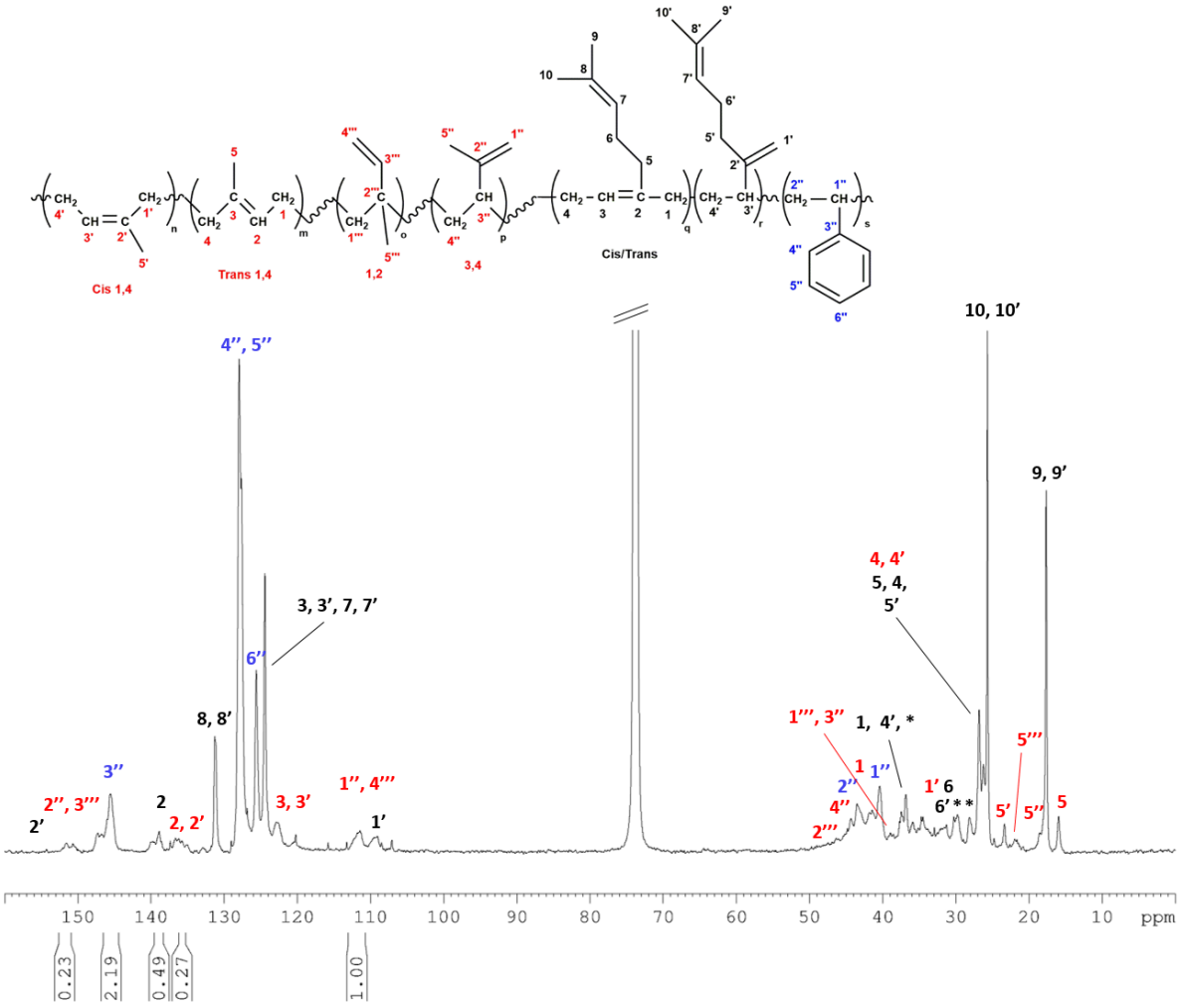

Figure 5S21. ^{13}C **NMR** spectrum (TCDE, 25 °C, 400 MHz) of PMSI from run 48 of Table 14

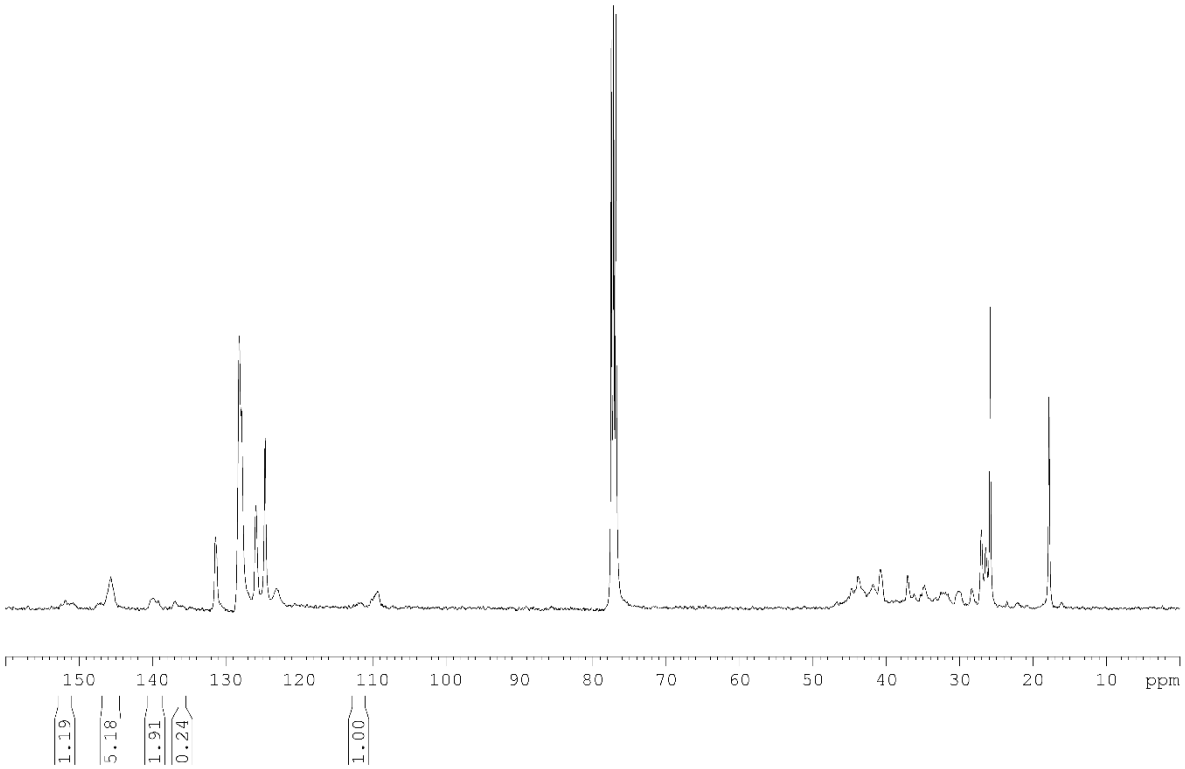

Figure 5S22. ^{13}C **NMR** spectrum ($CDCl_3$, 25 °C, 400 MHz) of PMSI from run 49 of Table 14.

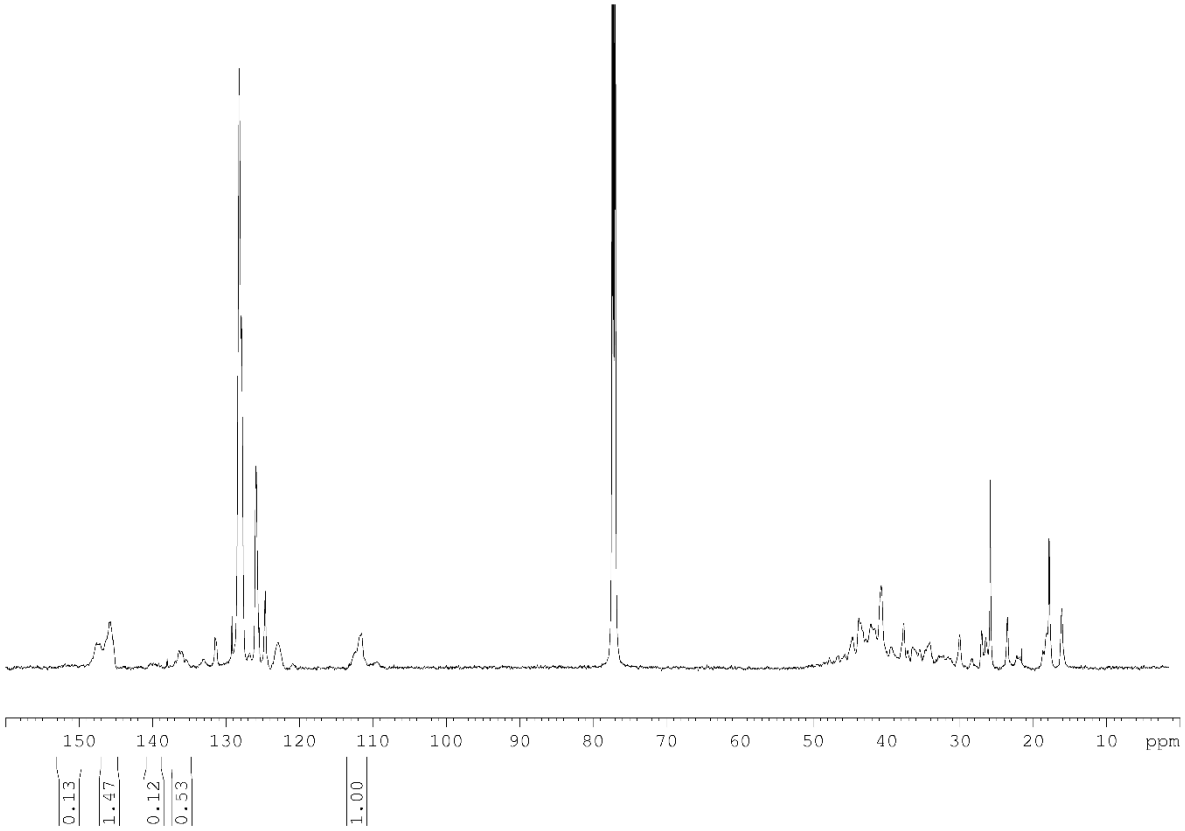

Figure 5S23. ^{13}C **NMR** spectrum (TCDE, 25 °C, 400 MHz) of PMSI from run 50 of Table 14.

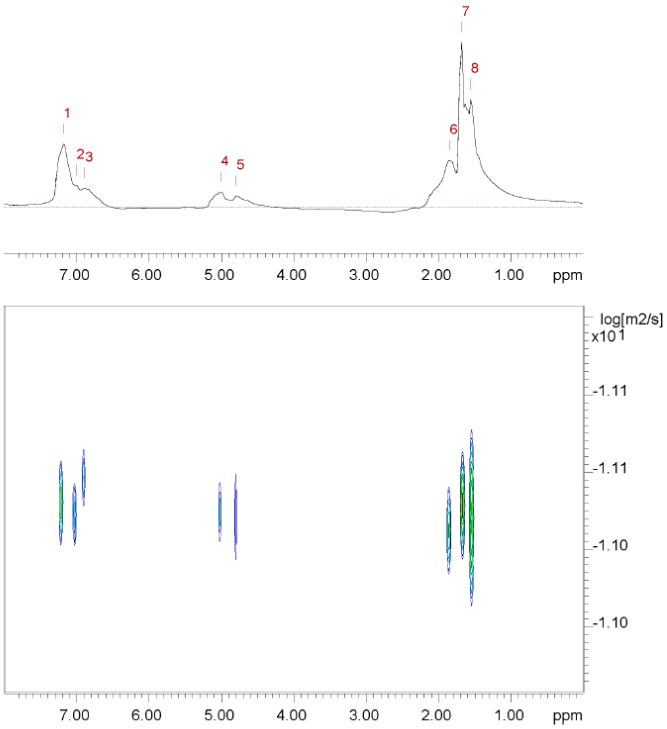

Fitted function:	f (x) = A * exp (-D * x^2 * gamma^2 * littleDelta^2 (bigDelta-littleDelta/3)* 10^4
used gamma:	26752 rad/(s*Gauss)
used little delta:	0.0050000 s
used big delta:	0.14990 s
used gradient strength:	variable
Random error estimation of data:	RMS per spectrum (or trace/plane)
Systematic error estimation of data:	worst case per peak scenario
Fit parameter Error estimation method:	from fit using arbitray y uncertainties
Confidence level:	95%
Used peaks:	automatically picked peaks
Used integrals:	peak intensities
Used Gradient strength:	all values (including replicates) used

Peak name	F2 [ppm]	D [m2/s]	error
1	7.190	8.09e-12	3.034e-13
2	7.008	8.28e-12	3.385e-13
3	6.889	7.89e-12	2.786e-13
4	5.013	8.62e-12	3.627e-13
5	4.795	9.39e-12	7.118e-13
6	1.854	8.84e-12	3.726e-13
7	1.683	8.57e-12	3.458e-13
8	1.558	8.74e-12	6.227e-13

Figure 5S24. DOSY **NMR** spectrum ($CDCl_3$, 25 °C, 600 MHz) of PMS copolymers from run 43 of Table 14

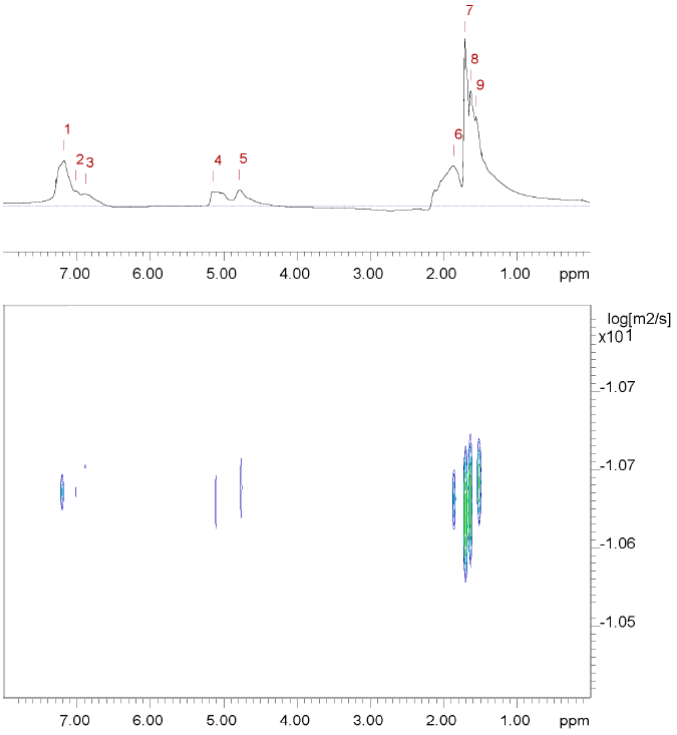

Fitted function:	f (x) = A * exp (-D * x^2 * gamma^2 * littleDelta^2 (bigDelta-littleDelta/3)* 10^4
used gamma:	26752 rad/(s*Gauss)
used little delta:	0.0050000 s
used big delta:	0.14990 s
used gradient strength:	variable
Random error estimation of data:	RMS per spectrum (or trace/plane)
Systematic error estimation of data:	worst case per peak scenario
Fit parameter Error estimation method:	from fit using arbitray y uncertainties
Confidence level:	95%
Used peaks:	automatically picked peaks
Used integrals:	peak intensities
Used Gradient strength:	all values (including replicates) used

Peak name	F2 [ppm]	D [m2/s]	error
1	7.190	2.05e-11	6.259e-13
2	7.018	2.05e-11	5.955e-13
3	6.883	1.97e-11	3.899e-13
4	5.138	2.97e-11	3.340e-12
5	4.790	2.79e-11	2.901e-12
6	1.859	2.29e-11	1.212e-12
7	1.709	2.62e-11	2.167e-12
8	1.636	2.59e-11	2.299e-12
9	1.558	2.20e-11	1.393e-12

Figure 5S25. DOSY **NMR** spectrum ($CDCl_3$, 25 °C, 600 MHz) of PMS diblock copolymers from run of 51 Table 14

5.6 DSC Thermal Analysis

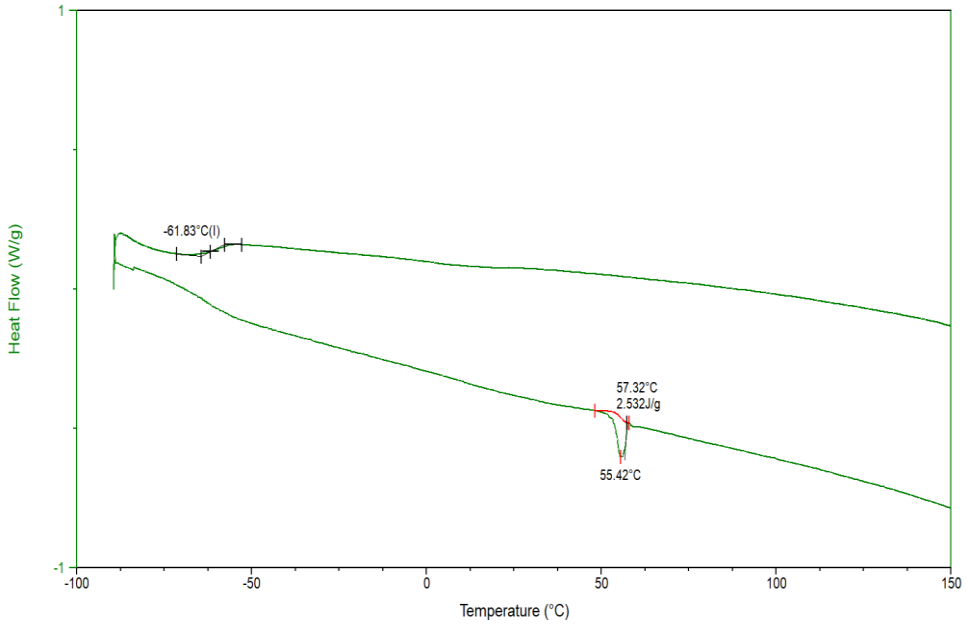

Figure 5S26. DSC thermogram of PM from run 31 of **Table 13**.

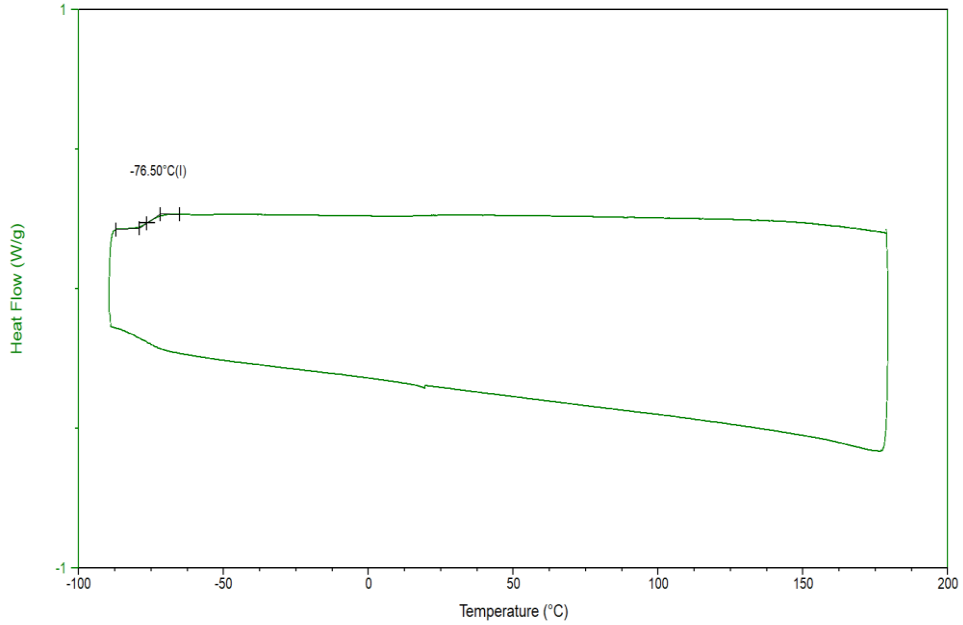

Figure 5S27. DSC thermogram of PM from run 34 of **Table 13**.

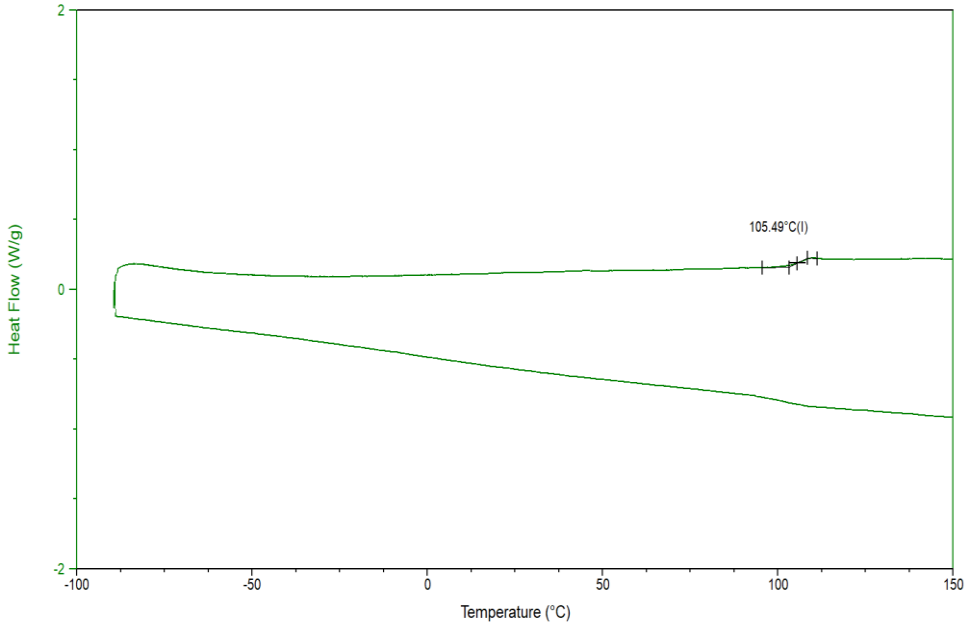

Figure 5S28. DSC thermogram of PS from run 35 of **Table 13**.

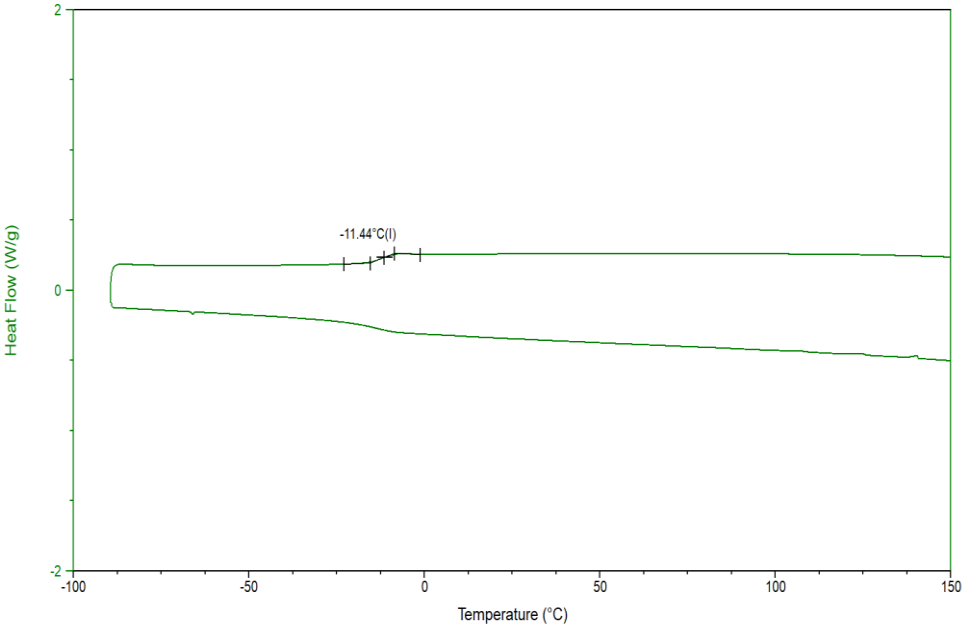

Figure 5S29. DSC thermogram of PI from run 38 of **Table 13**.

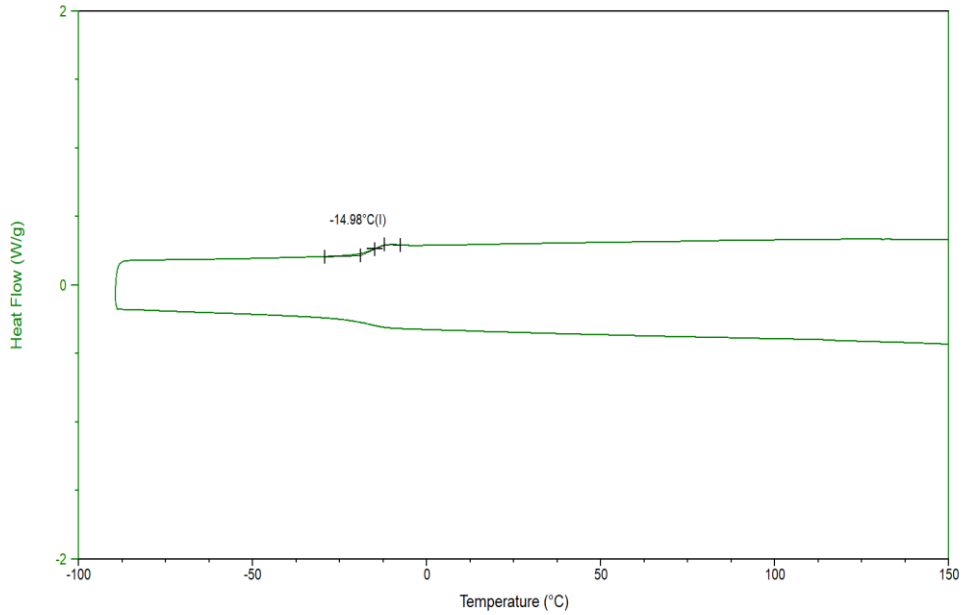

Figure 5S30. DSC thermogram of PI from run 39 of **Table 13**.

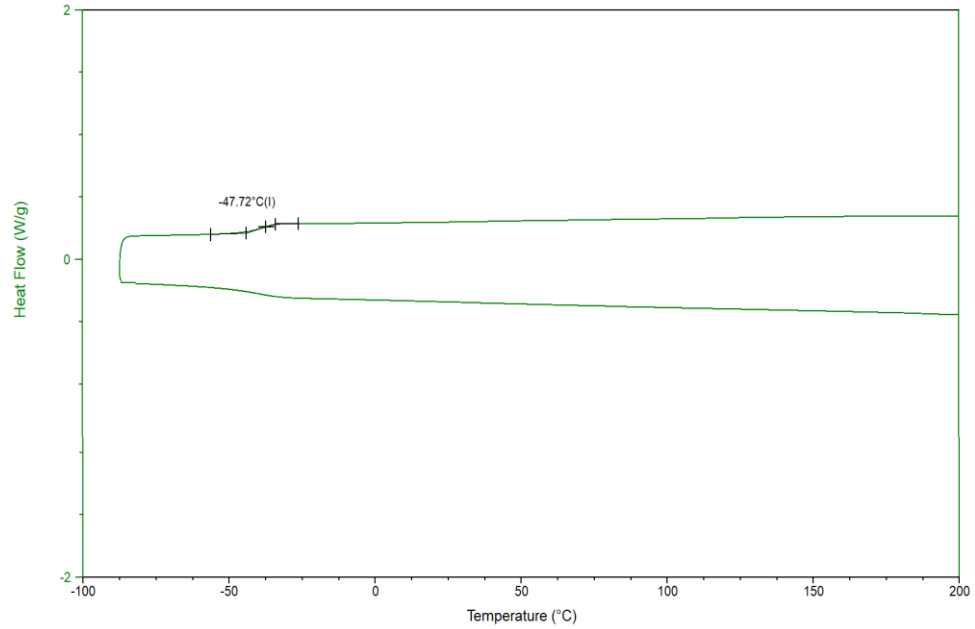

Figure 5S31. DSC thermogram of PMS from run 40 of **Table 14.**

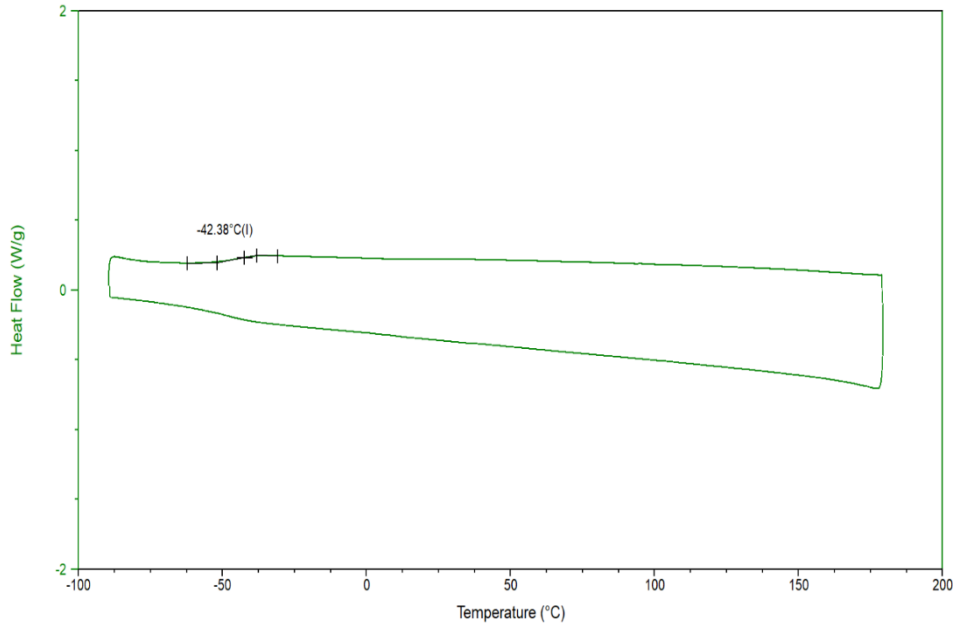

Figure 5S32. DSC thermogram of PMS from run 42 of **Table 14.**

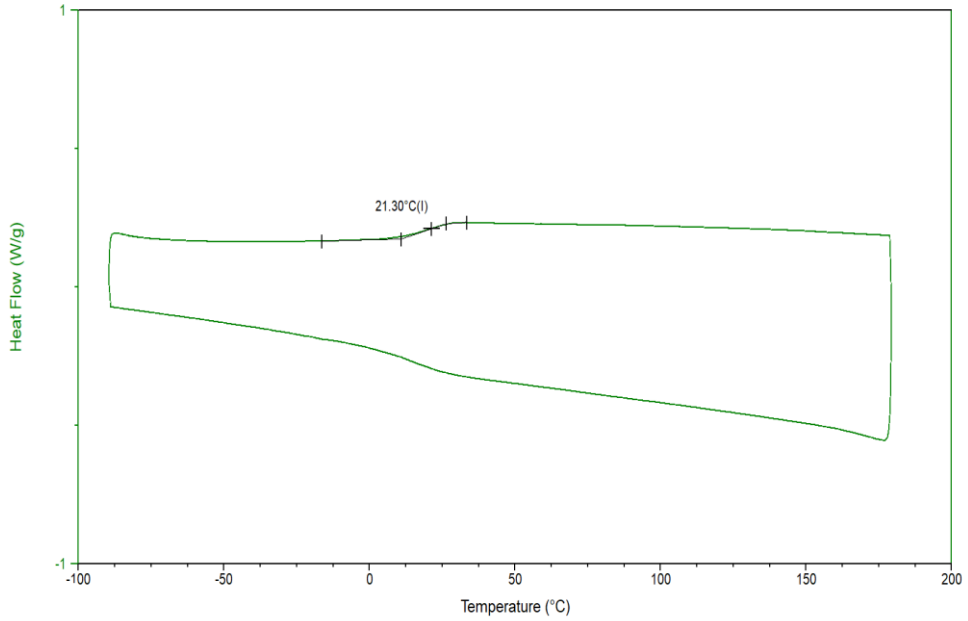

Figure 5S33. DSC thermogram of PMS from run 44 of **Table 14.**

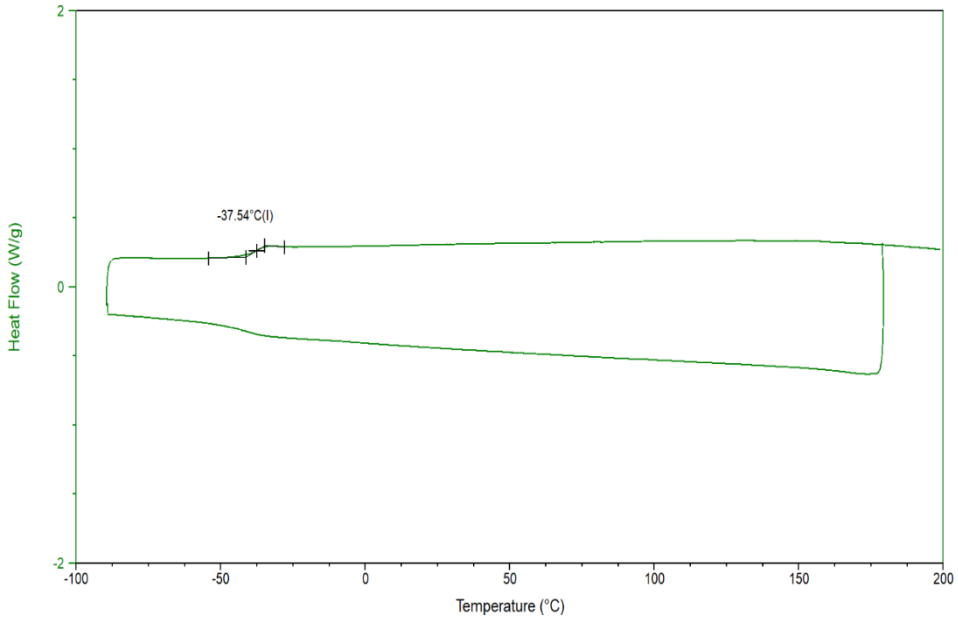

Figure 5S34. DSC thermogram of PMI from run 46 of **Table 14**.

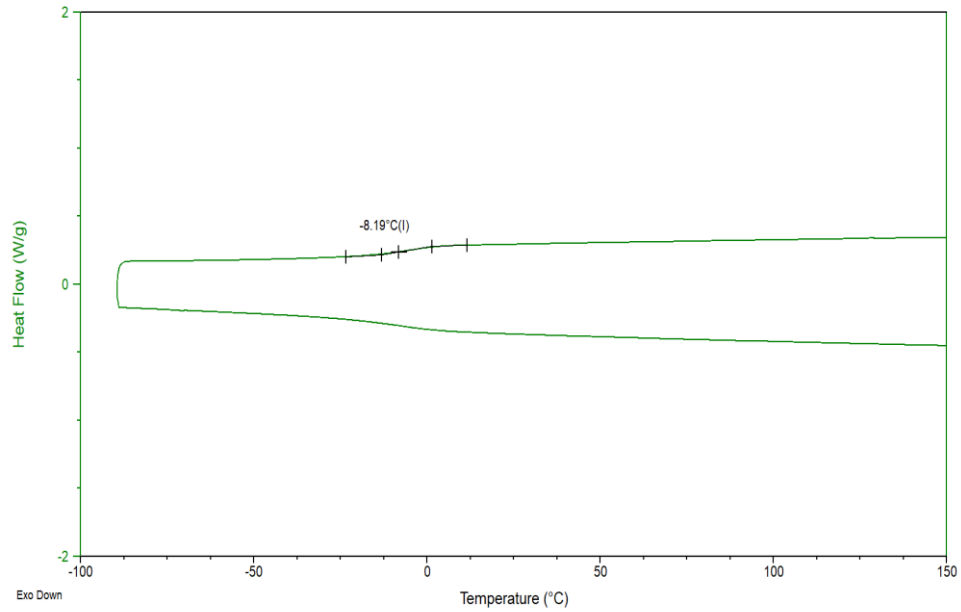

Figure 5S35. DSC thermogram of PMSI from run 48 of **Table 14**.

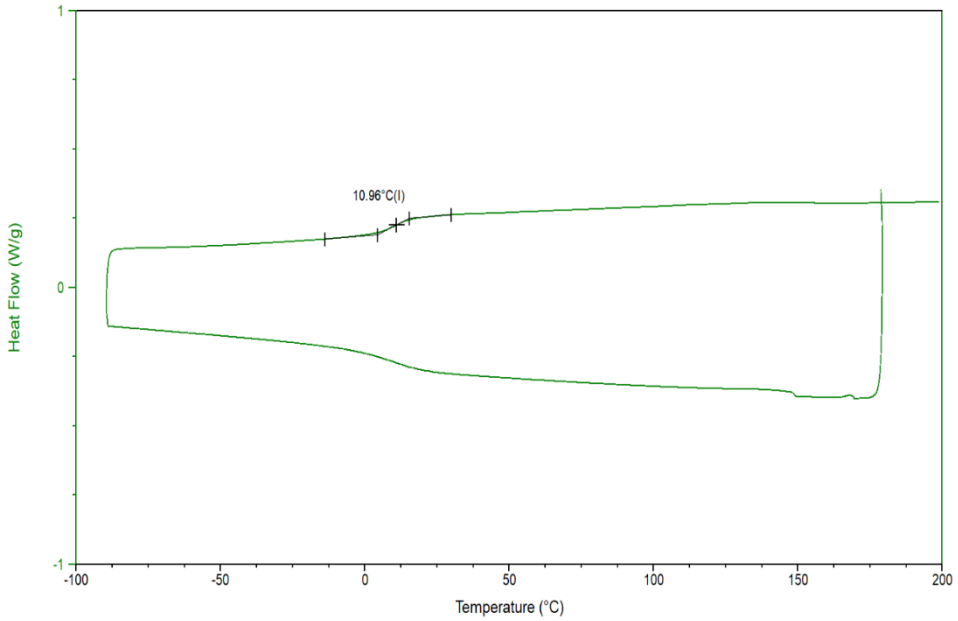

Figure 5S36. DSC thermogram of PMSI from run 50 of **Table 14.**

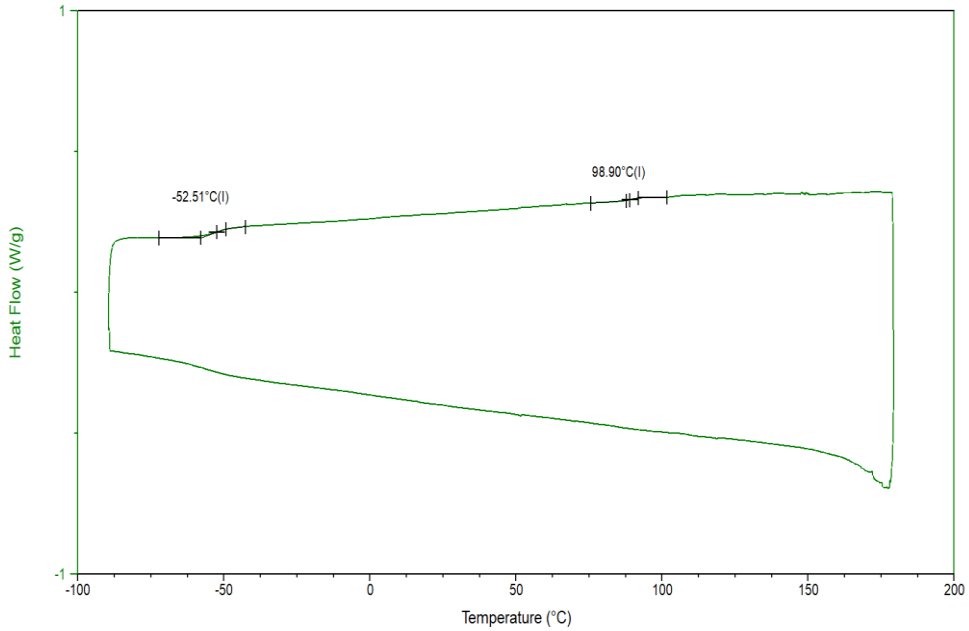

Figure 5S37. DSC thermogram of diblock PMS from run 51 of **Table 14**.

5.7 TGA Analysis

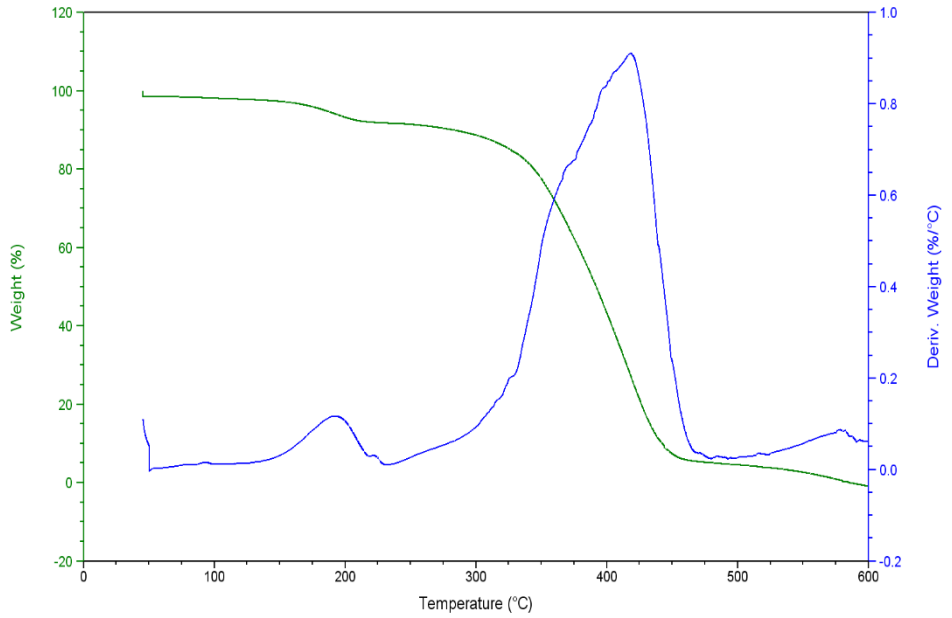

Figure 5S38. TGA thermogram of PM from run 31 of **Table 13**.

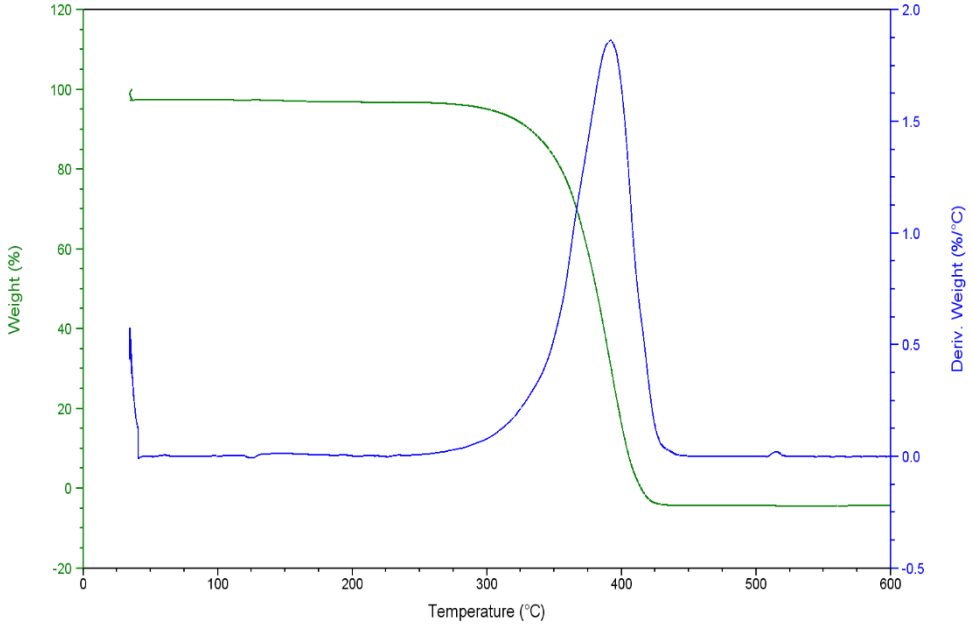

Figure 5S39. TGA thermogram of PS from run 35 of **Table 13**.

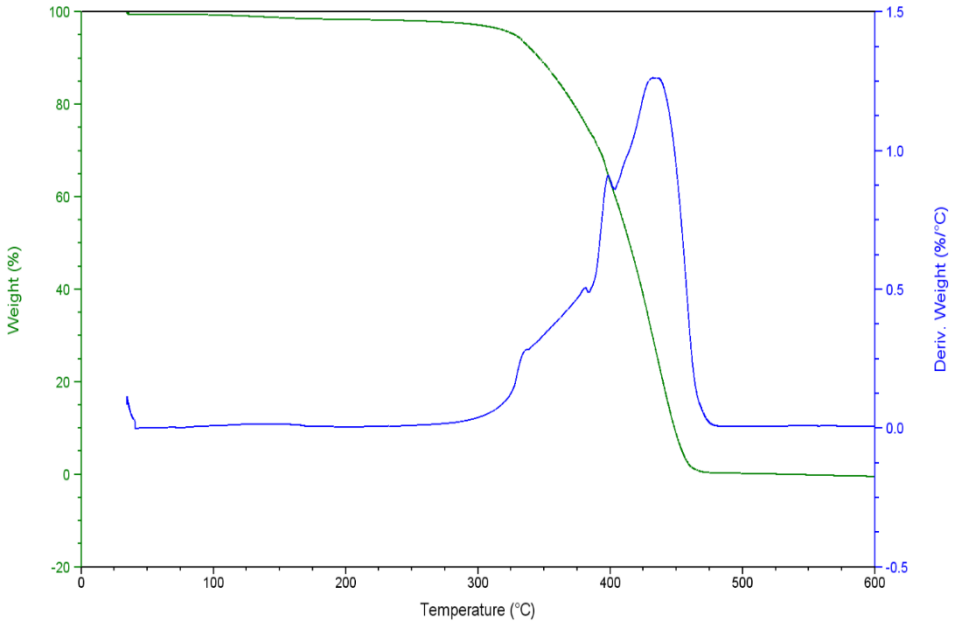

Figure 5S40. TGA thermogram of PI from run 38 of **Table 13**.

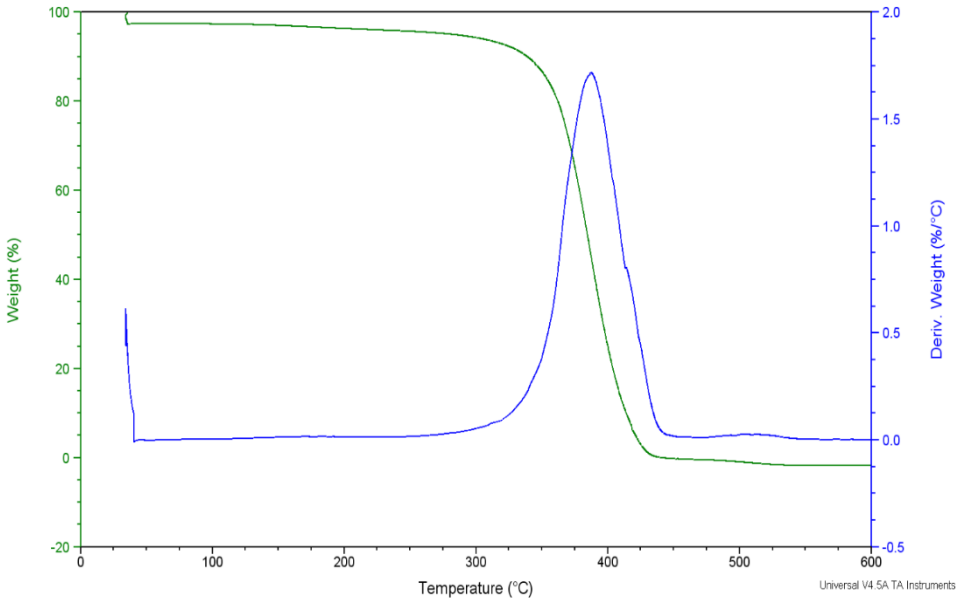

Figure 5S41. TGA thermogram of PMS from run 42 of **Table 14**.

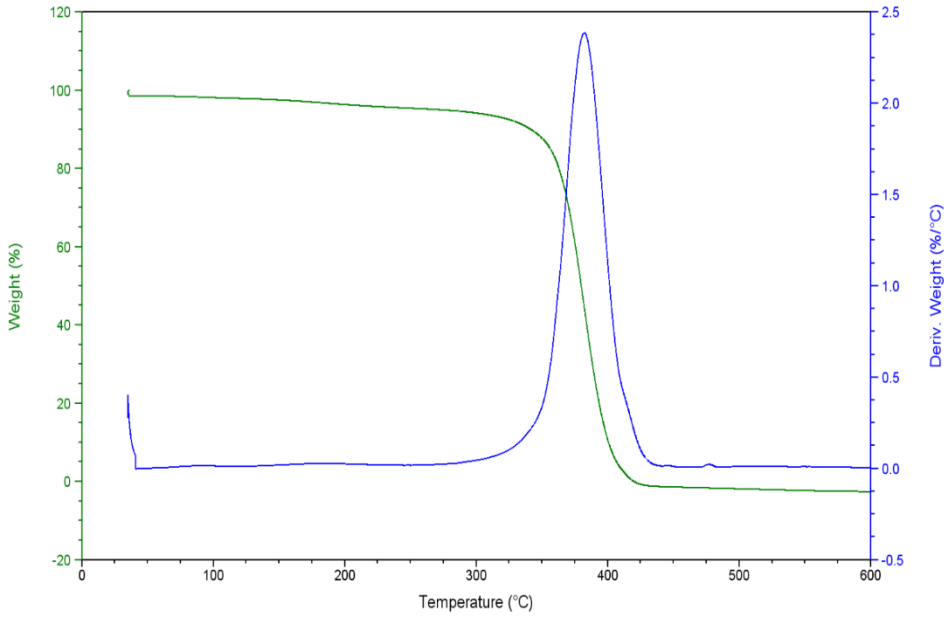

Figure 5S42. TGA thermogram of PMS from run 44 of **Table 14**.

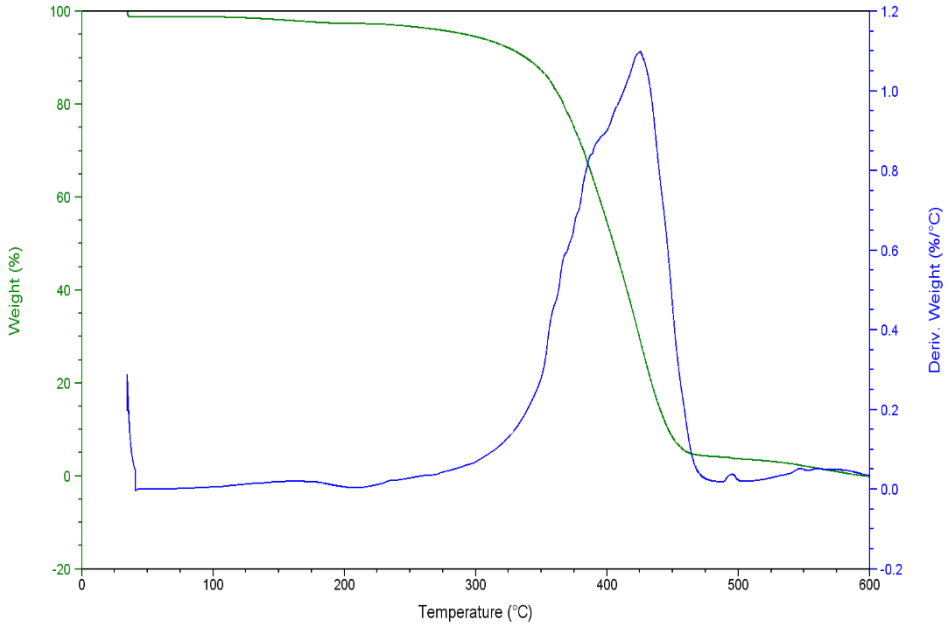

Figure 5S43. TGA thermogram of PMI from run 45 of **Table 14**.

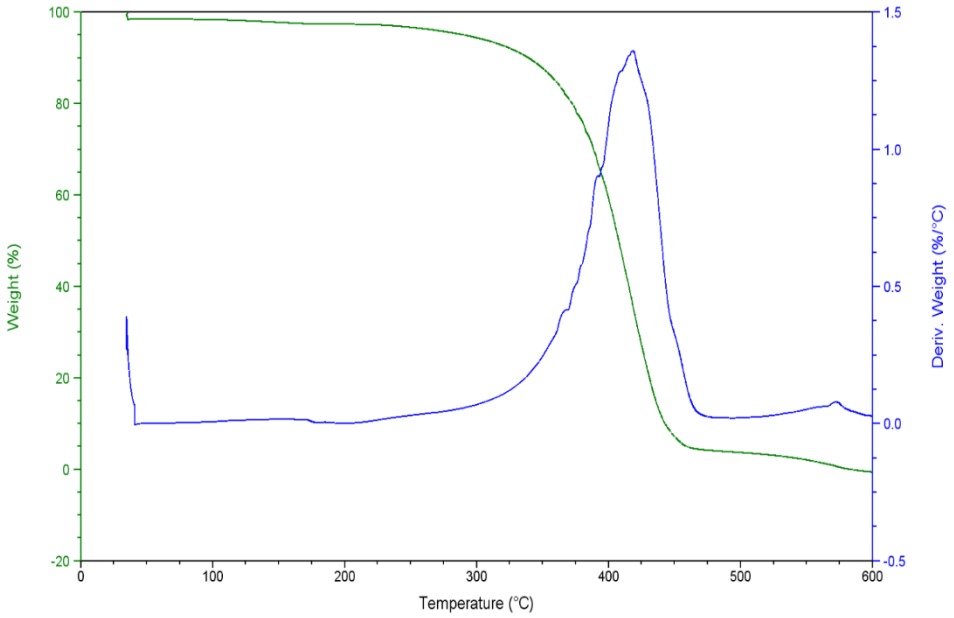

Figure 5S44. TGA thermogram of PMI from run 46 of **Table 14**.

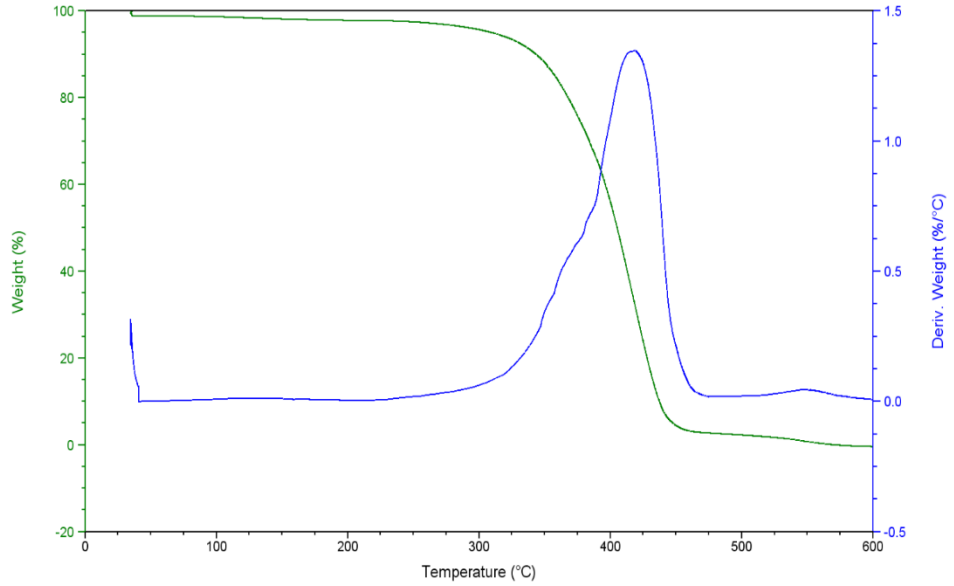

Figure 5S45. TGA thermogram of PMI from run 47 of **Table 14**.

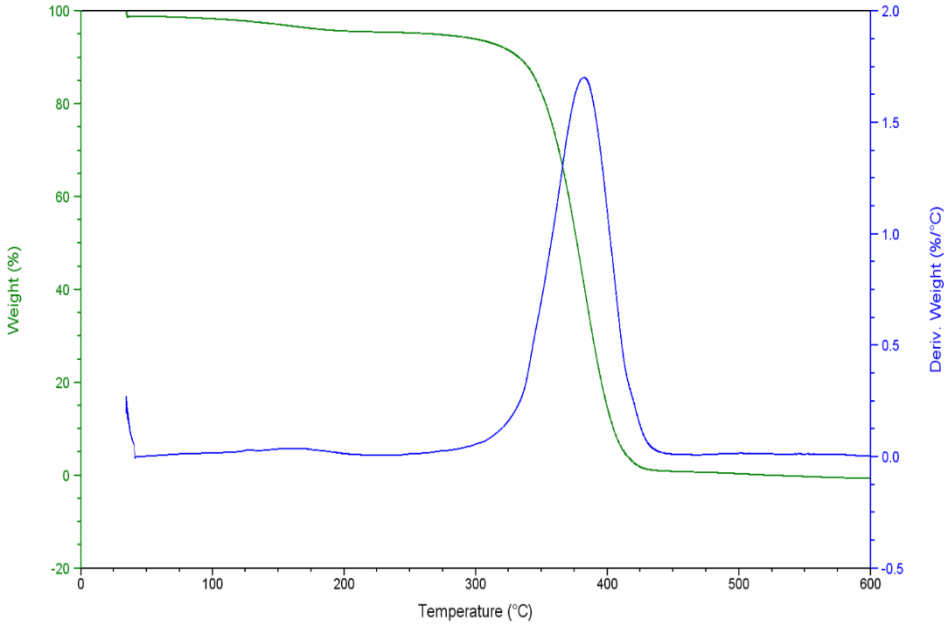

Figure 5S46. TGA thermogram of PMSI from run 50 of **Table 14**.

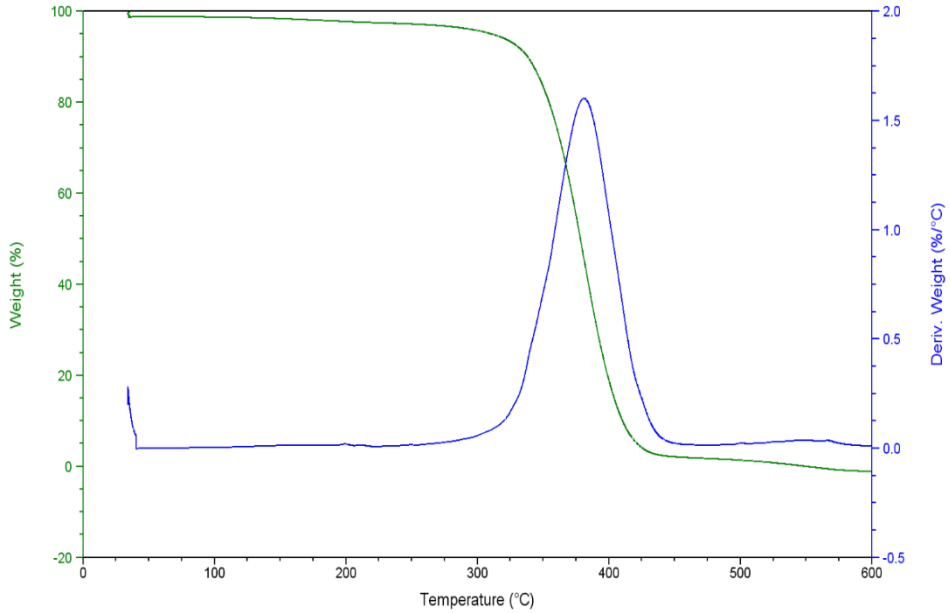

Figure 5S47. TGA thermogram of diblock PMS from run 51 of **Table 14**.

5.8 GPC Analysis

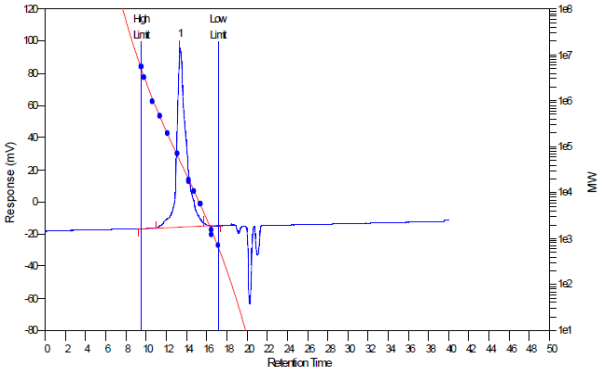

Figure 5S48. GPC curve of PM from run 31 of **Table 13**.

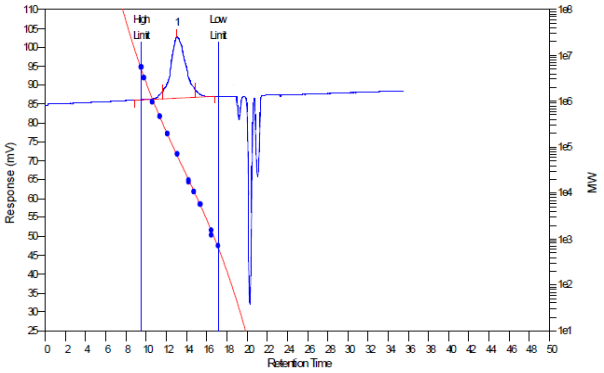

Figure 5S49. GPC curve of PM from run 32 of **Table 13**.

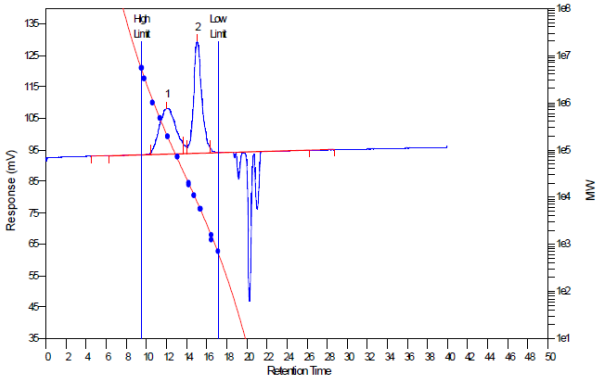

Figure 5S50. GPC curve of PM from run 33 of **Table 13**.

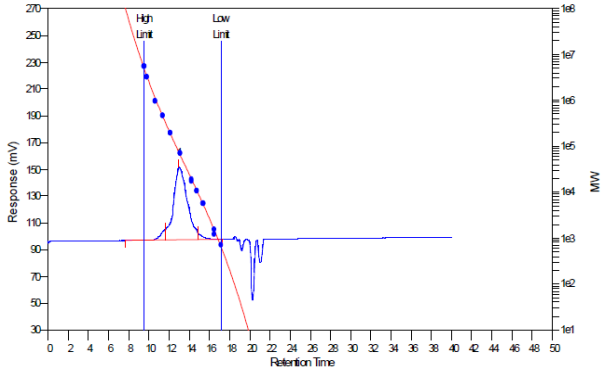

Figure 5S51. GPC curve of PM from run 34 of **Table 13**.

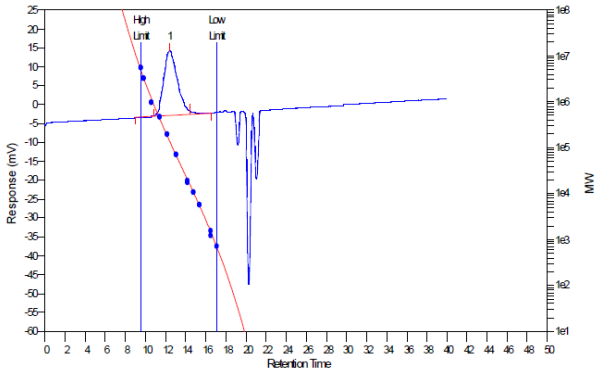

Figure 5S52. GPC curve of PS from run 35 of **Table 13**.

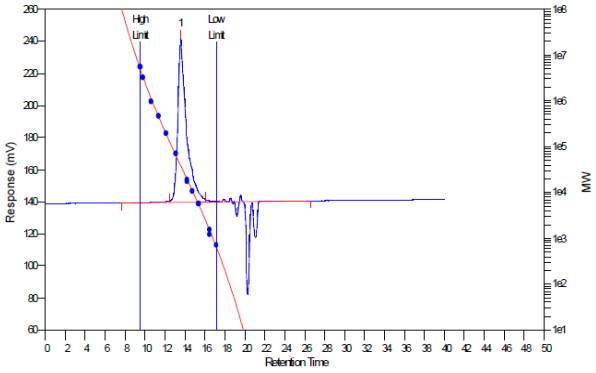

Figure 5S53. GPC curve of PI from run 38 of **Table 13**.

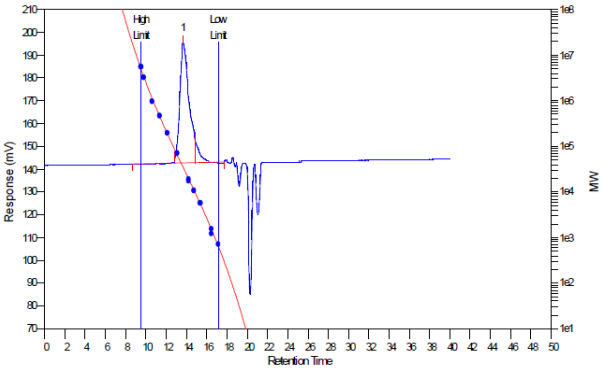

Figure 5S54. GPC curve of PI from run 39 of **Table 13**.

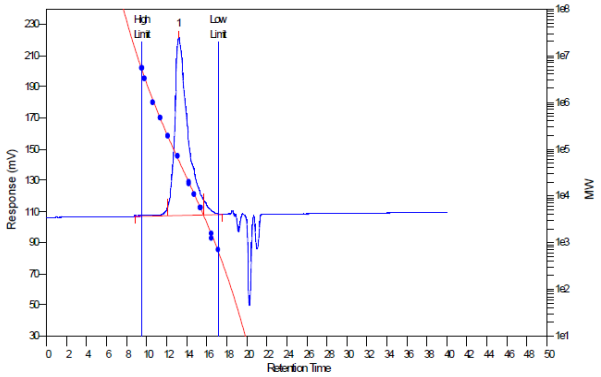

Figure 5S55. GPC curve of PMS from run 40 of **Table 14**.

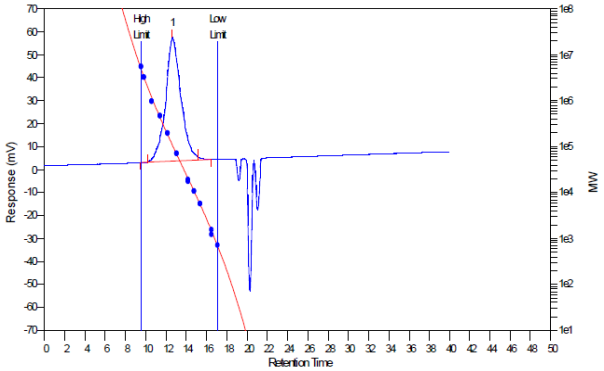

Figure 5S56. GPC curve of PMS from run 42 of **Table 14**.

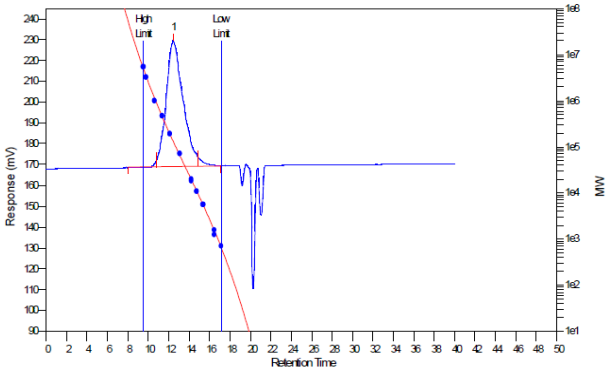

Figure 5S57. GPC curve of PMS from run 43 of **Table 14**.

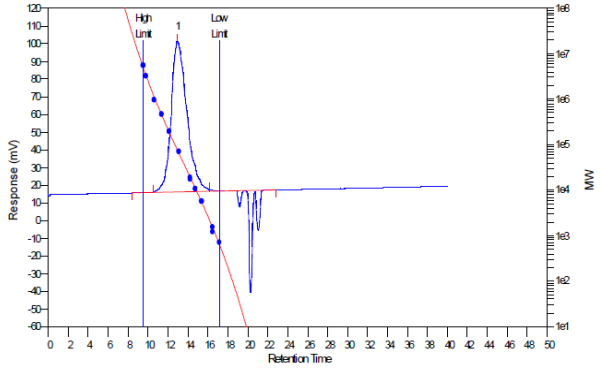

Figure 5S58. GPC curve of PMI from run 46 of **Table 14**.

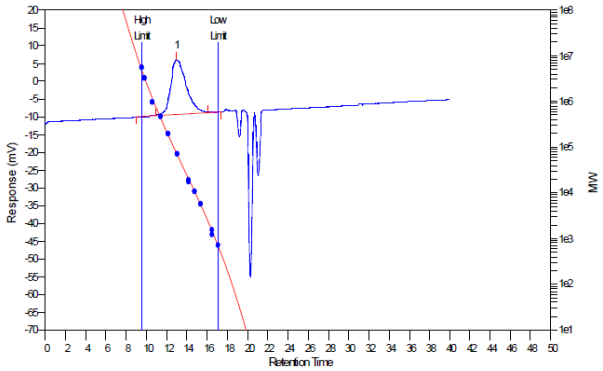

Figure 5S59. GPC curve of PMI from run 47 of **Table 14**.

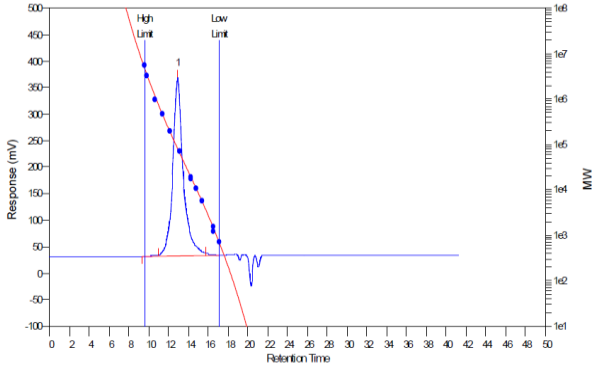

Figure 5S60. GPC curve of PMSI from run 50 of **Table 14**.

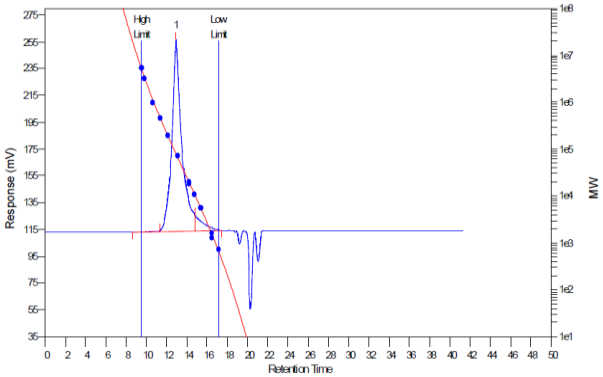

Figure 5S61. GPC curve of diblock PMS from run 51 of **Table 14**.

5.9 CAM Analysis

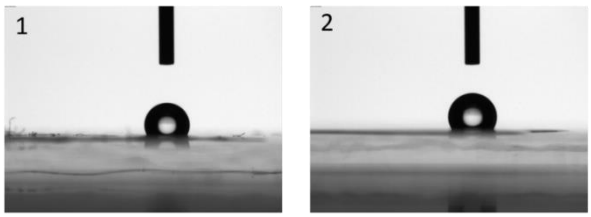

The CAM profiles of PI From run 7 Table 1

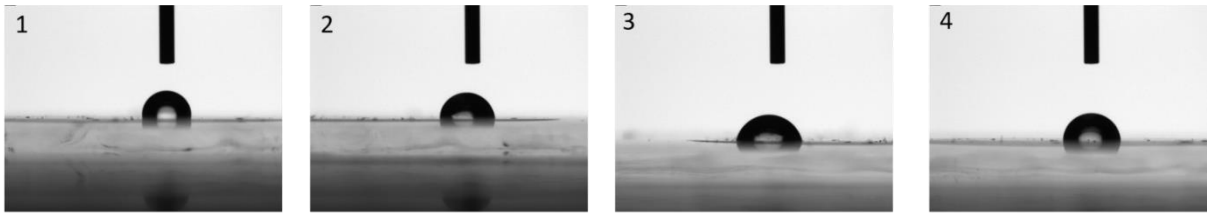

The CAM profiles of PMS From run 14 Table 2

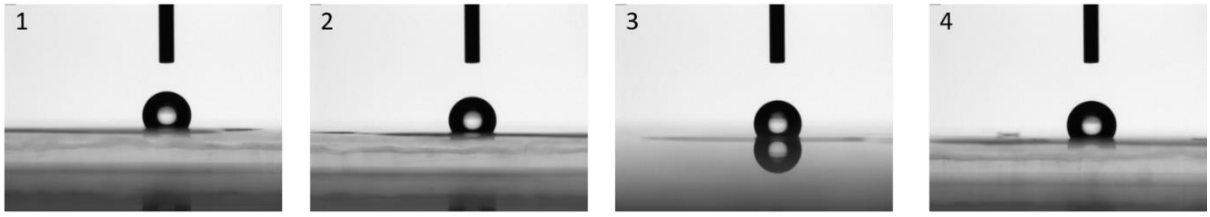

The CAM profiles of PMI From run 17 Table 2

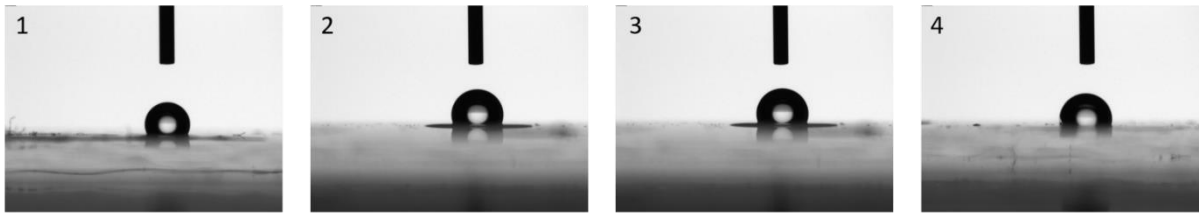

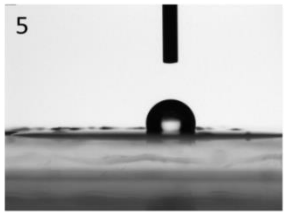

The CAM profiles of PMI From run 19 Table 2

Table T7 – Contact angles for tested samples

Sample	⊙ left	⊙ right	Contact angle
Run 7	114,5	115,6	115,05
"	116,1	112,4	114,25
Run7			**114,85**
Run 14	84,3	84,7	84,5
"	84,1	92,1	88,1

"	77,1	77,8	77,45
"	82,9	86,6	84,75
Run 14			**83,7**
Run 17	125,6	125,8	125,7
"	121	120,2	120,6
"	121,4	120,7	121,05
"	120,8	121,3	121,05
Run 17			**122,1**
Run 19	118,9	120,1	119,5
"	113,7	109,2	111,45
"	108	102	105
"	101,2	110,5	105,85
"	110,8	106,7	108,75
Run 19			**110,11**

5.10 SEM Analysis

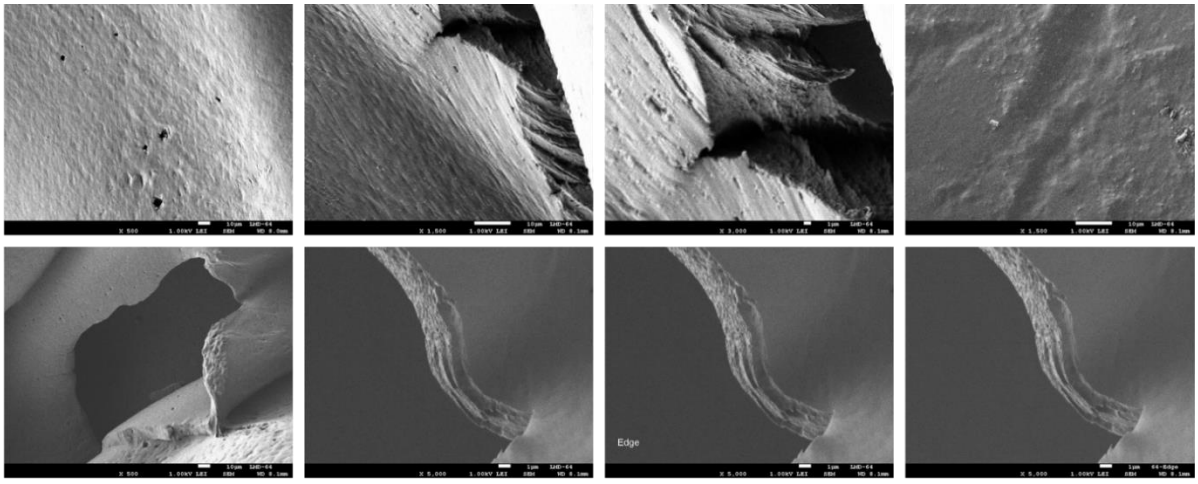

SEM image of PMS from run 14 Table 2

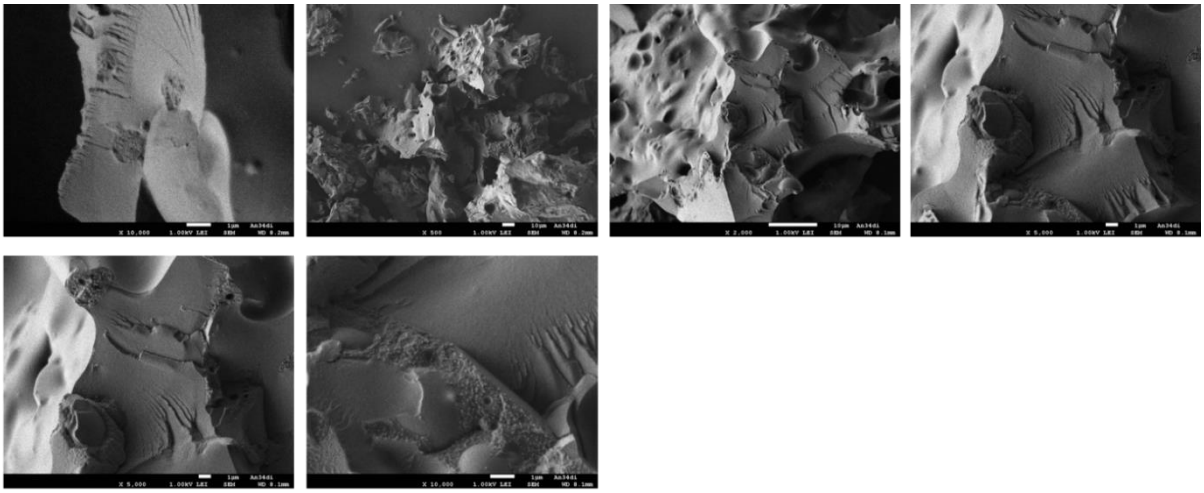

SEM image of PMS from run 21 Table 2

5.11 Kinetic studies

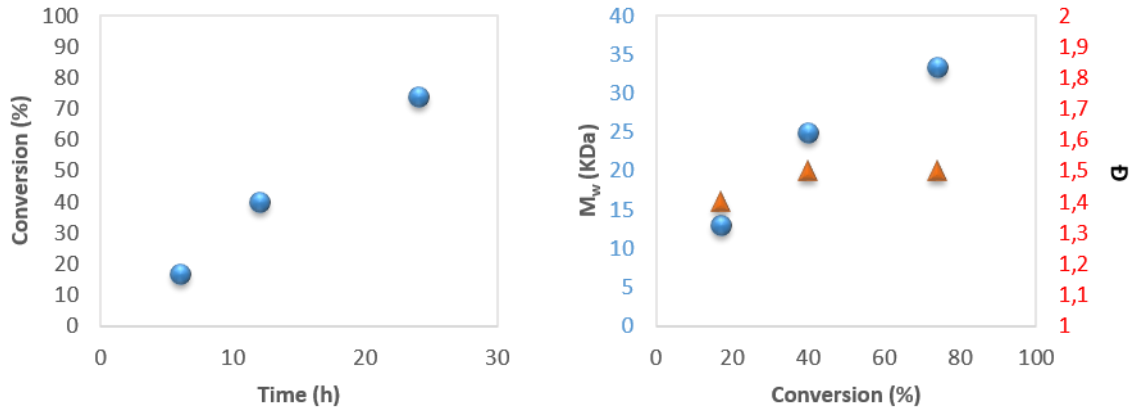

Figure 5S61. Conversion vs. time plot for isoprene polymerization (on left); plots of M_W (and $Đ$) vs conversion (on right); same experimental conditions of run 37 of Table 13 (except for time).

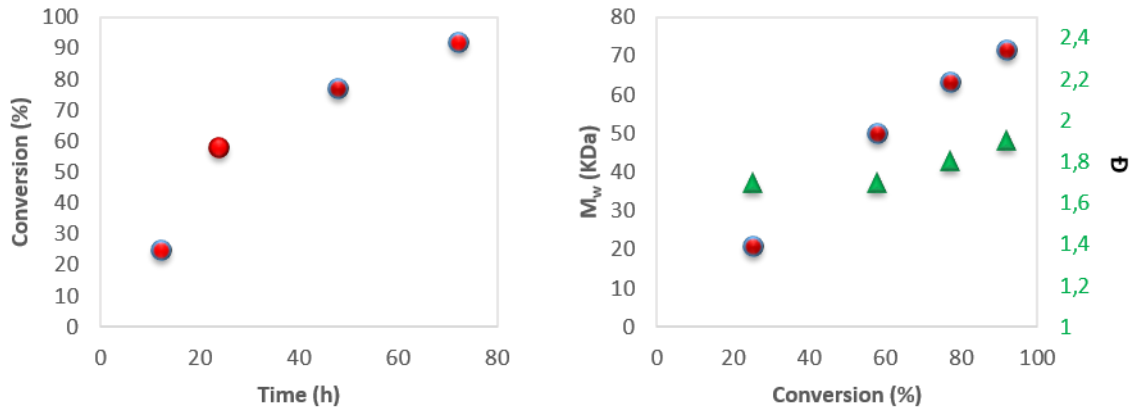

Figure 5S62. Conversion vs. time plot for myrcene polymerization (on left); plots of M_W (and $Đ$) vs conversion (on right); same experimental conditions of run 31 of Table 13 (except for time).

Chapter 6 – Supporting information

6.1 NMR Spectra

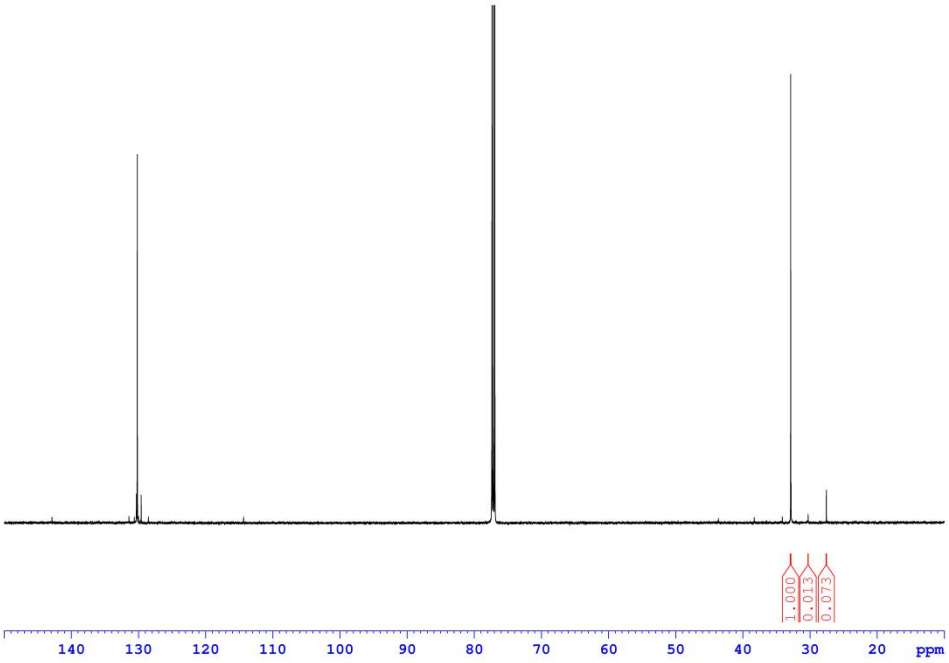

Fig. 6S1. ^{13}C **NMR** spectrum ($CDCl_3$, 25 °C, 600 MHz) of sample A of **Table 16**

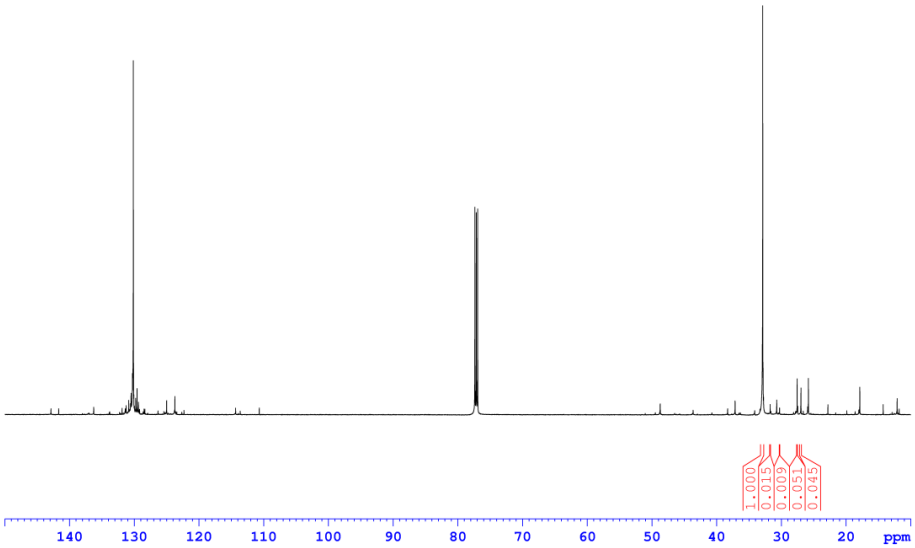

Fig. 6S2. ^{13}C **NMR** spectrum ($CDCl_3$, 25 °C, 600 MHz) of sample B of **Table 16**

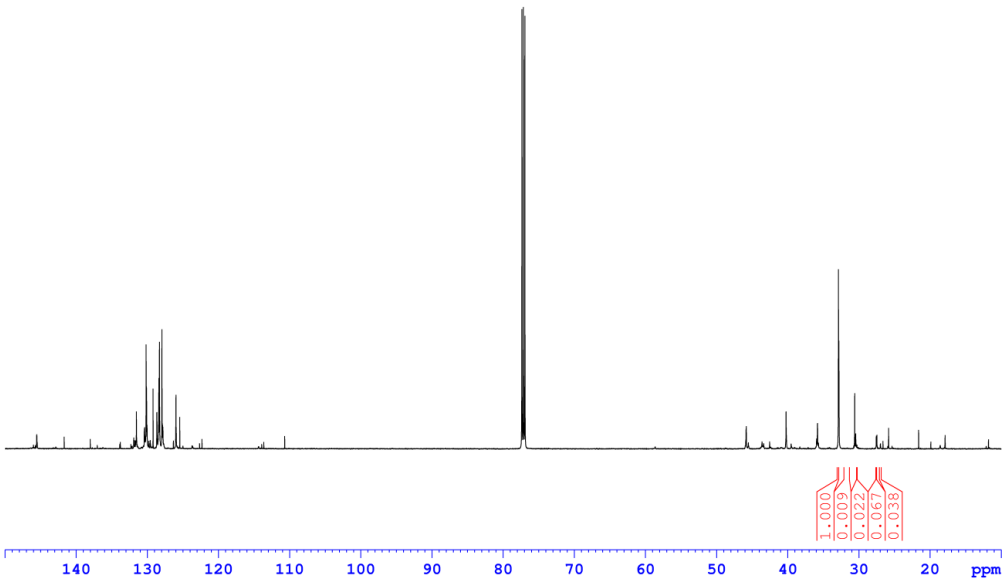

Fig. 6S3. ^{13}C **NMR** spectrum ($CDCl_3$, 25 °C, 600 MHz) of sample C of **Table 16**

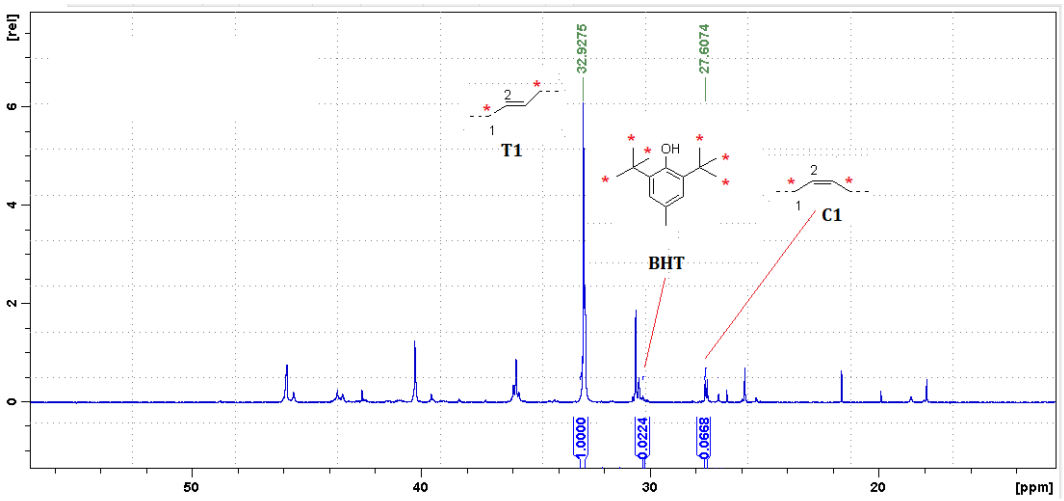

Fig. 6S4. ^{13}C **NMR** spectrum ($CDCl_3$, 25 °C, 600 MHz) of sample C of **Table 16**

6.2 DSC Thermal Analysis

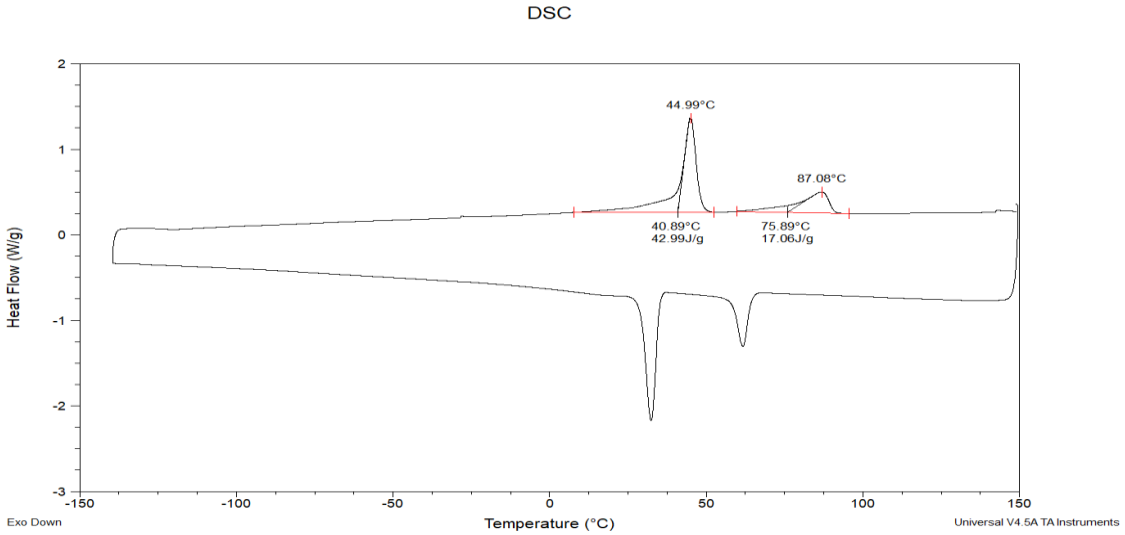

Figure 6S5. DSC thermogram of sample A of **Table 16**.

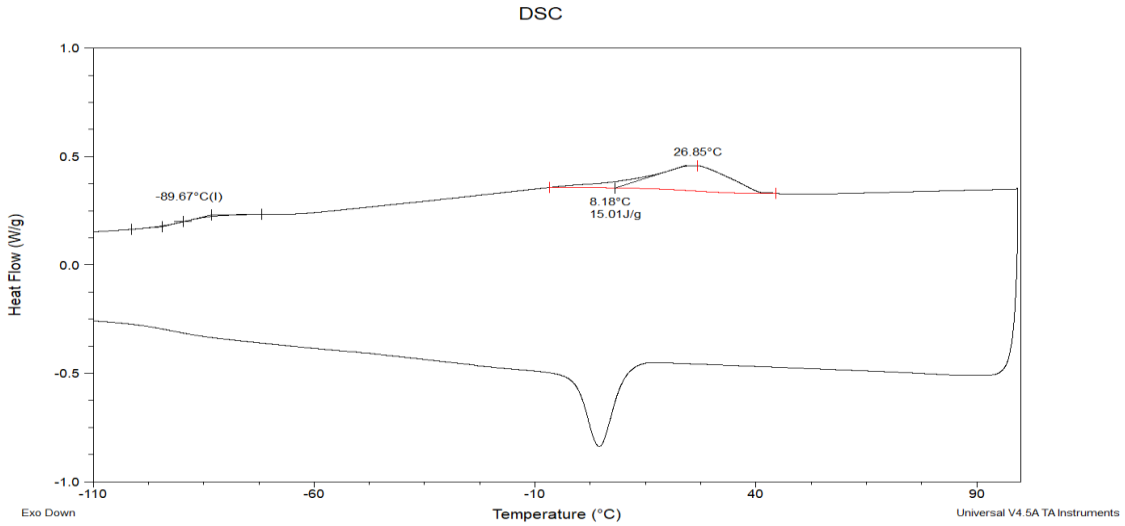

Figure 6S6. DSC thermogram of sample B of **Table 16**.

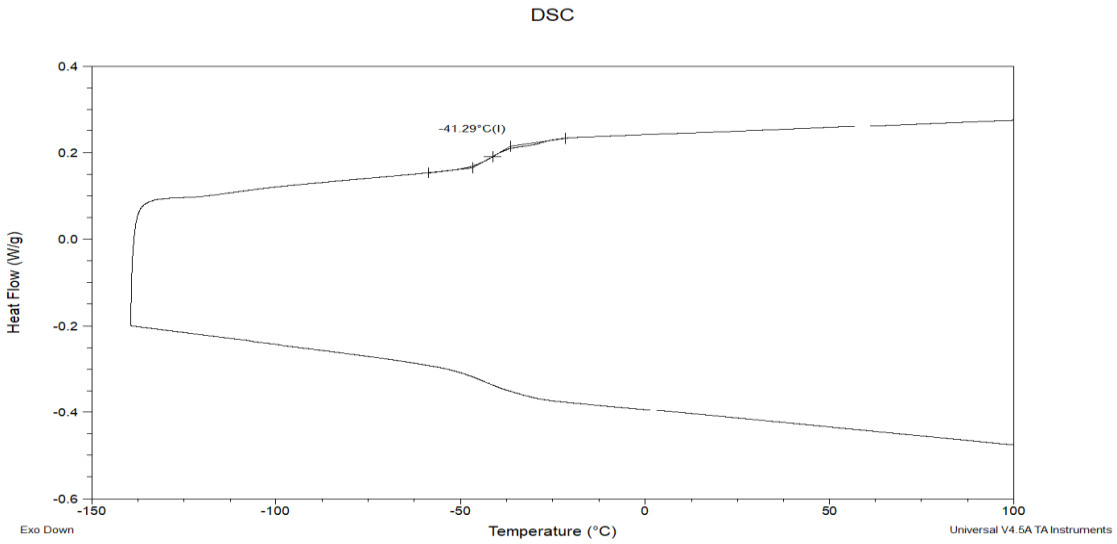

Figure 6S7. DSC thermogram of sample C of **Table 16**.

6.3 GPC Analysis

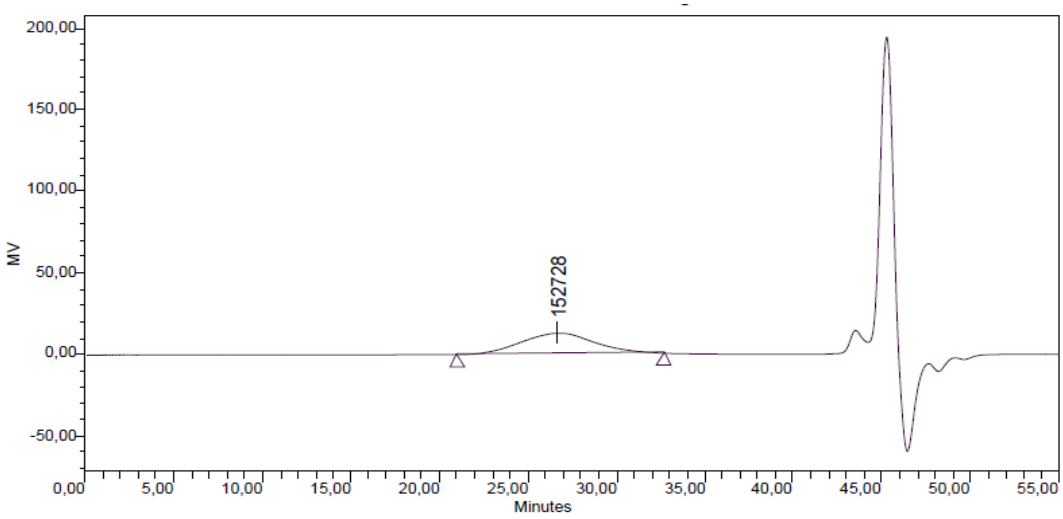

Broad Unknown Relative Peak Table

	Distribution Name	Mn (Daltons)	Mw (Daltons)	MP (Daltons)	Mz (Daltons)	Mz+1 (Daltons)	Polydispersity	Mz/Mw	Mz+1/Mw
1		*111411*	*225807*	*152728*	*464618*	*810848*	*2,026785*	*2,057591*	*3,590893*

Figure 6S8. GPC curve of sample A of **Table 16**.

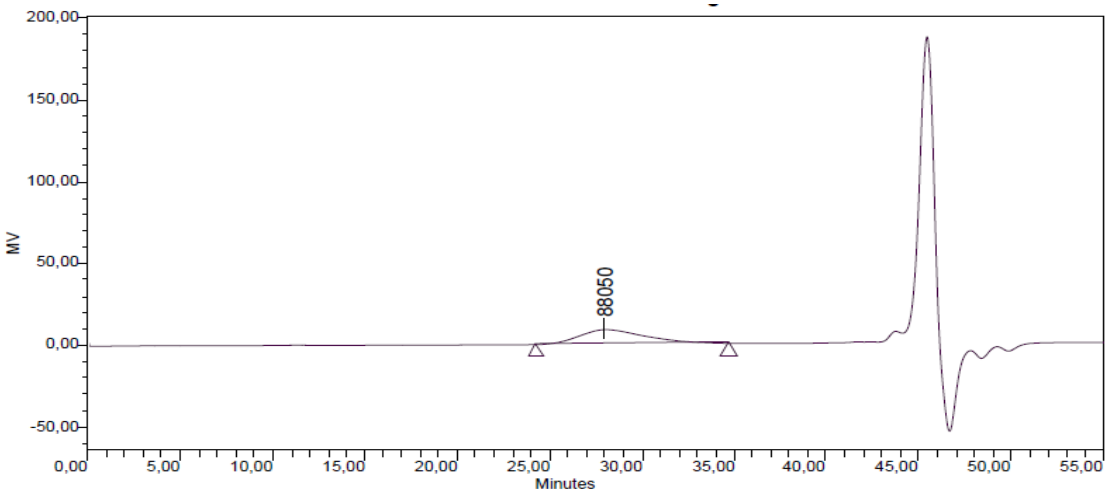

Broad Unknown Relative Peak Table

	Distribution Name	Mn (Daltons)	Mw (Daltons)	MP (Daltons)	Mz (Daltons)	Mz+1 (Daltons)	Polydispersity	Mz/Mw	Mz+1/Mw
1		*55509*	*86385*	*88050*	*124451*	*166311*	*1,556229*	*1,440654*	*1,925236*

Figure 6S9. GPC curve of sample B of **Table 16**.

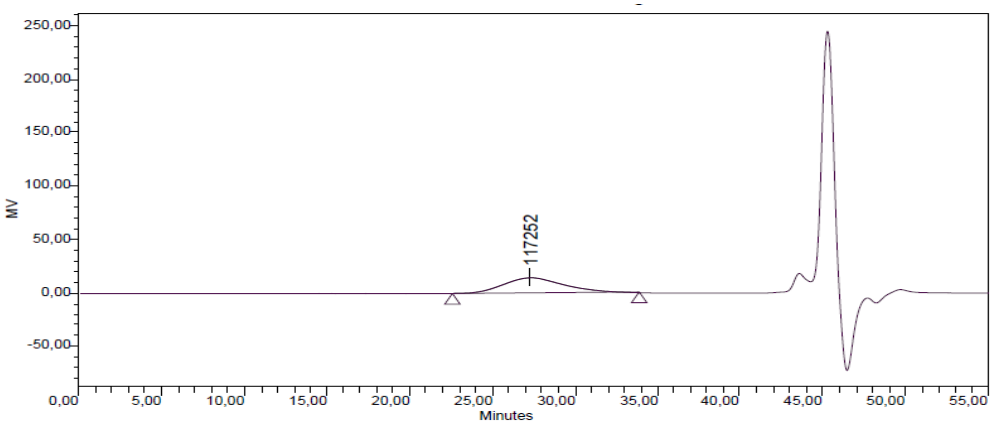

Broad Unknown Relative Peak Table

	Distribution Name	Mn (Daltons)	Mw (Daltons)	MP (Daltons)	Mz (Daltons)	Mz+1 (Daltons)	Polydispersity	Mz/Mw	Mz+1/Mw
1		*77968*	*132304*	*117252*	*212689*	*317739*	*1,696903*	*1,607584*	*2,401590*

Figure 6S10. GPC curve of sample C of **Table 16**.

Permissions

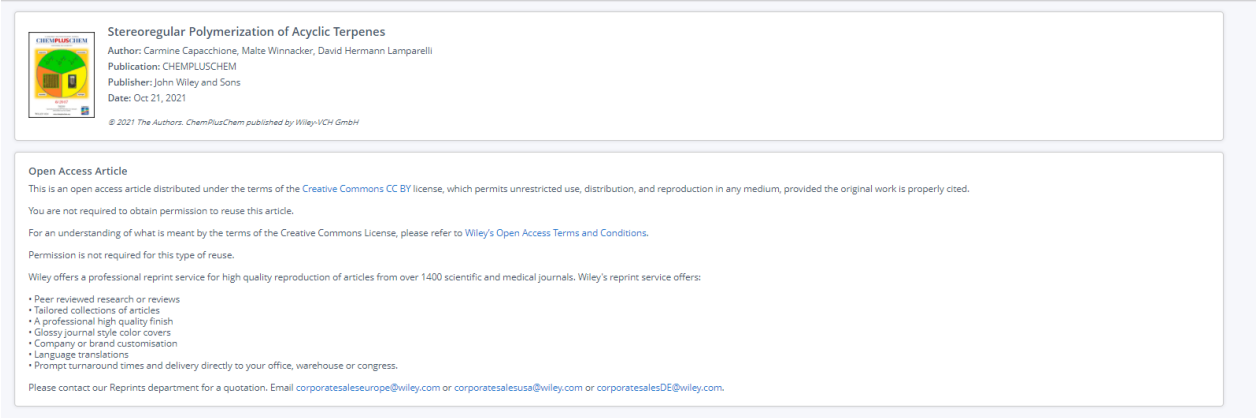

Stereoregular Polymerization of Acyclic Terpenes
Author: Carmine Capacchione, Malte Winnacker, David Hermann Lamparelli
Publication: CHEMPLUSCHEM
Publisher: John Wiley and Sons
Date: Oct 21, 2021
© 2021 The Authors. ChemPlusChem published by Wiley-VCH GmbH

Open Access Article
This is an open access article distributed under the terms of the Creative Commons CC BY license, which permits unrestricted use, distribution, and reproduction in any medium, provided the original work is properly cited.

You are not required to obtain permission to reuse this article.

For an understanding of what is meant by the terms of the Creative Commons License, please refer to Wiley's Open Access Terms and Conditions.

Permission is not required for this type of reuse.

Wiley offers a professional reprint service for high quality reproduction of articles from over 1400 scientific and medical journals. Wiley's reprint service offers:

- Peer reviewed research or reviews
- Tailored collections of articles
- A professional high quality finish
- Glossy journal style color covers
- Company or brand customisation
- Language translations
- Prompt turnaround times and delivery directly to your office, warehouse or congress.

Please contact our Reprints department for a quotation. Email corporatesaleseurope@wiley.com or corporatesalesusa@wiley.com or corporatesalesDE@wiley.com.

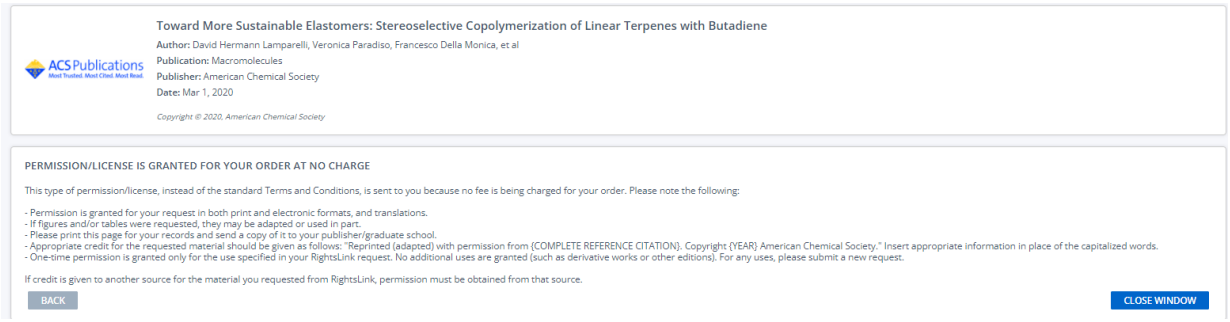

Toward More Sustainable Elastomers: Stereoselective Copolymerization of Linear Terpenes with Butadiene
Author: David Hermann Lamparelli, Veronica Paradiso, Francesco Della Monica, et al
Publication: Macromolecules
Publisher: American Chemical Society
Date: Mar 1, 2020
Copyright © 2020, American Chemical Society

PERMISSION/LICENSE IS GRANTED FOR YOUR ORDER AT NO CHARGE

This type of permission/license, instead of the standard Terms and Conditions, is sent to you because no fee is being charged for your order. Please note the following:

- Permission is granted for your request in both print and electronic formats, and translations.
- If figures and/or tables were requested, they may be adapted or used in part.
- Please print this page for your records and send a copy of it to your publisher/graduate school.
- Appropriate credit for the requested material should be given as follows: "Reprinted (adapted) with permission from {COMPLETE REFERENCE CITATION}. Copyright {YEAR} American Chemical Society." Insert appropriate information in place of the capitalized words.
- One-time permission is granted only for the use specified in your RightsLink request. No additional uses are granted (such as derivative works or other editions). For any uses, please submit a new request.

If credit is given to another source for the material you requested from RightsLink, permission must be obtained from that source.

BACK CLOSE WINDOW

References

1. Jones, K. P. & Allen, P. W. Historical Development of the World Rubber Industry. in *Developments in Crop Science* vol. 23 1–25 (Elsevier, 1992).

2. Kohjiya, S. & Ikeda, Y. A short history of natural rubber research. in *Chemistry, Manufacture, and Application of Natural Rubber* 407–427 (Elsevier, 2021). doi:10.1016/B978-0-12-818843-9.00006-0.

3. De, S. K., White, J. R., & Rapra Technology Limited. *Rubber technologist's handbook*. (Rapra Technology Ltd., 2001).

4. Drori, J. & Clerc, L. *Around the world in 80 trees*. (Laurence King Publishing, 2020).

5. Drabble, J. H. The Plantation Rubber Industry in Malaya up to 1922. *Journal of the Malaysian Branch of the Royal Asiatic Society* **40**, 52–77 (1967).

6. Morton, M. History of Synthetic Rubber. *Journal of Macromolecular Science: Part A - Chemistry* **15**, 1289–1302 (1981).

7. Baker, I. Rubber. in *Fifty Materials That Make the World* 199–203 (Springer International Publishing, 2018). doi:10.1007/978-3-319-78766-4_38.

8. *The Physics of Glassy Polymers*. (Springer Netherlands, 1997). doi:10.1007/978-94-011-5850-3.

9. *Handbook of elastomers*. (M. Dekker, 2001).

10. Brandt, H.-D. *et al.* Rubber, 5. Solution Rubbers. in *Ullmann's Encyclopedia of Industrial Chemistry* (ed. Wiley-VCH Verlag GmbH & Co. KGaA) o23_o02 (Wiley-VCH Verlag GmbH & Co. KGaA, 2011). doi:10.1002/14356007.o23_o02.

11. Valentini, L. & Lopez-Manchado, M. A. Classification of rubbers and components for harsh environmental systems. in *High-Performance Elastomeric Materials Reinforced by Nano-Carbons* 1–14 (Elsevier, 2020). doi:10.1016/B978-0-12-816198-2.00001-3.

12. Kadir, A. A. S. A. Advances in Natural Rubber Production. *Rubber Chemistry and Technology* **67**, 537–548 (1994).

13. Huang, C. *et al.* Research on architecture and composition of natural network in natural rubber. *Polymer* **154**, 90–100 (2018).

14. Tanaka, Y. & Tarachiwin, L. Recent Advances in Structural Characterization of Natural Rubber. *Rubber Chemistry and Technology* **82**, 283–314 (2009).

15. admin. 5 World's largest natural rubber producers in 2019. *The Science Agriculture* https://scienceagri.com/5-worlds-largest-natural-rubber-producers-in-2019/ (2021).

16. Lewandowski, L., Sibbald, M. S., Johnson, E. & Mallamaci, M. P. New Emulsion SBR Technology: Part I. Raw Polymer Study. *Rubber Chemistry and Technology* **73**, 731–742 (2000).

17. Bressi, S., Fiorentini, N., Huang, J. & Losa, M. Crumb Rubber Modifier in Road Asphalt Pavements: State of the Art and Statistics. *Coatings* **9**, 384 (2019).

18. Forrest, M. J. *Recycling and Re-use of Waste Rubber*. (De Gruyter, 2019). doi:10.1515/9783110644142.

19. Brundtland, G., ed., in. Our common future: the world commission on environment and development. Oxford University Press: Oxford, 1987.

20. Eneh, O. C. A Review on Petroleum: Source, Uses, Processing, Products and the Environment. *J. of Applied Sciences* **11**, 2084–2091 (2011).

21. *Springer Handbook of Petroleum Technology*. (Springer International Publishing, 2017). doi:10.1007/978-3-319-49347-3.

22. Kweku, D. *et al.* Greenhouse Effect: Greenhouse Gases and Their Impact on Global Warming. *JSRR* **17**, 1–9 (2018).

23. Rochman, C. M. *et al.* Classify plastic waste as hazardous. *Nature* **494**, 169–171 (2013).

24. Jambeck, J. R. *et al.* Plastic waste inputs from land into the ocean. *Science* **347**, 768–771 (2015).

25. Law, K. L. *et al.* Plastic Accumulation in the North Atlantic Subtropical Gyre. *Science* **329**, 1185–1188 (2010).

26. Suaria, G. *et al.* The Mediterranean Plastic Soup: synthetic polymers in Mediterranean surface waters. *Sci Rep* **6**, 37551 (2016).

27. Anastas, P. T. & Kirchhoff, M. M. Origins, Current Status, and Future Challenges of Green Chemistry. *Acc. Chem. Res.* **35**, 686–694 (2002).

28. Beach, E. S., Cui, Z. & Anastas, P. T. Green Chemistry: A design framework for sustainability. *Energy Environ. Sci.* **2**, 1038 (2009).

29. Zhu, Y., Romain, C. & Williams, C. K. Sustainable polymers from renewable resources. *Nature* **540**, 354–362 (2016).

30. Della Monica, F. & Kleij, A. W. From terpenes to sustainable and functional polymers. *Polym. Chem.* 10.1039.D0PY00817F (2020) doi:10.1039/D0PY00817F.

31. Winnacker, M. Pinenes: Abundant and Renewable Building Blocks for a Variety of Sustainable Polymers. *Angew. Chem. Int. Ed.* **57**, 14362–14371 (2018).

32. Winnacker, M. *et al.* Sustainable Polyesteramides and Copolyamides: Insights into the Copolymerization Behavior of Terpene-Based Lactams. *Macromol. Chem. Phys.* **221**, 2000110 (2020).

33. Winnacker, M., Neumeier, M., Zhang, X., Papadakis, C. M. & Rieger, B. Sustainable Chiral Polyamides with High Melting Temperature via Enhanced Anionic Polymerization of a Menthone-Derived Lactam. *Macromol. Rapid Commun.* **37**, 851–857 (2016).

34. Wahlen, C. & Frey, H. Anionic Polymerization of Terpene Monomers: New Options for Bio-Based Thermoplastic Elastomers. *Macromolecules* acs.macromol.1c00770 (2021) doi:10.1021/acs.macromol.1c00770.

35. Gandini, A. Polymers from Renewable Resources: A Challenge for the Future of Macromolecular Materials. *Macromolecules* **41**, 9491–9504 (2008).

36. Silvestre, A. J. D. & Gandini, A. Terpenes: Major Sources, Properties and Applications. in *Monomers, Polymers and Composites from Renewable Resources* 17–38 (Elsevier, 2008). doi:10.1016/B978-0-08-045316-3.00002-8.

37. Christianson, D. W. Structural and Chemical Biology of Terpenoid Cyclases. *Chem. Rev.* **117**, 11570–11648 (2017).

38. Jaeger, R. & Cuny, E. Terpenoids with Special Pharmacological Significance: A Review. *Natural Product Communications* **11**, 1934578X1601100 (2016).

39. Rohmer, M. & Rohmer, M. The discovery of a mevalonate-independent pathway for isoprenoid biosynthesis in bacteria, algae and higher plants†. *Nat. Prod. Rep.* **16**, 565–574 (1999).

40. *Handbook of essential oils: science, technology, and applications*. (CRC Press, 2020).

41. Behr, A. & Johnen, L. Myrcene as a Natural Base Chemical in Sustainable Chemistry: A Critical Review. *ChemSusChem* **2**, 1072–1095 (2009).

42. Mumm, R., Posthumus, M. A. & Dicke, M. Significance of terpenoids in induced indirect plant defence against herbivorous arthropods. *Plant Cell Environ* **31**, 575–585 (2008).

43. Hillier, S. G. & Lathe, R. Terpenes, hormones and life: isoprene rule revisited. *Journal of Endocrinology* **242**, R9–R22 (2019).

44. Arroo, R. Eberhard Breitmaier. Terpenes—flavors, fragrances, pharmaca, pheromones. Wiley-VCH, 2006, 214 pp ISBN 3-527-31786-4. *Appl. Organometal. Chem.* **21**, 377–377 (2007).

45. Breitmaier, E. *Terpenes: flavors, fragrances, pharmaca, pheromones*. (WILEY-VCH, 2006).

46. Mathers, R. T. & Meier, M. A. R. *Green Polymerization Methods: Renewable Starting Materials, Catalysis and Waste Reduction.* (Wiley, 2011).

47. Sahu, P., Bhowmick, A. K. & Kali, G. Terpene Based Elastomers: Synthesis, Properties, and Applications. *Processes* **8**, 553 (2020).

48. Kim, E.-M., Eom, J.-H., Um, Y., Kim, Y. & Woo, H. M. Microbial Synthesis of Myrcene by Metabolically Engineered *Escherichia coli*. *J. Agric. Food Chem.* **63**, 4606–4612 (2015).

49. Kunert, G., Reinhold, C. & Gershenzon, J. Constitutive emission of the aphid alarm pheromone, (E)-β-farnesene, from plants does not serve as a direct defense against aphids. *BMC Ecol* **10**, 23 (2010).

50. Benjamin, K. R., Silva, I. R., Cherubim, J. P., McPhee, D. & Paddon, C. J. Developing Commercial Production of Semi-Synthetic Artemisinin, and of β-Farnesene, an Isoprenoid Produced by Fermentation of Brazilian Sugar. *Journal of the Brazilian Chemical Society* (2016) doi:10.5935/0103-5053.20160119.

51. George, K. W., Alonso-Gutierrez, J., Keasling, J. D. & Lee, T. S. Isoprenoid Drugs, Biofuels, and Chemicals—Artemisinin, Farnesene, and Beyond. in *Biotechnology of Isoprenoids* (eds. Schrader, J. & Bohlmann, J.) vol. 148 355–389 (Springer International Publishing, 2015).

52. Yao, K. & Tang, C. Controlled Polymerization of Next-Generation Renewable Monomers and Beyond. *Macromolecules* **46**, 1689–1712 (2013).

53. Winnacker, M. & Rieger, B. Recent Progress in Sustainable Polymers Obtained from Cyclic Terpenes: Synthesis, Properties, and Application Potential. *ChemSusChem* **8**, 2455–2471 (2015).

54. Winnacker, M. & Sag, J. Sustainable terpene-based polyamides *via* anionic polymerization of a pinene-derived lactam. *Chem. Commun.* **54**, 841–844 (2018).

55. Wilbon, P. A., Chu, F. & Tang, C. Progress in renewable polymers from natural terpenes, terpenoids, and rosin. *Macromolecular Rapid Communications* **34**, 8–37 (2013).

56. Winnacker, M. Pinenes: Abundant and Renewable Building Blocks for a Variety of Sustainable Polymers. *Angewandte Chemie International Edition* 2–12 (2018) doi:10.1002/anie.201804009.

57. Carmody, M. O. & Carmody, Wm. H. Polymerization of Terpenes. *J. Am. Chem. Soc.* **59**, 1312–1312 (1937).

58. Wilbon, P. A., Chu, F. & Tang, C. Progress in Renewable Polymers from Natural Terpenes, Terpenoids, and Rosin. *Macromol. Rapid Commun.* **34**, 8–37 (2013).

59. Naddeo, M. *et al.* Stereoselective polymerization of biosourced terpenes β-myrcene and β-ocimene and their copolymerization with styrene promoted by titanium catalysts. *Polymer (United Kingdom)* **131**, 151–159 (2017).

60. Loughmari, S. *et al.* Highly stereoselective coordination polymerization of β-myrcene from a lanthanide-based catalyst: Access to bio-sourced elastomers. *Journal of Polymer Science, Part A: Polymer Chemistry* **50**, 2898–2905 (2012).

61. Georges, S., Bria, M., Zinck, P. & Visseaux, M. Polymyrcene microstructure revisited from precise high-field nuclear magnetic resonance analysis. *Polymer (United Kingdom)* **55**, 3869–3878 (2014).

62. Georges, S., Touré, A. O., Visseaux, M. & Zinck, P. Coordinative chain transfer copolymerization and terpolymerization of conjugated dienes. *Macromolecules* **47**, 4538–4547 (2014).

63. Liu, B. *et al.* Renewable β-myrcene polymerization initiated by lutetium alkyl complexes ligated by imidophosphonamido ligand. *Chin J Polym Sci* **33**, 792–796 (2015).

64. Raynaud, J., Wu, J. Y. & Ritter, T. Iron-catalyzed polymerization of isoprene and other 1,3-dienes. *Angewandte Chemie - International Edition* **51**, 11805–11808 (2012).

65. Jia, X. *et al.* Dual Catalysis of the Selective Polymerization of Biosourced Myrcene and Methyl Methacrylate Promoted by Salicylaldiminato Cobalt(II) Complexes with a Pendant Donor. *Organometallics* **38**, 278–288 (2019).

66. Li, W., Zhao, J., Zhang, X. & Gong, D. Capability of PN ^{3} -type Cobalt Complexes toward Selective (Co-)Polymerization of Myrcene, Butadiene, and Isoprene: Access to Biosourced Polymers. *Ind. Eng. Chem. Res.* **58**, 2792–2800 (2019).

67. Marvel, C. S. & Hwa, C. C. L. Polymyrcene. *J. Polym. Sci.* **45**, 25–34 (1960).

68. Naddeo, M. *et al.* Stereoselective polymerization of biosourced terpenes β-myrcene and β-ocimene and their copolymerization with styrene promoted by titanium catalysts. *Polymer* **131**, 151–159 (2017).

69. Paradiso, V., Capaccio, V., Lamparelli, D. H. & Capacchione, C. [OSSO]-bisphenolate metal complexes: A powerful and versatile tool in polymerization catalysis. *Coordination Chemistry Reviews* **429**, 213644 (2021).

70. Ricci, G., Pampaloni, G., Sommazzi, A. & Masi, F. Dienes Polymerization: Where We Are and What Lies Ahead. *Macromolecules* **54**, 5879–5914 (2021).

71. Peng, D. *et al.* Regio- and Stereochemical Control in Ocimene Polymerization by Half-Sandwich Rare-Earth Metal Dialkyl Complexes. *Macromol. Rapid Commun.* **37**, 987–992 (2016).

72. Yang, F. & Li, X. Novel cationic rare earth metal alkyl catalysts for precise olefin polymerization. *J. Polym. Sci. Part A: Polym. Chem.* **55**, 2271–2280 (2017).

73. Ren, X. *et al.* Scandium-catalyzed copolymerization of myrcene with ethylene and propylene: convenient syntheses of versatile functionalized polyolefins. *Polym. Chem.* **9**, 1223–1233 (2018).

74. Guo, G. *et al.* Unprecedentedly High Activity and/or High Regio-/Stereoselectivity of Fluorenyl-Based CGC Allyl-Type η3:η1-tert-Butyl(dimethylfluorenylsilyl)amido Ligated Rare Earth Metal Monoalkyl Complexes in Olefin Polymerization. *Polymers* **11**, 836 (2019).

75. Yu, X., Li, M., Hong, J., Zhou, X. & Zhang, L. Living 3,4-(Co)Polymerization of Isoprene/Myrcene and One-Pot Synthesis of a Polyisoprene Blend Catalyzed by Binuclear Rare-Earth Metal Amidinate Complexes. *Chem. Eur. J.* **25**, 2569–2576 (2019).

76. Li, W., Jiang, X., So, Y.-M., He, G. & Pan, Y. Lutetium and yttrium complexes supported by an anilido-oxazoline ligand for polymerization of 1,3-conjugated dienes and ε-caprolactone. *New J. Chem.* **44**, 121–128 (2020).

77. You, F., Zhai, J., So, Y.-M. & Shi, X. Rigid Acridane-Based Pincer Supported Rare-Earth Complexes for *cis* -1,4-Polymerization of 1,3-Conjugated Dienes. *Inorg. Chem.* **60**, 1797–1805 (2021).

78. Georges, S., Touré, A. O., Visseaux, M. & Zinck, P. Coordinative Chain Transfer Copolymerization and Terpolymerization of Conjugated Dienes. *Macromolecules* **47**, 4538–4547 (2014).

79. Valente, A., Mortreux, A., Visseaux, M. & Zinck, P. Coordinative Chain Transfer Polymerization. *Chem. Rev.* **113**, 3836–3857 (2013).

80. Liu, B., Liu, D., Li, S., Sun, G. & Cui, D. High trans-1,4 (co)polymerization of β-myrcene and isoprene with an iminophosphonamide lanthanum catalyst. *Chin J Polym Sci* **34**, 104–110 (2016).

81. Loughmari, S. *et al.* Highly stereoselective coordination polymerization of β-myrcene from a lanthanide-based catalyst: Access to bio-sourced elastomers. *J. Polym. Sci. A Polym. Chem.* **50**, 2898–2905 (2012).

82. Georges, S. *et al.* Efficient One-Pot Synthesis of End-Functionalized *trans* -Stereoregular Polydiene Macromonomers. *Macromolecules* **52**, 1210–1219 (2019).

83. Díaz de León Gómez, R. E. *et al.* Synthesis and characterization of high *cis* -polymyrcene using neodymium-based catalysts. *Can. J. Chem. Eng.* **94**, 823–832 (2016).

84. Díaz de León, R. *et al.* Towards Bioelastomers via Coordination Polymerization of Renewable Terpenes Using Neodymium-Based Catalyst Systems. *KEM* **779**, 115–121 (2018).

85. Ren, Y. *et al.* Halide-free neodymium phosphate based catalyst for highly *cis* -1,4 selective polymerization of dienes. *RSC Adv.* **9**, 3345–3350 (2019).

86. Laur, E. *et al.* Stereoselective Copolymerization of Styrene with Terpenes Catalyzed by an Ansa-Lanthanidocene Catalyst: Access to New Syndiotactic Polystyrene-Based Materials. *Catalysts* **7**, 361 (2017).

87. Liu, B. *et al.* Isoselective 3,4-(co)polymerization of bio-renewable myrcene using NSN-ligated rare-earth metal precursor: an approach to a new elastomer. *Chem. Commun.* **51**, 1039–1041 (2015).

88. Liu, B. *et al.* Renewable β-myrcene polymerization initiated by lutetium alkyl complexes ligated by imidophosphonamido ligand. *Chin J Polym Sci* **33**, 792–796 (2015).

89. Li, L., Li, S. & Cui, D. Chemo- and stereoselective polymerization of 3-methylenehepta-1,6-Diene and Its thiol-ene modification. *J. Polym. Sci. Part A: Polym. Chem.* **55**, 1031–1039 (2017).

90. Jing, C. *et al.* Enhancing Thermal Stability in Aminopyridine Iron(II)-Catalyzed Polymerization of Conjugated Dienes. *Organometallics* **39**, 4019–4026 (2020).

91. Zhao, J. *et al.* Polymerization of Isoprene Promoted by Aminophosphine(ory)-Fused Bipyridine Cobalt Complexes: Precise Control of Molecular Weight and *cis* -1,4- *alt* -3,4 Sequence. *Inorg. Chem.* **57**, 4088–4097 (2018).

92. Jia, X. *et al.* Dual Catalysis of the Selective Polymerization of Biosourced Myrcene and Methyl Methacrylate Promoted by Salicylaldiminato Cobalt(II) Complexes with a Pendant Donor. *Organometallics* **38**, 278–288 (2019).

93. Xu, Y. *et al.* Synthesis and properties investigation of hydroxyl functionalized polyisoprene prepared by cobalt catalyzed co-polymerization of isoprene and hydroxylmyrcene. *Polym. Chem.* **11**, 2034–2043 (2020).

94. Gong, D., Tang, F., Xu, Y., Hu, Z. & Luo, W. Cobalt catalysed controlled copolymerization: an efficient approach to bifunctional polyisoprene with enhanced properties. *Polym. Chem.* 10.1039.D1PY00101A (2021) doi:10.1039/D1PY00101A.

95. Ziegler, K., Holzkamp, E., Breil, H. & Martin, H. Das Mülheimer Normaldruck-Polyäthylen-Verfahren. *Angew. Chem.* **67**, 541–547 (1955).

96. Busico, V. Ziegler-Natta catalysis: Forever young. *MRS Bull.* **38**, 224–228 (2013).

97. Natta, G. & Corradini, P. CRYSTALLINE STRUCTURE OF CIS-1,4-POLYBUTADIENE AND OF CIS-1,4-POLYISOPRENE. in *Stereoregular Polymers and Stereospecific Polymerizations* 137 (Elsevier, 1967). doi:10.1016/B978-1-4831-9883-5.50024-6.

98. Lütjering, G. & Williams, J. C. *Titanium*. (Springer, 2007).

99. Capacchione, C. *et al.* Ancillary Ligand Effect on Single-Site Styrene Polymerization: Isospecificity of Group 4 Metal Bis(phenolate) Catalysts. *J. Am. Chem. Soc.* **125**, 4964–4965 (2003).

100. Milione, S. *et al.* Stereoselective Polymerization of Conjugated Dienes and Styrene−Butadiene Copolymerization Promoted by Octahedral Titanium Catalyst. *Macromolecules* **40**, 5638–5643 (2007).

101. Capacchione, C., Saviello, D., Avagliano, A. & Proto, A. Copolymerization of ethylene with isoprene promoted by titanium complexes containing a tetradentate [OSSO]-type bis(phenolato) ligand. *J. Polym. Sci. A Polym. Chem.* **48**, 4200–4206 (2010).

102. Auriemma, F. *et al.* Structure of Isotactic Ethylene/4-Methyl-1,3-pentadiene Alternating Copolymers Obtained from Postmetallocene Catalysts. *Macromolecules* **48**, 6931–6940 (2015).

103. Buonerba, A. *et al.* Binary Copolymerization of *p* -Methylstyrene with Butadiene and Isoprene Catalyzed by Titanium Compounds Showing Different Stereoselectivity. *Macromolecules* **46**, 8449–8457 (2013).

104. Loria, M., Proto, A. & Capacchione, C. Binary copolymerization of 4-methyl-1,3-pentadiene with styrene, butadiene and isoprene catalysed by a titanium [OSSO]-type catalyst: Titanium complex-catalysed copolymerization of 4-methyl-1,3-pentadiene. *Polym. Int.* **66**, 144–150 (2017).

105. Proto, A., Avagliano, A., Saviello, D., Ricciardi, R. & Capacchione, C. Living, Isoselective Polymerization of Styrene and Formation of Stereoregular Block Copolymers via Sequential Monomer Addition. *Macromolecules* **43**, 5919–5921 (2010).

106. Laur, E. *et al.* Stereoselective Copolymerization of Styrene with Terpenes Catalyzed by an Ansa-Lanthanidocene Catalyst: Access to New Syndiotactic Polystyrene-Based Materials. *Catalysts* **7**, 361 (2017).

107. Benjamin, K. R., Silva, I. R., Cherubim, J. P., McPhee, D. & Paddon, C. J. Developing Commercial Production of Semi-Synthetic Artemisinin, and of β-Farnesene, an Isoprenoid Produced by Fermentation of Brazilian Sugar. *Journal of the Brazilian Chemical Society* (2016) doi:10.5935/0103-5053.20160119.

108. Energy Department Announces $11.3 Million for MEGA-BIO: Bioproducts to Enable Biofuels. *Energy.gov* https://www.energy.gov/eere/articles/energy-department-announces-113-million-mega-bio-bioproducts-enable-biofuels.

109. Choi, S.-S., Kwon, H.-M., Kim, Y., Ko, E. & Lee, K.-S. Hybrid factors influencing wet grip and rolling resistance properties of solution styrene-butadiene rubber composites: Wet grip and rolling resistance of SSBR composite. *Polym. Int.* **67**, 340–346 (2018).

110. Ishihara, N., Seimiya, T., Kuramoto, M. & Uoi, M. Crystalline syndiotactic polystyrene. *Macromolecules* **19**, 2464–2465 (1986).

111. Capacchione, C. *et al.* Isospecific Styrene Polymerization by Chiral Titanium Complexes That Contain a Tetradentate [OSSO] -Type Bis (phenolato) Ligand. *Society* 2971–2982 (2005) doi:10.1021/om050120l.

112. Ricci, G., Bosisio, C. & Porri, L. Polymerization of 1,3-butadiene, 4-methyl-1,3-pentadiene and styrene with catalyst systems based on biscyclopentadienyl derivatives of titanium. *Macromol. Rapid Commun.* **17**, 781–785 (1996).

113. Ricci, G., Boccia, A., Leone, G. & Forni, A. Novel Allyl Cobalt Phosphine Complexes: Synthesis, Characterization and Behavior in the Polymerization of Allene and 1,3-Dienes. *Catalysts* **7**, 381 (2017).

114. Ricci, G., Forni, A., Boglia, A., Sommazzi, A. & Masi, F. Synthesis, structure and butadiene polymerization behavior of CoCl2(PRxPh3−x)2 (R=methyl, ethyl, propyl, allyl, isopropyl, cyclohexyl; x=1, 2). Influence of the phosphorous ligand on polymerization stereoselectivity. *Journal of Organometallic Chemistry* **690**, 1845–1854 (2005).

115. Mello, I. L. *et al.* Solvent effect in cis-1,4 polymerization of 1,3-butadiene by a catalyst based on neodymium. *European Polymer Journal* **40**, 635–640 (2004).

116. Sherman, J., Chin, B., Huibers, P. D., Garcia-Valls, R. & Hatton, T. A. Solvent replacement for green processing. *Environmental Health Perspectives* **106**, 253–271 (1998).

117. Ricci, G. *et al.* Synthesis and Characterization of Syndiotactic 1,2-Poly(3-methyl-1,3-pentadiene). *Macromolecules* **40**, 7238–7243 (2007).

118. Naddeo, M. *et al.* Stereoselective polymerization of biosourced terpenes β-myrcene and β-ocimene and their copolymerization with styrene promoted by titanium catalysts. *Polymer* **131**, 151–159 (2017).

119. Lamparelli, D. H. *et al.* Toward More Sustainable Elastomers: Stereoselective Copolymerization of Linear Terpenes with Butadiene. *Macromolecules* acs.macromol.9b02646 (2020) doi:10.1021/acs.macromol.9b02646.

120. Matyjaszewski, K. & M??ller, A. H. E. *Controlled and Living Polymerizations From Mechanisms to Applications*. (2009).

121. Szwarc, S., M. 'Living' Polymers. *Nature* **178**, 1168–1169 (1956).

122. *Anionic Polymerization: Principles, Practice, Strength, Consequences and Applications*. (Springer Japan, 2015). doi:10.1007/978-4-431-54186-8.

123. Hou, G. *et al.* Effect of the structural characteristics of solution styrene–butadiene rubber on the properties of rubber composites. *J. Appl. Polym. Sci.* **135**, 45749 (2018).

124. Obrecht, W. *et al.* Rubber, 4. Emulsion Rubbers. in *Ullmann's Encyclopedia of Industrial Chemistry* (ed. Wiley-VCH Verlag GmbH & Co. KGaA) o23_o01 (Wiley-VCH Verlag GmbH & Co. KGaA, 2011). doi:10.1002/14356007.o23_o01.

125. Newmark, R. A. & Majumdar, R. N. 13C-NMR spectra of cis-polymyrcene and cis-polyfarnesene. *J. Polym. Sci. A Polym. Chem.* **26**, 71–77 (1988).

126. Quirk, R. P. & Huang, T.-L. Alkyllithium-Initiated Polymerization of Myrcene New Block Copolymers of Styrene and Myrcene. in *New Monomers and Polymers* (eds. Culbertson, B. M. & Pittman, C. U.) 329–355 (Springer US, 1984). doi:10.1007/978-1-4684-4619-7_19.

127. Bolton, J. M., Hillmyer, M. A. & Hoye, T. R. Sustainable Thermoplastic Elastomers from Terpene-Derived Monomers. *ACS Macro Lett.* **3**, 717–720 (2014).

128. Glatzel, J., Noack, S., Schanzenbach, D. & Schlaad, H. Anionic polymerization of dienes in 'green' solvents. *Polym Int* pi.6152 (2020) doi:10.1002/pi.6152.

129. Yoo, T. & Henning, S. K. SYNTHESIS AND CHARACTERIZATION OF FARNESENE-BASED POLYMERS. *Rubber Chemistry and Technology* **90**, 308–324 (2017).

130. Bareuther, J. *et al.* Temperature Variation Enables the Design of Biobased Block Copolymers via One-Step Anionic Copolymerization. *Macromol. Rapid Commun.* 2000513 (2020) doi:10.1002/marc.202000513.

131. Brown, H. C., Schlesinger, H. I., Sheft, I. & Ritter, D. M. Addition Compounds of Alkali Metal Hydrides. Sodium Trimethoxyborohydride and Related Compounds [1]. *J. Am. Chem. Soc.* **75**, 192–195 (1953).

132. Ashby, E. C., Arnott, Robert. & Srivastava, Suresh. Reactions of alkali metal hydrides with magnesium alkyls. Preparation of MMgR2H and MMg2R4H compounds. *Inorg. Chem.* **14**, 2422–2426 (1975).

133. Kubas, G. J. & Shriver, D. F. Nature of dialkyl- and diarylzinc hydride complexes. *J. Am. Chem. Soc.* **92**, 1949–1954 (1970).

134. Ziegler, K., Köster, R., Lehmkuhl, H. & Reinert, K. Metallorganische Verbindungen, XXX Neue Komplexverbindungen der Aluminiumalkyle. *Justus Liebigs Ann. Chem.* **629**, 33–49 (1960).

135. Needles, H. L. Sodium hydride-initiated polymerizations of vinyl monomers in aprotic solvents. *J. Polym. Sci. A-1 Polym. Chem.* **7**, 1437–1445 (1969).

136. Carlotti, S. *et al.* Sodium Hydride/Trialkylaluminum Complexes for the Controlled Anionic Polymerization of Styrene at High Temperature. *Macromol. Rapid Commun.* **27**, 905–909 (2006).

137. Carlotti, S., Desbois, P., Warzelhan, V. & Deffieux, A. Retarded anionic polymerization (RAP) of styrene and dienes. *Polymer* **50**, 3057–3067 (2009).

138. Kalita, U., Samanta, S., Banerjee, S. L., Das, N. C. & Singha, N. K. Biobased Thermoplastic Elastomer Based on an SMS Triblock Copolymer Prepared *via* RAFT Polymerization in Aqueous Medium. *Macromolecules* **54**, 1478–1488 (2021).

139. Sarkar, P. & Bhowmick, A. K. Terpene Based Sustainable Elastomer for Low Rolling Resistance and Improved Wet Grip Application: Synthesis, Characterization and Properties of Poly(styrene- *co* -myrcene). *ACS Sustainable Chem. Eng.* **4**, 5462–5474 (2016).

140. Zhang, S. *et al.* Investigation on Synthesis and Application Performance of Elastomers with Biogenic Myrcene. *Ind. Eng. Chem. Res.* **58**, 12845–12853 (2019).

141. Labbé, A., Carlotti, S., Shcheglova, L., Desbois, P. & Deffieux, A. Dienes polymerization in the presence of metal hydrides and triethylaluminum. *Polymer* **47**, 3734–3739 (2006).

142. Sarkar, P. & Bhowmick, A. K. Terpene Based Sustainable Elastomer for Low Rolling Resistance and Improved Wet Grip Application: Synthesis, Characterization and Properties of Poly(styrene-co-myrcene). *ACS Sustainable Chem. Eng.* **4**, 5462–5474 (2016).

143. Hulnik, M. I. *et al.* Aqueous cationic homo- and co-polymerizations of β-myrcene and styrene: a green route toward terpene-based rubbery polymers. *Polym. Chem.* **9**, 5690–5700 (2018).

144. Grune, E. *et al.* Towards bio-based tapered block copolymers: the behaviour of myrcene in the statistical anionic copolymerisation. *Polym. Chem.* **10**, 1213–1220 (2019).

145. Jia, X., Zhang, X. & Gong, D. 1,2 Enriched polymerization of isoprene by cobalt complex carrying aminophosphory fused (PN^3) ligand: 1,2 Enriched Polymerization of Isoprene by Cobalt

Complex Carrying Aminophosphory Fused (PN ^{3}) Ligand. *J. Polym. Sci. Part A: Polym. Chem.* **56**, 2286–2293 (2018).

146. Oliveira, C., Albergaria De Mello Bandeira, R., Vasconcelos Goes, G., Schmitz Gonçalves, D. & D'Agosto, M. Sustainable Vehicles-Based Alternatives in Last Mile Distribution of Urban Freight Transport: A Systematic Literature Review. *Sustainability* **9**, 1324 (2017).

147. Huang, Y. *et al.* Eco-driving technology for sustainable road transport: A review. *Renewable and Sustainable Energy Reviews* **93**, 596–609 (2018).

148. Lamparelli, D. H., Paradiso, V. & Capacchione, C. NEW ELASTOMERIC MATERIALS FROM BIOMASS: STEREOSELECTIVE POLYMERIZATION OF LINEAR TERPENES AND THEIR COPOLYMERIZATION WITH BUTADIENE BY USING A COBALT COMPLEX WITH PHOSPHANE LIGANDS. *Rubber Chemistry and Technology* **93**, 605–614 (2020).

149. Lamparelli, D. H., Kleybolte, M. M., Winnacker, M. & Capacchione, C. Sustainable Myrcene-Based Elastomers via a Convenient Anionic Polymerization. *Polymers* **13**, 838 (2021).

150. Zhou, C., Wei, Z., Lei, X. & Li, Y. Fully biobased thermoplastic elastomers: synthesis and characterization of poly(L -lactide)-b-polymyrcene-b-poly(L -lactide) triblock copolymers. *RSC Adv.* **6**, 63508–63514 (2016).

151. Thaptong, P., Sae-oui, P. & Sirisinha, C. INFLUENCES OF STYRENE BUTADIENE RUBBER AND SILICA TYPES ON PERFORMANCE OF PASSENGER CAR RADIAL TIRE TREAD. *Rubber Chemistry and Technology* **90**, 699–713 (2017).

152. Hao, P. T., Ismail, H. & Hashim, A. S. Study of two types of styrene butadiene rubber in tire tread compounds. *Polymer Testing* **20**, 539–544 (2001).

153. Kane, M. & Edmondson, V. Tire/road friction prediction: introduction a simplified numerical tool based on contact modelling. *Vehicle System Dynamics* 1–20 (2020) doi:10.1080/00423114.2020.1832696.